PACIFIC EARTHQUAKE ENGINEERING RESEARCH CENTER

Ground Motion Evaluation Procedures for Performance-Based Design

Jonathan P. Stewart
Department of Civil and Environmental Engineering
University of California, Los Angeles

Shyh-Jeng Chiou
California Department of Transportation
Sacramento, California

Jonathan D. Bray
Department of Civil and Environmental Engineering
University of California, Berkeley

Robert W. Graves and Paul G. Somerville
URS Corporation
Pasadena, California

Norman A. Abrahamson
Pacific Gas and Electric Company
San Francisco, California

A report on research conducted under grant no. EEC-9701568 from the National Science Foundation

PEER 2001/09
SEPTEMBER 2001

Ground Motion Evaluation Procedures for Performance-Based Design

Jonathan P. Stewart
Department of Civil and Environmental Engineering
University of California, Los Angeles

Shyh-Jeng Chiou
California Department of Transportation
Sacramento, California

Jonathan D. Bray
Department of Civil and Environmental Engineering
University of California, Berkeley

Robert W. Graves and Paul G. Somerville
URS Corporation
Pasadena, California

Norman A. Abrahamson
Pacific Gas and Electric Company
San Francisco, California

A report on research conducted under
grant no. EEC-9701568 from the National Science Foundation

PEER Report 2001/09
Pacific Earthquake Engineering Research Center
College of Engineering
University of California, Berkeley

September 2001

EXECUTIVE SUMMARY

Introduction

The principal objective of the Pacific Earthquake Engineering Research Center (PEER) is to develop a sound, scientific basis for performance-based earthquake engineering. The development of this methodology includes three vital steps:

1. Evaluation of the distribution of ground motion **intensity measures** at a site, given certain seismological variables (i.e., fault characteristics, position of site relative to faults, etc.). Intensity measures may consist of traditional parameters such as spectral acceleration or duration, or newly defined parameters found to be useful for particular applications.
2. Evaluation of the distribution of system **response** or **damage measures**, given a particular set of intensity measures. These parameters describe the performance of a structure in engineering terms, such as inter-story drift (e.g., for buildings), plastic hinge rotation (e.g., for bridge columns) or slope displacement (e.g., for harbor revetment slopes).
3. Evaluation of the probability of exceeding **decision variables** within a given time period, given appropriate damage measures. Decision variables may include human or collateral loss, post-earthquake repair time, or other parameters of interest to an owner.

These three steps in the performance-based design methodology are linked through the theorem of total probability, and the outcome of the analysis is no better than the weakest (or most uncertain) link in the process. Accordingly, since its inception, PEER has recognized the vital role of high-quality ground motion characterization for performance-based design, and has developed and executed a plan for ground motion research that integrates the strengths of PEER researchers with those of experts in other organizations such as the Southern California Earthquake Center (SCEC) and the U.S. Geological Survey (USGS).

The PEER ground motion research plan is best understood by first recognizing the various components of a ground motion analysis, which involves the broad subjects of source characterization, travel path effects on seismic waves, and site effects. PEER has to a large extent deferred to other organizations such as SCEC and the USGS on the issue of source characterization, as these organizations have the seismological expertise appropriate to the topic.

The PEER ground motion research plan was developed with the objective of formulating a rational, scientifically-based set of procedures for the analysis of path and site effects. The majority of this work has been funded through the PEER Lifelines Program, but with specific, focused contributions from the Core Program as well.

Objective

This report was prepared to synthesize contemporary procedures for ground motion analysis within a performance-based design framework, and to document the past and future role of PEER research in developing these procedures. Each component of ground motion analysis is described, regardless of whether PEER has sponsored research on that topic. The subjects of source, path, and site effects are discussed in six chapters organized according to a traditional breakdown of topics. In the following two sections, we summarize the main technical content of the report (with PEER contributions identified), and describe the future research directions envisioned for the Core and Lifelines programs.

Technical Content of Report

The topics associated with a probabilistic evaluation of earthquake ground motions in seismically active regions consist of the following:

- *Source Characterization*: minimum and maximum magnitude, magnitude-recurrence relations
- *Attenuation Relations*: regression analysis procedures and factors affecting spectral acceleration and other ground motion parameters
- *Near-Fault Ground Motions*: rupture directivity and fling step effects
- *Site Effects*: observational studies of site effects, analysis procedures for one-dimensional ground response, basin response, and topographic effects
- *Ground Motion Simulation*: elements of simulation methods, example procedures, verification and future use of simulation
- *Time History Selection*: de-aggregation of hazard, time history selection, and scaling of time histories.

The discussion of source characterization and site effects is clear in the above topics. Path effects are covered within the topic categories of attenuation, near-fault ground motions, and simulation.

Source Characterization

We describe faults as a series of segments (or a single segment) that can either rupture individually or in groups. A fault segment is characterized by a length (or area), a probability density function describing the relative likelihood of the fault producing earthquakes of different magnitudes [$f(m)$], and a long term slip rate.

Fault models are constructed so as to only allow moment release between a minimum and maximum magnitude (denoted as m^0 and m^u, respectively). Minimum magnitude is often taken arbitrarily as five, although smaller values may be appropriate for stiff, brittle structures. Maximum magnitude is related to the stress drop that occurs on faults during earthquakes and the size (area) of the fault segment. Stress drop is generally observed to be reasonably consistent within a given tectonic regime (e.g., active regions such as California) and over a given magnitude range, which enables the development of magnitude-area scaling relationships from empirical data. These relationships can be used with known fault dimensions to assign probable values of m^u.

Several types of probability density functions for earthquake magnitude [$f(m)$] are used for seismic source zones, including truncated exponential, characteristic earthquake, and maximum magnitude models. The choice of an appropriate model is often made on the basis of fault size and slip rate, or from observations of historic seismicity. The rate of occurrence of earthquakes is derived by equating the rate of moment build-up on faults (derived from slip rate and fault size) to the rate of moment release [related to $f(m)$]. Earthquakes can be assumed to occur at a fixed rate according to a Poisson process, or at a time-varying rate that depends on the elapsed time since the previous event (time-predictable models).

PEER has not supported research related to source characterization, as SCEC and the USGS are better equipped to provide leadership in this area.

Ground Motion Attenuation Relations

The evaluation of seismic hazard requires the use of probabilistic distributions of intensity measures (*IMs*) conditioned on the occurrence of an earthquake with a particular magnitude (m) at a given site-source distance (r). The probability density function (PDF) for a single *IM* is written as $f(IM|m,r)$, and is usually log-normal. Attenuation relationships define the statistical moments of these PDFs (e.g., medians, standard error terms) in terms of parameters such as m and r. The attenuation relations are derived through regression of empirical data.

The most commonly used ground motion intensity measure is spectral acceleration at a specified damping level (usually 5%). A number of attenuation relations for this parameter are available for each of the three generally recognized tectonic regimes: active regions, subduction zones, and intra-plate regions. Attenuation relations for active regions are the most abundant, and these relations are distinguished to a large extent by the manner in which data is weighted, which in turn is related to different schemes for incorporating intra- and inter-event variability into the regression process. Other important distinguishing characteristics include the treatment of focal mechanism and site condition.

Attenuation relationships are also available for other intensity measures, including peak horizontal velocity, vertical spectral acceleration, Arias intensity, duration-related parameters, and mean period. The response of many classes of structures is sensitive to more than one of these intensity measures, and hence require a probabilistic representation of multiple *IM*s. Development of this methodology for hazard representation, termed vector hazard, is a key PEER research objective.

Almost all attenuation relations are derived from, or calibrated against, strong ground motion recordings. Current PEER research is performing the critical work of compiling and documenting uniformly processed strong motion and site condition databases for the next-generation of these relationships. Future work will develop relations for the critical intensity measures needed for structural and geotechnical applications.

Characteristics of Near-Fault Ground Motions

Ground motions in close proximity to the seismic source can be significantly influenced by near-fault effects referred to herein as "rupture directivity" and "fling step." Rupture directivity affects the duration and long-period energy content of ground motions, principally in the horizontal direction normal to the fault strike. Earthquake rupture towards a site tends to produce a short-duration, but large amplitude "pulse" of motion, and is called "forward directivity." Conversely, neutral or backward directivity of rupture away from the site produces long duration motion of relatively low amplitude. These effects are observed for site-source distances less than 20 to 60 km. Fling step is associated with the permanent displacement that occurs across a ruptured fault, and involves a large, unidirectional velocity pulse to accommodate this displacement in the slip-parallel direction.

Rupture directivity affects intensity measures related to the duration or long-period energy content of ground motions. Engineering models for conventional intensity measures such as spectral acceleration and duration are available that adjust the results of attenuation relations given near-fault geometric parameters (e.g., percentage of fault rupturing towards site, site-epicenter azimuth). However, nonlinear structural response studies have suggested that the feature of forward directivity ground motion that is most damaging to structures is the velocity pulse, which is best described in the time domain. PEER research has developed engineering models to describe the time-domain characteristics of these pulses, including peak velocity, pulse period, and number of significant pulses.

Fling step affects the peak velocity and displacement of ground motions, and is best described in terms of time-domain parameters. An engineering model for this effect is currently under development.

Site Effects

Ground motion attenuation relationships provide estimates of intensity measures that typically apply for broadly defined site conditions such as rock or soil. Actual conditions at strong motion recording sites are highly variable with respect to local ground conditions, possible basin effects, and surface topography, and hence estimates from attenuation relationships necessarily represent averaged values across the range of possible site conditions. Analyses of site effects seek to improve the accuracy and reduce the dispersion of ground motion predictions using information about site conditions. The PEER research program has taken a systematic approach to determine the impact of increasing levels of detail in site characterization on the accuracy of ground motion predictions. In particular, a series of complementary studies has investigated the use of the following models for evaluating site effects: (1) amplification factors defined on the basis of generalized site categories, (2) one-dimensional ground response analysis, and (3) basin response analysis. Although not researched in the PEER program, also significant for some sites are the effects of surface topography on ground motion.

Amplification factors represent the ratio of a ground motion intensity measure for a specified site condition to the value of the parameter that would have been expected for a reference site condition. Reference site conditions are typically rock or weathered soft rock. Amplification factors can be derived from observational data or numerical analyses. PEER researchers have developed nonlinear amplification factors as a function of detailed surface geology, shear wave velocity in the upper 30 m, and geotechnically based classification systems. Additional research has suggested that amplification factors may also be dependent on depth to basement rock (defined as having a shear wave velocity of 2.5 km/s).

One-dimensional ground response analyses are a means by which to adjust ground motion estimates at soil sites using detailed information on shallow soil conditions (i.e., these analyses are seldom performed for sediment depths > 100 – 200 m). All one-dimensional ground response calculation methods assume vertical propagation of seismic waves and horizontal soil layering. What distinguishes different analysis methods is the model for soil behavior, which ranges from relatively simple models requiring few input parameters (i.e., equivalent-linear) to more complex, fully nonlinear analyses requiring a greater number of input parameters. PEER research is evaluating the benefit of ground response analyses as compared to the use of attenuation models. Benefit is quantified in terms of the reduction of bias, which should be smaller for a more accurate model, and the reduction of prediction dispersion, as this dispersion is a measure of the degree to which the analysis procedure can capture site-to-site variations in ground motion. Results obtained to date using an equivalent-linear model suggest significant benefit for soft clay sites at periods < one second, but moderate to negligible benefit at longer periods and for stiffer soil conditions.

Basin response analyses provide a means by which to account for the effects of two- or three-dimensional deep basin structure on ground motion characteristics. Basin effects are defined for this report as deviations from the predictions of one-dimensional models resulting from the relatively complex wave propagation paths in basins. An important mechanism by which these basin effects occur is the propagation of seismic waves in the direction of basin thickening, which can trap the waves within the basin if post-critical incidence angles develop. Also possible is the focusing of seismic energy in spatially restricted areas on the surface due to folded deep sedimentary structure. PEER-sponsored research has sought to validate and calibrate existing analytical models for basin response, so that these models can be used to develop simple models for basin response.

Pronounced variations in ground motion can occur between level sites and areas with irregular surface topography such as ridges, canyons, or slopes. Numerical and analytical models for topographic effects are available, and indicate the amplification to be sensitive to the wave incidence angle, wave type, and some measure of the topographic irregularity (e.g., slope angle). Analyses also suggest that the effects are highly frequency dependant. Few strong ground motion data sets have been analyzed to calibrate these analysis procedures.

Ground Motion Simulation

Available data resources are inadequate to constrain models for a number of important problems such as ground motions from very large magnitude earthquakes, near-fault ground motions, and basin effects, as well as ground motions in intra-plate regions. Ground motion simulation refers to seismological methods for numerically simulating a rupture process, path effects, and site response effects within a unified framework. These types of analyses are attractive because they can be used to generate ground motion time histories for the aforementioned situations where actual recordings are sparse or unavailable.

A wide variety of models are available for simulating earthquake source, path, and site response effects. Several well-known simulation procedures are distinguished based on their models for these effects. Before any of these procedures can be used for practical application, however, it is vital that they be calibrated against recordings from actual earthquakes. The quality of a simulation procedure is measured from such calibration studies by average misfit (i.e., the average difference between data and prediction) and the dispersion of the misfit.

Spectral acceleration is the ground motion intensity measure most often used in these calibration studies, although duration has also been used. Work sponsored by PEER has validated a number of leading simulation methods against each other, and has begun the process of calibrating these codes against uniform data sets from several earthquakes.

Time History Selection

Probabilistic seismic hazard analyses produce estimates of ground motion intensity measures for specified annual probabilities of exceedance. For many applications in performance-based engineering, the ground motions may need to be specified not only as intensity measures but also by suites of time histories for input into time-domain nonlinear analyses of structures. Development of these time histories requires that the seismic hazard first be de-aggregated to identify the most critical ranges of magnitude and distance, that appropriate time histories be selected for these seismological conditions, and that the selected time histories be appropriately scaled. PEER has conducted relatively little research on these topics.

Future Research Directions

The PEER center has formulated a plan for future research that builds on the present momentum with the objective of developing rational, calibrated procedures for estimating ground motion intensity measures. This objective will be realized through synergistic research projects within the Core and Lifelines programs, as well as collaboration with non-PEER researchers.

The PEER Core Program has three principal objectives in ground motion research. The first is to identify existing or define new intensity measures (IMs) that provide the best possible correlation to damage measures for structures. These critical IMs are being defined in fundamental research characterizing the nonlinear dynamic response of geotechnical and structural systems. Once these critical IMs are defined, the second objective is to develop procedures for estimating these parameters with due consideration of near-fault and site effects. The third objective is to develop vector hazard capabilities, as the nonlinear response of many structures is described by multiple IMs.

The PEER Lifelines Program is currently engaged in the first stage of a three-year program of research on earthquake ground motions. The principal thrusts to this work remain the same —

the development of rational procedures for characterizing path effects (attenuation and near-fault ground motion models) and site effects.

The main thrust of the work within the broad category of path effects is to develop data that can be used to constrain attenuation and directivity models for large earthquakes, for which empirical data are scarce. Initial work is incorporating Turkey and Taiwan strong motion data into existing relations. Additional potential "data" sources that are being investigated as possible means of constraining the attenuation relations include the dating of precarious rocks near active faults, and simulation exercises. Physical models will be investigated as a means to evaluate rupture directivity effects. Finally, projects are planned to develop attenuation relations for intensity measures such as velocity, displacement, and differential displacement that are of vital importance for many lifelines structures.

The planned work within the broad subject of site effects is focused on the development of simple models and more complex analytical methodologies for ground response and basin response effects. Objectives of the ground response work are to establish guidelines for (1) when detailed response analyses are justified in terms of the their ability to reduce prediction bias and dispersion and (2) the use of equivalent-linear vs. nonlinear response analyses. Calibration exercises of ground response codes will also be performed using vertical array data. Objectives of the basin response work are to validate a series of basin response analysis methods against each other, calibrate them against strong motion data sets, and then use the calibrated analysis methods to help develop engineering models for basin response. The pursuit of these "global" objectives for ground and basin response is being supported with major data development and synthesis work, including strong motion data and geotechnical data from accelerograph sites.

In summary, the PEER Lifelines Program is developing data, models, and methods that are needed to meet the ground motion characterization needs for performance-based earthquake risk management for highway and electric power systems. This work is highly synergistic with planned work in the PEER Core Program, which will define the ground motion characterization needs for the next-generation of analysis and design methodologies for other classes of structures. The solid foundation of data and experience gained through the Lifelines Program will streamline the model development process for new intensity measures defined in the Core Program. All will benefit from close collaboration and coordination between these two, equally vital research programs.

ACKNOWLEDGMENTS

The authors would like to thank the following individuals who provided materials that were of assistance in the preparation of this report: Edward Field and William Elsworth of the U.S. Geological Survey, Walter Silva of Pacific Engineering and Analysis, and Allin Cornell of Stanford University. We would also like to thank the following reviewers of the manuscript: Maurice S. Power of Geomatrix Consultants, Clifford Roblee of the California Department of Transportation, Woody Savage of Pacific Gas and Electric Company, Walter Silva, and Y. Zeng of the University of Nevada, Reno.

This work was supported by the Pacific Earthquake Engineering Research Center through the Earthquake Engineering Research Centers Program of the National Science Foundation under Award number EEC-9701568. Support for the participation of Paul Somerville and Robert Graves was provided by the Lifelines Program of the Pacific Earthquake Engineering Research Center.

PREFACE

The Pacific Earthquake Engineering Research Center (PEER) is an Earthquake Engineering Research Center administered under the National Science Foundation Engineering Research Center program. The mission of PEER is to develop and disseminate technology for design and construction of buildings and infrastructure to meet the diverse seismic performance needs of owners and society. Current approaches to seismic design are indirect in their use of information on earthquakes, system response to earthquakes, and owner and societal needs. These current approaches produce buildings and infrastructure whose performance is highly variable, and may not meet the needs of owners and society. The PEER program aims to develop a performance-based earthquake engineering approach that can be used to produce systems of predictable and appropriate seismic performance.

To accomplish its mission, PEER has organized a program built around research, education, and technology transfer. The research program merges engineering seismology, structural and geotechnical engineering, and socio-economic considerations in coordinated studies to develop fundamental information and enabling technologies that are evaluated and refined using test beds. Primary emphases of the research program at this time are on older existing concrete buildings, bridges, and highways. The education program promotes engineering awareness in the general public and trains undergraduate and graduate students to conduct research and to implement research findings developed in the PEER program. The technology transfer program involves practicing earthquake professionals, government agencies, and specific industry sectors in PEER programs to promote implementation of appropriate new technologies. Technology transfer is enhanced through a formal outreach program.

PEER has commissioned a series of synthesis reports with a goal being to summarize information relevant to PEER's research program. These reports are intended to reflect progress in many, but not all, of the research areas in which PEER is active. The synthesis reports are geared toward informed earthquake engineering professionals who are well versed in the fundamentals of earthquake engineering, but are not necessarily experts in the various fields covered by the reports. Indeed, one of the primary goals of the reports is to foster cross-discipline collaboration by summarizing the relevant knowledge in the various fields. A related purpose of the reports is to identify where knowledge is well developed and, conversely, where significant gaps exist. This information will help form the basis to establish future research initiatives within PEER.

CONTENTS

LIST OF FIGURES

LIST OF TABLES

NOMENCLATURE

(partial list – additional variables used locally in the text)

A	Fault area
AD	Average displacement across ruptured fault
D_b	Depth to basement
DM	Damage Measure (defined in Section 1.1)
DV	Decision Variable (defined in Section 1.1)
f	Frequency
f_c	Corner frequency (defined in Section 1.2.2)
f_{max}	Cutoff frequency (defined in Section 1.2.2)
F	Focal mechanism parameter
F_a	Amplification factor at short period range (T = 0.1-0.5 s)
F_v	Amplification factor at intermediate period range (T = 0.4-2.0 s)
G	Soil shear modulus
G_{max}	Maximum (small strain) soil shear modulus
h	Focal depth
HW	Hanging wall parameter (Figure 3.2b)
i_{crit}	Critical angle for Moho reflection (Section 3.2.2d)
I_A	Arias intensity (defined in Section 1.2.3)
IM	Ground motion Intensity Measure (defined in Section 1.1)
m	Earthquake magnitude (generally moment magnitude unless indicated otherwise)
m^0	Minimum magnitude (defined in Section 2.2)
m^u	Upper-bound magnitude for use with truncated exponential distribution (defined in Section 2.3.1)
Δm_c	Width of characteristic magnitude range
m_{max}	Mean magnitude in maximum magnitude model (Section 2.3.1)
MD	Maximum displacement across ruptured fault
M_0	Seismic moment
$\dot{M}_0$	Rate of seismic moment build up
N	Equivalent number of uniform stress cycles

N_v	Number of half cycles of motion for near-fault velocity pulses (Section 4.2.1e)
PHA	Peak horizontal acceleration
PHV	Peak horizontal velocity
PHD	Peak horizontal displacement
Q	Seismic quality factor (Section 6.2.2)
r	Closest distance between site and seismic source
r_{crit}	Critical distance for Moho reflection (Section 3.2.2d)
r_{jb}	Closest distance between site and surface projection of source
r_{seis}	Closest distance between site and rupture surface below seismogenic depth
r_{hypo}	Closest distance between site and hypocenter
s	Fault slip rate
S	Site parameter (Chapter 3)
SD	Significant duration (defined in 1.2.3)
S_a	Spectral acceleration
t	Time
t_e	Time since last earthquake (Section 2.3.2)
T	Period
V_p	Pressure wave velocity
V_s	Shear wave velocity
t_r	Rise time (defined in 4.2.1d)
T_m	Mean period (defined in Section 1.2.2)
T_p	Predominant period (defined in Section 1.2.2)
T_v	Pulse period (defined in Section 1.2.2)
$T_{v\text{-}p}$	Pulse period as determined from peak in response spectrum (defined in Section 4.1.2)
X	Fraction of fault rupturing towards site, strike-slip focal mechanism (Figure 4.3)
Y	Fraction of fault rupturing towards site, dip-slip focal mechanism (Figure 4.3)
Z_t	Inter- vs. intra-slab earthquake parameter (Chapter 3)
α_t	Coefficient of variation of time between events for time-predictable model (Section 2.3.2)
δ	Scale parameter for Brownian motion (Section 2.3.2)
$\Delta\sigma$	Stress drop
ε	Standard normal variate (normalized residual)
κ	Parameter for damping function used for shallow crust in simulation procedures

λ	Seismic wavelength
μ	Friction coefficient between fault blocks (Section 2.3.2)
μ_t	Mean time between events for time-predictable model (Section 2.3.2)
υ	Poisson time rate of event occurring (event definition varies depending on context)
υ_c	Poisson rate of occurrence of characteristic earthquake
υ_m	Poisson rate of occurrence of earthquakes with magnitude > m
$\upsilon_{c,tp}$	Adjusted Poisson rate of occurrence of characteristic earthquakes based on time-predictable model
ϕ	Offset azimuth of site from dip-slip fault (Figure 4.3)
σ	Standard deviation or standard error
σ_m	Standard deviation in magnitude units for maximum magnitude model (Section 2.3.1)
θ	Offset azimuth of site from strike-slip fault (Figure 4.3)
η	Normalized frequency (Section 5.5.2)

1 INTRODUCTION

Ground motions are a fundamental mechanism by which earthquakes damage structures of all types. The Pacific Earthquake Engineering Research Center (PEER) is on the cutting edge of ground motion research, supporting numerous projects with significant short-term and long-term implications for the earthquake engineering profession. Ground motion research within PEER has been carefully coordinated with work in other organizations (such as the Southern California Earthquake Center and the U.S. Geological Survey) as part of a well-conceived plan to improve the scientific basis for ground motion characterization. The interconnection between PEER researchers and non-PEER researchers is a strength of the center's activities, and the outcome of this cooperative spirit is reflected by the diverse array of researchers whose work is synthesized in this document.

1.1 PERFORMANCE-BASED DESIGN

The mission of the PEER Center is to "develop, validate, and disseminate performance-based seismic design technologies for buildings and infrastructure to meet the diverse economic and safety needs of owners and society." While the words "ground motion" do not appear in this mission statement, the art and science of ground motion evaluation undeniably plays a vital role in performance-based design.

The role of ground motion characterization is demonstrated in the unifying equation commonly used to represent the performance-based design methodology:

$$\upsilon(DV) = \iint G\langle DV \mid DM \rangle \mid dG\langle DM \mid IM \rangle \| d\upsilon(IM) \mid \tag{1.1}$$

where

DV = a Decision Variable that can be understood and used by owners/policy makers (e.g., cost, down time, etc.).

DM = a Damage Measure representing the performance of the structure under consideration (e.g., displacement ductility for buildings/bridge, building settlement for foundations, slope displacement for waterfront structures).

IM = an Intensity Measure of the ground motion (e.g., spectral acceleration, duration).

$d\upsilon(IM)$ = Derivative with respect to *IM* of the Poisson rate of *IM* exceeding some threshold value.

$\upsilon(DV)$ = Poisson rate of *DV* exceeding some threshold value.

Equation 1.1 implies that functional relationships can be formed between parameters representing damage to structures (*DM*s) and ground motions (*IM*s), and between decision variables (*DV*s) and damage measures (*DM*s). Simply put, PEER's mission is to develop such relations. For simple structures, it may be possible to derive closed form expressions for the conditional probabilities of $DM|IM$ and $DV|DM$. However, for unique and complex structures, such relations will likely involve structure-specific simulation exercises utilizing carefully chosen ground motion parameters, or suites of time histories. This report is focused on synthesizing contemporary procedures for probabilistic evaluations of ground motion hazard for utilization within this performance-based design framework. While great strides have been made in recent years on these topics, this compilation also highlights a significant number of issues requiring new, original research before the promise of performance-based design can be fully realized.

To more clearly illustrate the components of a probabilistic ground motion evaluation and its use within the context of performance based design, we write the conventional hazard integral for *IM* (Cornell, 1968):

$$\upsilon(IM) = \sum_{i=1}^{N_{flt}} \upsilon_i \times \int_m \int_r f(m) f(r) P(IM > z \mid m, r) dm dr \tag{1.2}$$

where $\upsilon(IM)$ = Poisson rate of a single *IM* exceeding a threshold value z. Other terms in Equation 1.2 represent components of the hazard analysis. Term υ_i represents the rate of occurrence of earthquakes with magnitudes greater than a lower-bound threshold value, m^0 on fault i (the number of faults = N_{flt}). Term $f(m)$ represents a Probability Density Function (PDF) on magnitude (i.e., given an earthquake occurs, $f(m)$ represents the relative likelihood of it having different magnitudes). Term $f(r)$ is a PDF on site-source distance, which is generally broken down into additional PDFs pertaining to the rupture location on the fault and the size of the rupture conditioned on magnitude. Term $P(IM>z|m,r)$ is one minus the Cumulative

Distribution Function (CDF) for *IM* attenuation. The simple summation across N_{flt} sources in Equation 1.2 assumes statistical independence of earthquake occurrence on different faults. This may be incorrect for some areas, but could be accounted for in the υ terms.

Each of the elements in Equation 1.2 is retained when the hazard is expanded to encompass *DM*s. For the simplest possible case of one *DM* that depends on only one *IM*, the hazard can be written as,

$$\upsilon(DM) = \sum_{i=1}^{N_{flt}} \upsilon_i \times \int_m \int_r f(m) f(r) \int_{IM} f(IM \mid m,r) \times P(DM > y \mid IM) dm \cdot dr \cdot d(IM) \qquad (1.3a)$$

where $\upsilon(DM)$ = Poisson rate of *DM* exceeding a threshold value *y*. Note terms υ_i, *f(m)*, and *f(r)* are retained as in Equation 1.2. The term *f(IM|m,r)* is a PDF version of the *IM* attenuation. The additional term of *P*(*DM*>*y*|*IM*) describes the conditional CDF for *DV* in terms of *IM*, which as noted previously would generally require structure-specific analyses. The derivation of the CDF for *P*(*DM*>*y*|*IM*) is a significant challenge facing PEER, and will likely require the use of either a new ground motion parameter that incorporates elements of nonlinear structural response into the formulation, or suites (vectors) of two or more ground motion parameters. If the former is adopted for a particular class of structure, new attenuation relations for the critical *IM* will need to be derived. If a vector of *IM*s is selected, the hazard integral on $\upsilon(DM)$ would need to be re-written as,

$$\begin{aligned}\upsilon(DM) = & \sum_{i=1}^{N_{flt}} \upsilon_i \times \int_m \int_r f(m) f(r) \int_{IM_1} \int_{IM_2} f(IM_1, IM_2 \mid m,r) \times \\ & P(DM > y \mid IM_1, IM_2) dm \cdot dr \cdot d(IM_1) \cdot d(IM_2)\end{aligned} \qquad (1.3b)$$

where $f(IM_1, IM_2 \mid m,r)$ is a joint PDF on two ground motion parameters. Few joint PDFs of this type have been developed to date.

The extension of the hazard integral to *DV* is given below for the case of one *IM* to estimate *DM*, and one *DM* to estimate *DV*.

$$\begin{aligned}\upsilon(DV) = & \sum_{i=1}^{N_{flt}} \upsilon_i \times \int_m \int_r f(m) f(r) \int_{IM} f(IM \mid m,r) \int_{DM} f(DM \mid IM) \times \\ & P(DV > x \mid DM) \cdot dm \cdot dr \cdot d(IM) \cdot d(DM)\end{aligned} \qquad (1.4)$$

where $\upsilon(DV)$ = Poisson rate of *DV* exceeding a threshold value *x*. The only new term here is the *DV*|*DM* function, which would likely require structure-specific economic/use analysis. Regardless of the specific hazard equation being used, the prevailing need for terms associated with ground motion evaluation [υ, *f(m)*, and *f(r)*, and attenuation functions] is apparent. Also clear is a need for time history selection procedures (e.g., as would be used for structure-specific evaluation of $DM|IM$ functions).

The aforementioned functions and procedures are required to quantify ground motion hazard within the context of performance-based design. The intent of this report is to synthesize the present state of knowledge regarding these functions and procedures, and the PEER contributions to this state of knowledge. The following sections introduce the specific *IM*s considered here, and the strategies developed within PEER to meet the research needs associated with ground motion characterization.

1.2 DEFINITION OF INTENSITY MEASURES

Seismic demand is represented in design/analysis procedures for structures as either a series of parameters (i.e., intensity measures, *IM*s) or as a suite of time histories. Time history analyses provide the most direct and physically meaningful insights into the dynamic response of structures, and are becoming more common as computational speeds increase. It should be recognized, however, that both methods of demand characterization require the use of hazard analyses involving *IM*s. This need is obvious when demand is characterized with *IM*s. The need remains when demand is characterized with time histories because records are selected based on de-aggregation of hazard (which involves the use of *IM*s) into magnitude and distance bins.

A number of *IM*s can be used to represent the amplitude, frequency content, or duration characteristics of earthquake accelerograms. Kramer (1996) provides a fairly thorough listing and description of ground motion parameters, and no attempt is made here to reiterate all of these. Rather, the following describes a select group of parameters generally found to be most useful in demand characterization for geotechnical and structural systems. Records from the Palm Springs Airport site triggered by the 1992 m = 7.3 Landers and 1986 m = 6.0 North Palms Springs earthquakes are used to illustrate these parameters. The site-source distances for these two events were 38 km and 17 km, respectively.

1.2.1 Amplitude Parameters

The recorded accelerograms for the 360-degree component of motion at the Palm Springs Airport site are shown in Figure 1.1, along with velocities and displacements obtained through time-integration. The most direct amplitude measures are the peak values of acceleration, velocity, and displacement, which are identified in the figure. The integration process tends to dilute high-frequency components of the motion and enhance low-frequency components. For this reason, peak horizontal acceleration (PHA) is a relatively high-frequency ground motion parameter, whereas peak horizontal velocity (PHV) and peak horizontal displacement (PHD) are more sensitive to mid- and low-range frequencies, respectively. This is indicated in Figure 1.1 where the relatively low-frequency motion from the Landers earthquake produces a larger PHD than the North Palm Spring motion, despite the higher PHA for North Palm Springs. PHA can be related to the peak force induced in very stiff structures and can be scaled to estimate shear stresses at shallow depths in the ground, and hence has found widespread use both in structural and geotechnical engineering. PHV has been found to correlate well to earthquake damage in structures (e.g., Trifunac and Todorovska, 1997; Boatwright et al., 2001), and has been normalized by soil shear wave velocity (V_s) for use as a measure of shear strain in soil (Trifunac and Todorovska, 1996). PHD has not experienced much use as a demand parameter.

1.2.2 Frequency Content Parameters

The frequency content of accelerograms is best measured with the use of spectra. The two most common types of spectra are Fourier amplitude spectra and response spectra. Both Fourier amplitude and phase spectra are obtained by taking the Fourier transform of a time series. Mathematical procedures for performing Fourier transforms are presented in Kramer (1996). The Fourier amplitude spectra of the two recordings at the Palm Springs Airport site are shown in Figure 1.2(a). The spectra show that the Landers recording has more long-period energy (due to the higher magnitude) than the North Palm Springs recording. Figure 1.2(b) shows the Fourier amplitude spectra for the Landers motion plotted against frequency on a logarithmic scale. Shown on this plot are the corner frequency (f_c) and the cutoff frequency (f_{max}), which define the lowest and highest frequencies with significant energy content, respectively.

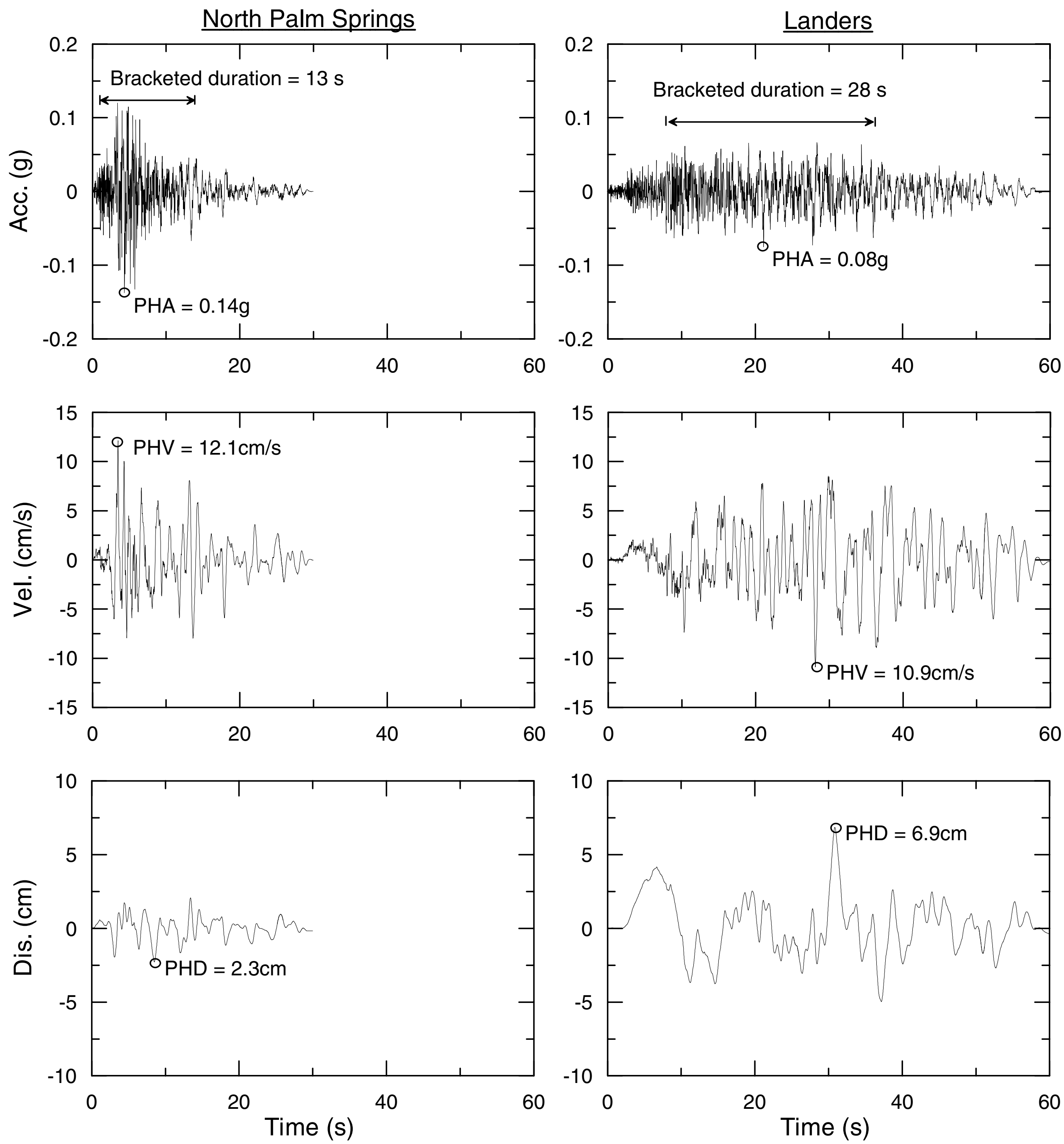

Fig. 1.1. Acceleration, velocity, and displacement time histories for ground motions recorded at Palm Springs Airport during 1986 North Palm Springs and 1992 Landers earthquakes.

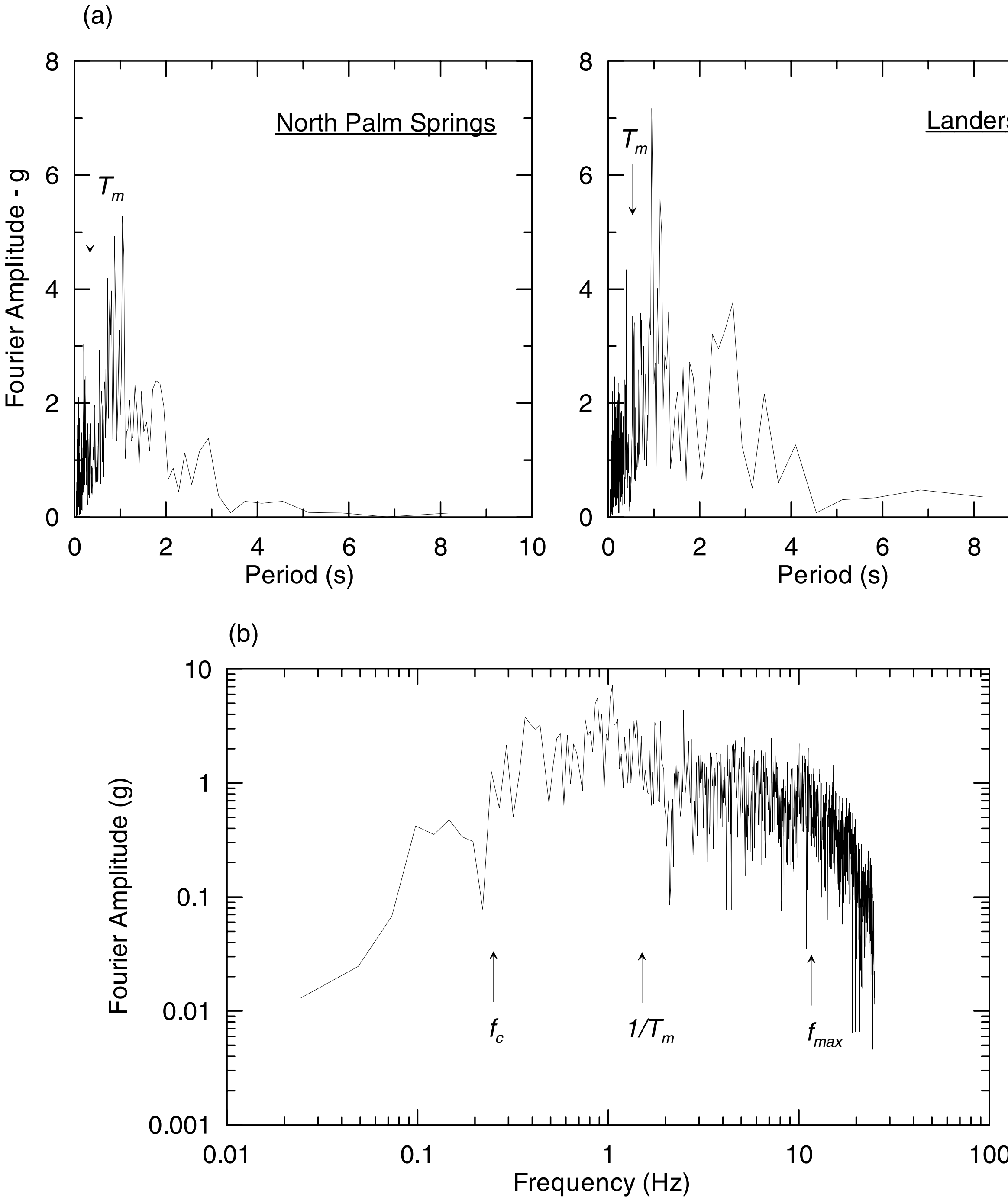

Fig. 1.2. (Upper frames) Fourier amplitude spectra of Palm Springs Airport motions; (Lower frame) Fourier amplitude spectra of Landers motion at Palm Springs Airport illustrating locations of frequency parameters.

Acceleration response spectral ordinates represent the period-dependent peak acceleration response of a single-degree-of-freedom elastic structure with a specified level of viscous damping. Mathematical procedures for calculating response spectra are presented by Chopra (2000). Unlike Fourier amplitude/phase spectra, response spectra are not unique (i.e., they cannot be converted back to the time history that generated the spectrum). The 5% damped acceleration response spectra for the two motions are illustrated in Figure 1.3. Acceleration response spectra are widely used in structural engineering, as the product of the spectral ordinate at the building period, and the structural mass can be used to approximate the base shear in elastic structures. Response spectral displacement and pseudo-velocity have also found use in structural engineering, particularly for long-period structures. However, these parameters are proportional to spectral acceleration, and hence do not require independent analyses. Limitations of response spectral ordinates are that they do not provide information on the duration of strong shaking nor the inelastic response of structures.

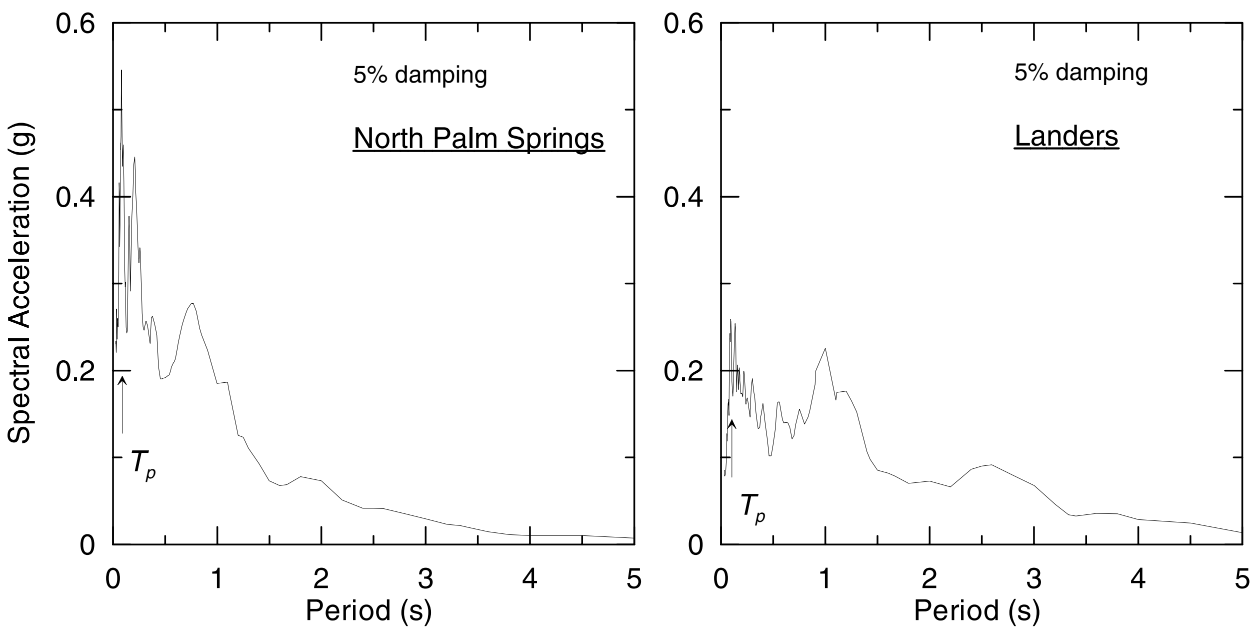

Fig. 1.3. Acceleration response spectra of Palm Springs Airport motions.

As an alternative to complete spectra, frequency content can be approximately measured by individual period parameters. The most widely used of these are predominant period and mean period. For near-fault motions, a third parameter known as pulse period (T_v) is used. The predominant period (T_p) is the period at which the maximum spectral acceleration occurs in an acceleration response spectrum calculated at 5% damping. The mean period (T_m) is defined as (Rathje et al., 1998):

$$T_m = \frac{\sum C_i^2 \left(\frac{1}{f_i} \right)}{\sum C_i^2} \quad \text{for} \quad 0.25 \le f_i \le 20 \text{ Hz} \tag{1.5}$$

where C_i = Fourier amplitudes of the entire accelerogram, and f_i = discrete Fourier transform frequencies between 0.25 and 20 Hz. The locations of T_p and T_m for the two Palm Springs Airport records are indicated in Figures 1.3 and 1.2(a), respectively. It is noted that these figures are drawn using a linear horizontal axis for period, and with this scale T_p and T_m may not appear to represent well the frequency content of these spectra. The plot of Fourier amplitude spectra against frequency on a logarithmic scale in Figure 1.2(b) better illustrates how T_m captures the mean period of the spectrum. Parameter T_v represents the period of near-fault velocity pulses, and is discussed further in Chapter 4. Geotechnical Engineers have sometimes used parameter T_p as a single-parameter representation of frequency content, but T_m and T_v are more physically meaningful and have been preferred in recent applications.

1.2.3 Duration Parameters

The duration of strong ground motion is related to the time required for rupture to spread across the fault surface, and thus is closely correlated to fault rupture area. As discussed in Section 2.1, fault rupture area is in turn correlated to magnitude, so duration tends to scale with magnitude. A number of duration measures are commonly used, a review of which is provided in Bommer and Martinez-Pereira (1999). The most common of these measures are bracketed duration (Bolt, 1969), defined as the time between the first and last exceedances of a threshold acceleration (usually 0.05g), and significant duration, defined as the time interval across which a specified amount of energy in the accelerogram is dissipated. Energy in the accelerogram can be quantified by the Arias intensity (Arias, 1970), defined as

$$I_A = \frac{\pi}{2g} \int_0^{\infty} a^2(t) dt \tag{1.6}$$

where $a(t)$ is the acceleration time history and g is the acceleration of gravity. Husid plots, used to track the build up of energy (Husid, 1969), are shown in Figure 1.4 for the two Palm Springs Airport accelerograms. Two common measures of significant duration are time intervals between

5-75% and 5-95% of I_A. The 5-75% durations are indicated in Figure 1.4. Bracketed durations for the same two accelerograms are indicated in Figure 1.1.

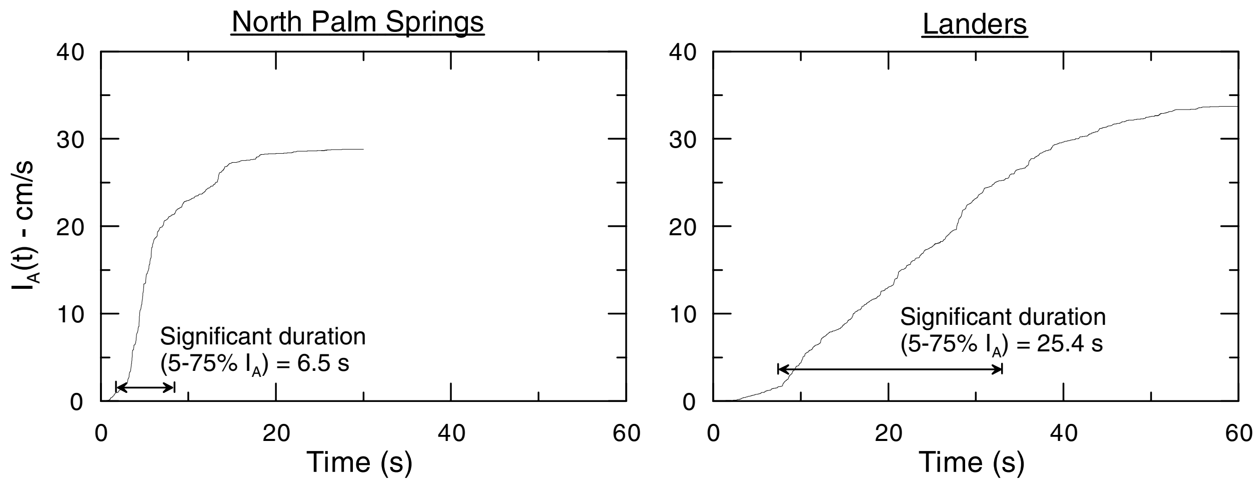

Fig. 1.4. Husid plots for Palm Springs Airport motions.

A quantity sometimes used as a substitute for duration is equivalent number of uniform stress cycles (N). Parameter N is obtained by counting a weighted number of cycles in an accelerogram, with the weighting factors being application-dependent. One common application is soil liquefaction analyses. Procedures for the evaluation of N for liquefaction applications have been developed by Liu et al. (2001), and using these procedures, N = 45 and 13 for the Landers and North Palm Springs earthquakes, respectively.

1.3 PEER RESEARCH STRATEGY AND SCOPE OF REPORT

The traditional elements of a ground motion analysis include characterization of source, travel path, and site effects. Characterization of seismic sources is traditionally performed by seismologists, and PEER has to a large extent deferred to other organizations such as SCEC and the USGS to continue to provide leadership in that area. PEER has focused its efforts on improving the engineering characterization of travel path and source effects. These effects can introduce the greatest degree of uncertainty in ground motion characterization for highly seismically active regions, and hence the results of this research are significantly improving the reliability of ground motion characterization for high-risk areas such as California's major urban centers.

At the time of PEER's inception, the needs faced by the earthquake engineering community related to ground motion characterization were great. Foremost among the problems were

- Lack of consensus on appropriate strategies for evaluating seismic site response with due consideration for local soil, geologic, and basin effects;
- Inadequate data and models for characterizing ground motions near seismic sources; and
- Unclear definitions of the critical ground motion parameters controlling the response of various types of structures.

To address these issues, PEER organized its ground motion research program into a Core Program intended to provide long-term, "next generation," methods for hazard characterization, and a user-driven Lifelines Program intended to provide relatively short-term results that could be immediately implemented into practice. The majority of the PEER-funded ground motion research has been within the Lifelines Program, which has implemented (and continues to execute) a systematic strategy for addressing the critical problems identified above. The research topic areas within both programs are briefly reviewed in the following paragraphs, and references are provided to chapters of the report that provide details of results obtained to date.

The Phase I effort in the Lifelines Program focused on the issue of site response, with the objective being to determine the impact of increasing levels of detail in site characterization on the accuracy of ground motion predictions. Studies were undertaken investigating the use of qualitative surface geology and geotechnical site categories, weak motion response measurements, and basin response codes to estimate ground motions. Work in Phase II continued to explore site response issues, but also addressed near-fault ground motions. A critical issue for near-fault ground motion characterization is a lack of near-fault recordings from large magnitude earthquakes. Accordingly, a major thrust of the Phase II work was to calibrate seismological simulation models, so that these models could be used to generate synthetic near-fault seismograms. These projects have produced meaningful results that have been implemented into seismic design practice, and work on these and other important topics is continuing at present in the first segment of an ongoing three-year coordinated research plan. The results of the completed work are synthesized into this report, principally in Chapters 4 and 5, which cover the topics of near-fault ground motions and site effects. We defer our discussion of the topic areas for future/ongoing research within the Lifelines Program to Chapter 8, where ground motion research directions for the PEER program as a whole are discussed.

Ground motion research in the Core Program is focused principally in the Hazard Assessment Thrust Area (Thrust Area 2), but important research helping to define critical ground motion intensity measures is occurring in the Global Methodology Thrust Area (Thrust Area 3). The original (1997) vision of the Thrust Area 2 research was to "define representative ground motions and ground motion parameters for engineering studies, as well as to define effective ways of representing earthquake hazards for use in performance-based design." Work funded within this program has developed fundamental new insights into the issues of near-fault ground motion characterization (discussed in Chapter 4) and strategies for effective, engineering characterization of site response (Chapter 5). This report does not specifically focus on the issue of defining critical ground motion parameters for particular classes of structures, which is covered in companion PEER synthesis reports.

The chapters of this report are organized to provide a complete synthesis of contemporary procedures for source characterization (Chapter 2), path effects including near-fault ground motions (Chapters 3-4), site effects (Chapter 5), ground motion simulation procedures (Chapter 6), and time history selection (Chapter 7). The chapters present relevant work on each topic, whether the research was performed within or outside of the PEER Center. Contributions from PEER researchers are identified at the end of each of Chapters 2-7. Finally, Chapter 8 summarizes from Chapters 2-7 many of the major accomplishments and tangible benefits of work performed over the past three years by PEER researchers on ground motion characterization. Future research directions for the Core and Lifelines programs are also presented.

2 SOURCE CHARACTERIZATION

2.1 OVERVIEW

The focus of this chapter is on source characterization for probabilistic seismic hazard analysis using models of fault systems derived from geologic/seismologic data. Source characterization for numerical simulation of ground motions is presented in Chapter 6.

A fault is characterized as a series of segments (or a single segment) that can either rupture individually or in groups. A fault segment is characterized by a length (or area), a probability density function describing the relative likelihood of the fault producing earthquakes of different magnitudes [$f(m)$], and a long-term slip rate. By balancing the rate of seismic moment build up on a fault (calculated from slip rate) with the rate of moment release (due to earthquakes), it is possible to derive the rate of occurrence of earthquake events on the fault. For future reference, it should be noted here that the measure of magnitude assumed herein is moment magnitude.

This chapter focuses on two issues: (1) the range of magnitudes that for a given fault should be considered in hazard analyses and (2) models describing the magnitude distribution of earthquakes on a fault and the rate of occurrence of these earthquakes. Other source characterization issues important to ground motion simulation are discussed in Chapter 6.

2.2 MAGNITUDE RANGE FOR SEISMIC SOURCES

The size of earthquakes generated along a fault can range from imperceptible events at very small magnitudes to highly destructive events during which entire fault segments rupture. The minimum magnitude (m^0) delineates the minimum level of energy release expected to produce ground motions damaging to structures. The largest magnitude earthquake that a fault is capable of producing depends on the largest possible fault area that could rupture in a single event and the stress drop. A constant stress drop is commonly assumed within a particular tectonic region (e.g., an active region such as California), which allows magnitude to be described in terms of fault area (A) only. These m-A relations are uncertain and are represented by a conditional probability density function, i.e., $f(m|A)$, estimated from empirical data.

Since magnitude is correlated with area, there is a need to characterize probable rupture surfaces along faults. For major faults this is best performed using the concept of fault segmentation, which assumes that faults are composed of segments that define the location and extent of future large earthquakes. The following sections describe considerations associated with the selection of m^0, the segmentation concept and how it has been implemented in northern and southern California, and magnitude-area scaling relations.

2.2.1 Minimum Magnitude

The minimum magnitude earthquake (m^0) is the smallest event that is expected to produce ground motions damaging to structures. The most appropriate value of m^0 for different classes of structures is unknown, but has often been taken as about 5.0. The use of smaller magnitudes might be appropriate for analysis of brittle structures that are sensitive to high-frequency ground motions.

2.2.2 Fault Segmentation

The fault segmentation concept has been implemented by the Working Group on California Earthquake Probabilities (Working Group, 1995, 1999) for northern and southern California. These regional assessments of large magnitude earthquake probabilities are based on characterizations of faults as series of segments that are assumed to rupture either individually or in contiguous groups. The fault segments are assumed to define the location and extent of future earthquakes, and are delineated based on geologic and geophysical data and by ruptures in past earthquakes. Segmentation models for the San Francisco Bay Region and for southern California produced by Working Group (1995, 1999) are shown in Figure 2.1, with data for major, strike-slip segments tabulated in Table 2.1. Complete information on the segmentation models is available in the Working Group references. In addition to these local models, faults across California have been classified as part of the state-wide CDMG-USGS hazard model (Petersen et al., 1996; Frankel et al., 1996) as A, B, and C faults, which are discussed further below.

Table 2.1(a) Source parameters for northern California faults (after Working Group, 1999)

Code	Name	s (mm/yr)	+/- 2σ	Last rupture	Length (km)	Width (km)
SGN	San Gregorio North	7	3	< 1776	109	13
SGS	San Gregorio South	3	2	< 1776	66	12
NCN	SA - North Coast North	24	3	1906	137	11
NCS	SA - North Coast South	24	3	1906	190	11
PN	SA - Peninsula	17	4	1906	85	13
SCZ	SA - Santa Cruz Mtns.	17	4	1906	62	15
RC	Rodgers Creek	9	2	1670-1776	63	12
NH	Northern Hayward	9	2	1640-1776	35	12
SH	Southern Hayward	9	2	1868	52	12
NC	Northern Calaveras	6	2	-	45	13
CC	Central Calaveras	15	3	< 1776	59	11
SC	Southern Calaveras	15	3	< 1776	19	11
NGV	Northern Green Valley	5	3	< 1776	14	14
SGV	Southern Green Valley	5	3	< 1776	22	14
CON	Concord	4	2	< 1776	20	16
NG	Northern Greenville	2	1	< 1776	20	15
CG	Central Greenville	2	1	< 1776	20	15
SG	Southern Greenville	2	1	< 1776	33	15
MTD	Mount Diablo thrust	3	2	< 1776	25	14.2

Table 2.1(b) Source parameters for southern California 'A' faults (after Working Group, 1995)

Zone	Name	s (mm/yr)	+	-	Disp (m)	+	-	$1/\nu_c$ (yr)	+	-	Last rupture	Length (km)
04	SA Carriz	34	3	3	7.0	4.0	4.0	206	149	125	1857	121
05	SA Mojave	30	8	8	4.5	1.5	1.5	150	123	71	1857	133
06	SA SanBer	24	5	5	3.5	1.0	1.0	146	91	60	1812	78
07	SA Coache	25	5	5	4.0	4.0	4.0	160	240	93	1690	114
	Total San Andreas											446
08	SJ SanBer	12	6	6	1.2	0.3	0.3	100	150	50	1890	35
09	SJ SanJac	2	6	6	1.0	0.2	0.2	83	117	39	1918	42
10	SJ Anza	12	7	5	3.0	1.0	1.0	250	321	145	1750	90
11	SJ CoyCre	4	2	2	0.7	0.3	0.3	175	325	108	1892	40
12	SJ Boreg	4	2	2	0.7	0.2	0.2	175	275	92	1968	29
13	SJ SupMtn	4	2	2	2.0	0.3	0.3	500	650	217	1430	23
14	SJ SupHil	4	2	2	1.0	0.3	0.3	250	400	133	1987	22
	Total San Jacinto											281
14	Whittier	2.5	1	1	1.9	0.2	0.2	760	640	274	650	38
16	GlenIvy	5	2	2	1.6	0.4	0.4	310	340	146	1910	35
17	Temecula	5	2	2	1.2	0.3	0.3	240	260	111	1818	42
18	Julian	5	2	2	1.7	0.2	0.2	340	293	126	1892	75
19	CoyoteM	4	2	2	2.5	0.5	0.5	625	875	292	1892	38
	Total Whittier											228

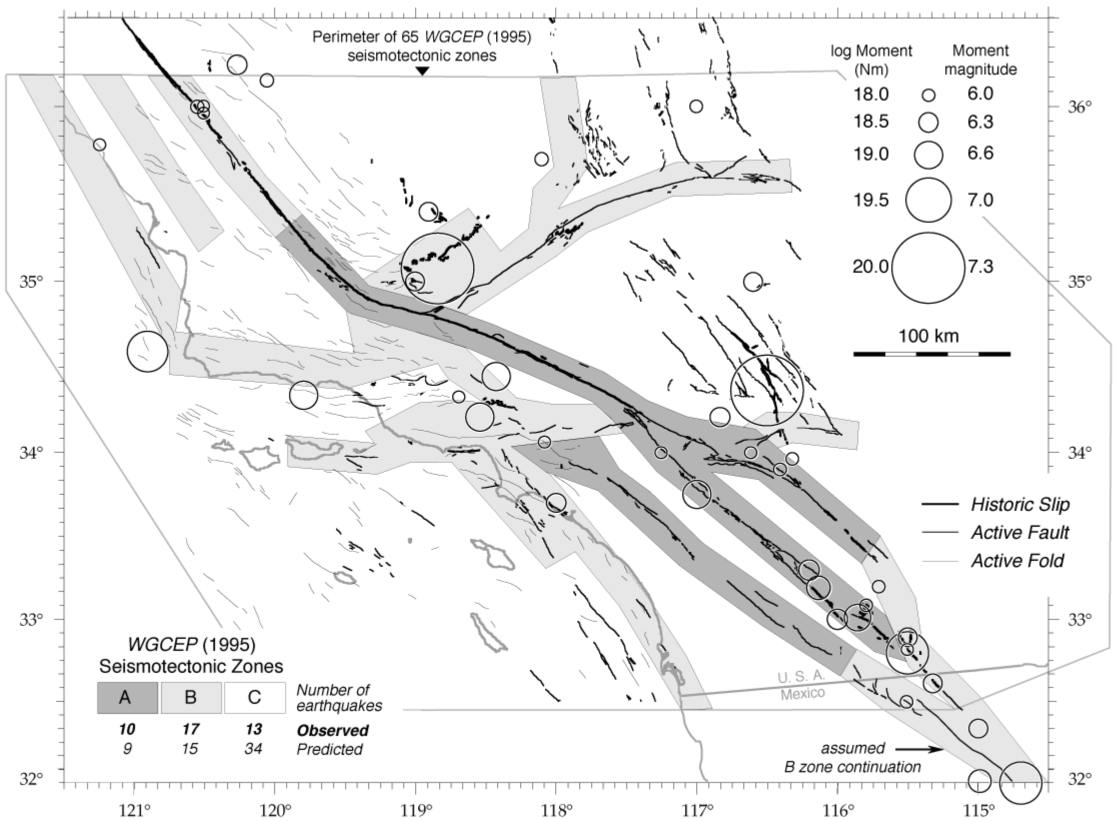

Fig. 2.1(a). Seismotectonic zones of WGCEP (1995) along with *m*≥6 earthquakes in southern California since 1903 (Stein and Hanks, 1998).

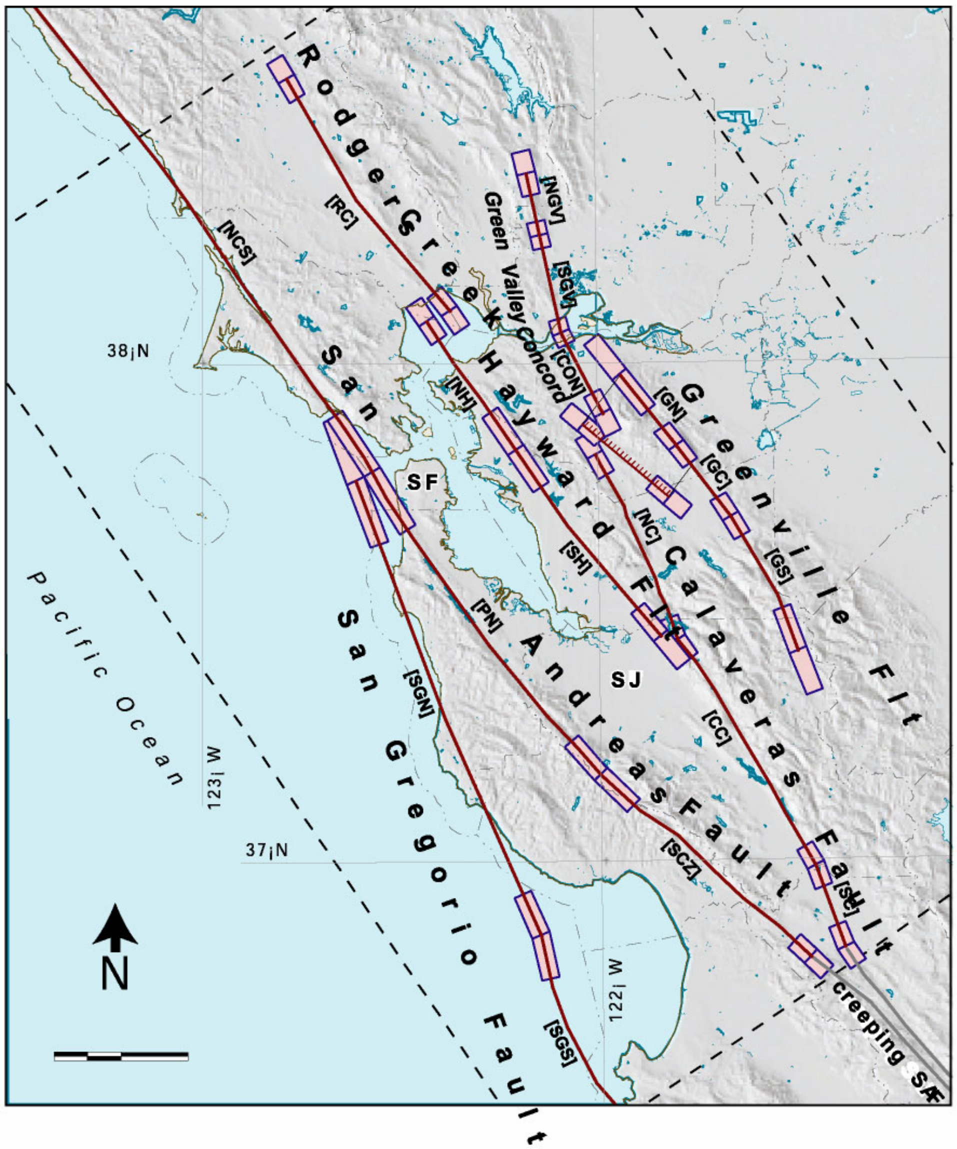

Fig. 2.1(b). Seismotectonic zones of WGCEP (1999) for San Francisco Bay region.

Regional models for earthquake generation allow for earthquakes both along known faults and background earthquakes along unrecognized or uncharacterized faults. Along known faults, earthquakes can occur within a segment, across multiple contiguous segments, or as floating events on segments whose boundaries are unknown (Working Group, 1999). Segment endpoints can have uncertain locations, as illustrated in Figure 2.1(b). Regional earthquake models allow for this variety of rupture sources, with the constraint that the long-term slip rate of each fault is accommodated. Working Group (1999) provides the following example to illustrate this concept for strike-slip faults (Figure 2.2). The Hayward-Rodgers Creek fault system is assumed to consist of three fault segments: the southern Hayward (SH), northern Hayward (NH), and Rodgers Creek (RC) segments. Each segment may fail alone or in combination with others. These combinations produce six possible earthquake rupture sources, each with an associated mean maximum magnitude. The relative degree to which the long-term slip is accommodated by each rupture source was determined by expert opinion.

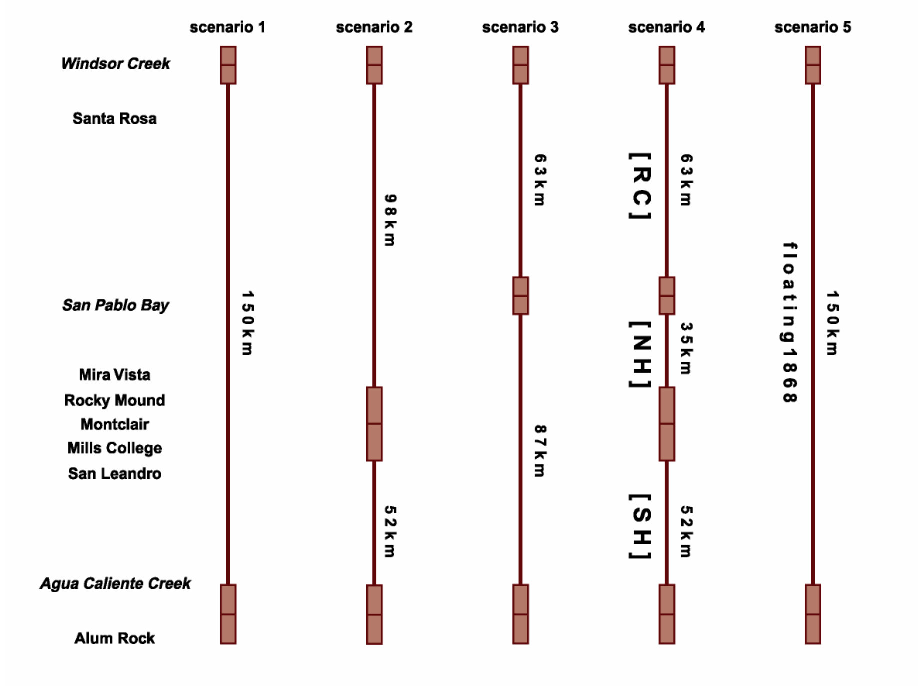

Fig. 2.2. Schematic representation of five scenario events on the Hayward-Rodgers Creek fault system. From WGCEP (1999).

Background earthquakes must be considered in broad zones not dominated by any single major fault, but which may contain diverse or hidden faults. Such events significantly contribute to the seismicity of southern California as a result of thrust faults created by significant north-south crustal compression associated with a "big bend" in the San Andreas fault. This compression results in reverse or thrust faults that can break the surface during earthquakes (e.g., 1971 San Fernando and 1952 Kern County events) and blind thrust faults that do not break the surface (e.g., 1987 Whittier and 1994 Northridge events). Background seismic models are used to represent the rupture areas and slip rates for blind thrusts. These parameters were estimated for broad background seismicity zones by Working Group (1995) based on limited available geologic data and expert consensus. Surface-breaking reverse fault locations can generally be mapped, and hence are considered as "known" and not "background" sources. However, it should be noted that the available data for surface-breaking reverse sources is seldom adequate to reliably define segmentation, displacement, or date of last earthquake (Working Group, 1995). Background seismicity is incorporated into San Francisco Bay Region source models as a result of several historical earthquakes that occurred on previously unrecognized faults. The rate of such earthquakes was assessed by Working Group (1999) using a Bayesian inference method to associate historical earthquakes with known faults. From the results it was possible to develop a Gutenberg-Richter relation for the rate of background earthquakes.

As noted previously, the CDMG-USGS model and the Working Group (1995) models delineate "known" and "background" seismic sources as A, B, or C faults. "A" faults are major strike-slip faults associated with the San Andreas fault system (e.g., faults listed in Table 2.1); "B" faults are most other faults in the state with slip rates, $s > 0.1$ mm/yr, and include both strike-slip and reverse faults; "C" faults account for poorly defined structures (e.g., blind thrust faults) and background seismicity. A complete listing of available data for A and B faults is provided in Petersen et al. (1996).

2.2.3 Magnitude-Area Scaling Relationships

Magnitude-area scaling relationships are used to relate the size of a ruptured fault segment (i.e., the "area") to the energy release from the event ("magnitude"). As energy release is also dependent on the average stress reduction, or stress drop, across the rupture, magnitude-area relations inherently assume a constant stress drop.

Wells and Coppersmith (1994) compiled a database of 421 earthquakes, 244 of which were used for the development of magnitude-area relations. The earthquakes in their database were shallow-focus (hypocentral depth < 40 km) events in active tectonic regions (i.e., along plate boundaries) and in mid-plate regions. Fault dimensions for these events were established primarily from the spatial pattern of early aftershocks. Relationships were developed between moment magnitude and fault length (along strike), fault width (dimension down dip), and fault area. The correlations between magnitude and fault length and fault area had less dispersion than those for other source dimensions, and are shown in Figures 2.3(a) and (b). The regression equations in the figures apply for all rupture mechanisms (strike-slip, reverse, normal), although no significant variation among mechanism-specific regressions was found. The regression equations give only the mean estimate of magnitude, the data are log-normally distributed with standard deviations of 0.24 in the magnitude-area relation and 0.26 in the magnitude-length relation (magnitude units). Somerville et al. (1999) found a very similar magnitude-area relation using rupture areas derived from waveform inversions for 15 shallow crustal events.

Recent work has suggested that stress drops for medium magnitude events ($6 \leq m \leq 7$) may be less than those for relatively rare, large magnitude ($m > \sim 7$) events (Working Group, 1999). Both the Wells and Coppersmith (1994) and Somerville et al. (1999) studies were based principally on data from m = 6-7 events, and presumably reflect stress drops across that magnitude range. Working Group (1999) have re-examined the following seven well documented strike-slip earthquakes in California with large magnitude:

*m*7.8 1857 Fort Tejon

*m*6.9 1868 Hayward

*m*7.6 1872 Lone Pine

*m*7.9 1906 San Francisco

*m*7.0 1940 Imperial Valley

*m*6.9 1989 Loma Prieta

*m*7.3 1992 Landers

The moment magnitudes and rupture areas for these events (based on Wells and Coppersmith data) are shown in Figure 2.4 along with the regression line by Wells and Coppersmith. It is clear from the results that the stress drop for large magnitude events significantly exceeds the prediction of the regression equation. Working Group (1999) derived a new regression equation

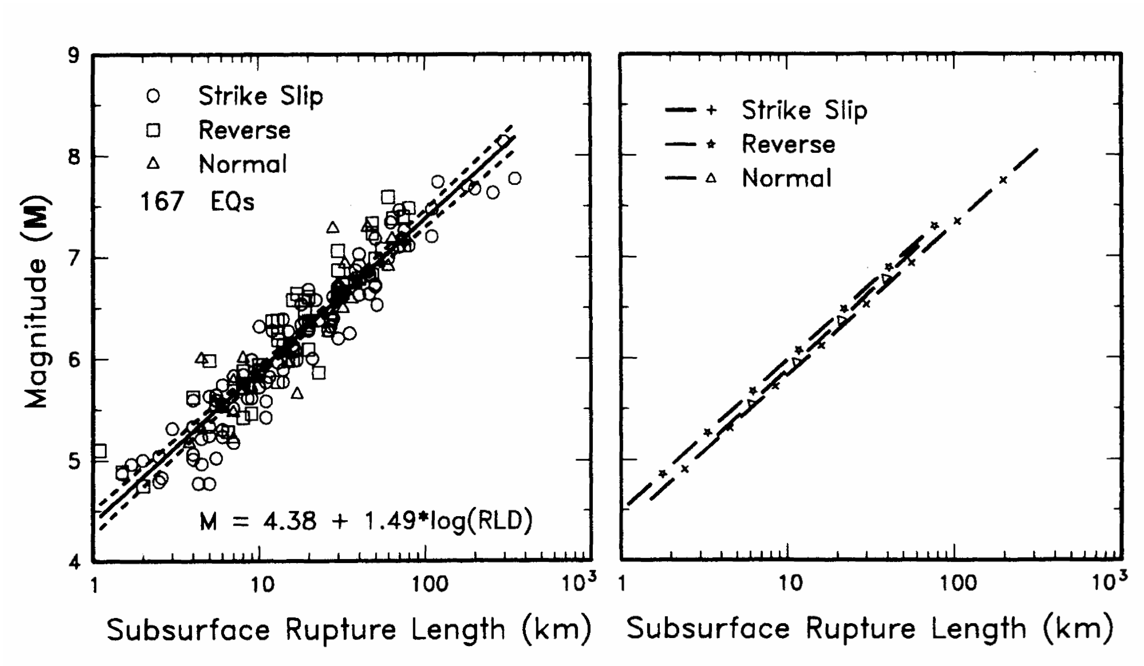

Figure 2.3(a): see caption below.

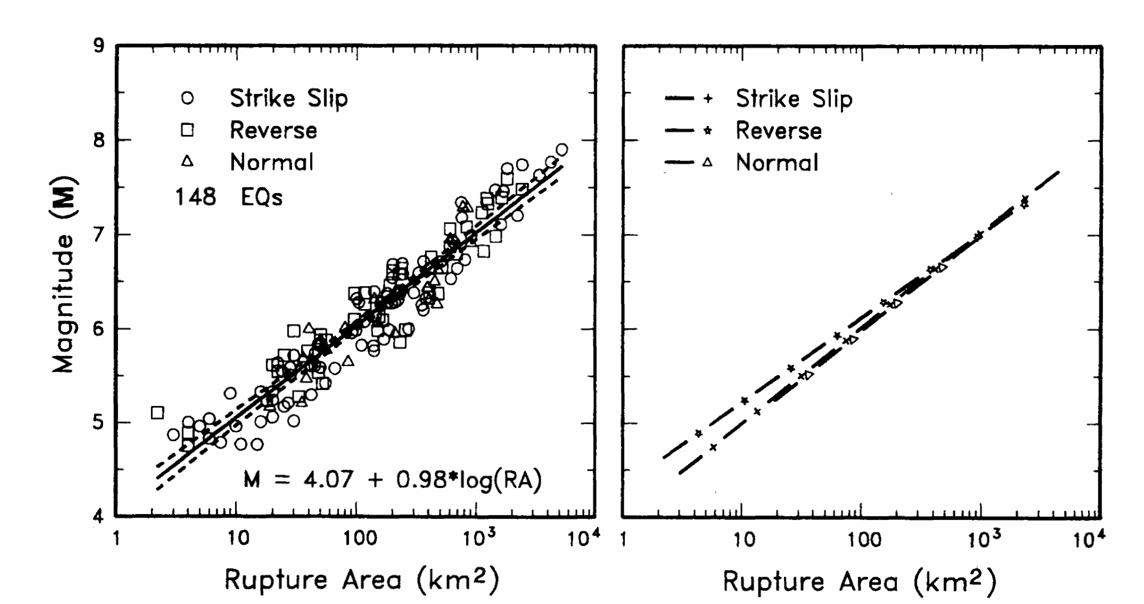

Fig. 2.3. Regression of (a) rupture length and (b) rupture area on magnitude by Wells and Coppersmith (1994). Left frame shows data, overall regression curve, and ± 95% confidence intervals. Right frame shows regression lines as function of focal mechanism.

for large magnitude earthquakes,

$$m = k + \log(A) \tag{2.1}$$

where k = 4.2-4.3. This relation plots near the mean plus one standard deviation line shown in Figure 2.4.

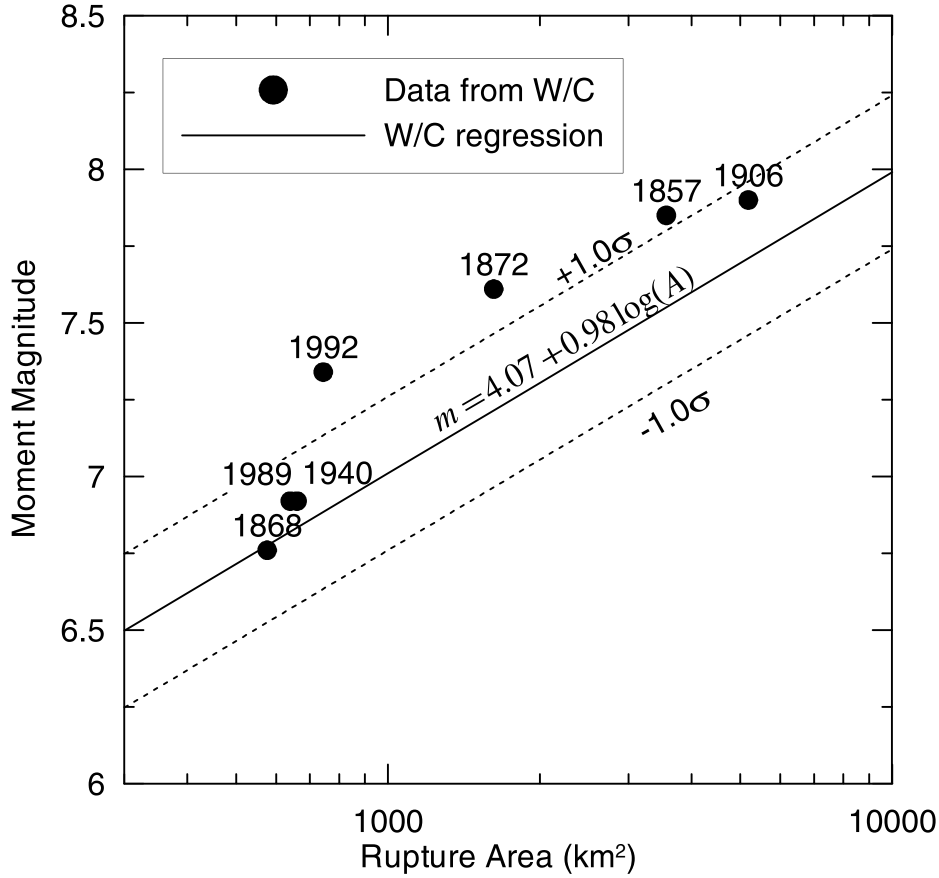

Fig. 2.4. Moment magnitudes and rupture areas for large California earthquakes analyzed by Wells and Coppersmith, W/C (1994), along with magnitude-area scaling relation by W/C (1994). Figure adapted from Working Group (1999).

2.3 MAGNITUDE RECURRENCE RELATIONS

Once the location and magnitude range for a seismic source have been identified, it is necessary to characterize the relative likelihood of different magnitude earthquakes on the fault, and the rate of occurrence of earthquakes. The development of such models must be constrained in such a way that the moment release (from earthquakes) balances moment build up. For a given fault, moment build up is proportional to slip rate (s), which is the long-term, time-averaged relative velocity of block movements on opposite sides of the fault. Slip rates for significant California faults are catalogued by Petersen et al. (1996), and for Bay Area and Los Angeles faults by Working Group (1999, 1995).

Characterization of magnitude recurrence relations involves two steps: (1) estimation of a probability density function on magnitude, *f(m)* and (2) estimation of the rate of earthquake occurrence. Models for these two steps in the characterization process are discussed below.

2.3.1 Probability Density Function on Magnitude, *f(m)*

Perhaps the most widely known magnitude recurrence relation is that developed by Gutenberg and Richter (1944), which is based on observations of the occurrence of earthquakes in southern California over many years. The Gutenberg-Richter relation relates the mean annual rate of occurrence of earthquakes with magnitudes > m (υ_m) to m as follows:

$$\log_{10} \upsilon_m = a - bm \tag{2.2}$$

Parameter b contains information on the relative likelihood of earthquakes with different magnitudes, and is typically about b = 0.8-1.0. Parameter a represents the annual rate of occurrence of earthquakes with $m > 0$.

The *truncated exponential* model for *f(m)* is based on the Gutenberg-Richter relation, but with two modifications: (1) natural logarithmic coefficients α and β are used, where $\alpha = 2.303a$ and $\beta = 2.303b$ and (2) the magnitude scale is truncated at lower- and upper-bound values, m^0 and m^u, respectively. Selection of m^0 and m^u is discussed in Section 2.2. With these modifications, and the constraint that *f(m)* must integrate to 1.0, *f(m)* is expressed as follows:

$$f(m) = \frac{\beta e^{-\beta\left(m-m^0\right)}}{1-e^{-\beta\left(m^u-m^0\right)}} \tag{2.3}$$

A plot of $f(m)$ for a fault with $m^0 = 5$ and $m^u = 7.5$ is shown in Figure 2.5(a) with a dashed line.

Seismological data compiled by Schwartz and Coppersmith (1984) and Wesnousky (1994) suggests that some individual faults and fault segments tend to repeatedly generate *characteristic* earthquakes of comparable magnitudes (within about 0.5 magnitude unit of each other). The characteristic earthquake model for $f(m)$ was proposed by Youngs and Coppersmith (1985) to adjust the truncated exponential model to allow for the increased likelihood of characteristic events. The form of the model is shown in Figure 2.5(a) with a solid line. The characteristic earthquake is uniformly distributed in the magnitude range of m^u-Δm_c to m^u, whereas lower magnitude earthquakes follow an exponential distribution. As discussed in the following section, two rate terms are necessary with the characteristic earthquake model — one rate for the characteristic event and another rate for earthquakes with $(m^u - \Delta m_c) > m > m^0$.

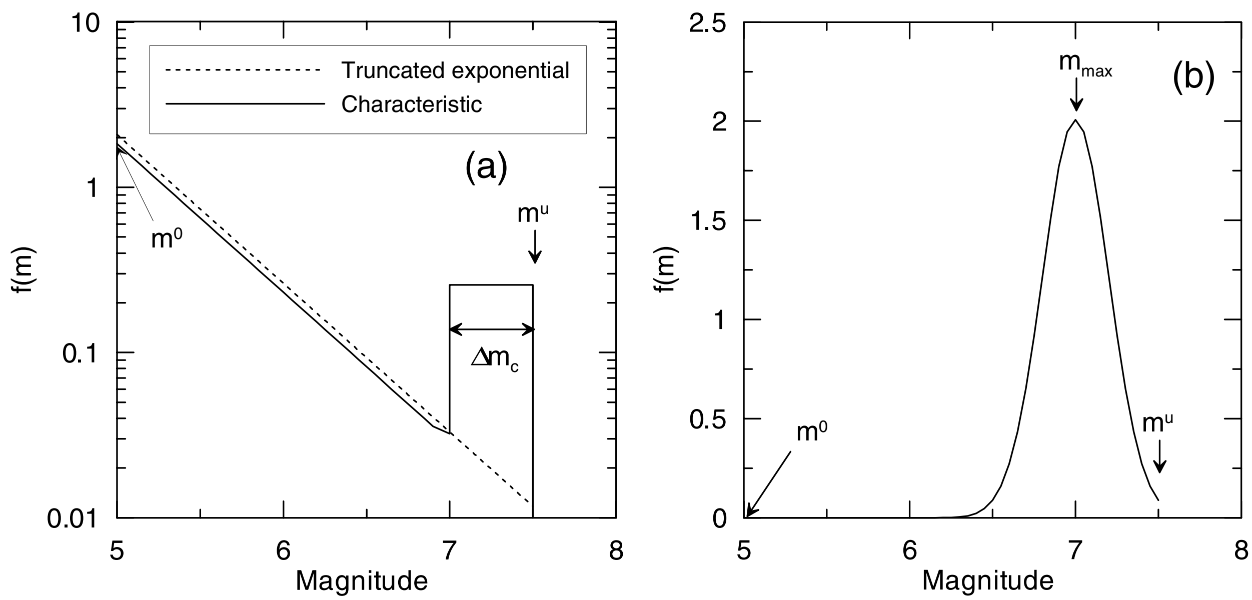

Fig. 2.5. Probability density functions for magnitude, *f(m)*; (a) truncated exponential and characteristic, (b) maximum magnitude.

A third model for $f(m)$ is sometimes used for faults that appear to generate earthquakes only within a relatively narrow magnitude range (Abrahamson, *pers. communication*). Such faults include certain segments of the San Andreas fault (e.g., the North Coast segment) and the Wasatch fault in Utah. This model is termed the *maximum magnitude* model, and consists of a truncated normal distribution for $f(m)$, with cutoff magnitudes of m^0 and m^u, mean magnitude of m_{max}, and a standard deviation of σ_m. The model is depicted in Figure 2.5(b) for $m^0 = 5$, $m^u = 7.5$,

m_{max} = 7.0, and σ_m = 0.2. A variation on the maximum magnitude model has been used by Petersen et al. (1996) and Wesnousky (1986) in which σ_m was taken as zero.

2.3.2 Rate of Earthquake Occurrence

Two philosophies are generally used to model the rate of earthquake occurrence. One philosophy holds that earthquakes occur as a Poisson process, i.e., the occurrence of an event has no influence on the timing of future events. A second philosophy, known as the time-predictable model, holds that the occurrence of an event releases stress on the fault and thus temporarily reduces the probability of future earthquakes (excluding aftershocks).

(a) *Rate derived as Poisson process*

The Poisson rate of earthquake occurrence on a given fault can be computed once a model for *f(m)* is selected. Assuming the fault area (A), friction coefficient between fault blocks (μ) and slip rate (s) are known, the rate of moment build up ($\dot{M}_0$) on a fault during quiescent periods (without earthquakes) is

$$\dot{M}_0 = \mu A s \tag{2.4}$$

For non-hybrid fault models (i.e., truncated exponential and maximum magnitude), moment release is calculated as

$$\dot{M}_0 = \upsilon \cdot \int_{m^0}^{m^u} f(m) M_0(m) dm \tag{2.5}$$

where υ = the Poisson rate of occurrence of earthquakes with $m>m^0$, and M_0 is related to m by the well known relation of Hanks and Kanamori (1979):

$$M_0 = 10^{1.5m+16.1} \tag{2.6}$$

By balancing moment build-up with moment release, the Poisson rate term υ can be readily calculated. For example, using a fault size of 100 x 15 km, $\mu = 3 \cdot 10^{11}$ dyne/cm^2, and slip rate of 5 mm/yr, the truncated exponential model of the fault considered in the previous section gives a Poisson rate of $m>5$ earthquakes of υ = 0.12 events/year. The same fault modeled with a maximum magnitude model (with parameters given above) gives a rate of υ = 0.005 events/year. This large rate difference occurs because the maximum magnitude model considered here has a higher likelihood of large magnitude, high moment-release events.

The characteristic fault model is hybrid in the sense that the characteristic earthquake occurs at a specified rate υ_c determined through Paleoseismic study, and a separate rate υ is determined for $m^0 \leq m < (m^u\text{-}\Delta m_c)$ through moment balance. In this case, moment build up is still evaluated using Equation 2.4, with moment release now evaluated as

$$\dot{M}_0 = \upsilon \cdot \int_{m^0}^{m^u - \Delta m_c} f(m) M_0(m) dm + \upsilon_c \cdot \int_{m^u - \Delta m_c}^{m^u} f(m) M_0(m) dm \qquad (2.7)$$

The Poisson rate term υ is evaluated by equating Eq. 2.4 and 2.7. For the fault discussed previously and υ_c = 0.002 events/year, υ = 0.20 events/year for the characteristic earthquake fault model.

A final comment with respect to the above models is that moment build up and release rates must not only balance for individual faults, but cumulative slip rates for all faults in a region must be consistent with geodetic measurements. This may require adjustments of slip rates for individual faults. This topic is discussed further by Working Group (1999).

(b) *Rate derived from time-predictable model*

A number of time-predictable models are available to adjust earthquake probabilities during a future time window based on the time elapsed since the previous major earthquake on the fault. These models consist of a probability distribution of the time from present until the next occurrence of a particular earthquake, $f(t)$, where t is the time to the next event. These models are used to update the rate of occurrence of a particular size event, which in practice is usually a large event such as the characteristic earthquake. Figure 2.6 illustrates the use of $f(t)$ to evaluate the rate of a characteristic event using a time-predictable model. In the figure, $f(t)$ is taken as normal with a mean of $1/\upsilon_c$ (where υ_c = annual rate of characteristic events = 1/300 years in this case). If time t_e = 200 years have passed since the last event, conditional density function $f(t|t>t_e)$ can be constructed, and the probability of an event within time Δt computed as shown. A new rate of characteristic event ($\upsilon_{c,tp}$) can then be evaluated as this probability normalized by Δt. For the example in the figure, $\upsilon_{c,tp}$ = 0.0039 events/year, which can be compared to υ_c = 1/300 = 0.0033 events/year. With the characteristic earthquake rate adjusted in this way, one could easily proceed with an overall moment balance for the fault, as described in the preceding section.

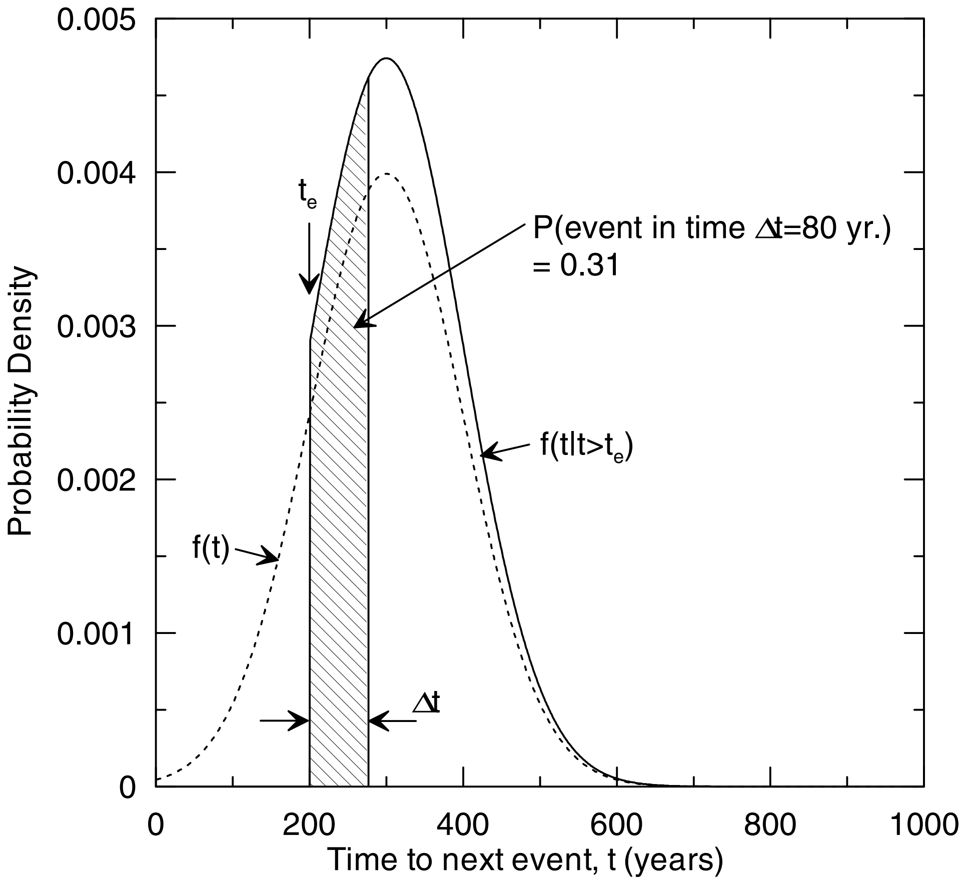

Fig. 2.6. Illustration of use of time-predictable model to update prediction of event probability.

From the above, it is clear that the key step in developing a time-predictable model is the construction of *f(t)*. As discussed by Ellsworth et al. (1999), statistical models used to construct these PDFs have historically included double exponential, Gaussian, Weibull, log-normal, and gamma distributions. Unfortunately, at present it is not possible to discriminate between these various models due to the limited and uncertain nature of earthquake recurrence data.

Given these limitations, recent practice (e.g., Working Group, 1999) has been to use a physically based renewal model for the earthquake cycle proposed by Mathews (1998). This model considers the moment on the fault at a particular time to have resulted from moment build up at a constant rate ($\dot{M}_0 \cdot t$, where $\dot{M}_0$ = rate of moment build up) and a random component [$\varepsilon(t)$] that is defined by Brownian motion. The random component is taken as the product of standard Brownian motion (W) and δ, a non-negative scale parameter [i.e., $\varepsilon(t) = W \cdot \delta$]. An earthquake occurs when a state variable describing the stress on the fault [$Y(t) = \dot{M}_0 \cdot t + \varepsilon(t)$]

reaches a fixed threshold (Y_f), at which time the state variable returns to a fixed ground state (Y_0). This process is illustrated in Figure 2.7. The PDF of passage times across the failure threshold [$f(t)$] is known as the Brownian Passage Time (BPT) distribution, described by

$$f(t) = \sqrt{\frac{\mu_t}{2\pi\alpha_t^2 t^3}} \exp\left[-\frac{(t-\mu_t)^2}{2\alpha_t^2 \mu_t t}\right] \qquad (2.8)$$

In Eq. 2.8, t is the time to the next event, and is reset after an event occurs. Parameter μ_t = mean time between events ($\mu_t = Y_f / \dot{M}_0$) and α_t = coefficient of variation of time between events ($\alpha_t = \delta \big/ \sqrt{Y_f \dot{M}_0}$). Parameter α_t can be interpreted as representing randomness associated with accumulating tectonic stress on a fault, spatial variations in the stress and strength of the fault, or perturbations to the stress state due to external causes such as nearby earthquakes (Ellsworth et al., 1999). This function gives a zero failure probability at t=0 and finite failure probability as $t \to \infty$. The "randomness" of the time to failure increases with α_t up to a limiting value of $\alpha_t = 1/\sqrt{2}$, at which point the model is equivalent to a Poisson process with failure rate μ_t.

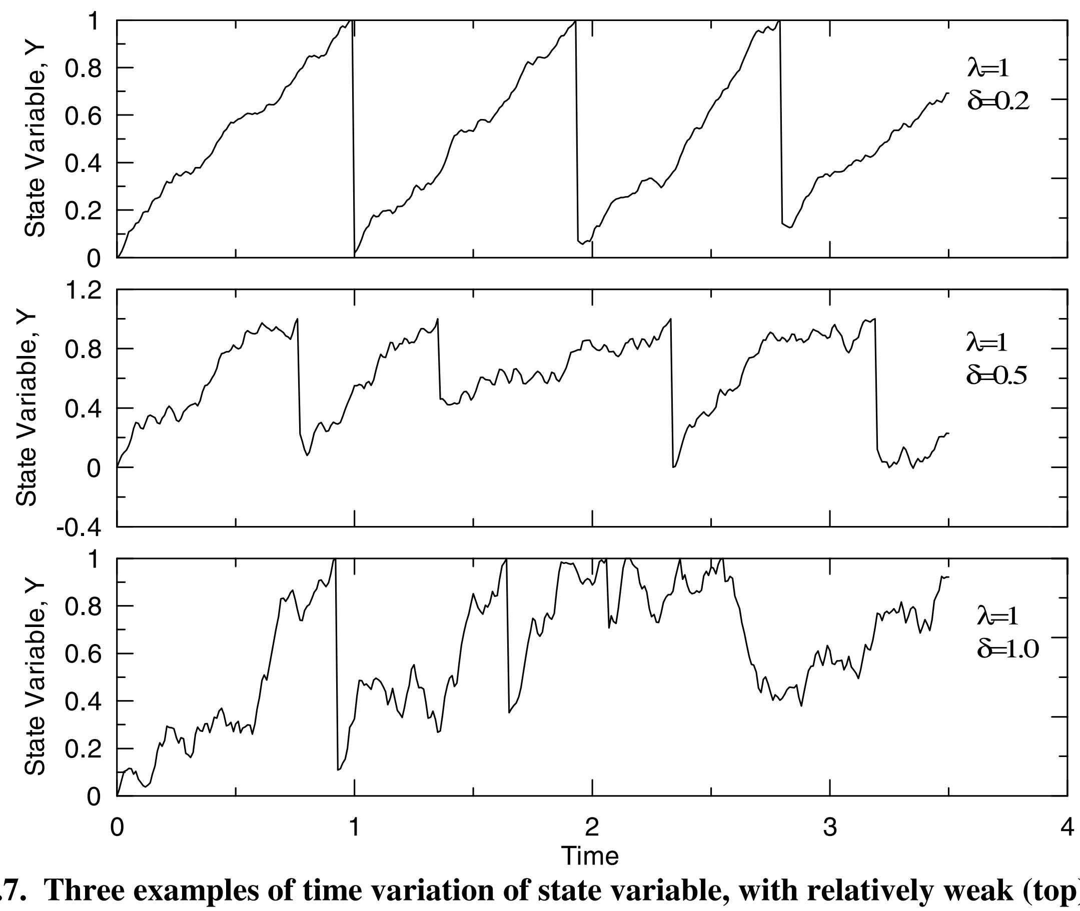

Fig. 2.7. Three examples of time variation of state variable, with relatively weak (top), moderate (middle), and strong (bottom) Brownian variability (after Mathews, 1998).

To apply the BPT model for time-predictable earthquake occurrence, the parameters μ_t and α_t are needed. Parameter μ_t is generally derived from fault-specific studies of Paleoseismic data. It should be noted that for faults modeled with a characteristic density function on magnitude, μ_t can be approximated as $1/\upsilon_c$, the rate of the characteristic earthquake. The rate υ_c has been tabulated by Petersen et al. (1996) for major California faults. Parameter α_t has been estimated by Ellsworth et al. (1999) from analysis of 37 recurrent earthquakes with m = -0.7 to 9.2. It was found that α_t = 0.5 can serve as a working estimate for recurrent earthquake sequences of all sizes and in all tectonic environments. A BPT density function calculated for α_t = 0.5 and μ_t =300 years is shown in Figure 2.8.

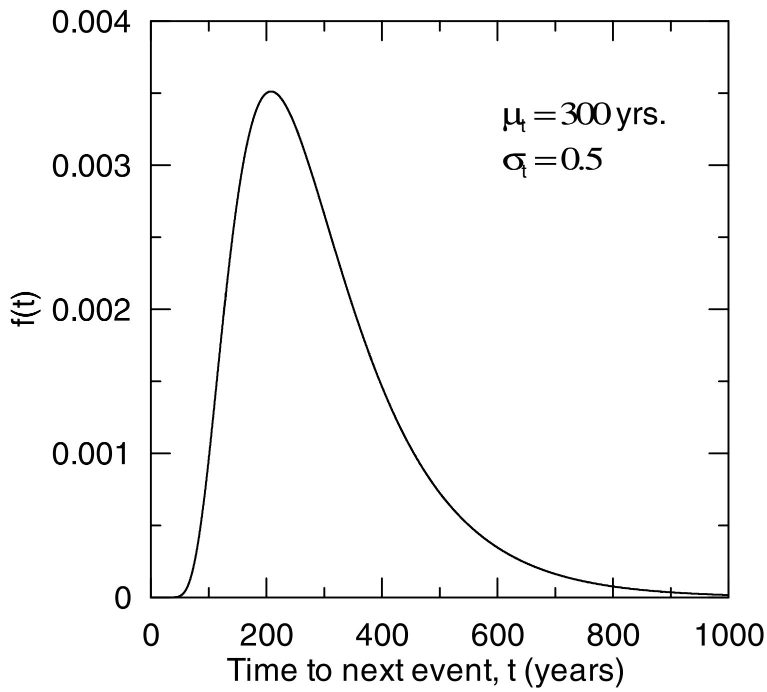

Fig. 2.8. Probability density of the Brownian Passage Time (BPT) distribution for mean period, μ_t = 300 years and coefficient of variation, σ_t = 0.5.

2.3.3 Example: State of California Recurrence Models

Magnitude recurrence relations for the CDMG-USGS state-wide hazard model are based on the A-B-C fault classification discussed in Section 2.2.2. As discussed by Petersen et al. (2000), approximately half the moment release in the CDMG-USGS model is associated with A-faults, and most of the remaining portion with B-faults. C-faults do not contribute significantly to the overall rate of earthquakes in California compared to the A- and B-faults.

A-faults have relatively well-constrained source parameters (e.g., Figure 2.1, Table 2.1) and large slip rates (s > 5 mm/yr). A maximum magnitude model is used by CDMG-USGS for these faults, with m_{max} determined from magnitude-area scaling relations coupled with fault segmentation models and $\sigma_m = 0$. B-faults include most other faults in the state with $s > 0.1$ mm/yr, and have relatively poorly constrained segmentation models and slip rates. These faults are modeled using a hybrid of (1) a maximum magnitude model similar to that for A-faults and (2) a truncated exponential model with m^0=6.5 and $m^u = m_{max}$. Half of the moment release is accommodated by the maximum magnitude model, and half by the truncated exponential model.

C-faults include poorly defined structures and background seismicity. These sources were modeled using a truncated exponential distribution, with m^0=6 and $m^u \leq 7.3$ for faults associated with poorly defined structures (e.g., blind thrusts), and m^0=5 and $m^u \leq 7$ for background seismicity. Background seismicity is characterized by spatially smoothing the historical earthquake catalogue for $m > 4$ earthquakes (after de-clustering aftershocks from mainshocks) over a uniform grid and summing the contribution from all earthquakes at each grid point. Background seismicity contributes all earthquakes with $m < 6$ in the CDMG-USGS model.

Petersen et al. (2000) have compared the cumulative number of earthquakes per year predicted by the above models with the historic earthquake catalogue in California. The model provides a good match to the data up to m=6, but overpredicts the number of earthquakes with m=6-7, and underpredicts for m>7. This rate discrepancy is primarily due to the poorly constrained B-faults in the model, which have not produced the number of events that would be expected based on the model during the past 150 years. This discrepancy can be readily resolved by adjusting the recurrence model, but the appropriate manner in which to make such adjustments is unknown and can be adequately resolved only with further geologic studies along these poorly characterized faults.

2.4 SYNTHESIS OF PEER RESEARCH

As noted in Chapter 1, the PEER Center has to date not sponsored research on empirical source characterization studies of the type described in this chapter. However, it should be noted that source models associated with seismological ground motion simulation algorithms have been calibrated in PEER-sponsored research. A discussion of this work is presented in Chapter 6.

In future work, the PEER Lifelines Program will sponsor a series of studies on earthquake occurrence. These studies will involve fault trenching and other data synthesis/collection exercises. Also planned is the development of a probabilistic rupture displacement map for California, which involves data collection and model development that are complementary to the source characterization needs for ground motion studies.

3 GROUND MOTION ATTENUATION RELATIONS

3.1 OVERVIEW

As outlined in Chapter 1, the evaluation of seismic hazard requires the use of probabilistic distributions of intensity measures (*IMs*) conditioned on the occurrence of an earthquake with a particular magnitude (m) at a given site-source distance (r). The probability density function (PDF) for a single *IM* is written as $f(IM|m,r)$, and is usually log-normal. Attenuation relationships define the statistical moments of these PDFs (e.g., median, standard deviation) in terms of m, r, and other seismological parameters, and are derived through regression of empirical data.

The most widely used *IM* in earthquake engineering is spectral acceleration. Accordingly, this chapter begins in Section 3.2 by reviewing spectral acceleration data characteristics that govern the form of relations to predict the median of $f(IM|m,r)$. We discuss common regression analysis procedures used to derive attenuation relations, and seismological parameters that have been found to affect the outcome of these regression analyses. In Section 3.3, we present attenuation models for single *IM*s other than spectral acceleration.

An important issue that has significant repercussions for performance-based design is that all of the attenuation relations presented in Sections 3.2 and 3.3 are for single *IM*s. As noted in Section 1.1, for certain applications there may be a need for joint PDFs on multiple *IM*s. This is necessary because some damage measures correlate to multiple *IM*s, which may in turn be correlated. Further discussion of this issue is provided in Section 3.4.

3.2 HORIZONTAL SPECTRAL ACCELERATION

3.2.1 Data Characteristics and Regression Procedures

Earthquake ground motions have been recorded by seismographs since the late nineteenth century (Bolt, 1993). Major initiatives to instrument seismically active regions around the world were undertaken in the twentieth century, and these instruments have provided a large inventory of recordings. Data from this inventory are used to develop attenuation relationships, which are either fully empirical, or rely on empirical data to calibrate theoretical models.

Despite the large ground motion inventory, the strong motion data set remains poorly sampled for the development of attenuation relations. To illustrate this point, we present in Figure 3.1 the magnitudes and distances that are sampled in the worldwide ground motion inventory of recordings from shallow crustal earthquakes in active tectonic regions. The horizontal "lines" of dots are in most cases single events that were well recorded. The sampling problems with the inventory are twofold. First, there are only 82 recordings of large magnitude earthquakes ($m > 7$) at close distance ($r < 20$ km), and 59 of these are from a single event (*m*7.6 1999 Chi Chi, Taiwan). This range of m and r is critical for seismic design practice in active tectonic regions, and the lack of data leads to significant *epistemic* uncertainty (i.e., uncertainty about the proper form of attenuation functions).

The second sampling problem is associated with the fact that the data set is dominated by a few well-recorded events. For example, the data set in Figure 3.1 contains approximately 1800 recordings, but 1055 of these are from only eight earthquakes (*m*6.6 1971 San Fernando, California; *m*6.5 1979 Imperial Valley, California; *m*6.4 1983 Coalinga, California; *m*6.0 1987 Whittier, California; *m*6.9 1989 Loma Prieta, California; *m*7.3 1992 Landers, California; *m*6.7 1994 Northridge, California; *m*7.6 1999 Chi Chi, Taiwan). While these well-recorded events allow for robust quantification of intra-event aleatory variability of ground motion (random variability within an event), this clustering of data in a few events is not sufficient to unambiguously evaluate inter-event aleatory variability (random variability across events). Stated another way, if inter-event variability were negligible, attenuation relations could be developed by weighting each data point equally, whereas if intra-event variability were negligible, the collective data from each event would be weighted equally. As neither source of variability is small, an important question is how data from sparsely and well-recorded events should be weighted relative to each other in the regression analysis.

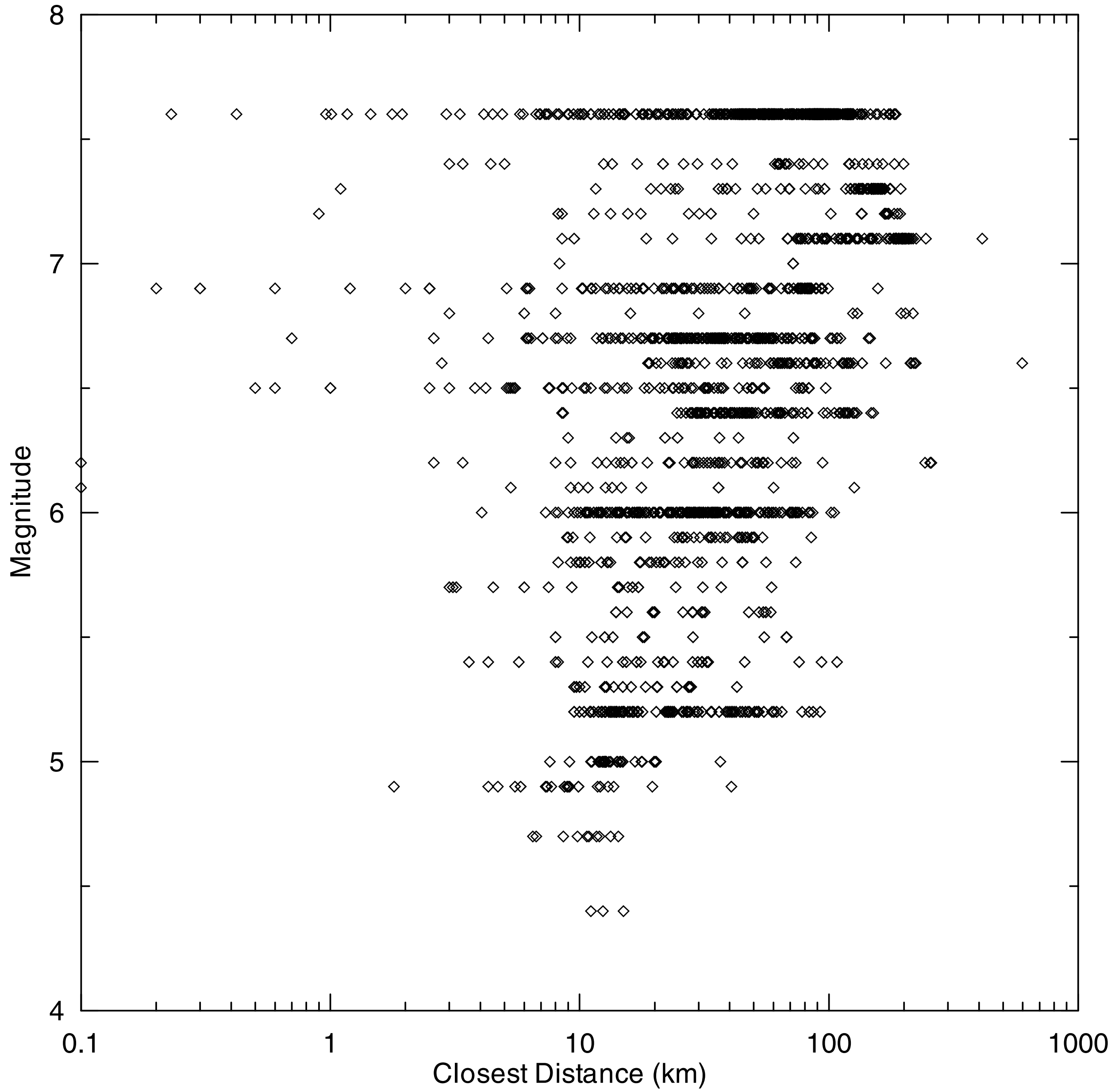

Fig. 3.1. Inventory of strong motion recordings from shallow crustal earthquakes in active tectonic regions; March 1933 Long Beach, California, earthquake to November 1999 Duzce, Turkey, earthquake (most data from PEER strong motion database).

Researchers involved in the development of attenuation relationships have developed a wide range of procedures for data analysis, each attempting to properly address data sampling issues so that the overall aleatory variability (i.e., sum of inter- and intra-event variability) in attenuation relations is properly quantified. Some of the common means by which these data weighting issues are treated are discussed in the following list:

- Joyner and Boore (1981) proposed a two-step regression procedure in which [1] all data points are weighted equally to derive the shape of the function describing the variation of spectral acceleration with distance (i.e., the change of S_a with changes in r), and [2] all events are weighted equally to derive the magnitude dependence of spectral quantities (i.e., the change of S_a with changes in m). Joyner and Boore (1993, 1994) have also proposed a one-step regression procedure that is similar in concept to the Brillinger and Preisler (1984, 1985) method discussed below, and produces regression results similar to the two-step procedure.
- Campbell (1981) uses a weighted least squares regression that is performed as follows: [1] The ground motion inventory (e.g., Figure 3.1) is first "binned" according to m and r (i.e., all data within a limited range of m and r is placed into a "bin"), [2] each bin of data is given equal weight in the regression, and [3] within a bin, the collective data from each event are weighted equally.
- Brillinger and Priesler (1984, 1985) developed a random effects model that is typically applied as described by Abrahamson and Youngs (1992). As part of the regression procedure, estimates of inter- and intra-event error are produced, as are "event terms" that represent the event-specific mean residuals in the data. Regression coefficients are estimated from a data set in which ground motion parameters are modified by subtraction of event terms. With the data set "corrected" in this manner, all data points are weighted equally. The standard error is the sum of the inter- and intra-event error. For earthquakes with large data residuals, the random effects method evaluates how much of the event term is likely due to random sampling of the intra-event distribution, and how much is due to true inter-event variability. For example, the event terms for a well-recorded event are taken essentially as the mean residuals (since the median of the data is well established from the large sample), whereas event terms for poorly sampled events are

less than the mean residual (since some of the residual may be due to intra-event variability).

- Idriss (1991, 1994) does not perform formal regression analysis, but has developed relations that are judgment based. The relations are formed by postulating a model, studying the residuals, and revising the model as necessary.

A number of modern attenuation relations implementing these data analysis schemes are summarized in Table 3.1. Also presented are various characteristics of the schemes, which are outlined in more detail in the following section.

Table 3.1 Selected attenuation models for horizontal spectral acceleration

Reference	Regression Method[1]	*m* range	*r* range (km)	*r type*[2]	site parameters[3]	other parameters[4]
Active Regions						
Boore et al. (1997)	2-step	5.5-7.5	0-100	r_{jb}	30-m V_s	F
Campbell (1997, 2000, 2001)	WLS	4.7-8.1	3-60	r_{seis}	S_{sr}, S_{hr}, D_b	F
Abrahamson & Silva (1997)	RE	>4.7	0-100	r	S	F, HW
Sadigh et al. (1997)	RE	4-8+	0-100	r	S	F
Idriss (1991, 1994)	judgement	4.6-7.4	1-100	r	rock only	F
Spudich et al. (1999): *ext. only*	1-step	5-7	0-100	r_{jb}	S	-
Subduction Zones						
Atkinson (1995)	2-step	4-8.2	< 500 (+/-)	r_{hypo}	S	h
Atkinson and Boore (1997a)	simulation	4-8.25	10-400	r_{hypo}	rock only	-
Anderson (1997)	none	3-8.1	14-255	r	rock only	-
Crouse (1991)	Equal	4.8-8.2	1-500	r_{cen}	firm soil only	h
Youngs et al. (1997)	RE	> 5	10-500	r	S	Z_t, h
Stable Continental Regions						
Atkinson and Boore (1995, 1997b)	simulation	4-7.25	10-500	r_{hypo}	rock only	-
Toro et al. (1997)	simulation	5-8	1-500	r_{jb}	rock only	-

[1] WLS = weighted least squares; RE = random effects; Equal = all date points weighted equally

[2] r = site-source distance; r_{jb} =surface projection distance; r_{seis} = seismogenic depth distance
r_{hypo} = hypocenter distance; r_{cen} = center of energy release distance

[3] S (rock/soil); S_{sr}, S_{hr}, soft rock, hard rock factors, D_b depth to basement rock

[4] F = style of faulting factor; HW = hanging wall factor; h = focal depth, Z_t = subduction zone source factor

3.2.2 Factors Affecting Attenuation

As described by Abrahamson and Shedlock (1997), the tectonic regime in which earthquakes occur is a fundamental factor affecting ground motion characteristics. Most earthquakes occur in one of three regimes: active tectonic regions (e.g., California), subduction zones (e.g., Washington, Alaska), and stable continental regions (e.g., central and eastern United States). In this section, we first illustrate the effects of a number of seismological variables on spectral accelerations using earthquake data from active tectonic regions. The section is concluded by discussing variations in ground motion across tectonic regimes. Characteristics of each of the attenuation models discussed below are presented in Table 3.1.

(a) *General formulation and effect of magnitude/distance*

Attenuation functions for median spectral acceleration generally have a form similar to the following:

$$\underbrace{\ln IM}_{1} = \underbrace{c_1 + c_2 m + c_3 m^{c_4}}_{2} + \underbrace{c_5 \ln r}_{3} + \underbrace{f(F) + f(HW) + f(S)}_{4} \tag{3.1}$$

where c_1 to c_5 are constants established by the regression, F is a factor related to the source rupture mechanism, HW is a hanging wall factor for dip-slip faults, and S is a site factor. Term m represents moment magnitude. Term r represents site-source distance, and is measured differently by different investigators. Common definitions of r are shown in Figure 3.2(a), along with the investigators using the respective distance measures. Figure 3.2(b) defines the geometric limits of the hanging wall for dip-slip faults. Explanations for the numbered terms in Eq. 3.1 are as follows:

1. As noted previously, *IM*s are generally log-normally distributed, hence regressions are performed on the natural logarithm of the data, which is normally distributed.
2. Several magnitude scales are derived from the logarithm of various peak ground motion parameters. Consequently, ln*IM* is approximately proportional to m. However, data from recent earthquakes suggest that this proportionality may break down for high-frequency ground motion parameters (e.g., PHA) at large magnitudes.

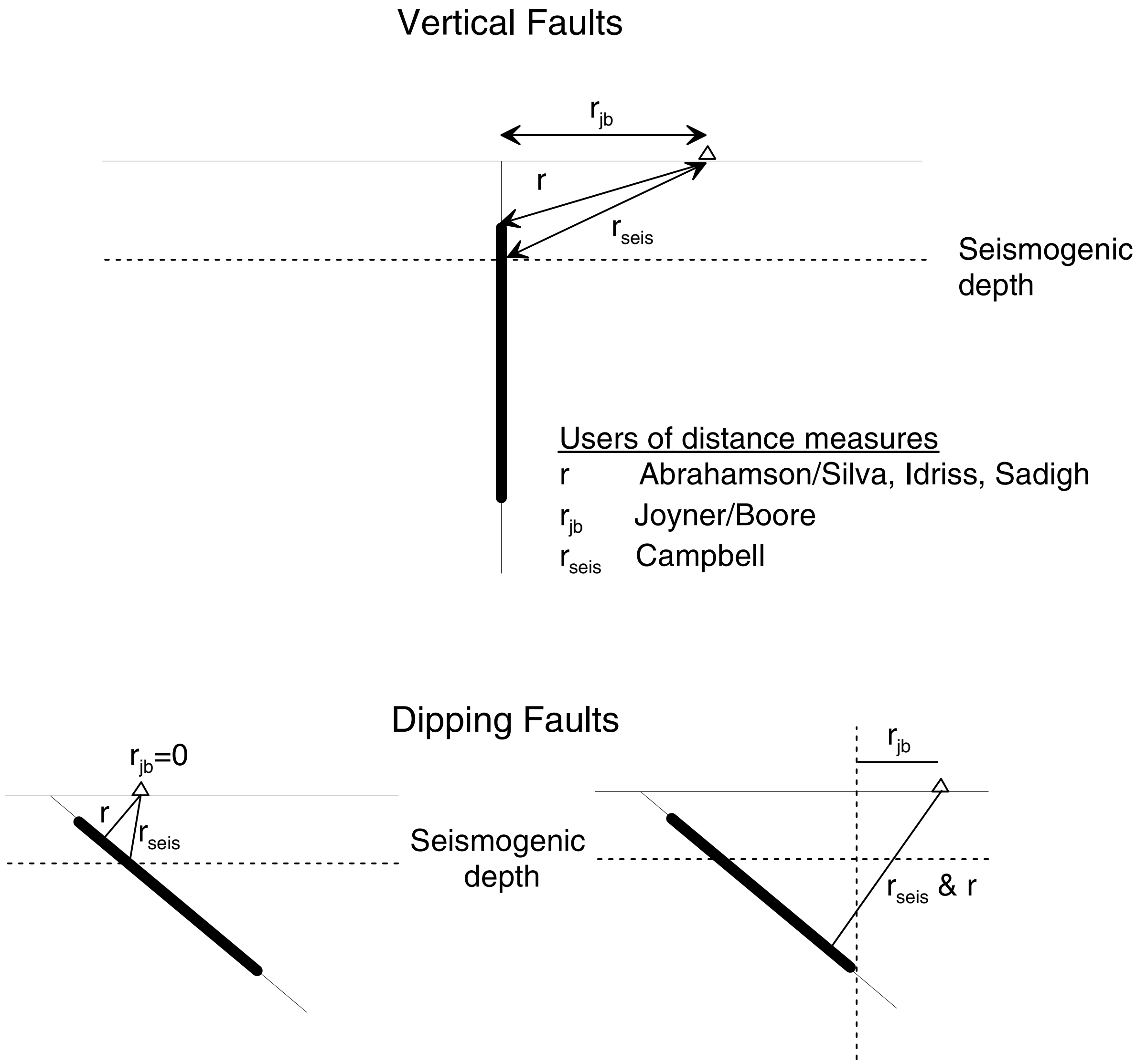

Fig. 3.2(a). Site-to-source distance measures for ground motion attenuation models (after Abrahamson and Shedlock, 1997). Seismogenic depth is the depth to the top orogenic part of the crust.

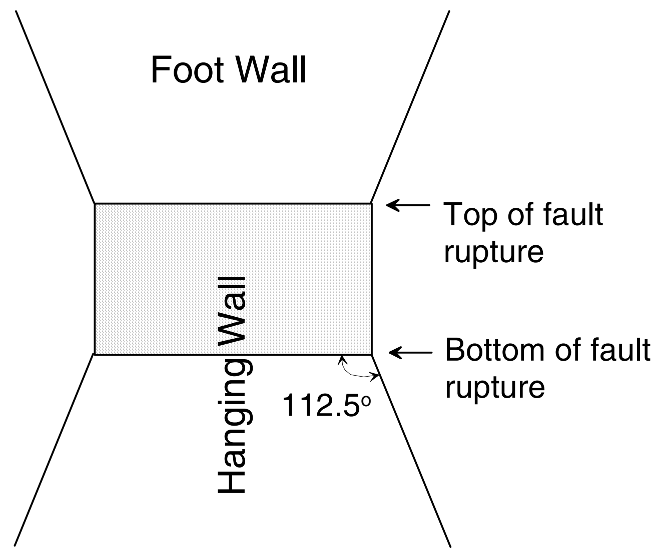

Fig. 3.2(b). Definition of footwall and hanging wall. The separation point is the vertical projection of the top of the fault rupture. After Abrahamson and Somerville (1996).

3. As body waves travel away from a seismic source, geometric spreading reduces their amplitude by $1/r$ (term c_5 is usually close to –1.0).
4. Fault rupture mechanism (F), the location of a site on or off the hanging wall of dip-slip faults (HW), and local site conditions (S) are observed to affect spectral accelerations, as discussed in Parts (b) and (c) below.

Error terms in attenuation relations are generally either constant (Boore et al., 1997) or functions of magnitude (Abrahamson and Silva, Idriss, Sadigh et al.). Available data generally indicate a decrease of standard error with increasing magnitude (Youngs et al., 1995). Specific regression equations used by various investigators and the corresponding regression coefficients are available on the USGS Engineering Seismology World Wide Web page, which can be found at **http://geohazards.cr.usgs.gov/engnseis/Eshmpage/eshmpage.htm** click on Ground Motion Information.

An example of the effect of m and r on ground motion is provided in Figure 3.3, which shows median values of PHA and T=3.0 s spectral acceleration for a strike-slip focal mechanism and rock site condition using the Abrahamson and Silva (1997) attenuation model. It can be observed from the figures that PHA attenuates more rapidly with distance than long-period spectral acceleration, and that long-period spectral acceleration is more magnitude sensitive.

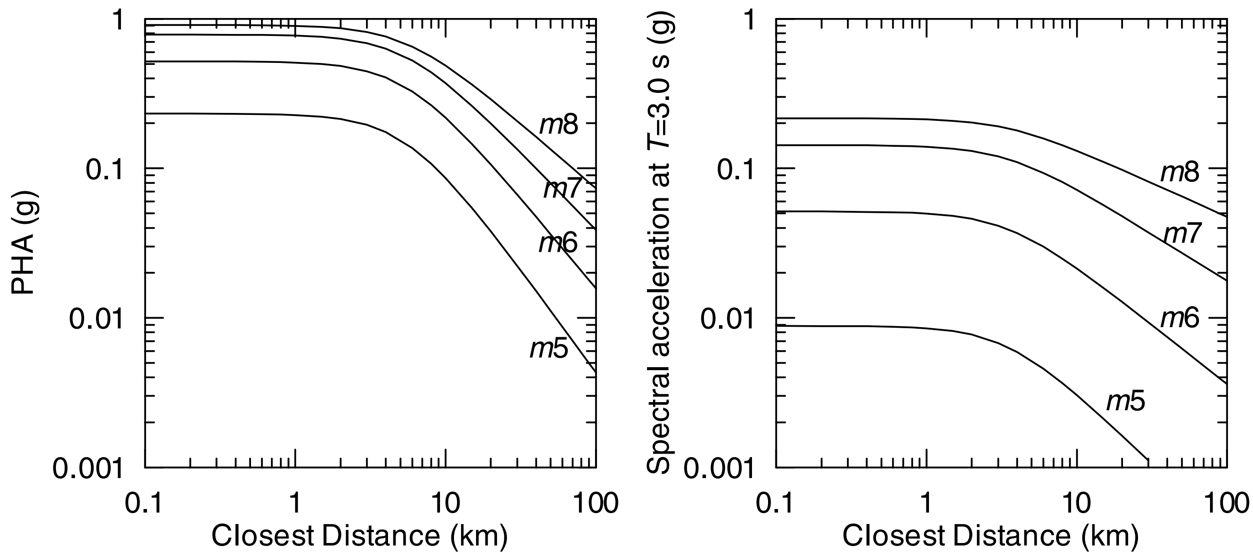

Fig. 3.3. Attenuation of PHA and 3.0 s spectral acceleration for strike-slip focal mechanism and rock site condition; Abrahamson and Silva (1997) attenuation relation.

Figure 3.3 shows an increase of PHA with magnitude, although the amount of this increase is larger at large distances than at short distances. At short distances, the limited available data suggest a "saturation" of high-frequency ground motion parameters such as PHA. This effect has also been found in some simulation exercises (Anderson, 2000). Recent data from the 1999 Kocaeli, Turkey, and Chi Chi, Taiwan, earthquakes have raised the question of whether PHA could *decrease* with increasing magnitude, as observed PHAs from these events at close distance were less than expected from existing attenuation relationships. This issue remains unresolved.

(b) ***Effect of focal mechanism***

Most earthquakes in active tectonic regions have one of four focal mechanisms: strike-slip, reverse, oblique, and normal. The strike-slip mechanism is generally taken as a "reference" mechanism, and no correction is necessary (i.e., $f(F) = 0$). Significant differences are observed between reverse earthquake motions and strike-slip, which are discussed below. No corrections are generally made for normal-slip earthquakes, although a separate set of attenuation relations is necessary for extensional tectonic regimes (see Part (e) below). Relatively little data are available for oblique-slip earthquakes, and the $f(F)$ correction for oblique-slip is often taken as half of $f(F)$ for reverse earthquakes.

Observations from the Northridge earthquake and other reverse events indicate that median ground motions from these earthquakes are higher than those from strike-slip events (e.g., Campbell, 1982; Somerville et al., 1996). This bias is present on both the footwall and hanging wall sides of reverse faults, but is particularly pronounced on the hanging wall side (Abrahamson and Somerville, 1996). The bias that results solely from rupture mechanism is represented in each of the major attenuation relationships for active regions (listed in Table 3.1) through use of an *f(F)* term in the regression equation (e.g., Equation 3.1). Researchers have taken this term as constant, period-dependent, distance-dependent, and/or magnitude-dependent. The analyses presented in Figure 3.3 are repeated in Figure 3.4 for a reverse focal mechanism to illustrate the influence of style-of-faulting with the Abrahamson and Silva attenuation relation. Factor *f(F)* generally increases median ground motion estimates, with the exception of long-period spectral components at large magnitudes, which are decreased.

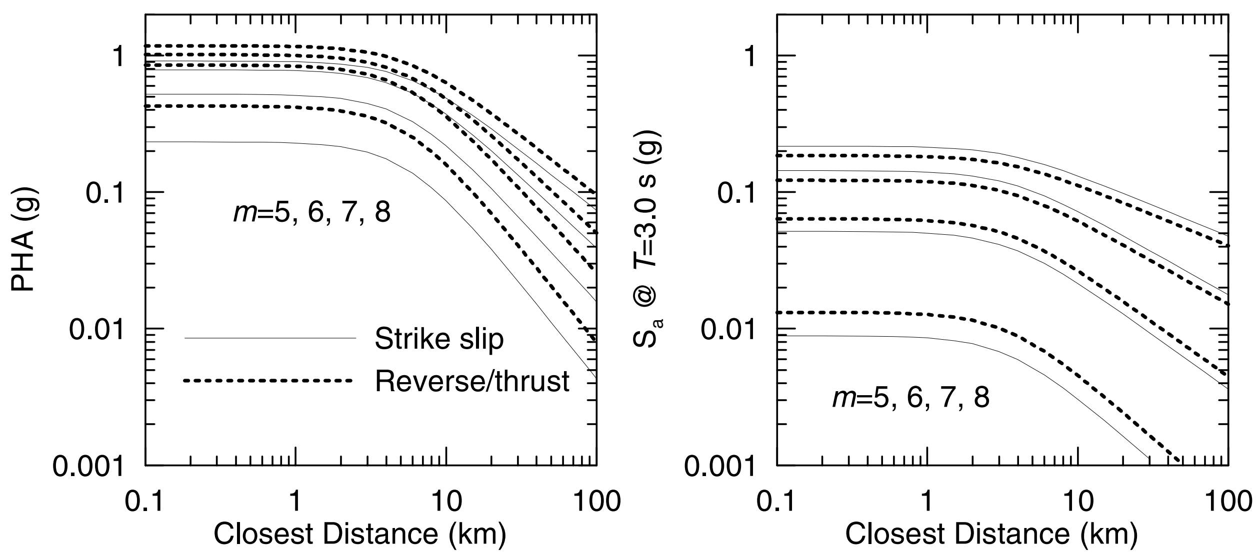

Fig. 3.4. Effect of focal mechanism on attenuation of PHA and 3.0 s spectral acceleration; Abrahamson and Silva (1997) attenuation relation.

The second source of bias for ground motions near thrust faults is associated with the positioning of sites on or off the hanging wall side of the fault. Analysis of data recorded during the 1994 Northridge earthquake showed positive residuals of up to 50% for hanging wall sites, and similar effects have been observed from other events as well (Abrahamson and Somerville, 1996). This bias is not surprising, as sites located over the hanging wall are closer to a larger area of the source than footwall sites. As a result of this bias, a magnitude-dependent hanging wall factor is included in the Abrahamson and Silva attenuation model. The analyses in Figures 3.3-3.4 are repeated in Figure 3.5 to illustrate the hanging wall effect, which diminishes attenuation with distance for $r < 25$ km. Hanging wall effects are not included in the Idriss, Sadigh et al., or Campbell attenuation relations. The distance definition used by Boore et al. incorporates the hanging wall effect to a limited extent, because $r_{jb} = 0$ for sites located over the hanging wall (e.g., Figure 3.2a).

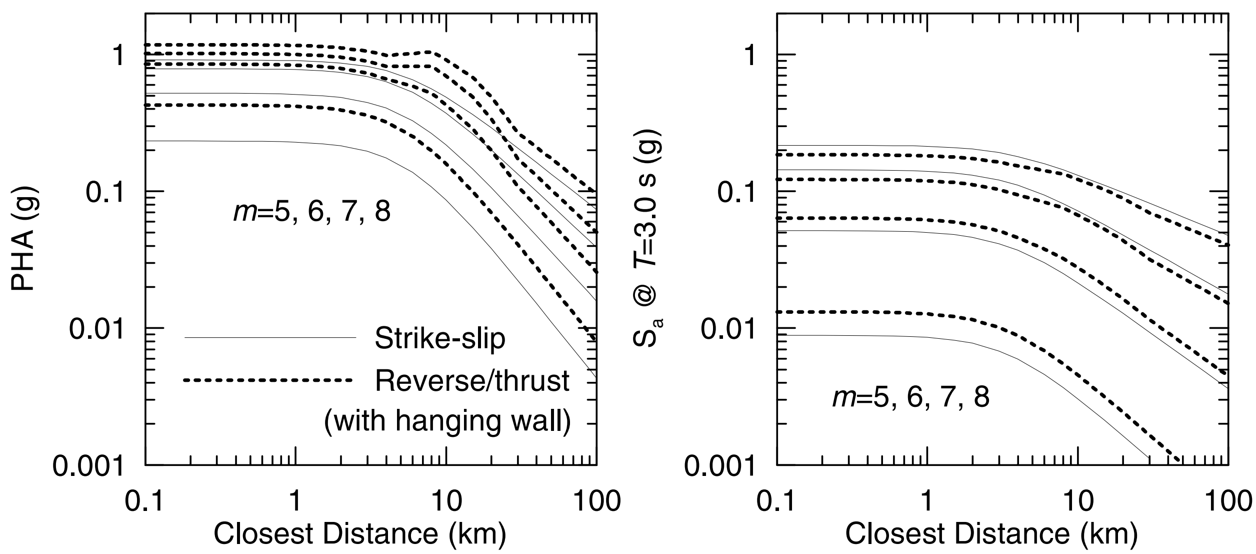

Fig. 3.5. Effect of focal mechanism and hanging wall effect on attenuation of PHA and 3.0 s spectral acceleration; Abrahamson and Silva (1997) attenuation relation.

(c) *Effect of site condition*

The effect of geologic and local soil conditions underlying seismographs can significantly influence the characteristics of recorded ground motion. To partially account for this effect, a site term, $f(S)$, is generally included in regression equations for median spectral acceleration (e.g., Equation 3.1). Standard error terms in attenuation relations are generally assumed to be unaffected by site condition. This section will address two issues related to the use of $f(S)$: the process by which sites are classified (i.e., quantification of S) and the form of the site term $f(S)$. The discussion is limited to site terms that have been used to date in attenuation relations. It should be noted that these site terms are simplified so as to not over-partition the data, which could result in regression instability. A review of work that has directly evaluated more elaborate site amplification factors (which have not, as yet, been included in attenuation functions) is presented in Section 5.2.

Some attenuation models use a simple rock/soil classification of ground conditions, setting S=1 for soil and S=0 for rock (e.g., Abrahamson and Silva, Sadigh et al.). Boore et al. (1997) use the 30-m shear wave velocity (V_S), calculated as 30 m/(shear wave travel time), as the site parameter. Campbell (1997) uses three parameters — S_{sr} and S_{hr} for local site conditions, as well as depth to basement rock (D_b). The local site condition parameters are $S_{sr} = S_{hr} = 0$ for soil (> 10 m depth), $S_{sr} = 1$ and $S_{hr} = 0$ for soft rock (Tertiary age and soft volcanics), and $S_{sr} = 0$ and $S_{hr} = 1$ for hard rock (e.g., Cretaceous, metamorphic or crystalline rock, hard volcanics). Parameter D_b is taken as the depth to Cretaceous or older deposits with $V_p \geq 5$ km/s or $V_s \geq 3$ km/s.

Analytical forms of site correction factors $f(S)$ vary from simple constants to more complex functions that attempt to account for nonlinearity in the local ground response. Boore et al. take $f(S)$ as the product of a period-dependent constant and 30-m V_s. Campbell incorporates distance r_{seis} into the site term to allow the deviation between rock and soils sites to increase with distance, as would be expected from soil nonlinearity. Abrahamson and Silva use the median peak acceleration on rock predicted by their attenuation relation as an input parameter to the site term. The value of the site term decreases as the rock acceleration increases, thus incorporating nonlinearity. Sadigh et al. do not use a site term, but perform the full regression separately for rock and soil sites.

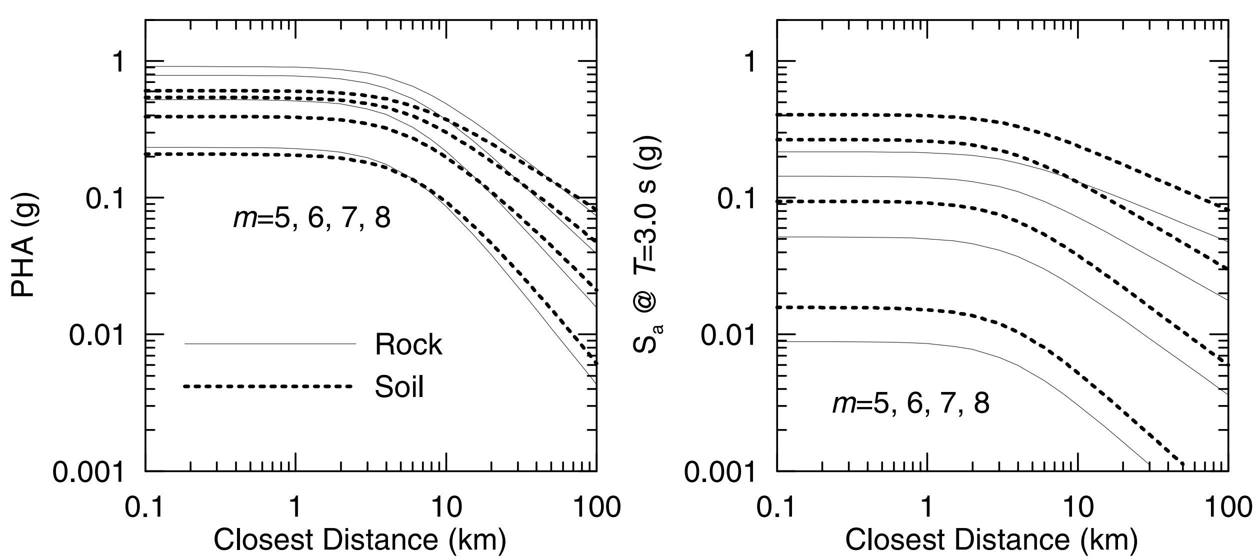

Fig. 3.6. Effect of site condition on attenuation of PHA and 3.0 s spectral acceleration; Abrahamson and Silva (1997) attenuation relation.

The analyses presented in Figure 3.3 are repeated in Figure 3.6 for a soil site condition to illustrate the effect of site response in the Abrahamson and Silva attenuation relation. For PHA, de-amplification occurs for rock accelerations greater than about 0.15g, with amplification at weaker levels of shaking. Long-period spectral acceleration is essentially uniformly amplified at all shaking levels.

(d) *Other effects observed in active regions*

The effects presented above in Sections (a)–(c) are generally well accepted as significantly influencing the attenuation of spectral acceleration. Several other effects have been postulated in the literature but are not incorporated into current attenuation relations. We discuss two such effects below, Moho bounce and surface fault rupture.

In the derivation of attenuation relations, the effects of different focal depths and travel paths on ground motion attenuation are averaged to obtain the median. The standard error reflects sources of epistemic variability such as variations in wave propagation conditions, source effects, and site effects, as well as aleatory variability. A particular path effect that can lead to localized amplification of motion at locations relatively far from the source occurs when body waves reflect at a critical angle off the Moho interface (i.e., crust-mantle boundary). A schematic illustration of this wave propagation scenario is shown in Figure 3.7. At close distances, ground motions are controlled by direct upgoing shear waves. At larger distances, reflections of shear waves off interfaces below the source reach a critical angle (i_{crit}) at which critical reflection occurs. At distances of $r \geq r_{crit}$, it has been postulated that these Moho reflections may contribute more strongly to the ground motion than the directly arriving shear waves, thus flattening the attenuation of ground motion with distance relative to what might otherwise be expected.

Empirical models have not been developed to predict the effects of Moho bounce. However, some general guidelines can be inferred from studies by Somerville et al. (1992, 1994). The effect tends to occur at $r \approx 60 - 120$ km, and can produce motions across all site conditions as high as one standard error above the median. For engineering problems in most major California urban centers, this effect is unlikely to be critical, as design is governed by more proximate faults. However, for areas relatively far from active faults, Moho bounce may be important.

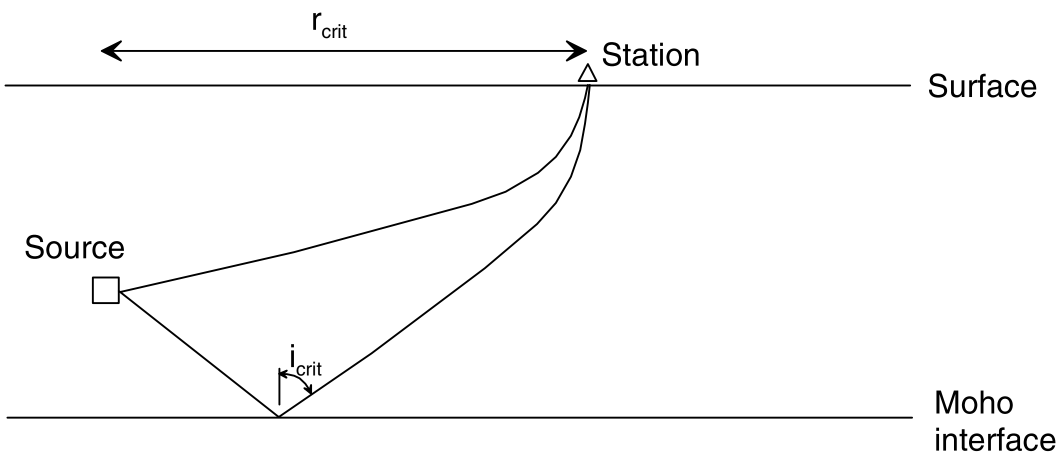

Fig. 3.7. Schematic diagram of direct and Moho reflected wave path. Reflection off shallower Conrad interface is also possible but is less significant than the Moho reflection. After Somerville et al. (1994).

Recent work by Somerville (2000) has suggested that ground motion characteristics may be affected by whether a fault rupture breaks the surface. Comparing ground motions records from the 1983 Coalinga, 1989 Loma Prieta, 1995 Northridge, and 1995 Kobe earthquakes (which either did not break the surface or did so over limited areas) with those from the 1999 earthquakes in Turkey and Taiwan (which had significant surface rupture), Somerville observed significantly lower spectral accelerations at $T < 3$ s for the Turkey/Taiwan events. These trends were also present to a lesser degree from other surface rupture earthquakes including the 1992 Landers, 1978 Tabas, 1971 San Fernando, and 1979 Imperial Valley earthquakes. The cause of these variations in the data is not well understood, and could be due to factors other than surface faulting. Additional study of these effects is needed.

(e) ***Ground motion variations across different tectonic regimes***

As noted above, worldwide earthquakes occur in one of three tectonic regimes: active tectonic regions, subduction zones, and stable continental regions. Previous discussion in this section has focused on active tectonic regions. Attenuation relationships for active regions are based principally on strong motion data from conservative (strike-slip) and/or compressive (reverse) earthquakes. In this section we summarize attenuation relations for extensional zones within active tectonic regions, as well as attenuation models for subduction zones and stable continental regions.

An attenuation model for ground motions in extensional regimes has been presented by Spudich et al. (1999). The model was developed using a worldwide database of extensional earthquakes in active tectonic regions. Data regression was performed using the Joyner and Boore (1993, 1994) one-step regression procedure, which produces results similar to the two-step analyses of Joyner and Boore (1981). Analyses similar to those presented in Figure 3.3 are repeated in Figure 3.8 to compare median ground motion predictions established from a global database of active tectonic regions (Boore et al., 1997) with those for extensional regions (Spudich et al., 1997). As both regressions were performed using similar data analysis procedures, the differences observed in this comparison should be meaningful. From Figure 3.8, no difference in PHA is observed for extensional regions at close distance, but more rapid attenuation occurs with distance from the source. Long-period spectral accelerations are smaller at all distances and magnitudes. It should be noted that Campbell (2000) has questioned these findings, citing controversy regarding the definitions of generic soil and generic rock between recordings in extensional regimes and other regimes, thus making direct comparisons difficult.

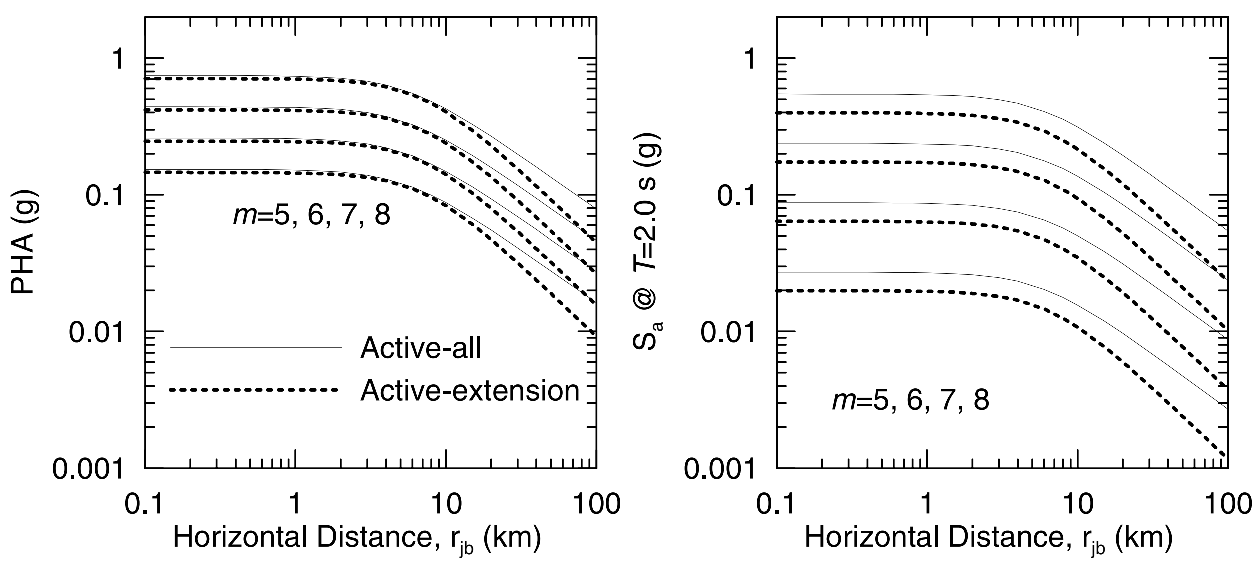

Fig. 3.8. Variation of attenuation of PHA and 2.0 s spectral acceleration within active tectonic regions (rock site condition). Median accelerations shown for strike-slip earthquakes in active regions (full database) and earthquakes in extensional regions. Boore et al. (1997) and Spudich et al. (1999) attenuation relations.

A number of attenuation models are available for earthquakes in subduction zones. These are primarily based on data from Japan and South America, as few recordings were available from U.S. earthquakes prior to the February 2001 Nisqually, Washington, earthquake. The database consists mostly of recordings at large distances. The only near-fault recordings are of the 1985 Michoacan earthquake from the Guerrero array (r as small as 13 km). This paucity of near-fault data leads to large epistemic uncertainty in the attenuation models for $r < 30$ km. Recent attenuation models for subduction zones include Youngs et al. (1997), Atkinson (1995), Atkinson and Boore (1997a), and Anderson (1997). An important older attenuation model is that of Crouse (1991). The Youngs et al. (1997) model is based on analyses of worldwide data performed with the random effects regression procedure. This model distinguishes between inter-slab earthquakes (i.e., reverse events at the interface of subducting and overriding plates, $Z_t = 0$) and intra-slab earthquakes (i.e., normal events resulting from tension in the down-bending subducting slab, $Z_t = 1$). The model also demonstrates the importance of focal depth as a parameter independent of site-source distance. Atkinson (1995) performed Joyner-Boore two-step regression analyses using a worldwide data set somewhat smaller than that of Youngs et al., and did not distinguish between inter-slab and intra-slab earthquakes. The Atkinson and Boore (1997a) model is based on stochastic point-source simulations and is applicable to the Cascadia subduction zone only. The Anderson (1997) model is based on PHA data from only the Guerrero, Mexico seismograph network. The Youngs et al. and Atkinson models were developed using procedures most comparable to those for active tectonic regions, and thus allow direct comparisons of ground motion attenuation characteristics.

A comparison of the Youngs et al. and Abrahamson and Silva attenuation models is made in Figure 3.9, which shows that PHA and long-period spectral acceleration from inter-plate subduction zone events are smaller at close distance, but attenuate more slowly with distance, than ground motions from active regions. Intra-slab events (not shown) produce larger amplitude ground motions more comparable at close distance to those from active regions, but which still attenuate relatively slowly with distance. The Atkinson (1995) model predicts ground motion amplitudes for large (m7) Cascadia events that are similar to California events, which may be due to the grouping together of inter-plate and intra-slab earthquakes in the data analysis.

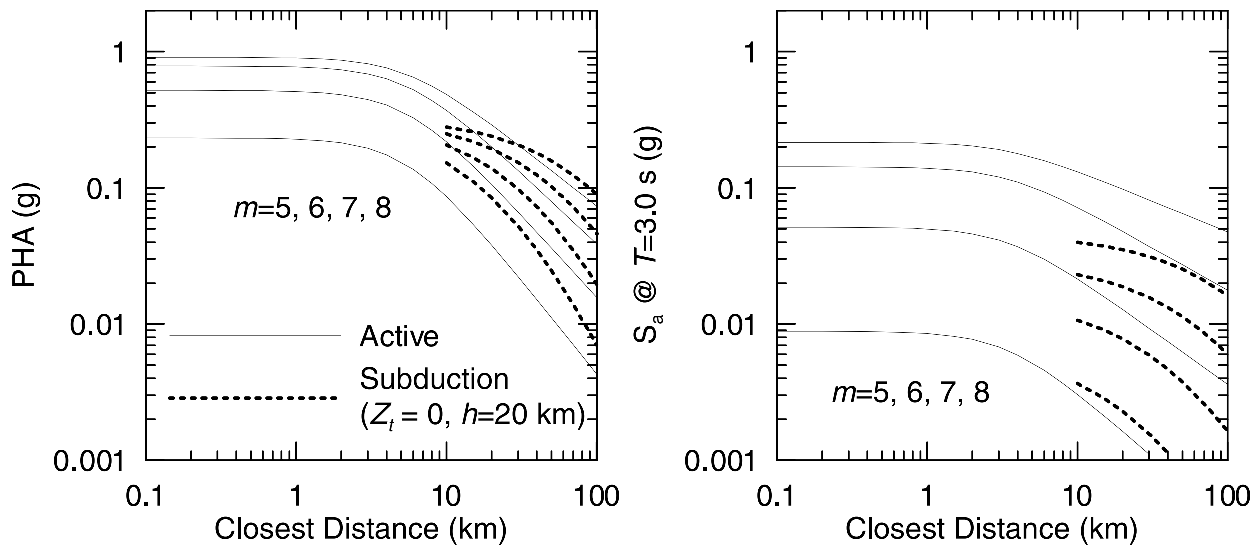

Fig. 3.9. Variation of attenuation of PHA and 3.0 s spectral acceleration between active tectonic regions and subduction zones (rock site condition). Median accelerations shown for strike-slip earthquakes in active regions and interplate earthquakes in subduction zones with focal depth = 20 km. Abrahamson and Silva (1997) and Youngs et al. (1997) attenuation relations.

Very little strong motion data are available for stable continental regions, and as a result, attenuation relationships are generally based on simulated ground motions instead of recordings. Regression analyses utilizing these simulated motions are used to develop attenuation functions. Two such relations are Atkinson and Boore (1995, 1997b), and Toro et al. (1997), both of which use a stochastic point-source simulation procedure (discussed further in Chapter 6). A comparison between ground motions from stable continental and active tectonic regions is made in Figure 3.10 using the Toro et al. and Boore et al. (1997) attenuation models. The most significant difference is much larger high-frequency ground motions in stable continental regions. Figure 3.10 indicates that mid-plate earthquakes have rates of attenuation with distance that are somewhat higher for $r < 100$ km, but the attenuation at larger distance is significantly less than that for active regions (not shown in figure).

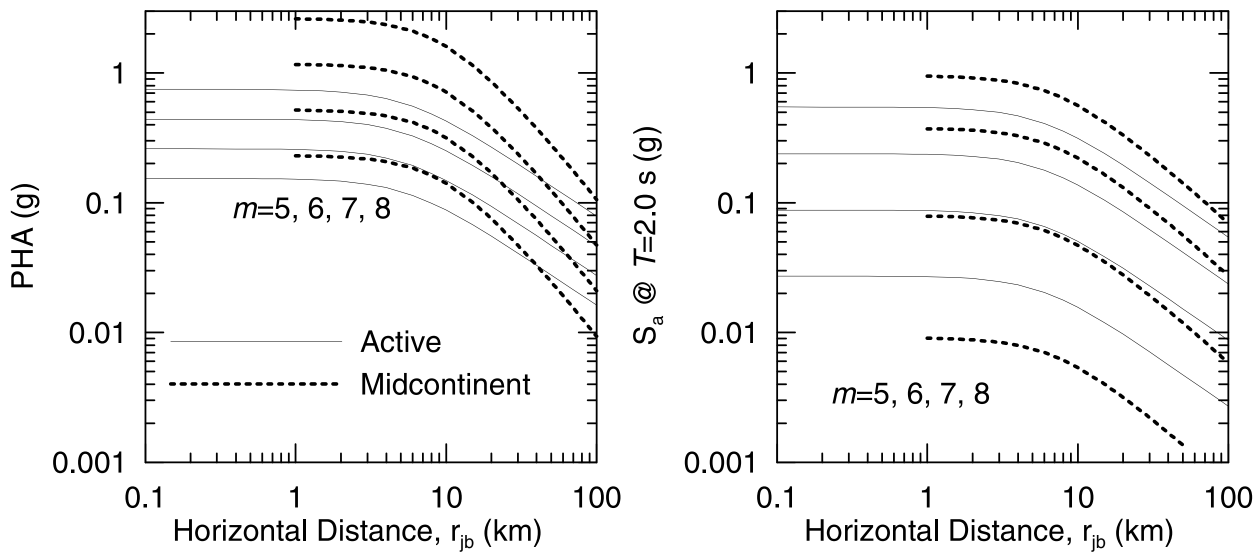

Fig. 3.10. Variation of attenuation of PHA and 2.0 s spectral acceleration between active stable continental regions (rock site condition). For active regions, the median accelerations are for strike-slip earthquakes. Boore et al. (1997) and Toro et al. (1997) attenuation relations.

3.2.3 Recommended Attenuation Relations for Horizontal Spectral Acceleration

As noted in Section 3.2.1, sampling problems associated with the strong motion database give rise to numerous possible means by which to account for inter-event vs. intra-event variability in regression analyses. Each of the attenuation relationships discussed above and summarized in Table 3.1 are viable from a technical standpoint, and the variability in median ground motions predicted by them represents epistemic uncertainty. Because it is desirable to incorporate this uncertainty into hazard analyses, the use of multiple attenuation relations is recommended.

Logic tree approaches are often used to incorporate into hazard analyses the epistemic uncertainty of attenuation models. In a logic tree approach, the hazard analysis is repeated using each selected attenuation model, and the respective results are assigned judgment-based weights. When using multiple relations, care must be taken to apply consistent distance measures. Moreover, to facilitate comparisons across models with different site parameters, Boore et al. (1997) indicated that 30-m V_s can be taken as 310 m/s for soil and 620 m/s for rock, and Campbell (2000) indicates that his parameters for rock sites should be taken as S_{sr}=1, S_{hr}=0, and D_b=1 km, and for soil sites as S_{sr}=0, S_{hr}=0, and D_b=5 km.

3.3 OTHER GROUND MOTION PARAMETERS

A number of ground motion parameters other than spectral acceleration and PHA can significantly affect the nonlinear response and performance of structures. The identification of such critical parameters for building and bridge structures is the focus of companion reports by Krawinkler and Mahin (manuscripts in preparation). The final identification of these parameters is not yet complete but may include duration, mean period, peak velocity, and vertical ground motion parameters (for long-span structures). For geotechnical structures, such parameters may include Arias intensity, duration, mean period, and equivalent number of uniform stress cycles (e.g., Kayen and Mitchell, 1997; Bray et al., 1998; Liu et al., 2001). Each of these parameters is defined in Section 1.2, and attenuation relations for them are presented in the sections that follow. These relations are summarized in Table 3.2.

Table 3.2 Attenuation models for ground motion parameters other than horizontal S_a

Reference	Tectonic Regime	Regres. Method[1]	*m* range	*r* range (km)	*r type*	site param.[2]	other param.[3]
Peak Ground Velocity							
Campbell (1997, 2000)	Active	WLS	4.7-8.1	3-60	r_{seis}	S_{sr}, S_{hr}, D	F
Atkinson and Boore (1997a)	Subduc.	sim.	4-8.25	10-400	r_{hypo}	rock only	-
Atkinson and Boore (1997b)	Mid-Pl.	sim.	4-7.25	10-500	r_{hypo}	rock only	-
Vertical Spectral Acceleration							
Abrahamson & Silva (1997)	Active	RE	>4.7	0-100	r	S	F, HW
Campbell (1997, 2000, 2001)	Active	WLS	4.7-8.1	3-60	r_{seis}	S_{sr}, S_{hr}, D_b	F
Sadigh et al. (1993)	Active	not given	not given	not given	r	rock only	-
Anderson (1997)	Subduc.	none	3-8.1	14-255	r	rock only	-
Arias Intensity							
Wilson (1993) and Kayen and Mitchell (1997)	Active	not given	not given	1-100	r*	S + soft soil	h
Duration/N							
Abrahamson & Silva (1996)	Active	Equal	>4.7	0-100	r	S	-
Liu et al. (2001)	Active	RE	>4.7	0-100	r	S	-
Mean Period							
Rathje et al. (1998)	Active	Equal	>5	0-100	r	-	-

[1] WLS = weighted least squares; RE = random effects, Equal = all data equally weighted, sim.= data from simulation

[2] S (rock/soil); S_{sr}, S_{hr}, soft rock, hard rock factors, D_b depth to basement rock

[3] F = style of faulting factor; HW = hanging wall factor; h = focal depth

It should be noted that in the future new ground motion parameters based on simplified nonlinear systems will be identified in ongoing PEER research. Such parameters may provide better representations of the nonlinear response of structures than is possible with existing parameters.

3.3.1 Peak Horizontal Velocity

Attenuation relations for peak horizontal velocity (PHV) have been developed for active tectonic regions by Campbell (1997, 2000, 2001), for the Cascadia subduction zone by Atkinson and Boore (1997a), and for eastern North America by Atkinson and Boore (1997b). Attenuation of PHV follows trends similar to mid-period spectral acceleration (i.e., S_a at $T \approx 1$ s). Specific regression equations used by these investigators and the corresponding regression coefficients are available on the USGS Engineering Seismology World Wide Web page at **http://geohazards.cr.usgs.gov/engnseis/Eshmpage/eshmpage.htm** click on Ground Motion Information.

3.3.2 Vertical Spectral Acceleration

Attenuation relationships for vertical spectral acceleration (including peak vertical acceleration, PVA) have been developed for active tectonic regions by Abrahamson and Silva (1997), Campbell (1997, 2000, 2001), and Sadigh et al. (1993), and for subduction zones by Anderson (1997). Figure 3.11 presents a comparison of median PVA values for strike-slip earthquakes in active regions (using Abrahamson and Silva relation) with those for subduction zones (by Anderson). As with the horizontal attenuation functions, subduction zones are seen to have small peak accelerations at close distance, but to attenuate more slowly with distance. Also shown is the attenuation of long-period vertical spectral accelerations for active regions (spectral values for subduction zones are not available). Bozorgnia et al. (1999) have examined ratios of vertical to horizontal spectra, and have found strong dependence of this ratio on period, distance, and site condition. High V/H ratios (~1.5) were found for Holocene soil conditions, short periods (~0.1 s), and short distances. Values of V/H ≤ 0.5 were found at longer periods (0.2 – 2.0 s).

Specific regression equations used by these investigators and the corresponding regression coefficients are available on the USGS Engineering Seismology World Wide Web page (see reference above).

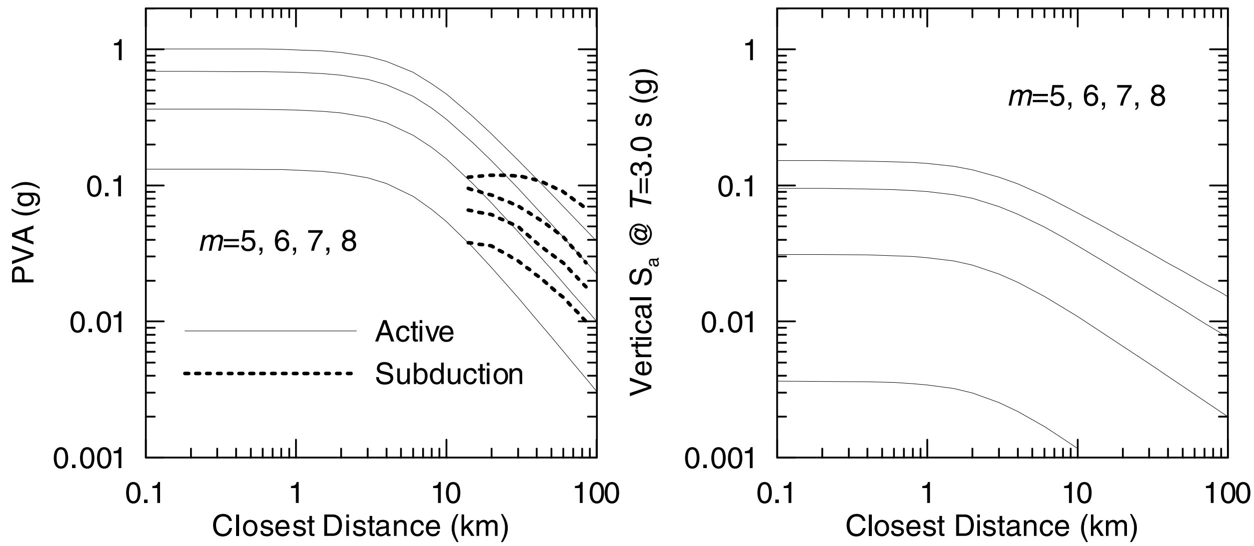

Fig. 3.11. Variation of attenuation of PVA and 3.0 s vertical spectral acceleration between active tectonic regions and subduction zones. For strike-slip regions, the median accelerations are for strike-slip earthquakes. Abrahamson and Silva (1997) and Anderson (1997) attenuation relations.

3.3.3 Arias Intensity

Attenuation relationships for Arias intensity (I_A) have been compiled by Wilson (1993) and Kayen and Mitchell (1997). These relations apply for California and active tectonic regions, respectively. Kayen and Mitchell assume the data to be log-normally distributed. Separate regressions were performed for rock, alluvium, and soft soil conditions. Equations for median values of I_A are as follows:

$$\log_{10}(I_A) = M - 4.0 - 2\log_{10}(r^*) : \text{rock sites}$$

$$\log_{10}(I_A) = M - 3.8 - 2\log_{10}(r^*) : \text{alluvial sites}$$

$$\log_{10}(I_A) = M - 3.4 - 2\log_{10}(r^*) : \text{soft soil sites} \tag{3.2}$$

where $r^* = \sqrt{r_{jb}^2 + h^2}$, and h = focal depth. Standard error terms are 0.63 for rock, 0.61 for alluvium, and are undefined for soft soil due to insufficient data. These error terms are of approximately the same size as those for high-frequency spectral quantities.

The variation of median I_A with magnitude and distance according to this relation is presented in Figure 3.12. As the I_A parameter contains a combination of amplitude and duration information, it is more magnitude sensitive than peak acceleration (i.e., compare to Figures 3.3

or 3.11). Applications of I_A have included liquefaction triggering analysis procedures by Kayen and Mitchell (1997).

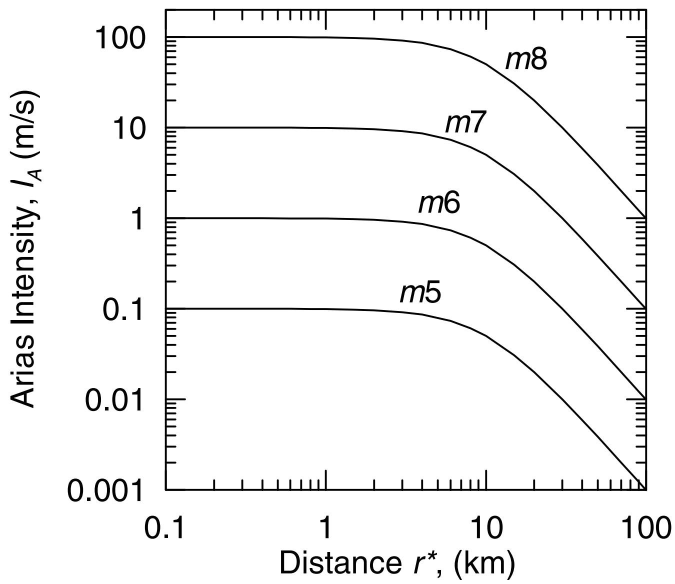

Fig. 3.12. Attenuation of Arias intensity for rock site condition; Kayen and Mitchell (1997) attenuation relation.

3.3.4 Duration and Equivalent Number of Uniform Stress Cycles

An introduction to duration parameters was provided in Section 1.2.3. The most common duration parameters are bracketed duration and the time across which a specified percentage of the Arias intensity is generated (usually 5-75% or 5-95%, and referred to as significant duration). Another parameter used as a proxy for duration in some geotechnical applications is the equivalent number of uniform stress cycles (N). Of these parameters, attenuation relationships are available for significant duration and N. Both apply for active tectonic regions, and use as input m,r, and S, as shown in Table 3.2.

The models for significant duration were compiled by Abrahamson and Silva (1996) using strong motion data up through the 1994 Northridge earthquake. The data were found to be log-normally distributed. The model for the median of significant duration (SD) for the horizontal and vertical directions is

$$\ln(SD) = \ln\left[\frac{\left(\dfrac{\exp(b_1 + b_2(m - m^*))}{10^{1.5m+16.05}}\right)^{-\frac{1}{3}}}{4.9 \cdot 10^6 \beta} + Sc_1 + c_2(r - r_c)\right] + D_{rat}, \quad r \geq r_c$$

$$\ln(SD) = \ln\left[\frac{\left(\dfrac{\exp(b_1 + b_2(m - m^*))}{10^{1.5m+16.05}}\right)^{-\frac{1}{3}}}{4.9 \cdot 10^6 \beta} + Sc_1\right] + D_{rat}, \qquad r < r_c \tag{3.3}$$

where β, b_1, b_2, m^*, c_1, c_2, D_{rat} and r_c are regression coefficients (listed in Table 3.3). Parameter D_{rat} is related to the percent of normalized Arias intensity used to define significant duration, and values for 5-75% and 5-95% significant duration are listed in Table 3.3. Standard error terms are also listed in Table 3.3. Shown in Figure 3.13(a) is the variation of median 5-75% significant duration with magnitude and distance. Duration is seen to be highly magnitude sensitive, and to increase with distance for $r > 10$ km (r_c).

Table 3.3 Regression coefficients for ground motion parameters related to duration

Reference	Parameter	β	b_1	b_2	m^*	c_1	c_2	r_c	D_{rat}	σ
A&S (1996)	5-75% S.D., H	3.2	5.204	0.851	6	0.805	0.063	10	0	0.55
A&S (1996)	5-75% S.D., V	3.2	4.61	1.536	6	1.076	0.107	10	0	0.46
A&S (1996)	5-95% S.D., H	3.2	5.204	0.851	6	0.805	0.063	10	0.845	0.49
A&S (1996)	5-95% S.D., V	3.2	4.61	1.536	6	1.076	0.107	10	0.646	0.45
Liu et al., 2001	No. cycles, H	3.2	1.53	1.51	5.8	0.75	0.095	0	-	0.56

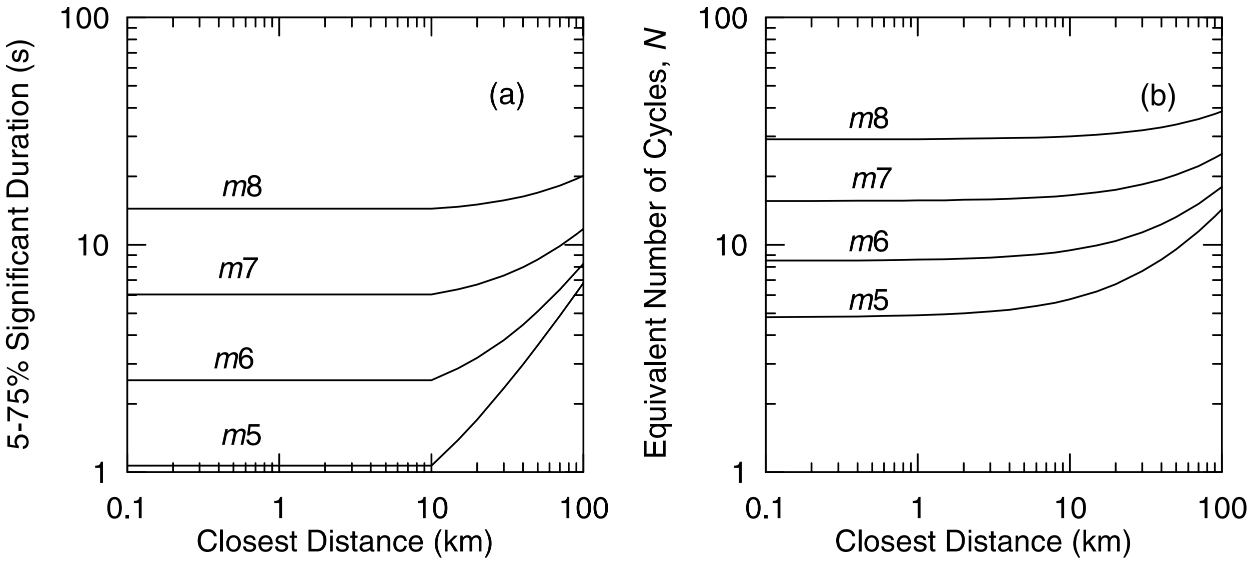

Fig. 3.13. Attenuation for rock sites of (a) 5-75% significant duration and (b) equivalent number of uniform stress cycles; Abrahamson and Silva (1996) and Liu et al. (2001) attenuation relations.

The model for equivalent number of uniform stress cycles (N) was compiled by Liu et al. (2001) using strong motion data up through the 1999 Duzce, Turkey, earthquake. Values of N were evaluated from the data using weighting factors applicable for analyses of the triggering of soil liquefaction. Several such weighting factors were derived based on analyses of laboratory and field case histories of liquefaction, and the recommended factors are a weighted average of the laboratory and field factors. A database of N values was evaluated from time histories using these averaged factors. Regression of these data revealed a log-normal distribution, with a median that can be computed as

$$\ln(N) = \ln\left[\frac{\left(\dfrac{\exp(b_1 + b_2(m - m^*))}{10^{1.5m+16.05}}\right)^{-\frac{1}{3}}}{4.9 \cdot 10^6 \beta} + Sc_1 + rc_2\right] \tag{3.4}$$

Coefficients β, b_1, b_2, m^*, c_1, and c_2 were estimated by the regression, and are listed in Table 3.3 along with the standard error. The variation of median N-values with magnitude and distance are shown in Figure 3.13(b), and show similar trends to the duration values (although the N-values are significantly larger than 5-75% significant duration values).

3.3.5 Mean Period

As noted in Section 1.2.2, single parameters that can be used to represent the frequency content of ground motions are mean period (T_m) and pulse period (T_v). Parameter T_m represents the inverse of the mean frequency of a Fourier amplitude spectrum, and provides a reasonable single-parameter representation of ordinary (non-near-fault) ground motions. Parameter T_v represents the period of near-fault velocity pulses and is expected to provide a better representation than T_m of the frequency content of near fault motions. Empirical relations for pulse period are presented in Chapter 4; the focus of this section is T_m.

Empirical attenuation relationships for parameter T_m have been developed by Rathje et al. (1998) for active regions. Data from earthquakes up to the 1994 Northridge earthquake were used, and were found to be log-normally distributed. Regression equations for median values are

$$T_m = C_1 + C_2 \cdot (m-6) + C_3 \cdot r \qquad m \le 7.25$$

$$T_m = C_1 + 1.25 \cdot C_2 + C_3 \cdot r \qquad 7.25 \le m \le 8.0 \tag{3.5}$$

where parameters C_1, C_2, and C_3 are functions of site condition as indicated in Table 3.4. Standard error is also indicated in Table 3.4. Rathje et al. also developed theoretical models for T_m based on a stochastic point-source model that are applicable for the mid-plate tectonic regime. Equations that approximate the resulting relations for rock sites are

$$T_m = 0.208 + 0.0523 \cdot (m-6) + \left[0.00184 - 0.000148(m-8)^2\right] \cdot r \qquad m \le 7.25$$

$$T_m = 0.273 + \left[0.00184 - 0.000148(m-8)^2\right] \cdot r \qquad 7.25 \le m \le 8.0 \tag{3.6}$$

Shown in Figure 3.14 is the variation of median T_m with magnitude and distance for active and mid-plate regions. Parameter T_m is seen to be highly magnitude sensitive and to increase with distance for r > 10 km. The simulations indicate T_m to be significantly lower for mid-plate regions than for active regions.

Table 3.4 Coefficients for estimating T_m

Sites	C_1	C_2	C_3	σ
T_m, rock	0.411	0.0837	0.0021	0.437
T_m, soil	0.519	0.0837	0.0019	0.35

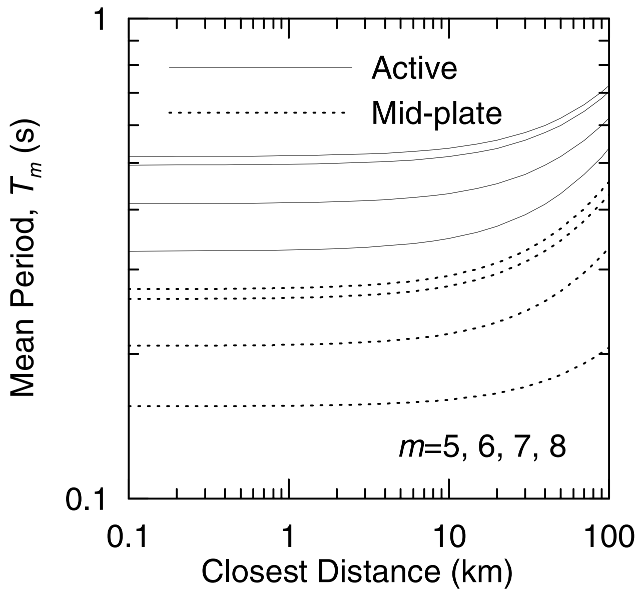

Fig. 3.14. Attenuation of mean period for rock site condition in active and mid-plate regions; Rathje et al. (1998) attenuation relationship.

3.4 JOINT-PROBABILITY DENSITY FUNCTIONS FOR MULTIPLE PARAMETERS

The nonlinear response of many types of structures is controlled by more than one ground motion intensity measure. For such cases, it is necessary to develop joint-probability density functions for multiple *IM*s. In the following, we review how such distributions can be integrated into the performance-based design framework, and the work that will be required to develop such distributions in the future.

In a standard, single-parameter hazard calculation, the rate with which *IM* will exceed a test value *z* is written as indicated in Equation 1.2, and repeated below.

$$\upsilon(IM > z) = \sum_{i=1}^{N_{flt}} \upsilon_i \times \int_m \int_r f(m) f(r) P(IM > z \mid m, r) dm dr \qquad (3.7, 1.2)$$

The probability term in Equation 3.7 is an implicit integration of the *IM* distribution given *m* and *r*. Writing out this integration leads to

$$\upsilon(IM > z) = \sum_{i=1}^{N_{flt}} \upsilon_i \times \int_m \int_r \int_\varepsilon f(m) f(r) f(\varepsilon) P(IM > z \mid m, r, \varepsilon) dm dr d\varepsilon \qquad (3.8)$$

where ε is the standard normal variate for *IM* integrated from -∞ to ∞ and given by

$$\varepsilon = \frac{\ln(z) - \ln(\mu_{IM\mid m,r})}{\sigma} \qquad (3.9)$$

where $\mu_{IM|m,r}$ = median value of *IM* given *m* and *r*, and σ is the standard error of *IM*. In Eq. 3.8, $f(\varepsilon)$ indicates the probability density function for ε, which is generally assumed to be normal. The probability term in Eq. 3.8 is either 0 or 1.

If we now expand the hazard equation to include two *IM*s, we can write the rate of exceeding both simultaneously as

$$\upsilon(IM_1 > z_1 \,\&\, IM_2 > z_2) = \sum_{i=1}^{N_{flt}} \upsilon_i \times \int_m \int_r \int_{\varepsilon_1} \int_{\varepsilon_2} f(m) f(r) f(\varepsilon_1, \varepsilon_2) P(IM_1 > z_1 \,\&\, IM_2 > z_2 \mid m, r, \varepsilon_1, \varepsilon_2)\, dm\, dr\, d\varepsilon_1\, d\varepsilon_2 \tag{3.10}$$

where the probability term is again either 0 or 1, and $f(\varepsilon_1,\varepsilon_2)$ is a joint distribution on the normalized residuals of IM_1 and IM_2. Eqs. 3.7-3.10 were written for hazard defined in terms of intensity measures, but the $f(\varepsilon_1,\varepsilon_2)$ term also appears when the hazard is written in terms of a damage measure or a decision variable (e.g., Eq. 1.3 and 1.4). Accordingly, the integration of a vector of intensity measures into the performance based design framework reduces to the evaluation of $f(\varepsilon_1,\varepsilon_2)$.

Research to define the joint-probability density function $f(\varepsilon_1,\varepsilon_2)$ for key *IM*s has been limited but follows several straightforward steps. First, a scatter diagram of ε_1 and ε_2 should be prepared to ensure the data are jointly normal. Provided this is the case, the correlation coefficient (ρ) between ε_1 and ε_2 should be evaluated, from which the joint-probability density function is defined as follows:

$$f(\varepsilon_1, \varepsilon_2) = \frac{1}{2\pi\sqrt{1-\rho^2}} \exp\left[\frac{-1}{2(1-\rho^2)}\left\{\varepsilon_1^2 - 2\rho\varepsilon_1\varepsilon_2 + \varepsilon_2^2\right\}\right] \tag{3.11}$$

From the above, it is clear that the key quantity needed to define $f(\varepsilon_1,\varepsilon_2)$ for jointly normal data is the correlation coefficient. Correlation coefficients for 5% damped spectral acceleration at different periods have been evaluated by Inoue and Cornell (1990). Similar work for other pairs of parameters represents a research need for the PEER Center.

3.5 SYNTHESIS OF PEER RESEARCH

Researchers affiliated with the PEER Center have strongly contributed to the development of modern attenuation relations, both for spectral acceleration and other ground motion parameters. Much of the research discussed in this chapter was completed immediately prior to the inception of the PEER Center and was published in an issue of *Seismological Research Letters* in 1997. Since that time, several developments have triggered PEER research initiatives related to attenuation relations, including (1) the 1999 earthquakes in Turkey and Taiwan, which have significantly enhanced the strong motion database for active regions, (2) the ongoing development of next-generation ground motion intensity measures for building structures, which will require new attenuation relationships for predicting these intensity measures from seismological variables, and (3) recognition of the need for multiple intensity measures to properly characterize the seismic response of nonlinear structures of various types. Further discussion on research related to these developments is provided below.

In response to the 1999 earthquakes, the PEER Lifelines Program has engaged in a long-term series of projects to gather necessary strong motion and site data, and to develop new attenuation models. Work completed to date has focused on data generation and database development, including the following projects:

- ROSRINE IV: Characterization of geotechnical conditions at California strong motion sites (Lifelines Phase II, PI: Henyey).
- Web enabling of Pacific Engineering & Analysis strong motion database (Lifelines Phase II with supplemental support from Core Program, PI: Silva).

Ongoing data generation projects include SASW measurements at strong motion sites in Turkey and California (PI: Stokoe), additional support to the ROSRINE program for geotechnical characterization of strong motion sites (PI: Nigbor), and geotechnical testing to support the development of models of nonlinear soil behavior (PI: Anderson). In addition, a project was recently completed to update the ground motion database with recordings from the 1999 earthquakes (PI: Silva). Major initiatives for new attenuation model development are planned, including the development of new attenuation relationships incorporating the 1999 earthquake data, and attenuation relationships for PHV, PHD, and differential displacement.

Work in the PEER Core Program (Thrust Area 3, PI: Conte) is developing next-generation intensity measures for the nonlinear dynamic response of building structures. These parameters measure the ability of time histories to generate in simple structures specified realizations of nonlinearity such as peak ductility or cumulative hysteretic energy dissipated. These parameters are intended to be used jointly with S_a, thus requiring the use of vector hazard. Future research will likely develop engineering models for estimating these important parameters, using the databases developed within the Lifelines Program.

The need for vectors of ground motion intensity measures (i.e., so-called vector hazard) has been recognized for many classes of structures. Preliminary work to develop the analytical formulation for vector hazard is presented in Section 3.4. In the Hazard Assessment Thrust Area in the PEER Core Program, future work will evaluate the correlation coefficients needed for development of vector hazard capabilities.

4 CHARACTERISTICS OF NEAR-FAULT GROUND MOTIONS

4.1 INTRODUCTION

4.1.1 Near-Fault Effects

Ground motions close to a ruptured fault can be significantly different than those further away from the seismic source. The near-fault zone is typically assumed to be within a distance of about 20-60 km from a ruptured fault. Within this near-fault zone, ground motions are significantly influenced by the rupture mechanism, the direction of rupture propagation relative to the site, and possible permanent ground displacements resulting from the fault slip. These factors result in effects termed herein as "rupture-directivity" and "fling step." The estimation of ground motions close to an active fault should account for these characteristics of near-fault ground motions.

Forward directivity occurs when the rupture propagates toward a site and the direction of slip on the fault is also toward the site. This occurs because the velocity of fault rupture is close to (generally slightly less than) the shear wave velocity of the rock near the source. As shown in Figure 4.1 for a strike-slip focal mechanism, as the rupture front propagates away from the hypocenter and toward a site, energy is accumulated near the rupture front from each successive zone of slip along the fault. The wave front arrives as a large pulse of motion (a shock wave effect) that occurs at the beginning of the record (Somerville et al. 1997a) and is polarized in the strike-normal direction. The pulse of motion is typically characterized by large amplitude at intermediate to long periods and short duration.

If a site is located near the epicenter, i.e., rupture propagates away from the site, the arrival of seismic waves is distributed in time. This condition, referred to as backward directivity, is characterized by motions with relatively long duration and low amplitude. Neutral directivity occurs for sites located off to the side of the fault rupture surface (i.e., rupture is neither predominantly toward nor away from the site).

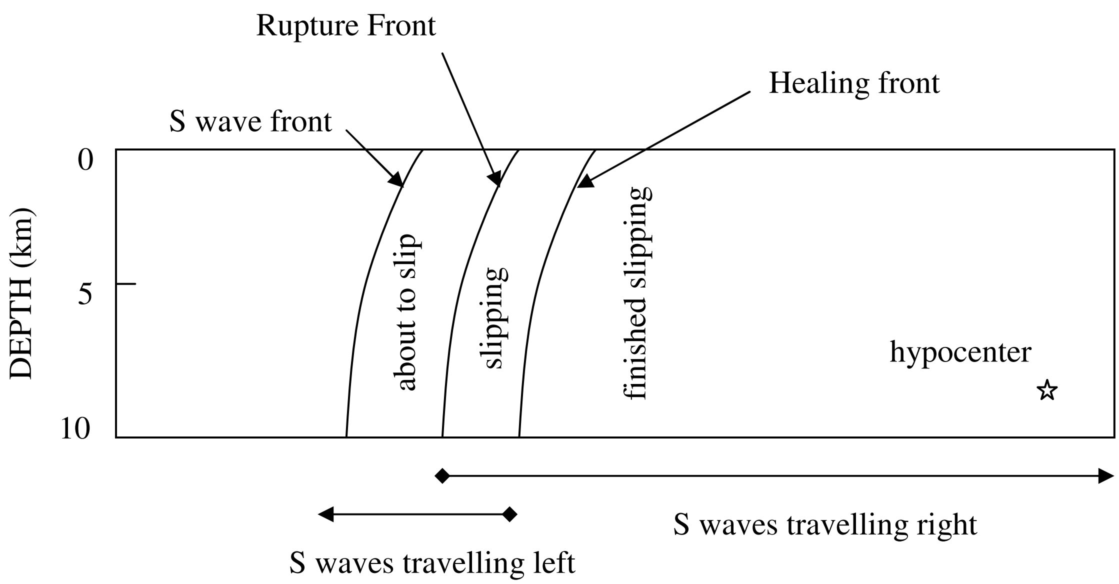

Fig. 4.1. Schematic diagram of rupture-directivity effects for a vertical strike-slip fault. The rupture begins at the hypocenter and spreads at a speed that is about 80% of the shear wave velocity. The figure shows a snapshot of the rupture front at a given instant (from Somerville et al. 1997a).

The effects of rupture-directivity on ground displacements recorded during the 1989 Loma Prieta earthquake are shown in Figure 4.2. The epicenter of the earthquake is near Corralitos and Branciforte Drive, where the horizontal ground displacements are moderate on both fault-normal and fault-parallel components. This is attributed to backward directivity. At the ends of the fault, however, at Lexington Dam and Hollister, forward directivity causes the horizontal ground motions in the fault-normal direction to be impulsive and much larger than the fault-parallel motions, which are similar to those near the epicenter. The large impulsive motions occur only in the fault-normal direction and only away from the epicenter.

Rupture-directivity effects can be present both for strike-slip and dip-slip events. In dip-slip events, forward-directivity conditions occur for sites located near the up-dip projection of the fault plane. As with strike-slip focal mechanisms, the radiation pattern of the shear dislocation on a reverse fault causes the pulse of motion to be oriented perpendicular to the fault strike (Somerville et al., 1997a).

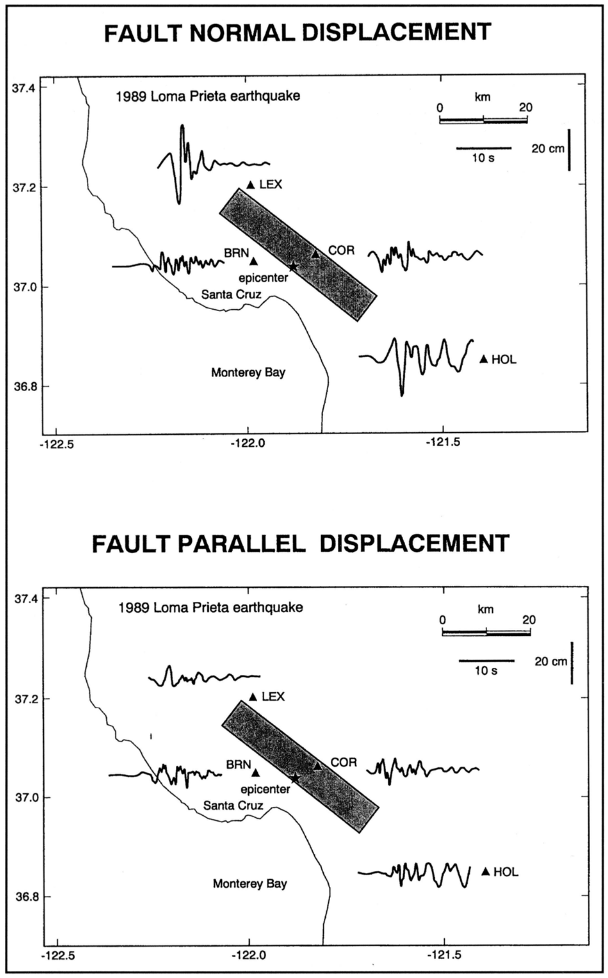

Fig. 4.2. Rupture-directivity effects in the recorded displacement time histories of the 1989 Loma Prieta earthquake, for the fault-normal (top) and fault-parallel (bottom) components. Source: EERI, 1995.

Modern digital recordings of near-fault ground motions, for example from the 1999 Turkey and Taiwan earthquakes, contain permanent ground displacements due to the static deformation field of the earthquake. These static displacements, termed "fling step," occur over a discrete time interval of several seconds as the fault slip is developed. Fling step displacements occur in the direction of fault slip, and therefore are not strongly coupled with the aforementioned dynamic displacements referred to as the "rupture-directivity pulse." In strike-slip faulting, the directivity pulse occurs on the strike-normal component while the fling step occurs on the strike parallel component. In dip-slip faulting, both the fling step and the directivity pulse occur on the strike-normal component. The orientations of fling step and directivity pulse for strike-slip and dip-slip faulting are shown schematically in Figure 4.3, and time histories in which these contributions are shown together and separately are shown schematically in Figure 4.4.

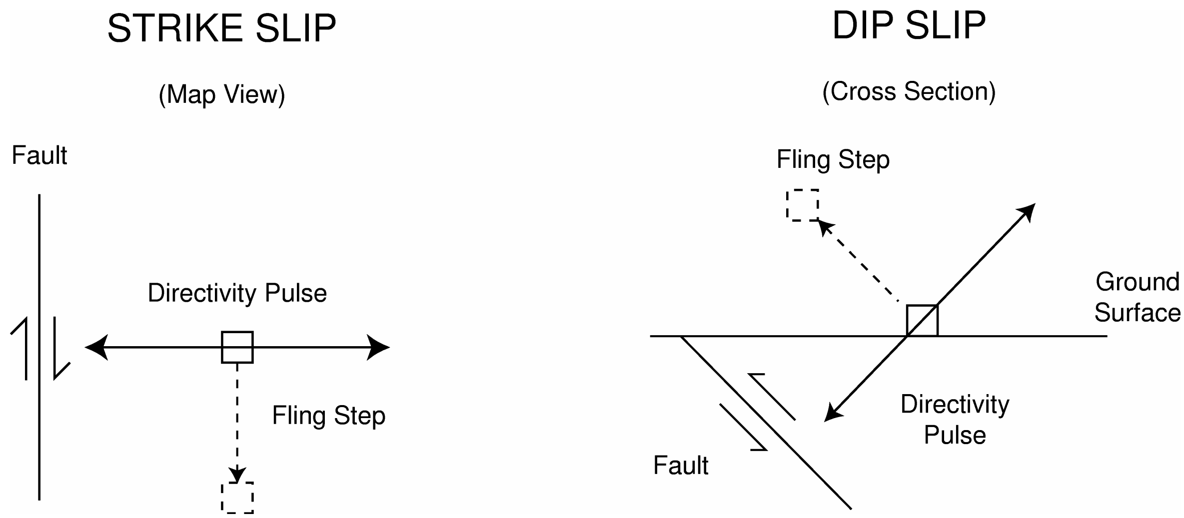

Fig. 4.3. Schematic diagram showing the orientations of fling step and directivity pulse for strike-slip and dip-slip faulting.

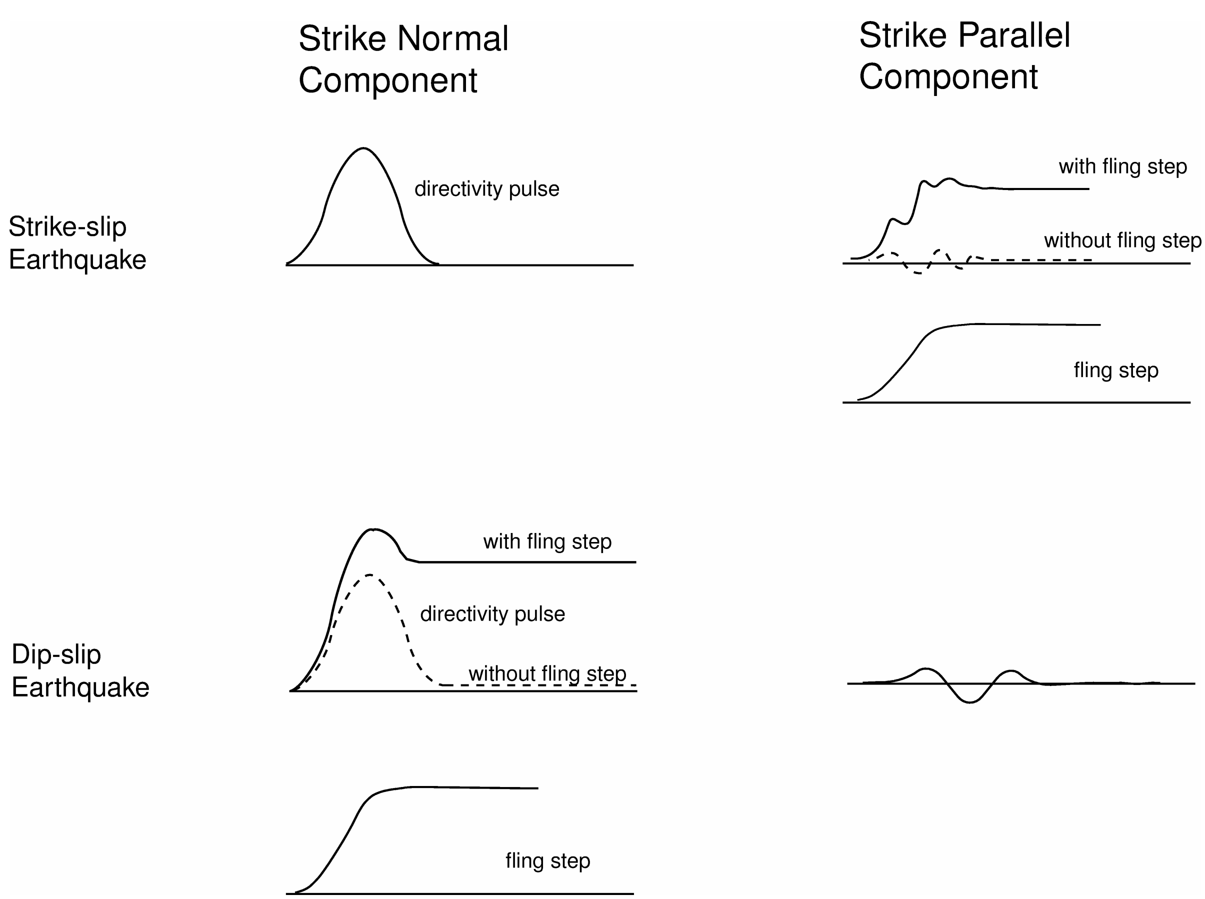

Fig. 4.4. Schematic diagram of time histories for strike-slip and dip-slip faulting in which the fling step and directivity pulse are shown together and separately.

The available strong motion data that can be used to quantify these effects are limited, although the recent earthquakes in Turkey and Taiwan have significantly supplemented the near-fault ground motion database. The remaining sections of this chapter describe currently available models for these near-fault effects and the steps required to incorporate these effects into hazard calculations. Rupture-directivity effects, with an emphasis on forward directivity, are discussed first, followed by fling step effects.

4.1.2 Parameterization of Near-Fault Ground Motion

Somerville et al. (1997a) parameterized the conditions that lead to forward and backward-directivity. As shown in Figure 4.5, the spatial variation of directivity effects depends on the angle between the direction of rupture propagation and the direction of waves traveling from the fault to the site (θ for strike-slip faults, and ϕ for dip-slip faults), and on the fraction of the fault rupture surface that lies between the hypocenter and the site (X for strike-slip faults and Y for dip-slip faults). More significant forward-directivity results from smaller angles between the site and fault and for larger fractions of ruptured fault between the site and hypocenter. It should be noted that even when the geometric conditions for forward directivity are satisfied, the effects of forward directivity may not occur. This could happen if a station is at the end of a fault and rupture occurs toward the station but slip is concentrated near the end of the fault where the station is located.

To account for directivity effects, Somerville et al. (1997a) correlated the residuals of response spectral ordinates (at 5% damping) to the geometric parameters defined in Figure 4.5, with the results shown in Figure 4.6. The ground motion parameters that are modified are the average horizontal response spectra and the ratios of fault-normal to fault-parallel response spectra. Details of the model are presented in Section 4.2.1. The 1997 UBC accounts for near-fault effects by means of near-source factors, N_a and N_v, applied to the low period (acceleration) and intermediate period (velocity) parts of the acceleration response spectrum, respectively. The near-source factors are specified for distances less than 15 km and for three different fault types (Table 4.1). The near-source factors in the UBC are compatible with the average of the fault-normal and fault-parallel components in the Somerville et al. (1997a) model, and hence, the code provisions do not address the larger fault-normal component of motion (Somerville, 1998).

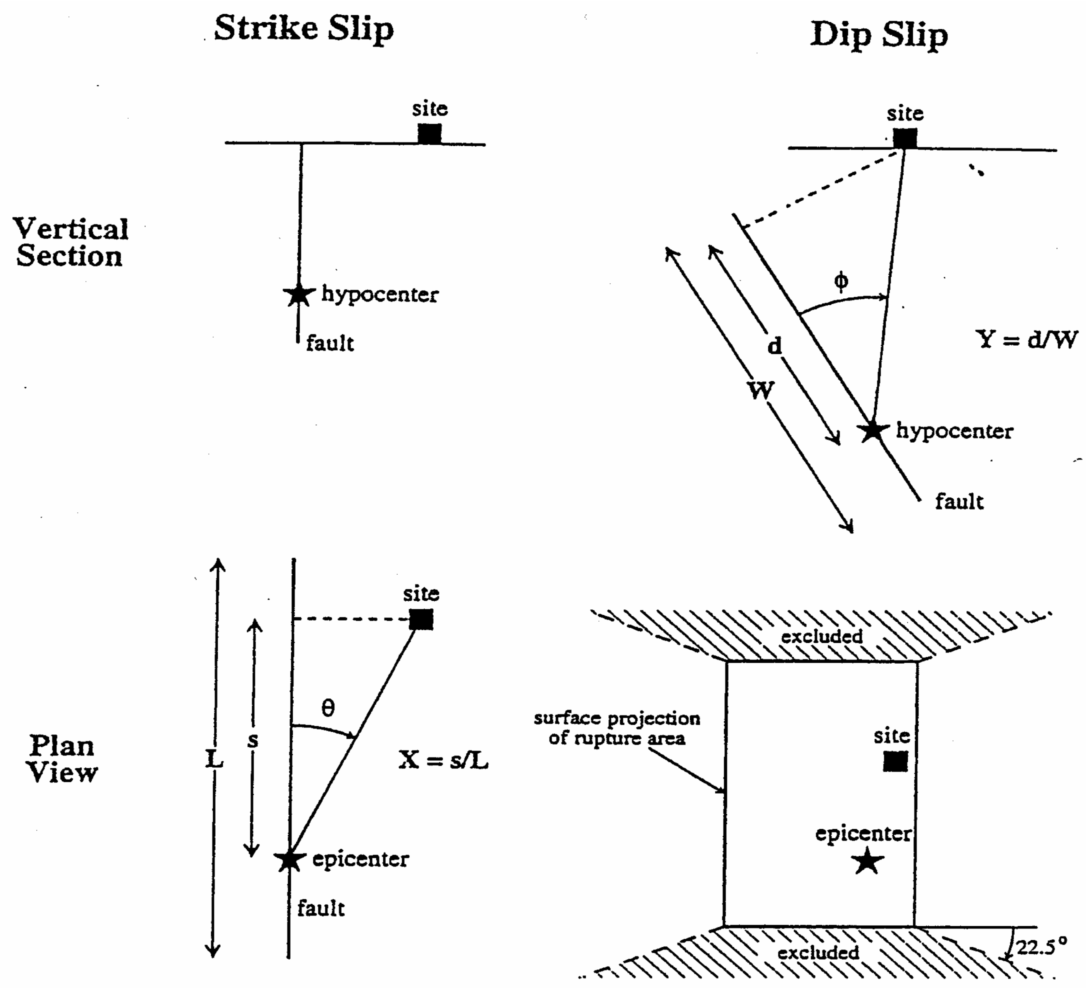

Fig. 4.5. Parameters used to define rupture-directivity conditions (adapted from Somerville et al. 1997a).

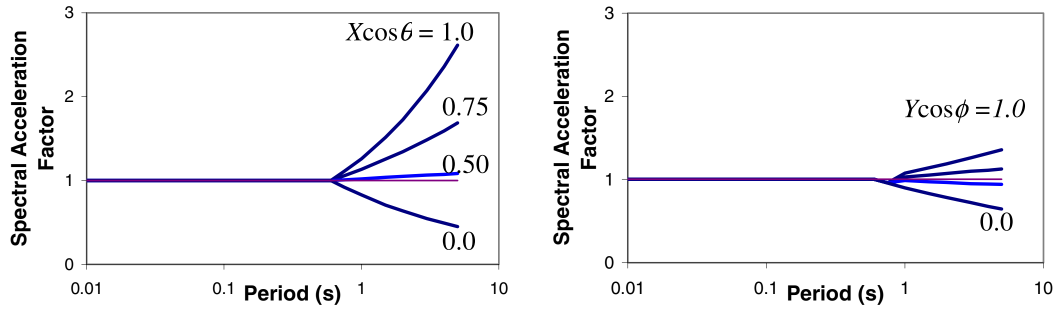

(a) Average response spectra ratio, showing dependence on period and on directivity parameters

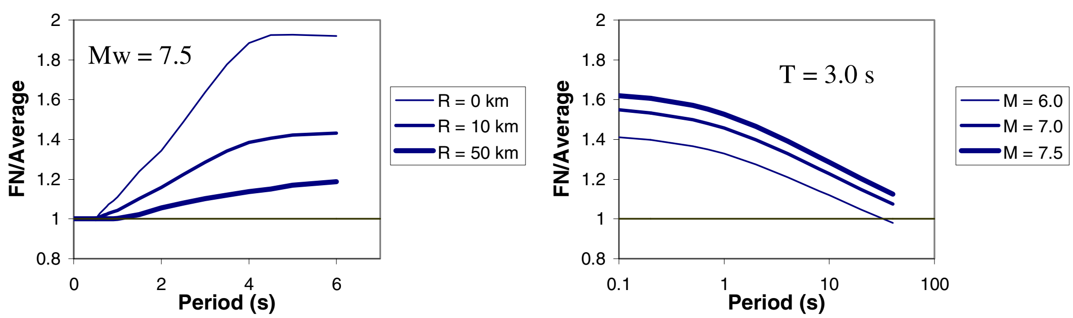

(b) Strike-normal to average horizontal response spectral ratio for maximum forward-directivity conditions ($X\cos\theta = 1$)

Fig. 4.6. Predictions from the Somerville et al. (1997a) relationship for varying directivity conditions.

Table 4.1. Near-source factors from the 1997 Uniform Building Code

(a) Short-period factor (N_a)

Seismic Source Type	Closest Distance to Known Seismic Source[1]		
	≤ 2 km	5 km	≥ 10 km
A	1.5	1.2	1.0
B	1.3	1.0	1.0
C	1.0	1.0	1.0

(b) Intermediate-period factor (N_v)

Seismic Source Type	Closest Distance to Known Seismic Source[1]			
	≤ 2 km	5 km	10 km	≥ 15 km
A	2.0	1.6	1.2	1.0
B	1.6	1.2	1.0	1.0
C	1.0	1.0	1.0	1.0

(c) Description of seismic source types

Seismic Source Type	Description	Seismic Source Definition	
		Maximum Moment Magnitude, m	Slip Rate, s (mm/year)
A	Faults that are capable of producing large magnitude events and that have a high rate of seismic activity	$m \geq 7.0$	$s \geq 5$
B	All faults other than Types A and C	$m \geq 7.0$ $m < 7.0$ $m \geq 6.5$	$s > 5$ $s > 2$ $s < 2$
C	Faults that are not capable of producing large magnitude earthquakes and that have a relatively low rate of seismic activity	$m < 6.5$	$s \leq 2$

[1] The closest distance to seismic source shall be taken as the minimum distance between the site and the surface projection of the fault plane. The surface projection need not include portions of the source at depths of 10 km or greater.

Research on the response of structures to near-fault motions has found a time history representation of the motions to be preferable to a response spectrum representation (e.g. Somerville, 1998; Alavi and Krawinkler, 2000; Sasani and Bertero, 2000; Rodriguez-Marek, 2000). A time history representation is preferable because the frequency-domain characterization of ground motion (i.e. through a response spectrum) implies a stochastic process having a relatively uniform distribution of energy throughout the duration of the motion. When the energy is concentrated in a few pulses of motion, the resonance phenomenon that the response spectrum was conceived to represent may have insufficient time to build up (Somerville, 1998).

Studies by Krawinkler and Alavi (1998) and Sasani and Bertero (2000) have shown that simplified representations of the velocity pulse can capture the salient response features of structures subjected to near-fault ground motions. Some simplified pulses are shown in Figure 4.7. The simplified sine-pulse representations of velocity time histories are defined by the number of equivalent half-cycles, the period of each half-cycle, and the corresponding amplitudes. To represent bidirectional shaking, a sine-pulse representation of the fault-parallel component is needed along with the time lag between initiation of the fault-normal and fault-parallel components. Table 4.2 provides definitions of common near-fault ground motion parameters, and these parameters are illustrated in Figure 4.8. A simple characterization is possible with the use of peak horizontal velocity (PHV), approximate period of the dominant pulse (T_v), and the number of significant half-cycles of motion in the (larger) fault-normal direction.

The definition of pulse period uses either the zero crossing time or the time at which velocity is equal to 10% of the peak velocity for this pulse. This is necessary for pulses preceded by a small drift in the velocity time history. A degree of subjectivity is involved in this definition and can lead to variations in estimates of T_v. However, the uncertainty associated with predicting T_v from seismological variables is much larger than the errors in estimating it from zero crossings. Krawinkler and Alavi (1998) identify the velocity pulse by a clear and global peak in the velocity response spectrum of the ground motion. Hence, this estimate of equivalent pulse period (T_{v-p}) is relatively unambiguous. For single-pulse motions, these different definitions of pulse period provide roughly equivalent results, but for more complex records, they can differ significantly. Overall, the ratio between T_v and T_{v-p} is 0.84 with a standard deviation of 0.28 (Rodriguez-Marek 2000). The coincidence of T_v and T_{v-p} for an earthquake ground motion indicates that the velocity pulse contains energy in a narrow period band.

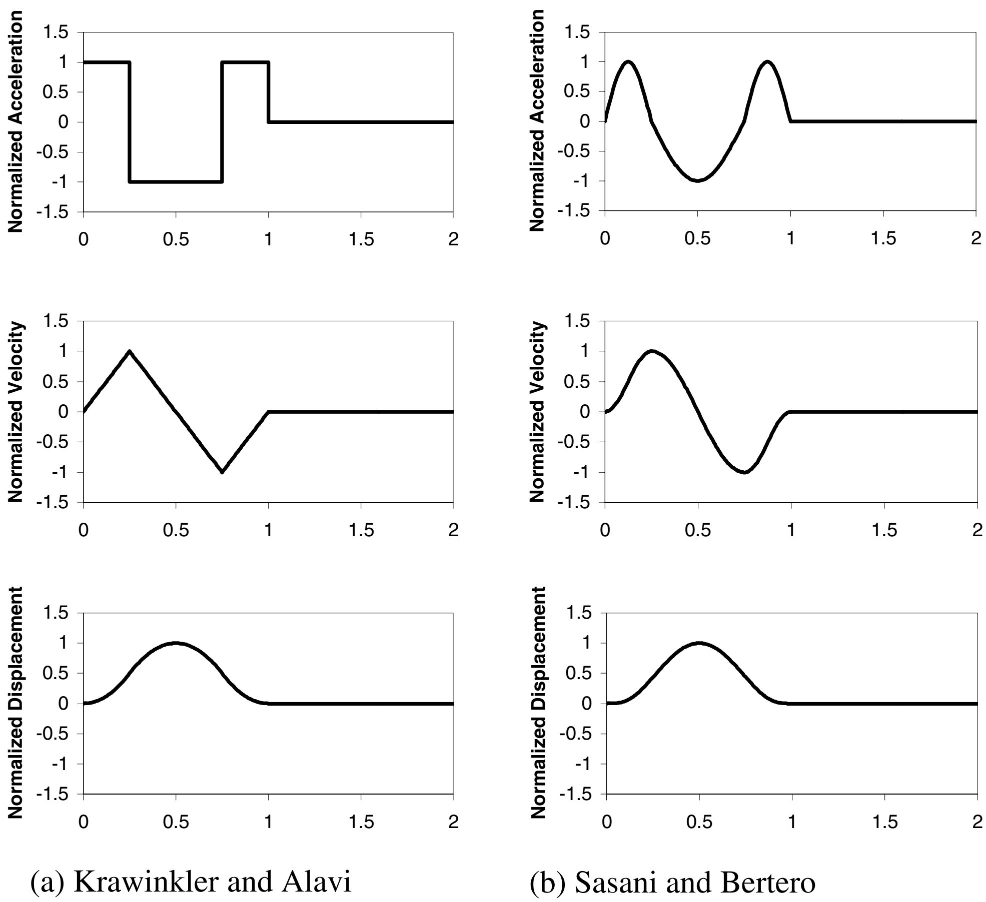

Fig. 4.7. Simplified pulses that have been used by some researchers.

Table 4.2. Parameters used to define the simplified sine-pulse ground motions (after Rodriguez-Marek 2000)

Parameter	Abbreviation	Methodology to obtain parameter
Number of significant pulses.	N	Number of half-cycle pulses in the velocity-time history with amplitudes at least 50% of the peak ground velocity of the record.
Pulse period.	$T_{v,i}$	For each half sine pulse, $T_{v,i} = 2\,(t_2 - t_1)$, where t_1 and t_2 are either the zero-crossing time, or the time at which velocity is equal to 10% of the peak velocity for the pulse if this time is significantly different than the zero crossing time. T_v corresponding to the pulse with maximum amplitude is the overall representative velocity pulse period.
Predominant period from pseudo-velocity response spectra.	$T_{p\text{-}v}$	Period corresponding to a clear and global peak in the pseudo-velocity response spectra at 5% damping.
Pulse amplitude.	A_i	For each half sine pulse, the peak ground velocity in the time interval $[t_1, t_2]$.
Peak ground velocity	PHV	Maximum velocity, defined by the maximum value of A_i. Note, however, that in very few exceptions, the maximum value of A_i in the fault parallel direction does not occur concurrently with the fault normal pulse.
Ratio of fault parallel to fault normal amplitude	$PHV_{P/N}$	Defined by the ratio of maximum A_P divided by maximum A_N, where the subscripts P and N denote fault-parallel and fault-normal motions respectively.
Time delay between fault normal and fault parallel pulse	t_{off}	Time of initiation of fault parallel pulse minus the time of initiation of fault normal pulse.

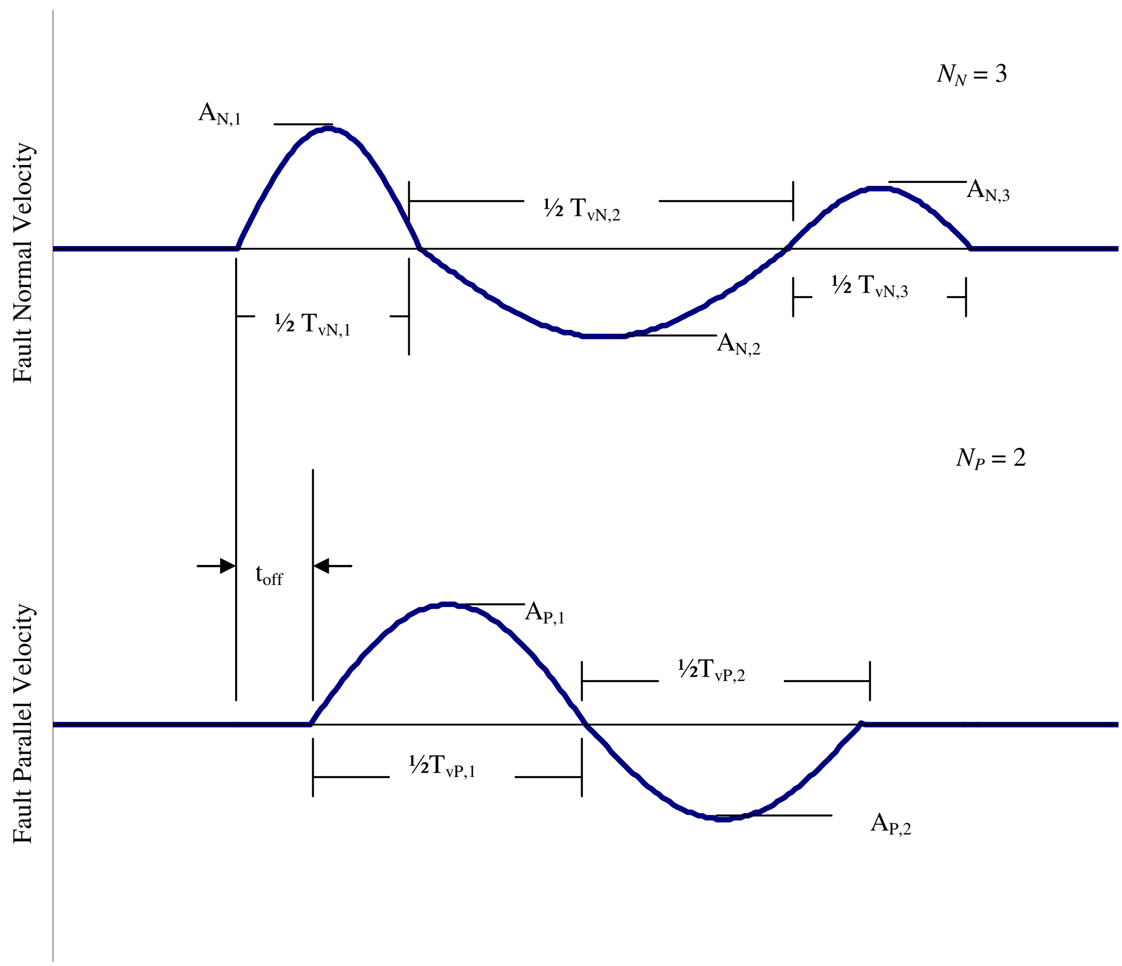

Fig. 4.8. Parameters needed to define the fault-parallel and fault-normal components of simplified velocity pulses. Subscripts *N* and *P* indicate fault-normal and fault-parallel motions, respectively (from Rodriguez-Marek 2000).

Studies of structural response to near-fault motions have focused on the effects of the larger fault-normal component (e.g. Alavi and Krawinkler 2000). However, there are applications for which the fault-parallel motion may also be important. For example, the softening of soil stiffness in response to the large fault-normal component of motion will allow more strain to develop in the fault-parallel direction as the soil responds to the fault-parallel component of motion. Nonlinear bidirectional soil response analyses by Rodriguez-Marek (2000) indicate that local soil conditions can affect values of PHV and T_v in both directions. Two near-fault motions with significantly different fault-parallel motions are shown in Figure 4.9. These differences can be depicted with the horizontal velocity trace plot on the right side of the figure. Additional research is warranted to discern the effects of bidirectional shaking on soil and structural response in the near-fault zone where the two components of horizontal ground motion can differ significantly. An examination of recorded near-fault motions exhibiting forward directivity by Rodriguez-Marek (2000) found that the simplified motions shown in Figure 4.10 could be used to investigate the importance of bidirectional shaking in future studies. If important to structural performance, vertical motions in the near-fault zone may need to be estimated as well.

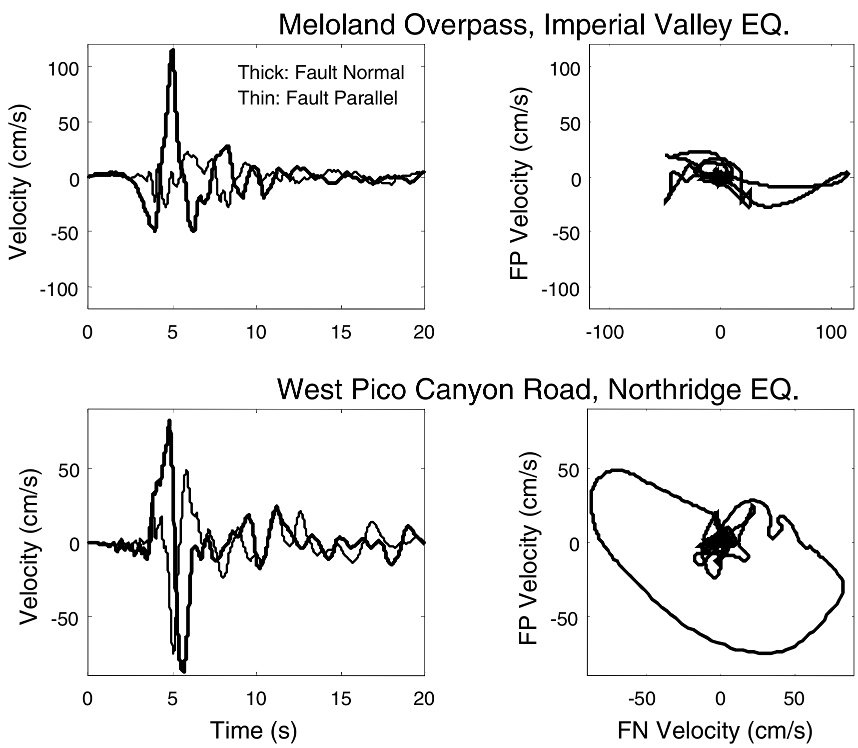

Fig. 4.9. Fault-normal (FN) and fault-parallel (FP) velocity time histories and horizontal velocity trace plots for two near-fault recordings. Both recordings have significant fault-normal velocities, but the Meloland has lower relative FP velocities.

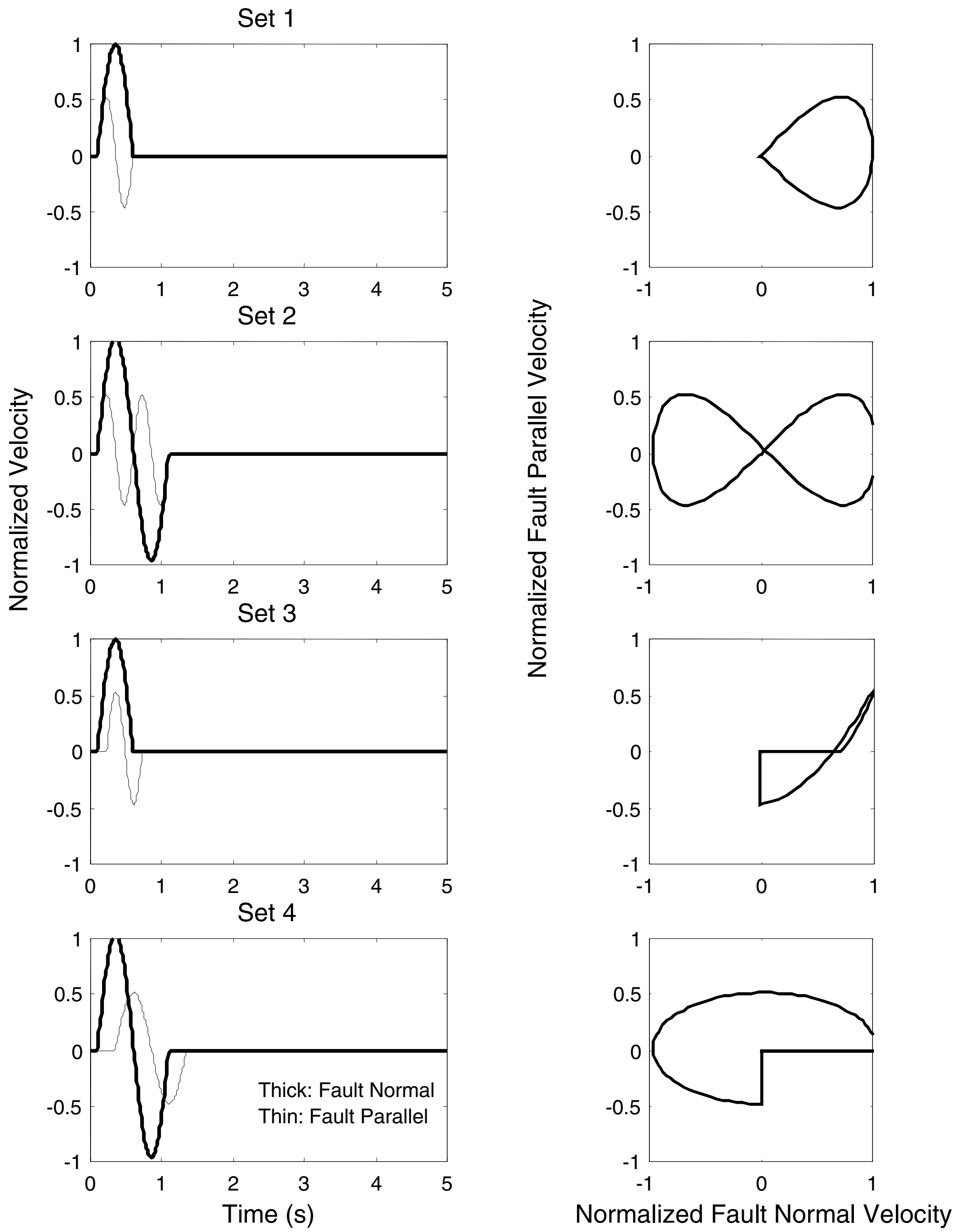

Fig. 4.10. Simplified sine-pulse representation of near-fault ground motions. The fault-parallel PHV is set to 50% of the fault-normal PHV (from Rodriguez-Marek 2000).

4.2 RUPTURE-DIRECTIVITY EFFECTS

4.2.1 Available Models

(a) *Spectral acceleration*

Somerville et al. (1997a) and Abrahamson (2000) have presented models for the modification of 5%-damped response spectral ordinates from the Abrahamson and Silva (1997) attenuation relationship. The models were developed by regressing the residuals of this attenuation relationship to the near-fault geometric parameters indicated in Figure 4.5. Models are presented for modification of the geometric mean of both horizontal components and the ratio of fault-normal/average horizontal spectral ordinates. Details of the models are indicated in the top two rows of Table 4.3.

(b) *Duration and equivalent number of uniform stress cycles*

Somerville et al. (1997a) presented a model for the modification of 5-75% significant duration from the Abrahamson and Silva (1996) attenuation relationship. The model was developed by regressing the residuals of this attenuation relationship to the near-fault geometric parameters indicated in Figure 4.5. The model applies to the duration of the geometric mean of both horizontal components. A similar model was developed by Liu et al. (2001) for equivalent number of uniform stress cycles (*N*). Details of the duration and *N* models are indicated in the bottom two rows of Table 4.3.

Table 4.3. Modification to ground motion parameters to account for directivity effects. Parameters X, Y, θ, and ϕ are defined in Figure 4.5, along with exclusion zones for strike-slip faults. The modifications to spectra are illustrated in Figure 4.6. The reader is referred to the references indicated for the standard deviations and period-dependent coefficients.

Ground Motion Parameter (Reference)	Description	Equation	Range of Applicability
Spectral Acceleration: Ratio of data/model (Somerville et al., 1997a; Abrahamson, 2000)	y=Bias in average horizontal response spectral acceleration (ln units) with respect to Abrahamson and Silva (1997)	Strike-Slip faults: $y = c_1 + 1.88c_2\,X\cos\theta$ ($X\cos\theta \leq 0.4$) $y = c_1 + 0.75c_2$ ($X\cos\theta > 0.4$) Dip-Slip faults: $y = c_1 + c_2\,Y\cos\phi$	$m > 6.5$ For $m < 6.5$, replace y with $T_m \times y$ Where $T_m = 0$ for $m \leq 6$ and $T_m = 1+(m-6.5)/0.5$ for $6.5 > m > 6$ $r < 30$ km For $r > 30$, replace y with $T_d \times y$ Where $T_d = 0$ for $r > 60$ and $T_d = 1-(r-30)/30$ for $60 > r > 30$ km
Spectral Acceleration: Ratio of Strike Normal/Average Amplitude (Somerville et al., 1997a)	Natural logarithm of the ratio of strike normal to average horizontal spectral acceleration	$y = \cos 2\xi\,[C_1 + C_2 \ln(r+1) + C_3(m-6)]$	$6.0 \leq m \leq 7.5$ $0 \leq r \leq 50$ km $\xi = \theta$ for strike-slip, ϕ for dip-slip. $0 < \xi < 90°$ C_1, C_2, C_3 function of period. Given separately for cases in which dependence on ξ is included, and cases in which dependence on ξ is ignored.
5-75% sig. duration: Ratio of data/model (Somerville et al., 1997a)	Bias in duration of acceleration with respect to Abrahamson and Silva (1996)	Strike-Slip faults: $y = C_1 + C_2\,X\cos\theta$ Dip-Slip faults: $y = C_1 + C_2\,Y\cos\phi$	$6.5 \leq m \leq 7.5$ $0 \leq r \leq 20$ km
Number of Cycles (N): Ratio of data/model (Liu et al., 2001)	Bias in N with respect to Liu et al. (2001)	Strike-Slip faults: $y = C_1 + C_2\,X\cos\theta$ Dip-Slip faults: $y = C_1 + C_2\,Y\cos\phi$	$6.5 \leq m \leq 7.5$ $0 \leq r \leq 20$ km

(c) *Peak horizontal velocity*

PHV is significantly affected by magnitude, distance, and site condition. Somerville (1998) proposed the use of a bilinear relationship between the logarithm of PHV, magnitude, and the logarithm of distance. Somerville (1998) performed a regression analysis using data from 15 recorded time histories augmented by 12 simulated time histories. The records correspond to a m = 6.2-7.5 and r=0-10 km. To avoid unrealistic predictions of PHV at short distances, Somerville (1998) used a distance cutoff of 3 km. The Somerville (1998) relationship for PHV in the near-fault zone is

$$\ln(\mathrm{PHV}) = -2.31 + 1.15\, m - 0.5 \ln(r) \tag{4.1}$$

where r is the closest distance to the ruptured fault but is constrained to be at least 3 km. A similar study relating PHV to moment magnitude and distance in the near-fault zone was presented by Alavi and Krawinkler (2000) based on the same data set used by Somerville (1998). The Alavi and Krawinkler (2000) PHV relationship is

$$\ln(\mathrm{PHV}) = -5.11 + 1.59\, m - 0.58 \ln(r) \tag{4.2}$$

Rodriguez-Marek (2000) performed regression analyses using 48 velocity time histories from 11 events. The data was for sites with site-source distances r < 20 km and m = 6.1-7.4. Separate analyses were performed for motions recorded at rock and soil sites, as well as for all sites. Based on the analysis of these records, the following relationship for PHV was proposed

$$\ln(\mathrm{PHV}) = a + b\, m + c \ln(r^2 + d^2) + \eta_i + \varepsilon_{ij} \tag{4.3}$$

where PHV is in units of cm/s, a, b, c and d are the model parameters, r is the closest distance to the fault, m is moment magnitude, η_i is the inter-event term, and ε_{ij} represent the intra-event variations with j representing the individual recording and i representing the event. The inter-event and the intra-event error terms are assumed to be independent normally distributed random variables with variances τ^2 and σ^2, respectively. The standard error associated with the estimate of PHV is then

$$\sigma_{total}^2 = \tau^2 + \sigma^2 \tag{4.4}$$

The values of the model parameters are presented in Table 4.4.

Table 4.4. Parameters from the regression analyses for PHV (Rodriguez-Marek 2000)

Data Set	*a*	*b*	*c*	*d*	σ	τ	σ_{total}	$Var(\sigma^2)$	$Var(\tau^2)$	$Cov(\sigma^2,\tau^2)$
All Motions	2.44	0.50	-0.41	3.93	0.47	0.41	0.62	0.0026	0.011	8.2e-4
Rock	1.46	0.61	-0.38	3.93	0.53	0.25	0.59	0.023	0.019	-0.0120
Soil	3.86	0.30	-0.42	3.93	0.43	0.41	0.59	0.014	0.0026	8.6e-4

Figure 4.11 compares the relationship for all sites recently proposed by Rodriguez-Marek (2000) with those previously developed by Somerville (1998) and Alavi and Krawinkler (2000). The relationships differ mainly in the magnitude scaling term. Somerville (1998) and Alavi and Krawinkler (2000) propose a much stronger variation of PHV with magnitude. The variation cannot be attributed to the addition of the simulated time histories because Somerville (1998) indicates that the PHV of the recorded time histories grows more rapidly with magnitude than for the simulated time histories. The differences are likely due to the larger amount of data included in the most recent study.

(d) *Pulse period*

The Somerville (1998) relationship for pulse period is

$$\log_{10} T_v = -2.5 + 0.425\, m \tag{4.5}$$

where T_v is the period of the largest cycle of motion and m is moment magnitude. In a larger study of slip distributions using slip models for 15 earthquakes, Somerville et al. (1999) provide justifications for the use of self-similar scaling relationships to constrain fault parameters. In a self-similar system, events of different sizes cannot be distinguished except by a scale factor. Using this self-similar scaling model, the magnitude scaling in the above relationship is 0.5 and the resulting equation is

$$\log_{10} T_v = -3.0 + 0.5\, m \tag{4.6}$$

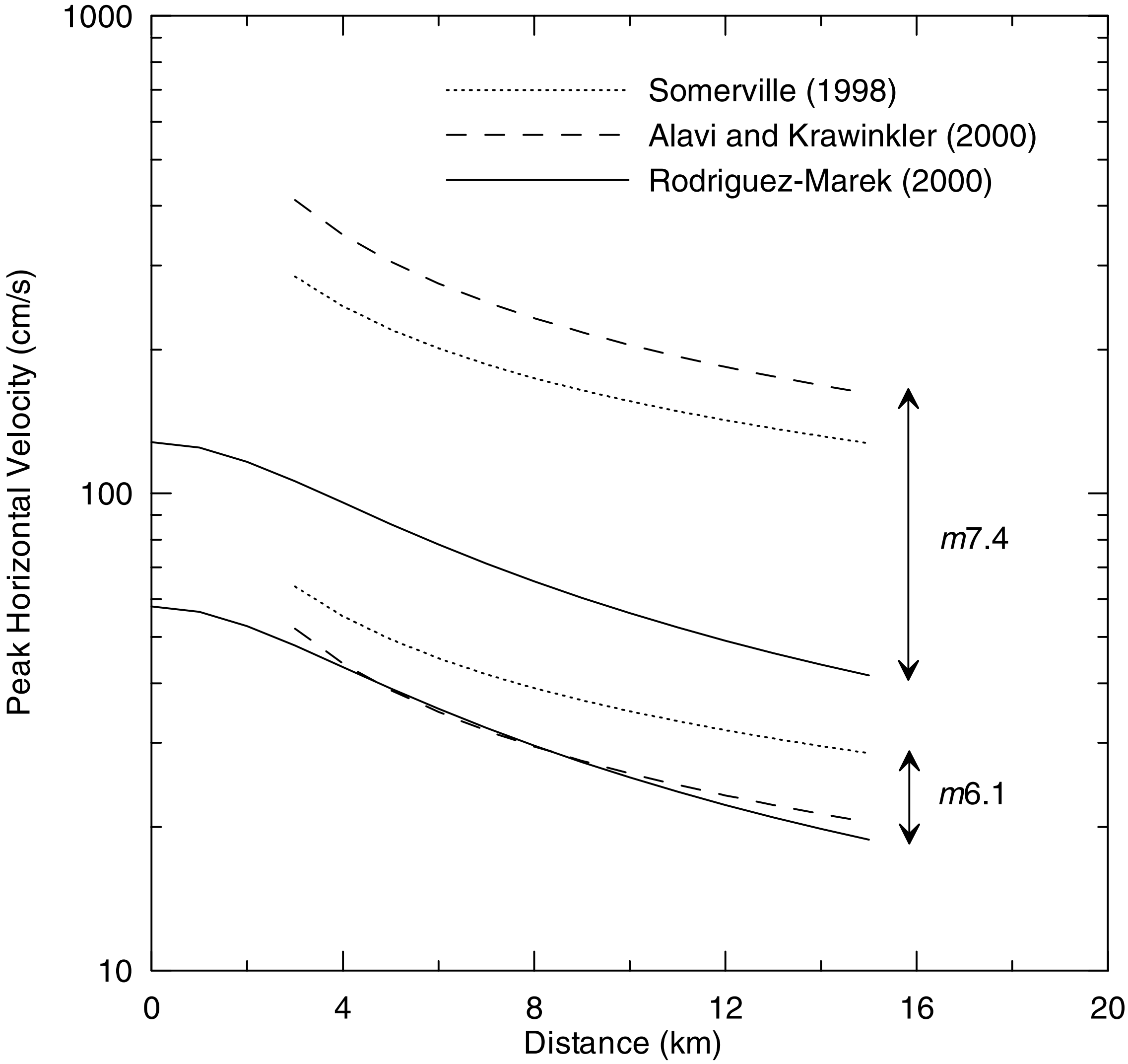

Rodriguez-Marek (2000):

$$\ln(\text{PHV}) = 2.44 + 0.5\,m - 0.41\,\ln(r^2 + 3.93^2)$$

Somerville (1998):

$$\ln(\text{PHV}) = -2.31 + 1.15\,m - 0.5\,\ln(r)$$

Alavi and Krawinkler (2000):

$$\ln(\text{PHV}) = -5.11 + 1.59\,m - 0.58\,\ln(r)$$

Fig. 4.11. Comparison of results from regression analysis for PHV with relationships proposed by other researchers for a database of near-fault, forward-directivity motions (from Rodriguez-Marek 2000).

The period of the velocity pulse is associated with the rise time of slip on the fault (T_R), which measures the duration of slip at a single point on the fault. The relationship between pulse period and rise time is (Somerville 1998):

$$T_v = 2.2\ t_r \tag{4.7}$$

The relationship between pulse duration and rise time can also be inferred from the physics of the fault rupture phenomenon. If a fault is modeled as a point and propagation effects are ignored, the duration of motion would be equal to the rise time (Somerville 1998). Fault finiteness and propagation effects contribute to widening of the pulse. Rise time is then, in essence, a lower bound for pulse period.

Alavi and Krawinkler (2000) defined the pulse period as the predominant period in a velocity response spectrum plot ($T_{v\text{-}p}$). Their relationship using this definition for pulse period is

$$\log_{10} T_{v\text{-}p} = -1.76 + 0.31\ m \tag{4.8}$$

Rodriguez-Marek (2000) developed the following relationship for pulse period:

$$\ln(T_v)_{\mathrm{ij}} = a + bm + \eta_{\mathrm{i}} + \varepsilon_{\mathrm{ij}} \tag{4.9}$$

where $(T_v)_{\mathrm{ij}}$ is the pulse period of the j^{th} recording from the i^{th} event, a and b are the model parameters, η_{i} is the inter-event term, and $\varepsilon_{\mathrm{ij}}$ represent the intra-event variations. Estimates are provided for both the pulse period, T_v, and the predominant period of the velocity spectrum, $T_{v\text{-}p}$. The values of the model parameters are presented in Table 4.5. The relationship is valid for m = 6.1-7.4 and for r < 20 km. The inter-event and the intra-event error terms are assumed to be independent normally distributed random variables with variances τ^2 and σ^2, respectively. The standard error associated with the estimate of T_v is then defined by Equation 4.4.

The recently proposed Rodriguez-Marek (2000) relationship is compared with those by Somerville (1998) and Alavi and Krawinkler (2000) in Figure 4.12. The Rodriguez-Marek (2000) relationships for T_v and $T_{v\text{-}p}$ predict systematically lower pulse periods than that of Somerville (1998) for T_v and that of Alavi and Krawinkler (2000) for $T_{v\text{-}p}$. The differences in the predictions are not likely significant for most cases due to the large uncertainties involved in estimating pulse period, especially for larger magnitude events (m > 7.0) where the regression lines are fairly close to each other.

Table 4.5. Parameters from the regression analyses for the period of the pulse of maximum amplitude, T_v, and the period corresponding to the maximum pseudo-velocity response spectral value, $T_{v\text{-}p}$ (Rodriguez-Marek 2000)

(a) T_v

Data Set	***a***	***b***	σ	τ	σ_{total}	$Var(\sigma^2)$	$Var(\sigma^2)$	$Cov(\sigma^2,\tau^2)$
All Motions	-8.33	1.33	0.36	0.40	0.54	0.0008	0.0078	-0.0003
Rock	-11.10	1.70	0.31	0.41	0.51	0.0029	0.0140	-0.0018
Soil	-5.81	0.97	0.32	0.40	0.51	0.0008	0.0100	-0.0003

(b) $T_{v\text{-}p}$

Data Set	***a***	***b***	σ	τ	σ_{total}	$Var(\sigma^2)$	$Var(\sigma^2)$	$Cov(\sigma^2,\tau^2)$
All Motions	-6.92	1.08	0.48	0.45	0.66	0.0028	0.0154	-0.0009
Rock	-9.53	1.42	0.37	0.61	0.71	0.0062	0.0555	-0.0041
Soil	-5.66	0.91	0.41	0.45	0.61	0.0022	0.0181	-0.0008

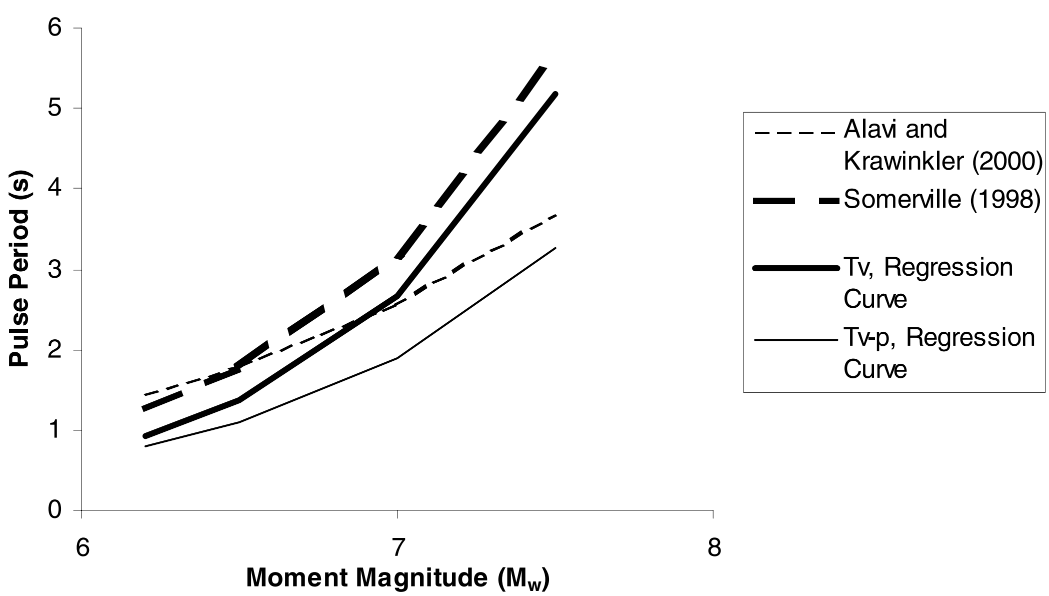

Fig. 4.12. Comparison of Rodriguez-Marek (2000) model with those proposed by Somerville (1998) for pulse period (T_v) and by Alavi and Krawinkler (2000) for the period of the maximum pseudo-velocity response spectral value ($T_{v\text{-}p}$) (from Rodriguez-Marek 2000).

The effect of site conditions can be investigated through the use of the Rodriguez-Marek (2000) pulse-period relationships for rock and soil. In Figure 4.13 the median and median ± one standard deviation values for pulse period as a function of *m* are shown for rock and soil site conditions. The difference between pulse period values at rock and soil sites is indistinguishable for large magnitude events ($m > 7$), but the pulse period is notably greater at soil sites than for rock sites for events with lower magnitudes. Examination of paired rock and soil stations and the results of nonlinear site response analyses confirm this observation (Rodriguez-Marek 2000).

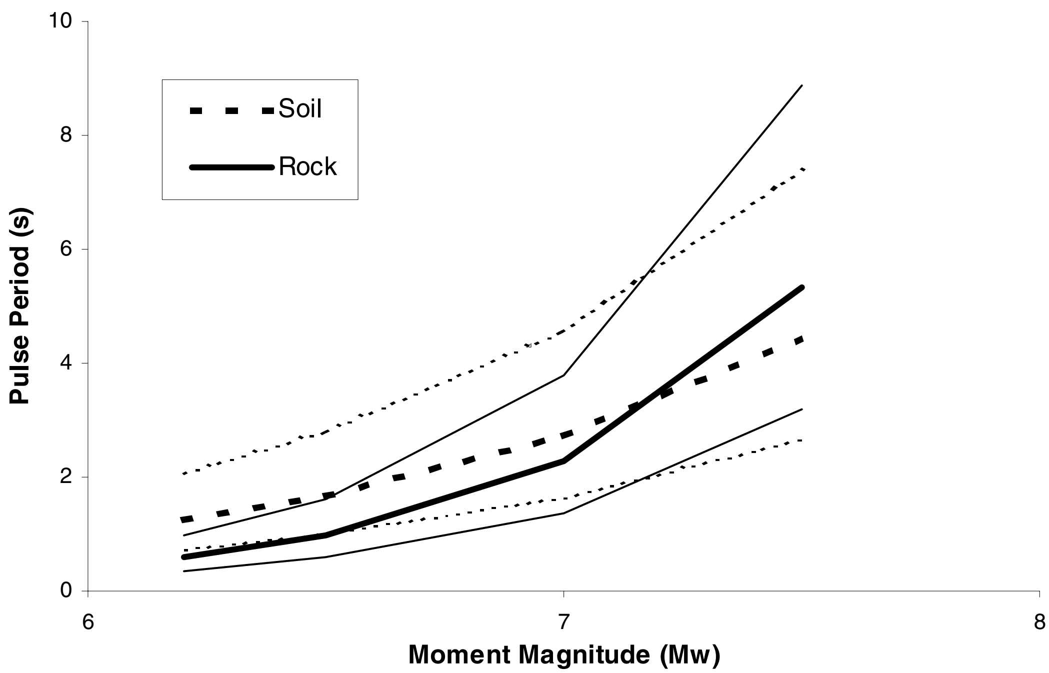

Fig. 4.13. Rodriguez-Marek (2000) model predictions for pulse period (T_v) for rock and soil site conditions. The bold lines represent the median and the lighter lines indicate the one standard deviation band (from Rodriguez-Marek 2000).

(e) *Number of significant pulses*

The number of half-cycles of motion (referred to as the number of significant pulses, N_v) is defined as the number of half-cycle velocity pulses that have amplitudes at least 50% of the peak ground velocity of the ground motion (Table 4.3). For evaluating the number of significant velocity pulses, only the fault-normal component of motion is considered. The 50% level chosen as a cutoff is arbitrary, and the number of significant pulses is somewhat sensitive to this value. The number of significant pulses in the fault-normal component of 48 near-fault records is presented in Table 4.6. Most records contain two significant pulses (i.e., one full cycle of pulse-type ground motion). Somerville (1998) suggests that the number of half sine pulses in the velocity time history might be associated with the number of asperities in a fault, which in turn is associated with fault slip distribution. This of course is a difficult phenomenon to estimate a priori. There are no models currently available for predicting the number of significant pulses in the velocity time history. For most cases, N_v will vary between 1 and 3, with $N_v = 2$ being a good general value to use in seismic evaluations.

Table 4.6. Number of half-cycle pulses (N_v) by event for 48 near-fault motions (fault-normal component). Value in parenthesis is the number of half-cycle pulses that corresponds to a cut-off value of 33% of the PHV (as opposed to 50% used to define N_v). From Rodriguez-Marek (2000).

Earthquake	Year	Number of Records	Number of Records with given number of half-cycle pulses (N_v)			
			1 pulse	2 pulses	3 pulses	> 3 pulses
Parkfield	66	2	0 (0)	1 (1)	0 (0)	1 (1)
San Fernando	71	1	1 (0)	0 (0)	0 (1)	0 (0)
Imperial Valley	79	13	1 (0)	10 (1)	1 (7)	1 (5)
Morgan Hill	84	2	0 (0)	0 (0)	1 (0)	1 (2)
Superstition Hills(B)	87	2	1 (0)	1 (1)	0 (0)	0 (1)
Loma Prieta	89	8	0 (0)	4 (0)	1 (1)	3 (7)
Erzincan, Turkey	92	1	0 (0)	0 (0)	1 (1)	0 (0)
Landers	92	1	1 (0)	0 (1)	0 (0)	0 (0)
Northridge	94	10	3 (0)	4 (4)	3 (2)	0 (4)
Kobe	95	4	0 (0)	1 (0)	0 (1)	3 (3)
Kocaeli,Turkey	99	4	0 (0)	3 (2)	0 (0)	1 (2)
Totals		48	7 (0)	24 (10)	7 (13)	10 (25)

4.2.2 Incorporation of Directivity into Hazard Analyses

Recently proposed relationships by Rodriguez-Marek (2000) include quantification of the uncertainty involved in predicting the effects of rupture-directivity. With these models, directivity can be incorporated into hazard analyses. However, uncertainties associated with these models are large, and additional work incorporating recent near-fault recordings, especially those from the 1999 Chi-Chi earthquake, are warranted. Additional studies are also needed to ensure that the near-fault ground motion parameters identified above provide a suitable representation of seismic demand for application to the nonlinear response of structures.

4.3 FLING STEP EFFECTS

The effects of fling step ground motions on the structural performance of buildings have received less attention than the effects of rupture-directivity. Recent earthquakes in Turkey and Taiwan have highlighted the importance of permanent ground deformation associated with surface rupture on the performance of buildings and lifelines that cross, or are situated close to, active fault traces. The effects of surface fault rupture are commonly evaluated as pseudo-static ground deformations that are decoupled from the ground shaking hazard. Distinct offsets across ruptures, differential settlement, ground warping, ground cracking, and extensional and compressional horizontal ground strains are the focus of these evaluations, as differential ground movements and ground strains are most damaging to overlying structures. As pointed out by numerous researchers (e.g., Byerly and DeNoyer 1958, Bonilla 1970, Bray et al. 1994, and Lazarte et al. 1994), significant ground deformation can occur away from the primary trace of the ruptured fault, so tectonic deformation associated with surface fault rupture can affect structures located some distance from the fault (although there are also many cases where relative ground displacements are restricted to a fairly narrow zone along the main fault trace). Bray (2001) summarizes the hazards associated with surface fault rupture, analytical procedures used to evaluate these hazards, and design methods that can be employed to mitigate these hazards. Our focus in this section is on the dynamic occurrence of these ground offsets near faults, i.e., fling step ground motions.

Fling step, being a result of a static ground displacement, is generally characterized by a uni-directional velocity pulse and a monotonic step in the displacement time history. The discrete step in the displacement time history occurs parallel to the direction of fault slip (i.e., along strike for strike-slip events and along dip for dip-slip events). To gain a sense of the magnitude of the fling step displacement that may be present in near-fault records, the compilation of empirical data by Wells and Coppersmith (1994) provides a useful starting point. For all fault types, the maximum fault displacement (*MD*) in meters can be related to the moment magnitude (*m*) of the event through the regression equation

$$\log_{10}(MD) = -5.46 + 0.82\, m \tag{4.10}$$

where the standard deviation for this estimate is 0.42 (in $\log_{10}$ units). The magnitude range over which Eq. 4.10 applies is m=5.2-8.1, and the range of *MD* is 0.01 m to 14.6 m. The estimate of fault displacement is somewhat dependent on fault type, and regression coefficients are given for strike-slip and normal faults separately in Wells and Coppersmith (1994). Regressions on reverse fault data set were not statistically significant. The maximum fault displacement occurs at one point along the fault with the amount of fault displacement varying along the fault trace. The average fault displacement (*AD*) for all fault types is

$$\log_{10}(AD) = -4.80 + 0.69\, m \tag{4.11}$$

where the standard deviation for this estimate is 0.36 (in $\log_{10}$ units). The magnitude range for these events is m=5.6-8.1. In general, the average displacement along the surface fault rupture is about half of the maximum displacement, although this ratio varies significantly.

Permanent ground surface displacement resulting from fault rupture can vary significantly with distance away from the fault trace. Tectonic displacement away from the fault can be localized on secondary fault traces and on other discontinuities. Relative movement across distinct surface ruptures is most damaging to structures, but as mentioned previously, this is outside the scope of this report. To provide a very approximate sense of amount of tectonic deformation that may occur away from the primary surface rupture, and hence be seen as a fling step effect in a displacement time history, findings from a study by Byerly and DeNoyer (1958) are presented. The tectonic displacement from the 1906 San Francisco earthquake ($m \approx 7.8$) was measured by geodetic surveys, and from these surveys Byerly and DeNoyer (1958) developed a model to quantify the amount of tectonic displacement (*TD*) in a general sense as a function of the distance from the primary fault trace. Their model, which is only appropriate for this event in this geologic setting, is

$$TD = 194 \cot^{-1}(0.325\, r_\perp) \tag{4.12}$$

where *TD* is the amount of tectonic displacement in cm and $r_\perp$ is the distance from the fault trace (in km) measured perpendicular to the strike. This relationship was developed using a maximum fault displacement at the fault trace of about 300 cm. For smaller magnitude events with lower values of maximum fault displacement at the fault trace, this relationship would need to be revised accordingly. As stated previously, the problem is more complex than this model would suggest, and it is presented here only to provide a sense of the order of the fling step displacement that may occur at a site located away from the fault trace. Surveys of the tectonic deformation resulting from other events with surface fault rupture, such as the 1999 Kocaeli and Chi-Chi earthquakes, will likely yield important data in this regard.

4.4 SYNTHESIS OF PEER RESEARCH

Through projects in both the Core and Lifelines programs, PEER researchers have been actively involved in developing the state of the art in near-fault ground motion characterization. In the Core Program, the work has focused on identifying critical intensity measures for nonlinear structural response in forward-directivity regions (discussed in Section 4.1), and in the development of engineering models for estimating intensity measures in these regions (Section 4.2). The projects in which the cited work was performed include

- Near-Fault Site Effects (Thrust Area 2, PI: Bray)
- Seismic Demands for Performance-Based Design (Thrust Area 3, PI: Krawinkler)

It should be noted that several additional projects in Thrust Area 5 have investigated the capacities of components or systems subjected to large velocity pulses. Mahin discusses these studies in a companion PEER synthesis report (in preparation).

The Lifelines Program has engaged in a research program seeking to enhance the limited empirical strong motion data set for near-fault effects with synthetic waveforms from simulations. The first component of this work was completed in Phase II of the Lifelines Program. In this work, three leading simulation codes were calibrated against existing near-fault data (PIs: Graves, Silva, Zeng). A thorough discussion of this work is provided in Chapter 6. Work currently in progress (Lifelines Projects 1D) is exploring the possibility of developing physical models for rupture-directivity. Future work will use the calibrated analysis tools and physical model results to provide synthetic "data" that can be used to supplement the empirical data set. This enhance data set will lead to improved models for near-fault ground motions, both in terms of directivity-pulse and fling step effects.

5 SITE EFFECTS

5.1 OVERVIEW

The ground motion attenuation relationships presented in Chapter 3 provide estimates of intensity measures that apply for a given site condition, which is typically defined as rock or soil. Actual conditions at strong motion recording sites are highly variable with respect to local geotechnical conditions, possible basin effects, and surface topography, and hence estimates from attenuation relationships necessarily represent averaged values across the range of possible site conditions. The intent of this chapter is to describe various means by which information on site conditions can be used to improve the accuracy of ground motion predictions, i.e., improve the estimate of $f(IM|m,r,S)$, where m=magnitude, r=site-source distance, and S=vector of site condition descriptors. This "improvement" in ground motion prediction generally involves (1) removing potential bias in median ground motion estimates and (2) reducing the uncertainty in ground motion estimates, as measured by standard error term, σ.

The term "site effects" means different things to different audiences. We take the term to represent local ground response, basin effects, and the influence of surface topography. The definition of surface topography is obvious. "Local ground response" refers to the influence of relatively shallow geologic materials on (nearly) vertically propagating body waves. These effects are ideally modeled using the full soil profile, but for deep alluvial basins the modeling domain generally does not extend beyond depths of 100-200 m. The term "basin effects" refers to the influence of two- or three-dimensional sedimentary basin structures on ground motions, including critical body wave reflections and surface wave generation at basin edges. Seismological models for basin effects are typically of a much larger scale than engineering models of local ground response. Where basin effects "end" and local ground response effects "begin" is somewhat ambiguous. For this report we define local ground response effects as representing essentially the one-dimensional response of the soil column (which is often modeled in practice using only the upper several hundred meters), and basin effects as producing ground motions that deviate from the predictions of one-dimensional models as a result of relatively complex wave propagation in basins.

The chapter begins with a review of observational studies of site amplification. Because these studies utilize actual field data, the identified amplification factors incorporate both ground response and basin effects to varying degrees (topographic effects are generally minimal, as most sites are nearly level). Subsequent sections focus specifically on one-dimensional ground response, basin effects, and topographic effects.

5.2 OBSERVATIONAL STUDIES OF SITE EFFECTS

Local ground response and basin effects can be quantified through a variety of means of varying sophistication. Amplification factors relative to a particular site condition (e.g., rock or weathered soft rock) can be derived from observational data or from the results of large suites of numerical analyses. The following sections describe approaches used to derive amplification functions from observational data, site categorization schemes used to delineate ground conditions, and the factors that have been found to affect amplification.

5.2.1 Types of Observational Studies

Quantification of site amplification effects from strong motion recordings requires the removal of source and path effects. Two categories of methods are used. The first compares soil motions with motions from a reference site (usually rock), while the second does not use a reference site.

With the reference site approach, if the rock and soil sites are close, both motions likely contain similar source and path effects, so a comparison of the two provides an estimate of site response effects. Investigations of this type (e.g., Table 5.1a) have compared the motions using either response spectral ordinates or Fourier amplitude spectra. A variation on this approach corrects the reference and site recordings to account for their different site-source distances. This was done using ratios of hypocentral distance by Borcherdt and Glassmoyer (1994) and Borcherdt (1996). Distance corrections incorporating frequency-dependent attenuation have been implemented by Hartzell et al. (2000) and Borcherdt (2001). Features of these studies are summarized in Table 5.1b. It should be noted that numerous studies not listed in Table 5.1 have been performed on individual selected rock-soil site pairs, typically as a verification exercise for ground response analysis routines. A discussion of these results is deferred to Section 5.2.2.

Table 5.1 Selected observation-based investigations of ground response effects using local reference rock recordings

Investigator	No. of sites[1]	No. ref. sites[2]	Location	Source	Soil site condition	Ground motion parameter
(a) No distance scaling						
Borcherdt, 1970; Borcherdt and Gibbs, 1976	37; 99	5	San Francisco, CA	Nevada explotions	w. rock, stiff & soft sediments	FAS
Seed and Idriss, 1971	4	1	San Francisco, CA	1957 San Francisco eq.	stiff sediments	S_a
Rogers et al. 1984	28	4	Los Angeles, CA	Nevada explotions, 1971 San Fernando eq.	rock, sediments	FAS
Idriss, 1990	8	na	San Francisco, CA	1989 Loma Prieta eq.	soft clay	S_a
Rathje et al., 2000	8	4	Izmit Bay, Turkey	1999 Kocaeli, Turkey eq.	stiff & soft sediments	S_a
(b) Distance scaling						
Hudson and Housner, 1958	4	1	San Francisco, CA	1957 San Francisco eq.	stiff sediments	S_a
Borcherdt and Glassmoyer, 1994	37	8	San Francisco, CA	1989 Loma Prieta eq.	w. rock, stiff & soft sediments	FAS
Borcherdt, 1996	133	27	Los Angeles, CA	1994 Northridge eq.	w. rock, stiff sediments	FAS
Hartzell et al., 1997	231	1	Los Angeles, CA	1994 Northridge eq. (AS)	w. rock, stiff sediments	FAS
Hartzell et al., 2000	30	2	Seattle, WA	Small eqks., airgun shots	till, fill, sand	FAS
Borcherdt, 2001	125	23	Los Angeles, CA	1994 Northridge eq.	w. rock, stiff sediments	FAS
(c) Generalized inversion approach						
Margheriti et al. 1994	14	1	San Jose, CA	1989 Loma Prieta eq. (AS)	w. rock, stiff & soft sediments	FAS
Carver and Hartzell, 1996	33	2	Santa Cruz, CA	1989 Loma Prieta eq. (AS)	w. rock, stiff sediments	FAS
Hartzell et al., 1996	90	1	Los Angeles, CA	1994 Northridge eq. (AS)	w. rock, stiff sediments	FAS
Bonilla et al. 1997	31	1	Los Angeles, CA	1994 Northridge eq. (AS)	w. rock, stiff sediments	FAS
Harmsen, 1997	281	1	Los Angeles, CA	1971 San Fer.; 1987 Whit.; 1991 S. Madre; 1994 Northr.	rock, sediments	FAS
Hartzell et al., 2000	30	2	Seattle, WA	Small eqks., airgun shots	till, fill, sand	FAS

[1] sites where amplification evaluated

[2] reference sites used for analysis of amplification

A third method for evaluating amplification using a reference site was developed by Andrews (1986). In this approach, generalized inversions are performed using the Fourier spectra of observed motions adjusted for geometric spreading to evaluate source and site terms simultaneously. A weighted least squares solution is developed in which the source term is allowed to have an arbitrary frequency dependence and the site response terms are taken as relative to the network average (Andrews, 1986) or relative to a single predetermined "reference" site for which the site term is unity (e.g., Boatwright et al., 1991; Hartzell et al., 1996). A list of several studies employing this generalized inversion approach is presented in Table 5.1c. Results of these studies have been found to compare favorably with more traditional reference site approaches (e.g., Field and Jacob, 1995). The principal advantage of this generalized inversion approach is that relatively large data sets can be utilized (e.g., Table 5.1). However, most of the studies utilizing this approach to date are somewhat limited for engineering application, in that weak motions dominate the data sets; thus nonlinearities in sediment response are not represented in the identified amplification factors.

The second category of approaches for evaluating ground motion amplification on soil does not require the presence of a reference site. Such approaches have the advantage of being able to incorporate essentially all available earthquake recordings. One such approach, termed horizontal-to-vertical spectral ratio (HVSR), involves normalizing the horizontal component spectra for a given site by the vertical component spectra for that same site, with the spectra computed over the shear-wave dominated portion of the record (Lermo and Chavez-Garcia, 1993). The HVSR method has generally been found to extract the same spectral peaks as reference site methods but different amplification levels (Field and Jacob, 1995; Bonilla et al., 1997), thus limiting its practical application. A second approach implements a generalized inversion scheme to identify source, path, and site effects for a given earthquake (Boatwright et al., 1991). The approach is similar to that of Andrews (1986) described above, but the source and path are now parameterized, and the site factor averaged across all frequencies and sites is constrained based on *a priori* information (Field and Jacob, 1995). While this approach can produce spectral ratios comparable to those observed from adjacent rock/soil sites (e.g., Field and Jacob, 1995), the need for *a priori* information on ground response is a limitation.

A third non-reference site approach consists of evaluating amplification by normalizing the spectra of recorded motions by a reference (rock) spectrum obtained from an attenuation relationship. This approach has been applied to specific basins by Sokolov (1997) and Sokolov et al. (2000) using locally derived attenuation functions for Fourier spectral amplitude, and for relatively broad areas using attenuation relations for spectral acceleration with event term corrections (Lee and Anderson, 2000; Field, 2000; Stewart et al., 2001) and without these corrections (Steidl, 2000). This approach offers several advantages to others previously identified:

1. A much larger inventory of strong motion data can be utilized than for reference site approaches. For example, the database of Stewart et al. includes 1032 recordings from 51 earthquakes, which is significantly larger than the databases summarized in Table 5.1.
2. No *a priori* information about site effects is required.
3. Amplification factors derived in this way can be readily incorporated into hazard analyses as adjustments to rock attenuation functions.

It should be noted, however, that the generalized inversion approach of Andrews (1986) could provide equally useful results provided that site terms are defined relative to an average site term for a large collection of "rock" sites (i.e., the sites used to develop attenuation relationships on rock).

5.2.2 Site Categorization Schemes

The observational studies described above have generally found distinct levels of amplification at sites with different geologic and geotechnical characteristics. Site categorization schemes that have been used include the following:

- Surface geology,
- Averaged shear wave velocity in the upper 30 m (30-m V_s),
- Geotechnical data, including sediment stiffness, depth, and material type, and
- Depth to basement rock (defined as V_s ~ 2.5 km/s).

A comparison of amplification factors derived using these three schemes is deferred to Section 5.2.3. The following presents details on the three methods of site categorization.

(a) *Surface geology*

Geology-based classification systems generally separate materials according to geologic age (e.g., Holocene-Pleistocene-Tertiary-Mesozoic). Separate categories are sometimes defined for granitic or volcanic rocks, or to subdivide Quaternary sediments. For example, Tinsley and Fumal (1985) categorized Los Angeles area Quaternary sediments according to age and texture, and these maps have recently been updated by Park and Elrick (1998) as shown in Figure 5.1. More detailed geologic data for southern California has recently become available through the Southern California Aerial Mapping Project (SCAMP), which provides for Quaternary materials information on sediment texture and depositional environment (e.g., Morton et al., 1999). In addition, the geology of the entire State of California is documented on 27 maps at 1:250,000 scale by the California Division of Mines and Geology (CDMG, 1959-1998). These maps distinguish Quaternary sediments based on age (Holocene-Pleistocene) and generalized descriptions of depositional environment. Given the availability of these data resources, Table 5.2 shows criteria that have been used for surface geologic classifications for general strong motion studies. A discussion of the degree to which these criteria delineate trends in site amplification functions is deferred to the following section. Classification systems based on specific geologic formations can of course be defined for local regions, and could be more effective than those listed in Table 5.2.

Table 5.2 Criteria for surface geology classifications (Stewart et al., 2001)

Age	Depositional Environment	Sediment Texture
Holocene	Fan alluvium	Coarse
Pleistocene	Valley alluvium	Fine
	Lacustrine/marine	Mixed
	Aeolian	
	Artificial Fill	
Tertiary		
Mesozoic + Igneous		

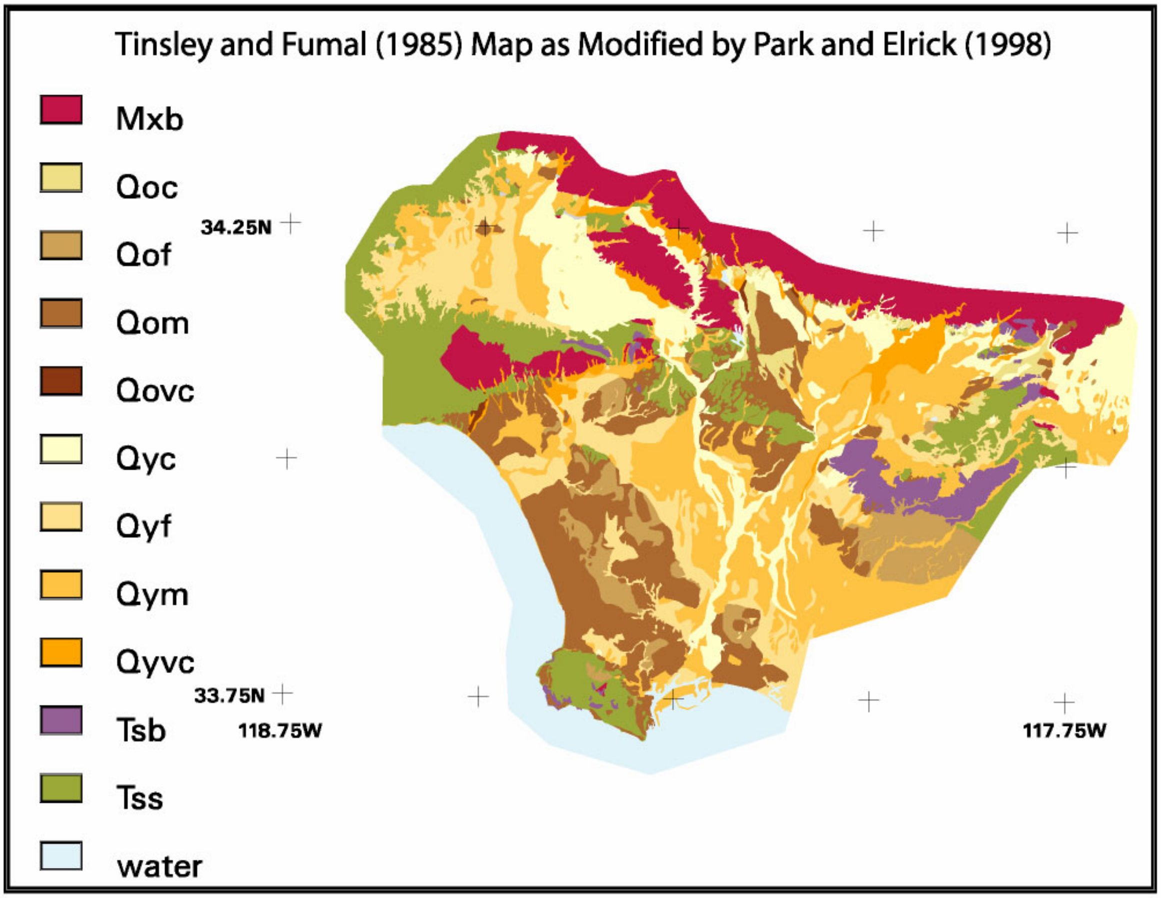

Fig. 5.1. Detailed geology map of Los Angeles area, modified by Park and Elrick (1998) from original map by Tinsley and Fumal (1985).

(b) ***30-m shear wave velocity (30-m V_s)***

Wave propagation theory suggests that ground motion amplitude should depend on the density and shear wave velocity of near-surface media (e.g., Bullen, 1965; Aki and Richards, 1980). Density has relatively little variation with depth, and so shear wave velocity is the logical choice for representing site conditions. Two methods have been proposed for representing depth-dependent velocity profiles with a single representative value. The first takes the velocity over the depth range corresponding to one-quarter wavelength of the period of interest (Joyner et al., 1981), which produces frequency-dependent values. Fumal and Tinsley (1985) developed 1-Hz V_s maps for the Los Angeles region by relating quarter-wavelength velocities inferred from 33 boreholes to geologic units.

A practical problem with the quarter wavelength V_s parameter is that the associated depths are often deeper than can economically be reached with boreholes. The 30-m V_s parameter was proposed to overcome this difficulty and has found widespread use in practice. Based on empirical studies by Borcherdt and Glassmoyer (1994), Borcherdt (1994) recommended 30-m V_s as a means of classifying sites for building codes, and similar site categories were selected for the NEHRP seismic design provisions for new buildings (Martin, 1994). The site classification scheme in the NEHRP provisions is presented in Table 5.3. The 30-m V_s parameter has been correlated with surface geology by Wills and Silva (1998), and this information has been used to generate state-wide maps of 30-m V_s by Wills et al. (2000).

Table 5.3 Site categories in NEHRP Provisions (Martin, 1994)

NEHRP Category	Description	Mean Shear Wave Velocity to 30 m
A	Hard Rock	> 1500 m/s
B	Firm to hard rock	760-1500 m/s
C	Dense soil, soft rock	360-760 m/s
D	Stiff soil	180-360 m/s
E	Soft clays	< 180 m/s
F	Special study soils, e.g., liquefiable soils, sensitive clays, organic soils, soft clays > 36 m thick	

(c) *Geotechnical data*

Geotechnical engineers have developed site classification schemes that can be used to estimate response spectra for soil sites. Early work on this topic is summarized in Seed and Idriss (1982), who recommended the following site classification scheme:

1. Rock sites
2. Stiff soil sites (< 60 m deep)
3. Deep cohesionless soil sites (> 75 m deep)
4. Sites underlain by soft to medium stiff clays

Response spectrum estimation procedures linked to this classification system were developed in which PHA on rock was first estimated from an attenuation relation, and then the ratio PHA(soil)/PHA(rock) and spectral shape were taken as a unique function of site condition (based on the work of Seed et al., 1976). Significant additional data gathered from the 1985 Mexico City, 1989 Loma Prieta, and 1994 Northridge earthquakes prompted revisions to the PHA rock-soil relations and spectral shapes, and the derivation of new site categories (e.g., Dickenson, 1994; Chang, 1996), which include information on sediment depth and near-surface shear wave velocity.

The most recent of the geotechnical classification schemes was proposed by Rodriguez-Marek et al. (2001) based on event-specific regressions of Loma Prieta and Northridge earthquake recordings. Data were grouped according to the categories in Table 5.4, and regressed using an attenuation function similar to that of Abrahamson and Silva (1997). Consistent trends were found for the Category D sites (deep stiff soil), as demonstrated by error terms smaller than those for the overall data population. However, large intra-category dispersion was found for Category C sites (shallow stiff soil), indicating that further subdivision of this category may be appropriate. Rodriguez-Marek et al. (2001) recommend use of their classification scheme over the 30-m V_s scheme as intra-category standard error terms were reduced through use of the geotechnical scheme.

Table 5.4 Geotechnical site categories proposed by Rodriguez-Marek et al. (2001)

Site	Description	Approx. Site Period (s)	Comments
A	Hard Rock	≤ 0.1	Crystalline Bedrock; $V_s \geq 1500$ m/s
B	Competent Bedrock	≤ 0.2	$V_s \geq 600$ m/s or < 10 m of soil. Most "unweathered" California Rock cases
C1	Weathered Rock	≤ 0.4	$V_s \approx 300$ m/s increasing to > 600 m/s, weathering zone > 10 m and < 30 m
C2	Shallow Stiff Soil	≤ 0.5	Soil depth > 10 m and < 30 m
C3	Intermediate Depth Stiff Soil	≤ 0.8	Soil depth > 30 m and < 60 m
D1	Deep Stiff Holocene Soil	≤ 1.4	Depth > 60 m and < 200 m
D2	Deep Stiff Pleistocene Soil	≤ 1.4	Depth > 60 m and < 200 m
D3	Very Deep Stiff Soil	≤ 2.0	Depth > 200 m
E1	Medium Thickness Soft Clay	≤ 0.7	Thickness of soft clay layer 3-12 m
E2	Deep Soft Clay	≤ 1.4	Thickness of soft clay layer > 12 m
F	Potentially Liquefiable Sand		Holocene loose sand with high water table ($z_w \leq 6$ m)

(d) *Depth to basement*

The site classification schemes presented above describe principally the characteristics of shallow sediments (i.e., at most, the upper few hundred meters). A parameter that can be used to supplement these classification schemes for ground motion studies is the depth to basement rock (i.e., rock with V_s > ~2.5 km/s). Recent work has shown this parameter to significantly impact amplification across a wide frequency range (Steidl, 2000; Lee and Anderson, 2000; Field, 2000). Information on the depth to basement is available for Los Angeles (Magistrale et al., 2000), the San Francisco Bay region (Brocher et al., 1998), Seattle (Frankel and Stephenson, 2000), the Kanto-Tokyo, Japan region (Sato et al., 1999), Kobe, Japan (Pitarka et al., 1998), and Taipei, Taiwan (Wen and Peng, 1998). Figures 5.2 and 5.3 present maps indicating depth to the 2.5 km/s shear wave velocity isosurface for the Los Angeles area (Magistrale et al., 2000) and the San Francisco Bay Area (Brocher et al., 1998), respectively.

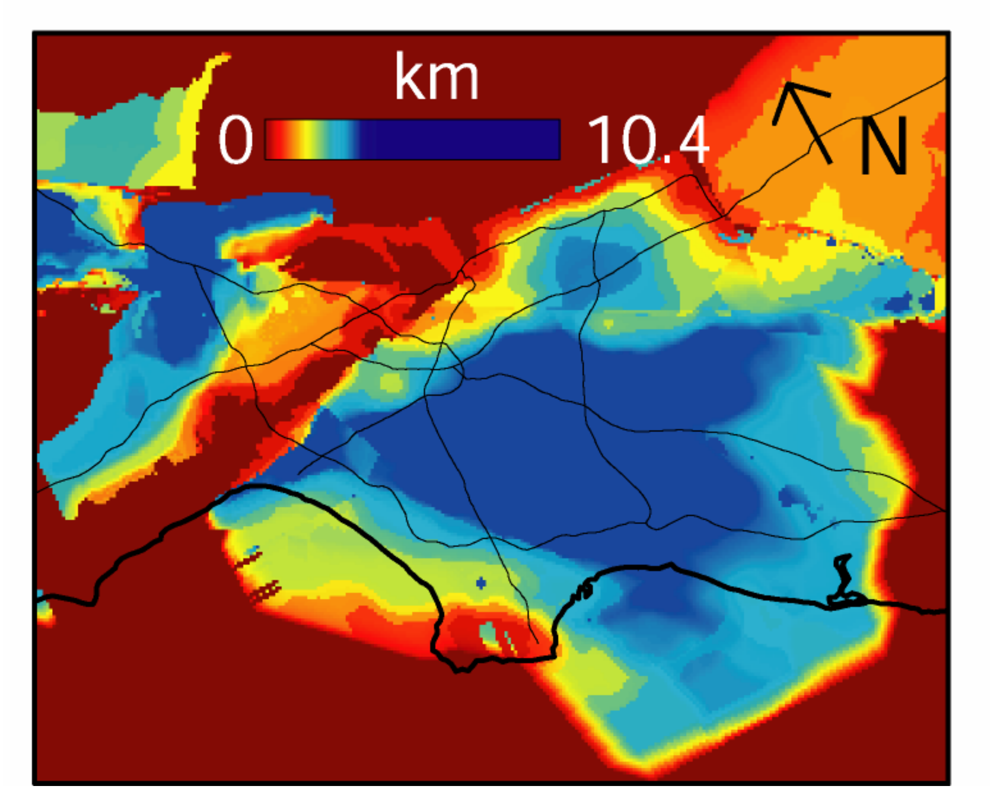

Fig. 5.2. Depth to the V_s = 2.5 km/s isosurface in Los Angeles (after Magistrale et al., 2000).

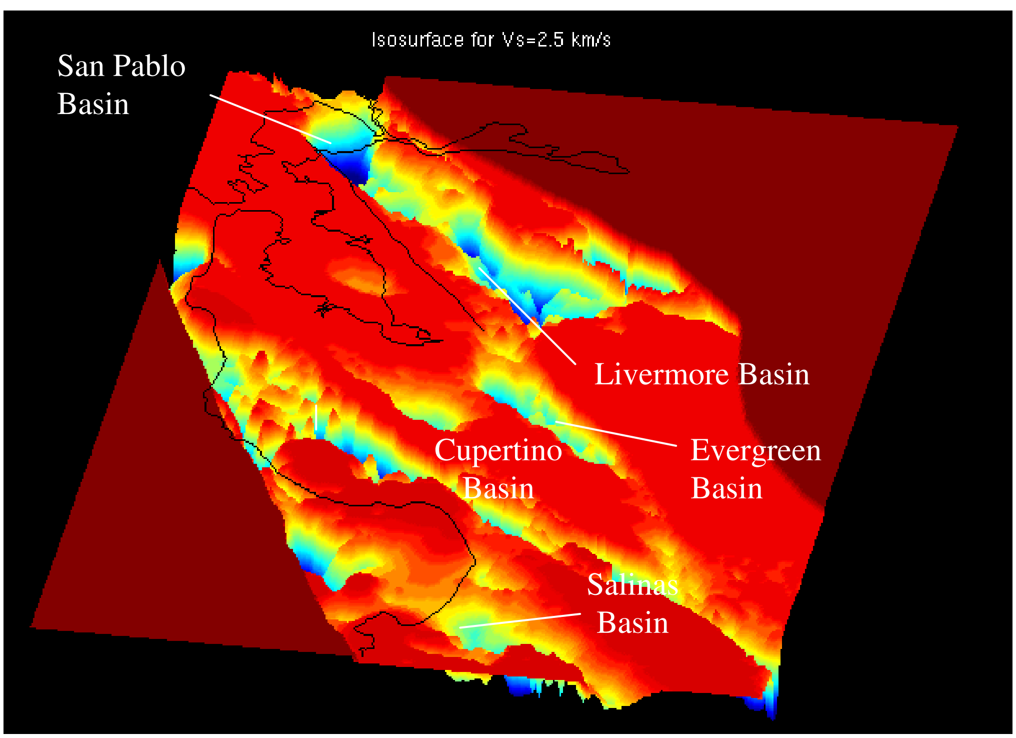

Fig. 5.3. Perspective view of the San Francisco Bay area showing depth to V_s = 2.5 km/s isosurface (after Brocher et al., 1998).

5.2.3 Outcomes of Observational Studies

In this section, we review significant findings from observational studies of ground motion amplification at soil sites. A feature of these studies is that the influence of ground response and basin effects cannot be readily distinguished in recordings from sedimentary basins, and hence amplification factors necessarily incorporate both effects.

(a) *Weak motion amplification*

Many studies of ground motion amplification have utilized low amplitude signals such as coda waves and recordings from relatively weak sources such as aftershocks, micro-tremors, distant nuclear explosions, or ambient noise. Field et al. (2000) reviewed the results of studies utilizing these recordings, and a brief summary of their critical findings is presented here.

Studies by Borcherdt and Gibbs (1976) and Rogers et al. (1984) examined recordings of Nevada nuclear explosions in the San Francisco and Los Angeles areas, respectively. Fourier spectra of recordings from instruments cited on various geologic media were compared to those on "crystalline rock." Figures 5.4 and 5.5 show amplification levels for (1) soft, marine clay deposits (i.e., Bay Mud), (2) alluvial sediments, (3) Tertiary-age sedimentary bedrock (e.g., Santa Clara Formation), and (4) relatively competent rock (e.g., Franciscan Formation, granite, and crystalline rock). Large amplification levels (about 10) occurred at Bay Mud sites near a predominant frequency of about 1 Hz. Amplification levels on alluvial sediments in both San Francisco and Los Angeles were considerably smaller (about 2-5), and the spectra generally do not indicate a predominant period of amplification. Amplification spectra for sedimentary rock sites also lack a predominant period, and indicate amplification levels on the order of one to three. Rogers et al. (1984) found high-frequency (> 2 Hz) amplification levels for the Los Angeles alluvial sites (> 2 Hz) to be influenced by near-surface void ratio (a crude proxy for V_s), as well as Holocene soil thickness and depth to basement. Quaternary thickness and basement depth were found to be most critical at lower frequencies.

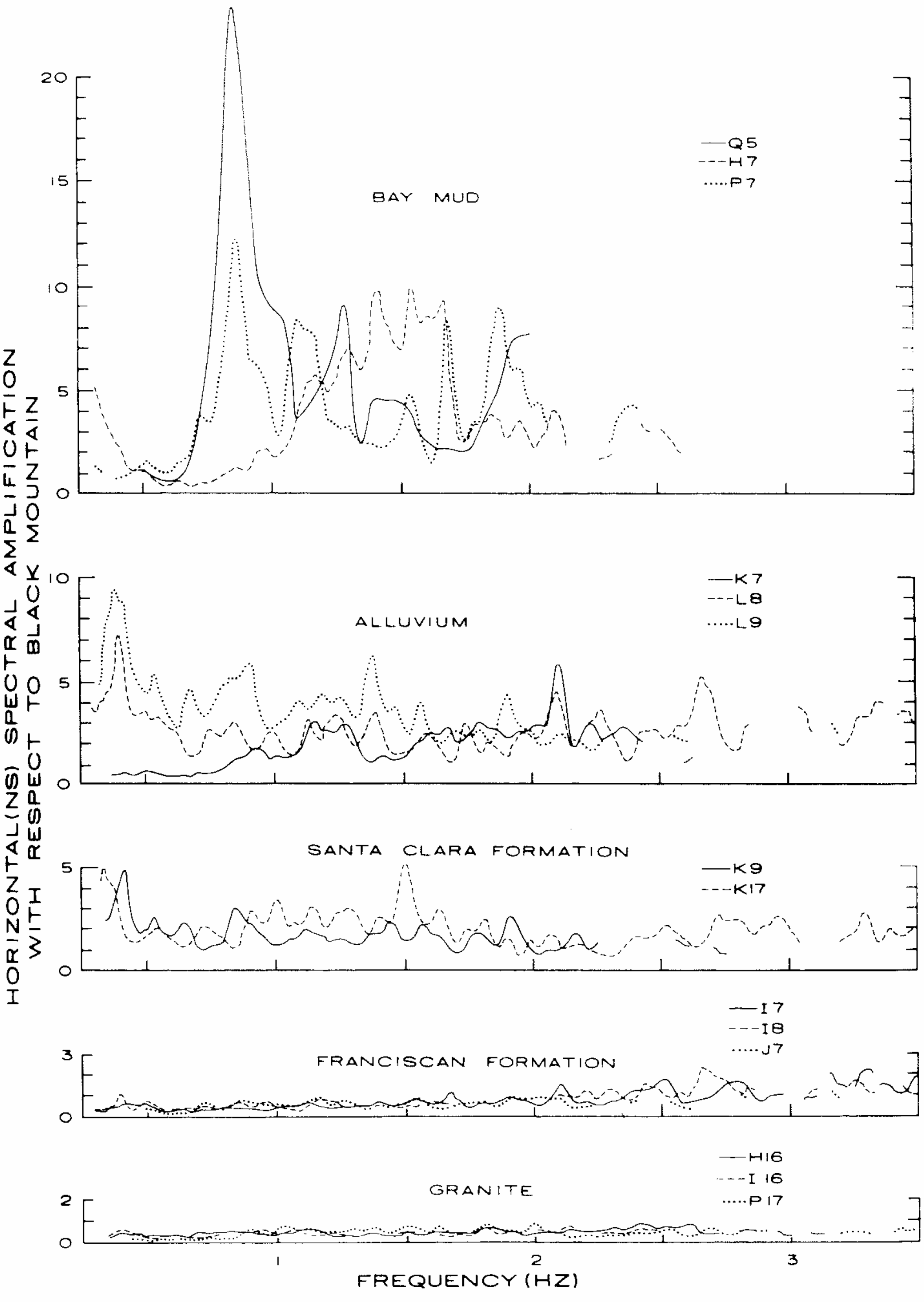

Fig. 5.4. Spectral amplification at San Francisco Bay Area recording sites relative to site underlain by Franciscan bedrock; data from Nevada nuclear explosions (Borcherdt and Gibbs, 1976).

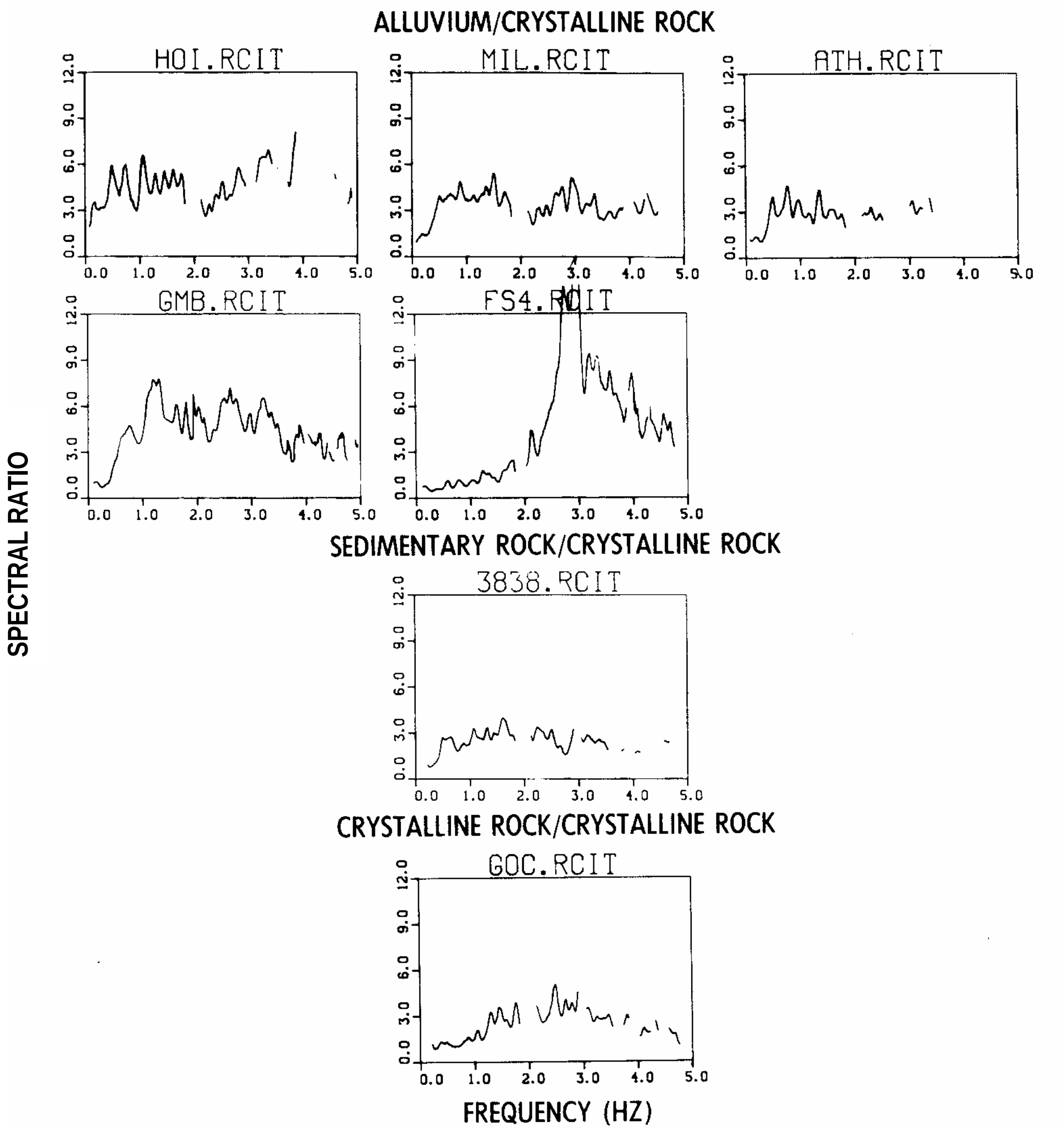

Fig. 5.5. Averaged spectral amplification at Los Angeles recording sites relative to crystalline rock site; data from Nevada nuclear explosions (Rogers et al., 1984).

The general trends in weak motion amplification factors derived from Nevada nuclear explosion data have generally been confirmed by subsequent studies employing weak seismic sources. For example, Figure 5.6 shows amplification factors for NEHRP category C-E sites (Tertiary rock, alluvial sediments, Bay Mud) derived from micro-tremors in the San Jose Area (Margheriti et al., 1994), while Figure 5.7 shows average amplification factors as a function of surface geology for a large number of sites derived from Northridge earthquake aftershock recordings (Bonilla et al., 1997). Amplification factors from these more recent studies are defined across a wider frequency range than those from nuclear explosions (e.g., Figures 5.4 and 5.5), and reveal relatively large low-frequency amplification, and small high-frequency amplification. Amplification levels across the mid-period band (1-3 Hz) are generally comparable to those from nuclear explosions, with the exception of relatively large soft rock amplification in the San Jose regional study.

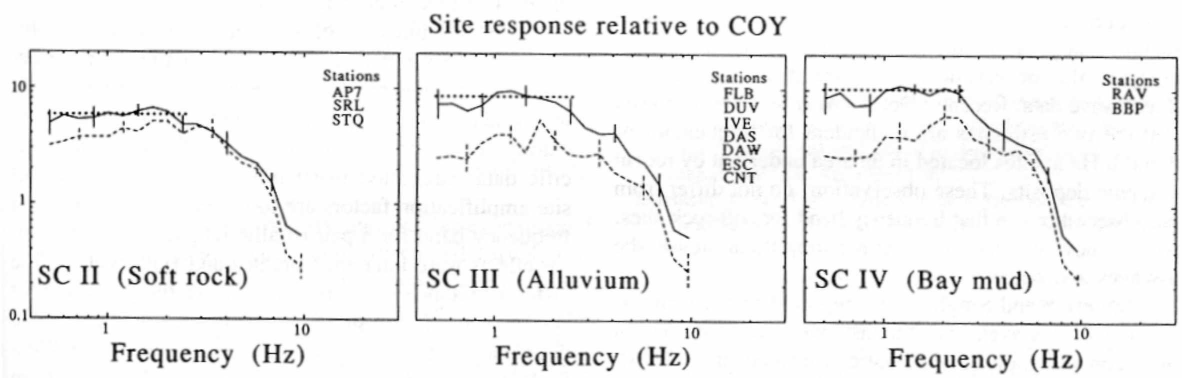

Fig. 5.6. Averaged spectral amplification at San Jose area recording sites relative to site underlain by Franciscan bedrock; data from microtremors (Margheriti et al., 1994).

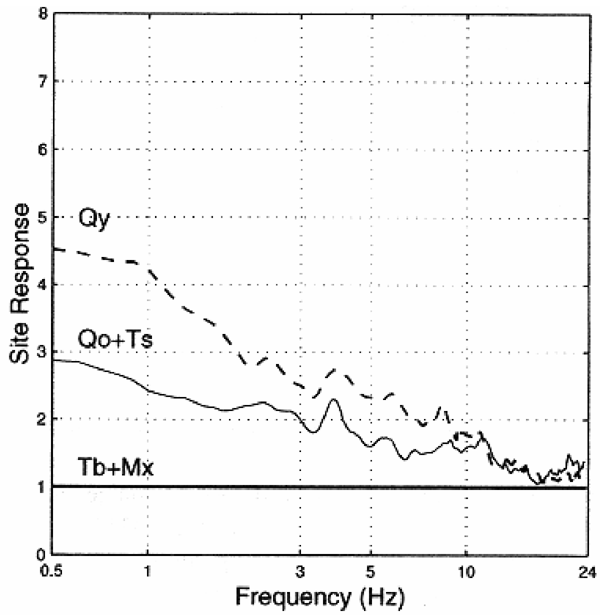

Fig. 5.7. Averaged spectral amplification at San Fernando Valley recording sites relative to site underlain by firm Mesozoic bedrock, data from aftershocks of 1994 Northridge earthquake (after Bonilla et al., 1997). Qy = young alluvium; Qo+Ts = older alluvium + Tertiary; Tb+Mx = Tertiary + Mesozoic basement units.

(b) ***Amplification from strong motion data — reference site approaches***

The 1989 Loma Prieta earthquake provided one of the first strong motion data sets with a sufficient number of recordings to evaluate amplification factors across a diverse array of surface geologic conditions. Borcherdt and Glassmoyer (1994) utilized 37 recordings from the San Francisco Bay region to evaluate site amplification factors as a function of 30-m V_s, which was generally evaluated from local downhole measurements. Amplification was evaluated relative to recordings from nearby rock sites, which consist of either Franciscan complex bedrock or well consolidated sedimentary bedrock of Tertiary-Mesozoic age. Where the reference recording is from a sedimentary bedrock site, the amplification factor was adjusted (increased) to a common reference site condition of "firm to hard rock," represented by the Franciscan complex. The resulting amplification factors for the 37 sites are plotted in Figure 5.8 for the T = 0.1-0.5 and 0.4-2.0 s period range (amplification factors across these ranges are denoted F_a and F_v, respectively). These amplification factors are similar to those evaluated by Borcherdt and Gibbs (1976) in weak motion studies, although it should be noted that the severity of "strong" shaking in the subject region was modest (e.g., PHA ≤ 0.1g at the reference rock sites).

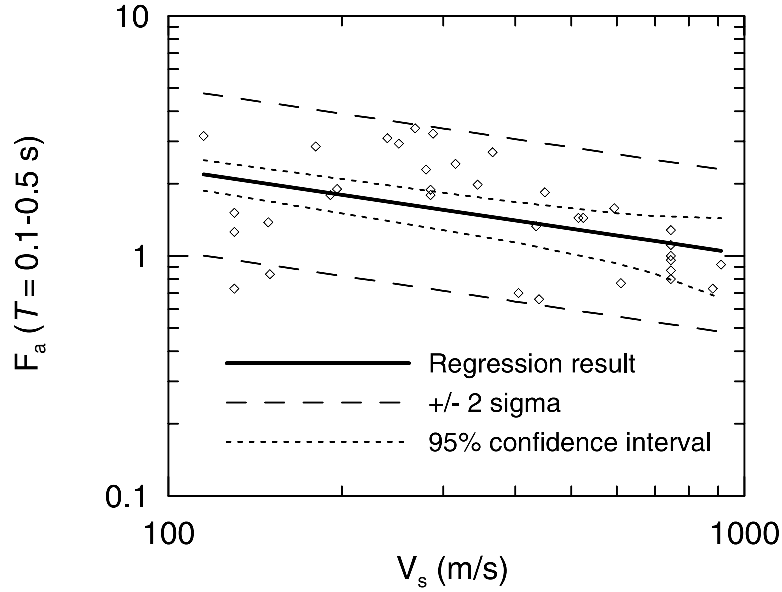

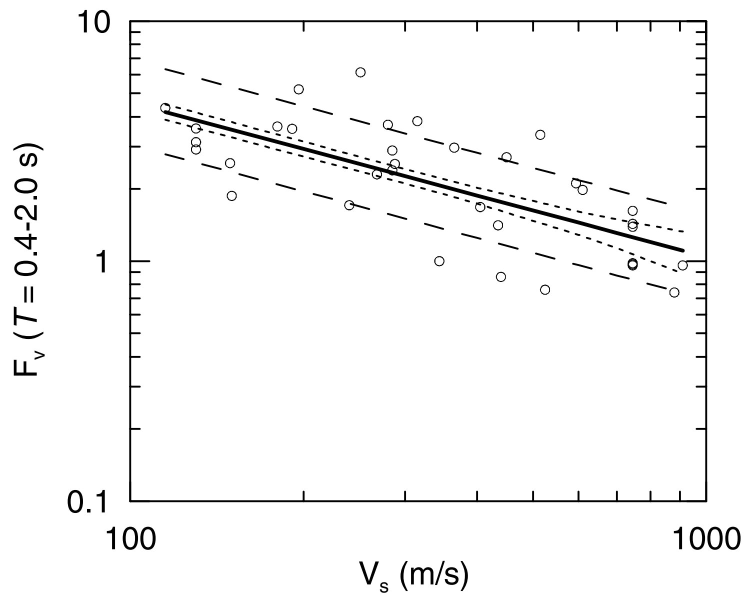

Fig. 5.8. Averaged spectral amplification vs. 30-m V_s for 37 sites in the San Francisco Bay Region that recorded the 1989 Loma Prieta earthquake (after Borcherdt and Glassmoyer, 1994).

Borcherdt (1996, 2001) performed a similar study using 125 recordings from the 1994 Northridge earthquake (mostly stiff soil and soft rock sites) and 8 recordings from the 1995 Hanshin-Awaji (Kobe) earthquake (soft soil sites only, Borcherdt, 1996). Reference motions for the Northridge recordings were taken from local stations with metamorphic rock (e.g., weathered granite, gneiss) or sedimentary rock. As was done for the Loma Prieta study, amplification factors derived from reference recordings at sedimentary rock sites were adjusted to reflect a hard rock site condition. The “hard rock” station at Kobe University was taken as the reference site for the Kobe recordings. Values of 30-m V_s were estimated for the recording sites using local borehole measurements or correlations with surface geology. As shown in Figure 5.9, for relatively small ground motion levels (PHA ≤ 0.1g on rock), Northridge amplification factors for deep soil sites at small period (i.e., F_a) are generally smaller than those obtained by Borcherdt and Glassmoyer (1994) for the Loma Prieta earthquake, but the amplification factors are comparable at longer periods (i.e., F_v). The Kobe amplification factors (Figure 5.10) are somewhat larger than those for Loma Prieta, although Borcherdt (1996) indicates these results as being preliminary. Both the Kobe and Northridge results demonstrate decreasing amplification with reference motion amplitude, which is evidence of nonlinearity in sediment response.

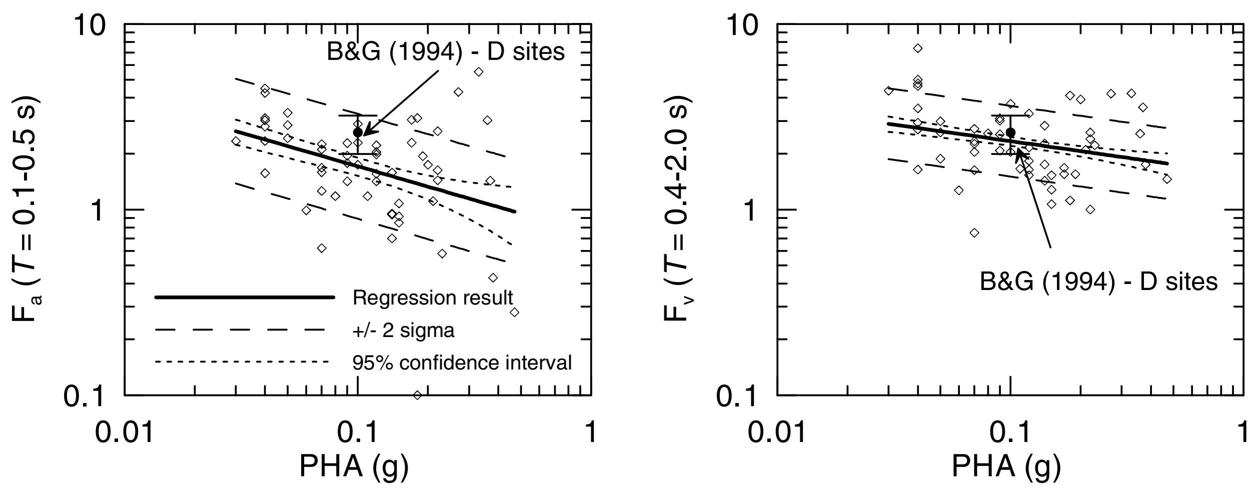

Fig. 5.9. Averaged spectral amplification vs. reference motion amplitude for Northridge earthquake deep stiff soil recordings (Borcherdt, 2001), as compared to low-amplitude results of Borcherdt and Glassmoyer (1994) for Loma Prieta earthquake (symbol indicates median ± one standard error). Reference motion amplitude is taken as a scaled motion from a nearby rock site.

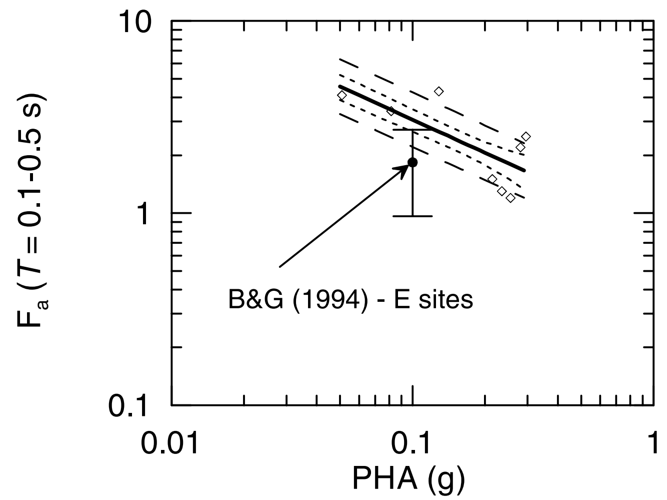

Fig. 5.10. Averaged spectral amplification vs. reference motion amplitude for Kobe earthquake soft soil recordings (Borcherdt, 1996), as compared to low-amplitude results of Borcherdt and Glassmoyer (1994) for Loma Prieta earthquake.

Harmsen (1997) evaluated mainshock recordings in the San Fernando Valley and Los Angeles basin from the 1971 San Fernando, 1987 Whittier, 1991 Sierra Madre, and 1994 Northridge events. Amplification factors relative to a single reference rock site (Caltech Seismic Lab) were derived using the inversion approach of Andrews (1986). The amplification factors were derived across intermediate (0.5-1.5 Hz) and high (2.0-6.0 Hz) frequency bands, and correlated to site classes defined by 30-m V_s (Table 5.3). As shown in Figure 5.11, the median regressions through these results indicate slightly higher amplification levels than those of Borcherdt and Glassmoyer (1994), which is opposite to the findings of Borcherdt (2001). The results were found to be similar to amplification levels derived from weak motion studies (e.g., Hartzell et al., 1996; Rogers et al., 1984). Based on this similarity, Harmsen suggested that amplification factors derived from weak motion data could be used for strong motion applications (i.e., hazard analyses). Adopting this suggestion, Hartzell et al. (1998) combined the Northridge aftershock results of Hartzell et al. (1996) with the mainshock results of Harmsen (1997) to produce Los Angeles basin site response maps (e.g., Figure 5.12).

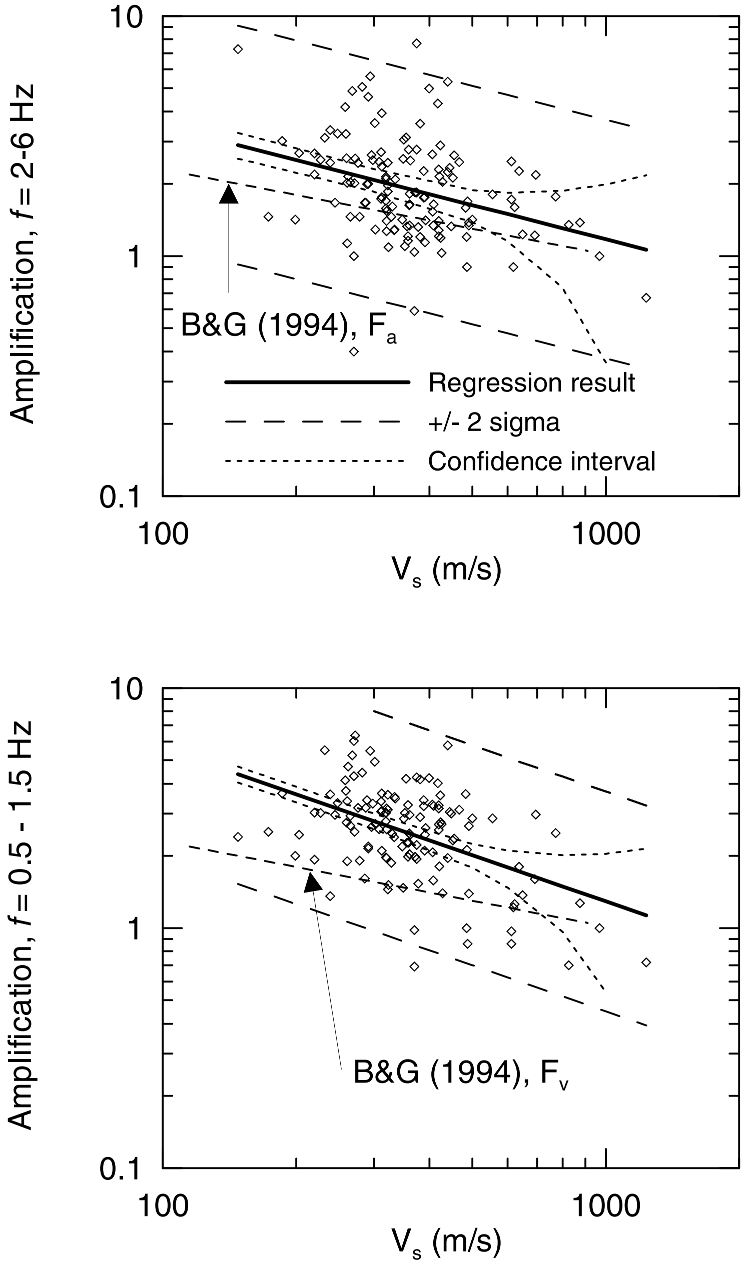

Fig 5.11. Averaged spectral amplification vs. 30-m V_s for Los Angeles region strong motion sites compared with results of Borcherdt and Glassmoyer (1994) for Loma Prieta earthquake. After Harmsen (1997).

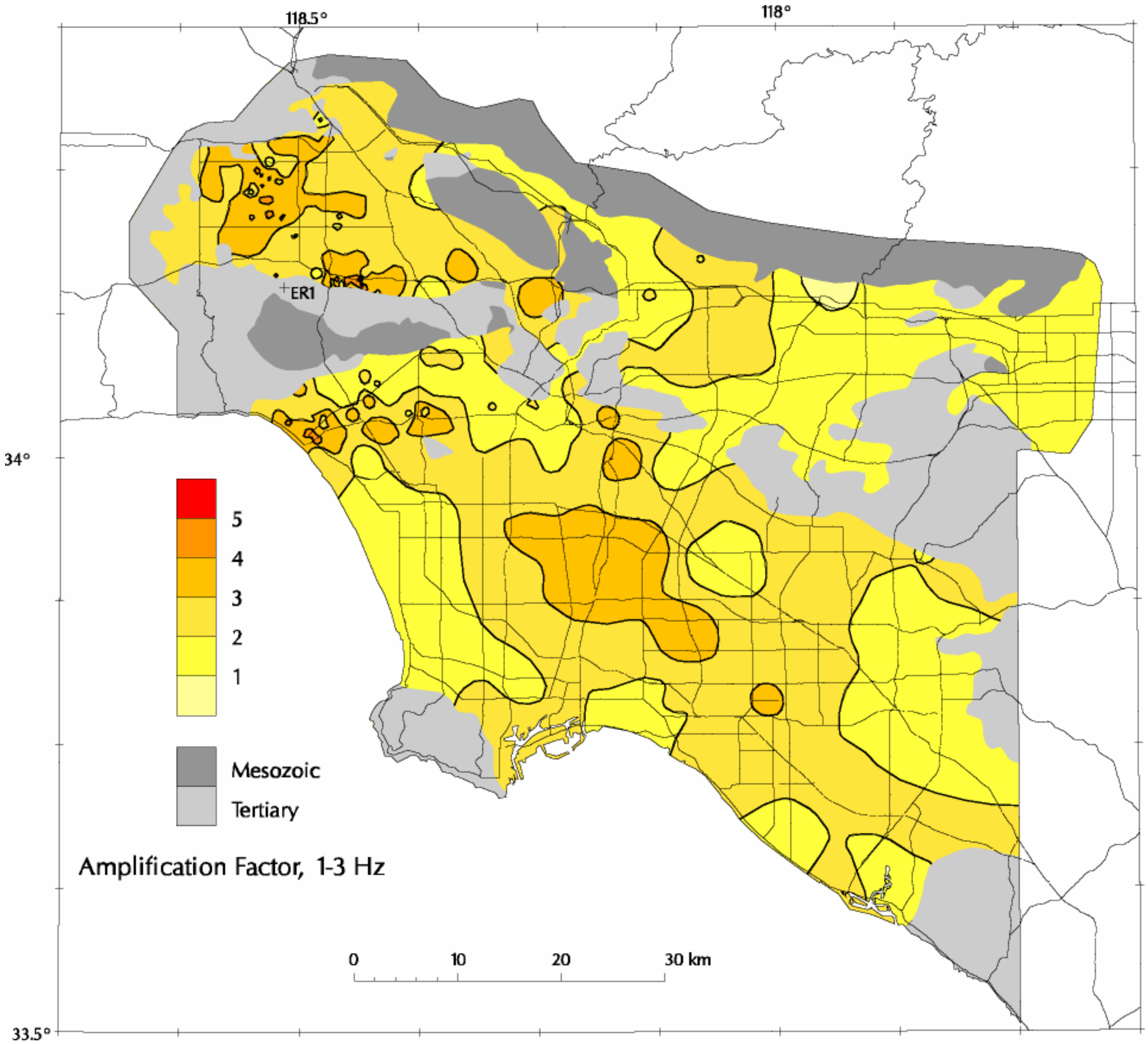

Fig. 5.12. Empirical sediment amplification map of Hartzell et al. (1998) for 1-3 Hz ground motion (as modified by Field et al., 2000).

(c) *Amplification from strong motion data — non-reference site approaches*

Three recent projects coordinated through the Southern California Earthquake Center (SCEC) developed amplification factors applicable to the southern California region by comparing recorded motions to predictions from attenuation relations (Field, 2000; Lee and Anderson, 2000; Steidl, 2000). Stewart et al. (2001) used a similar approach, but utilized a larger database that applies for all active tectonic regions. The following shows the attenuation relationships used to develop reference motions and the site classification systems used in these studies:

Investigator	Attenuation Relationship	Site Classification
Steidl (2000)	Sadigh (1993), rock	geology, basin depth, 30-m V_s
Lee and Anderson (2000)	Abrahamson and Silva (1997), soil	geology, basin depth, wk. motion amp., etc.
Field (2000)	revised Boore et al. (1997), V_s = 760 m/s	30-m V_s
Stewart et al. (2001)	Abrahamson and Silva (1997), rock	geology, 30-m V_s, geotech. scheme

In each study, amplification factors were inferred from residuals, i.e., differences between the natural logarithm of the data and the reference motion. Field, Lee and Anderson, and Stewart et al. removed event terms before evaluating residuals, while Steidl used unadjusted predictions. Some key results from these studies are presented in the following paragraphs.

The correlation between surface geology and amplification has been investigated by Steidl, Lee and Anderson, and Stewart et al.. As noted above, both Steidl and Stewart et al. evaluated amplification factors relative to a reference rock site condition, and so we focus on the outcomes of these studies in the following. Steidl classified strong motion stations using an age-based Q-T-M classification scheme as well as a more detailed classification scheme based on the mapping of Fumal and Tinsley (1985) in which younger Quaternary (Qy) is separated from older Quaternary (Qo), with Tertiary added to the Qo class. Stewart et al. performed more detailed classifications of Quaternary sediments, using the geologic mapping resources described in Section 5.2.1b. Steidl evaluated mean amplification factors (relative to soft rock) for spectral periods T = 0 (PHA), 0.3, 1.0, and 3.0 s using data with reference motion PHA values in the following ranges: < 0.05g, 0.05-0.1g, 0.1-0.2g, >0.2g. Stewart et al. regressed amplification factor (F) against control motion amplitude according to the function,

$$\ln(F) = a + b\ln\left(S_a^r\right) \tag{5.1}$$

where S_a^r = reference motion amplitude (taken as PHA), and a and b are regression parameters. These analyses were performed at the same four periods as Steidl, plus the period ranges associated with F_a and F_v.

The results of these studies are presented in Figure 5.13. Amplification factors at T = 0.3 and 1.0 s are presented for the following geologic categories: Holocene lacustrine/marine (Hlm), Quaternary alluvium (Qa), Tertiary (T), and Mesozoic (M). Materials belonging to the Hlm category (Figure 5.13b) have the highest levels of weak shaking amplification and soil nonlinearity. The nonlinearity in such materials is typically sufficiently pronounced that high-frequency spectral ordinates are de-amplified at strong levels of shaking (PHA > ~0.2g). Quaternary alluvial sediments (Figure 5.13a) experience less weak shaking amplification, but less nonlinearity as well. Stewart et al. found that amplification of Quaternary alluvial sediments is moderately age-dependent based on separate regression analyses for the Holocene and Pleistocene age groups. The statistical significance of the nonlinearity from the Stewart et al. work is demonstrated by hypothesis testing in which a b=0 model can be rejected for both the Hlm and Qa categories with nearly 100% confidence. In all Quaternary categories, ground motion amplification is found to be strongly period dependent, with less nonlinearity, and often more amplification, at longer spectral periods. "Rock-like" materials of pre-Pleistocene age (i.e., Tertiary or Mesozoic categories) generally have statistically insignificant nonlinearity and experience less amplification than Quaternary sediments. Amplification levels in Tertiary sediments are distinctly higher than those for Mesozoic (see Figures 5.13c and 5.13d).

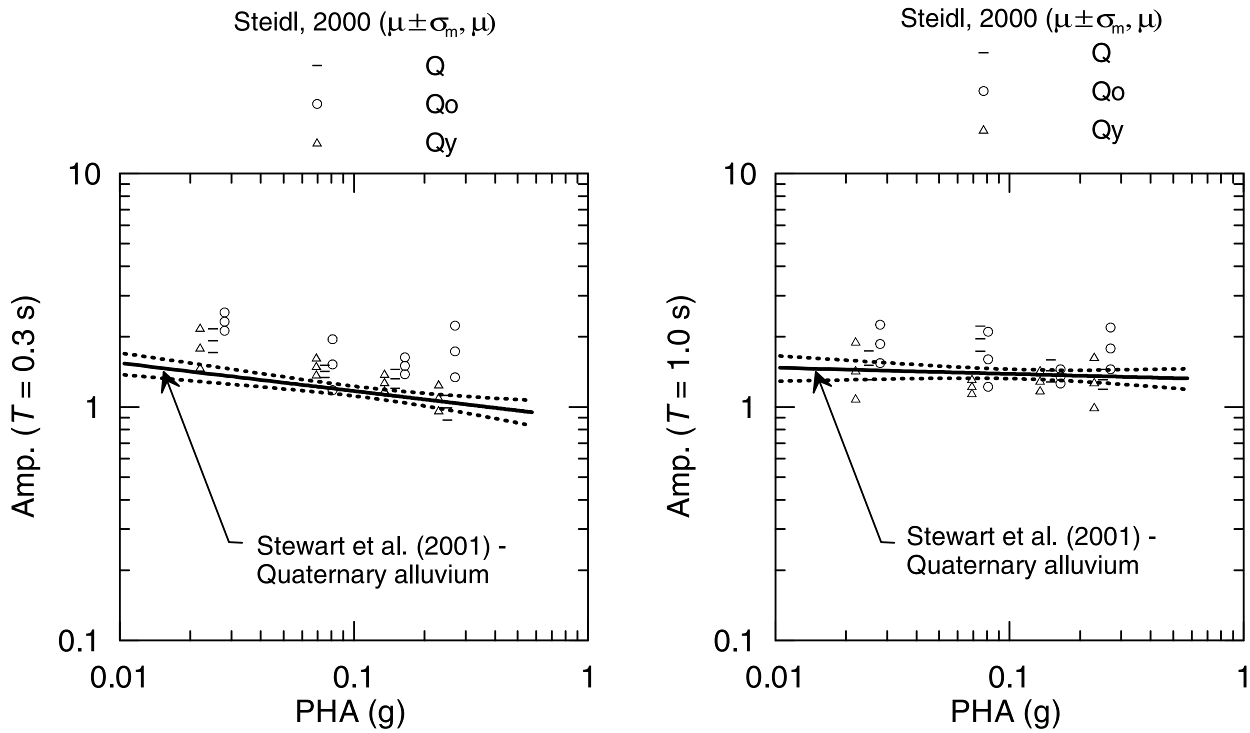

Fig. 5.13(a). Amplification of short- and mid-period spectral acceleration for Quaternary alluvial sediments. Results shown include median from regression analysis and standard deviation of the median (Steidl) and ± 95% confidence intervals on the regression (Stewart et al.).

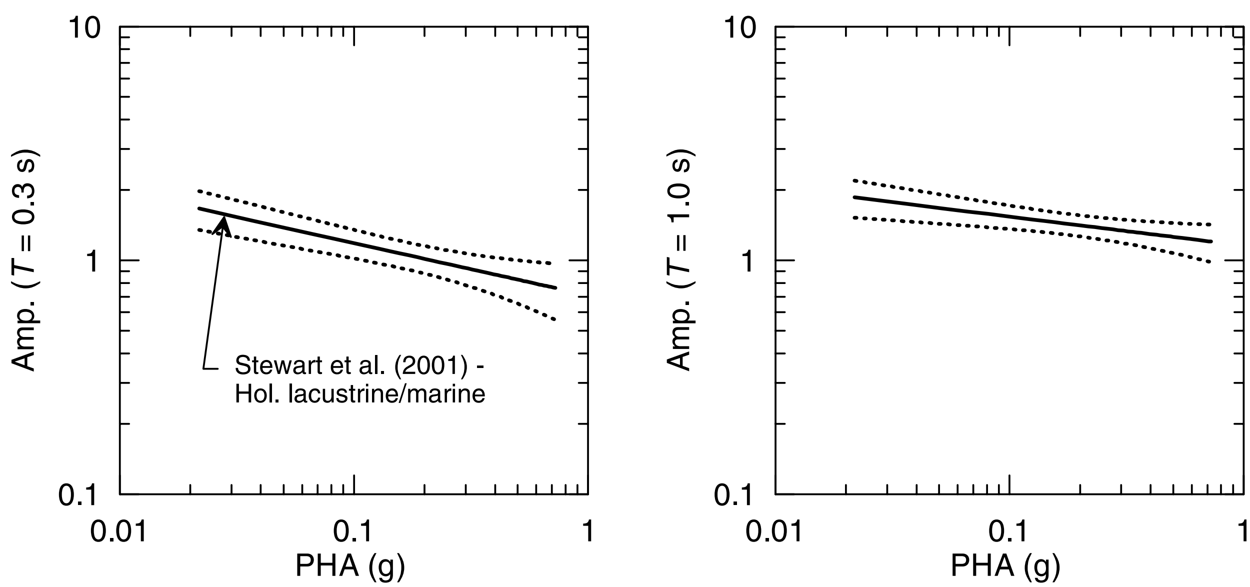

Fig. 5.13(b). Amplification factors for Holocene lacustrine/marine sediments. See caption for 5.13a.

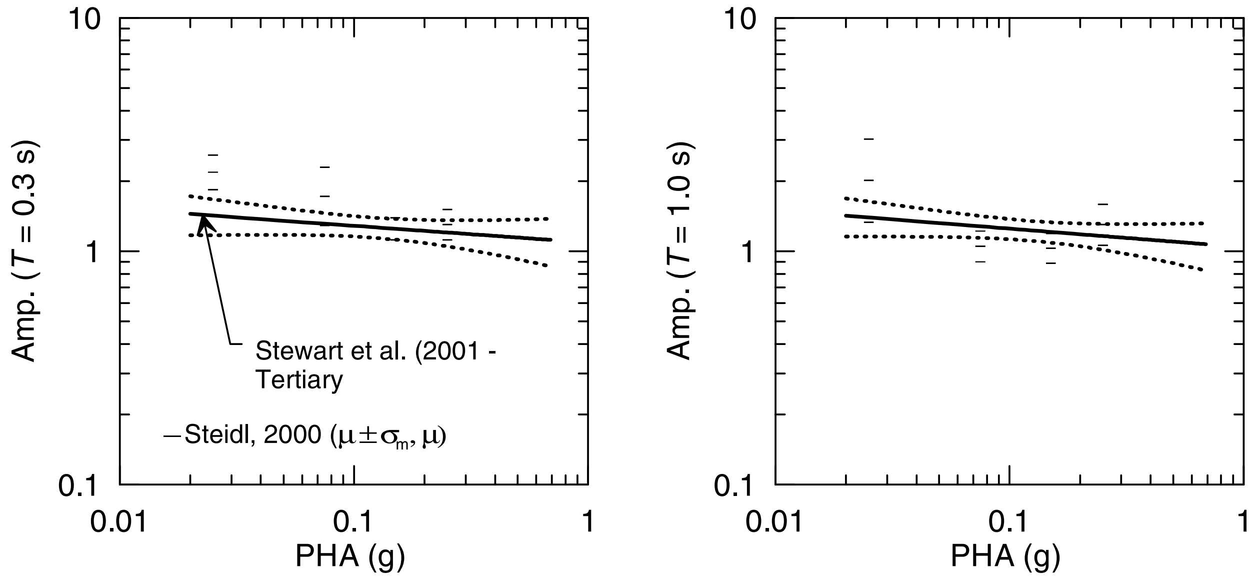

Fig. 5.13(c). Amplification factors for Tertiary sediments. See caption for 5.13a.

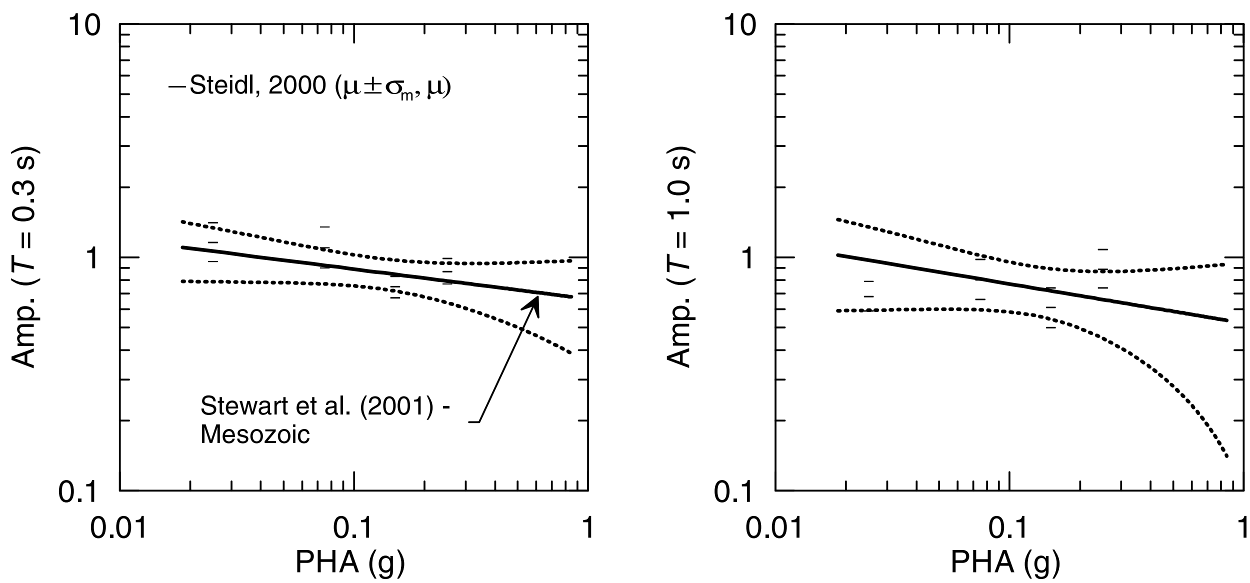

Fig. 5.13(d). Amplification for Mesozoic materials. See caption for 5.13a.

Field (2000), Steidl (2000), and Stewart et al. (2001) have evaluated amplification factors as a function of 30-m V_s. The 30-m V_s site classifications used by Field are based on maps by Wills et al. (2000) that correlate 30-m V_s to surface geology. The 30-m V_s site classifications used by Steidl and Stewart et al. are based on in situ measurements from nearby boreholes. Field found relatively distinct variations in weak motion amplification levels across different NEHRP site categories (e.g., Figure 5.14a). Steidl found a good correlation between amplification and 30-m V_s at long periods (T = 1.0 and 3.0 s); these results are similar to those of Harmsen (1997) previously reported (Fig. 5.11). At smaller periods, the correlation between amplification and 30-m V_s was relatively weak and dependent on shaking amplitude.

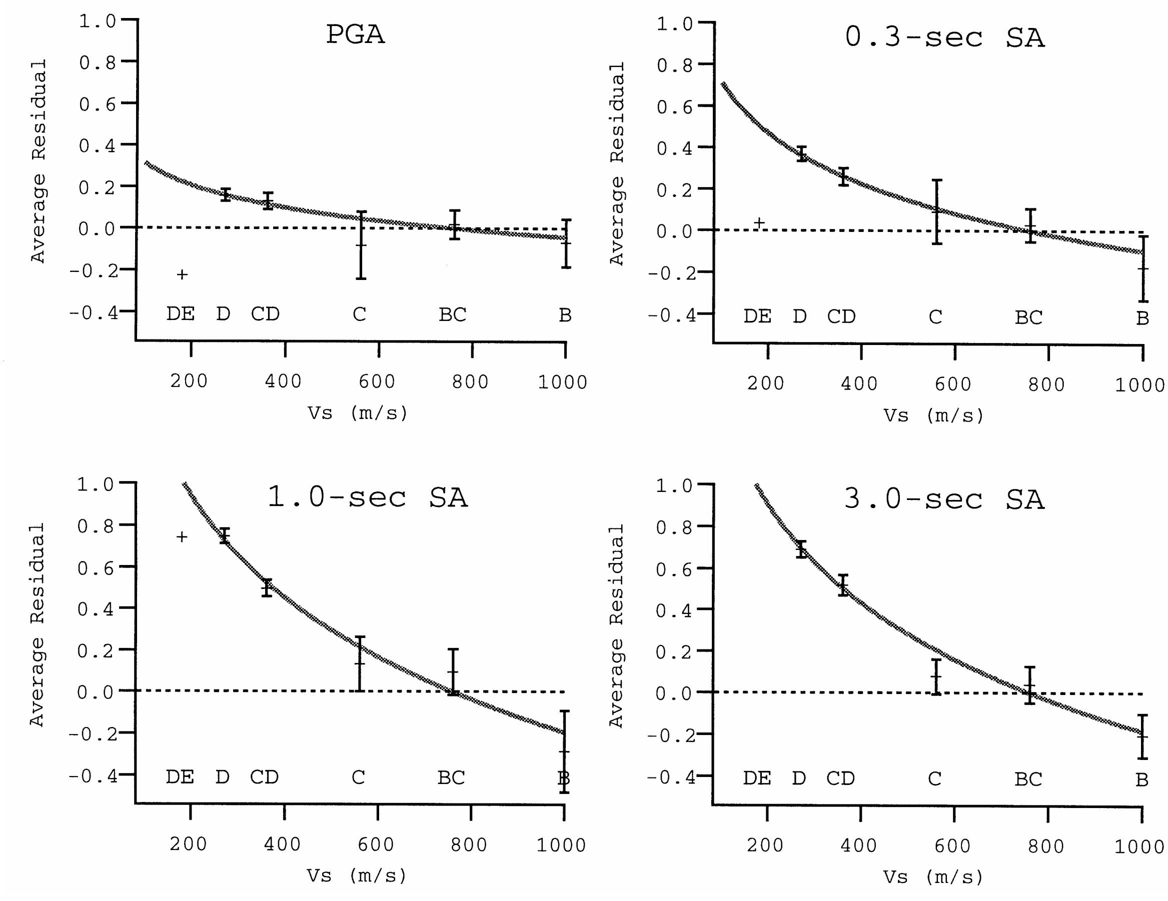

Fig. 5.14(a). Average residuals between southern California strong motion data and attenuation prediction for V_s = 760 m/s site condition as function of 30-m V_s (Field, 2000).

Stewart et al. found good correlations between amplification levels and 30-m V_s at short- and long-period ranges for the NEHRP C and D categories (the only categories with sufficient data to produce stable regression results). These results are shown in Figure 5.14b along with amplification factors in the NEHRP recommended provisions for new buildings (BSSC, 1998). Amplification factors for both categories are smaller than the corresponding site factors in the NEHRP provisions.

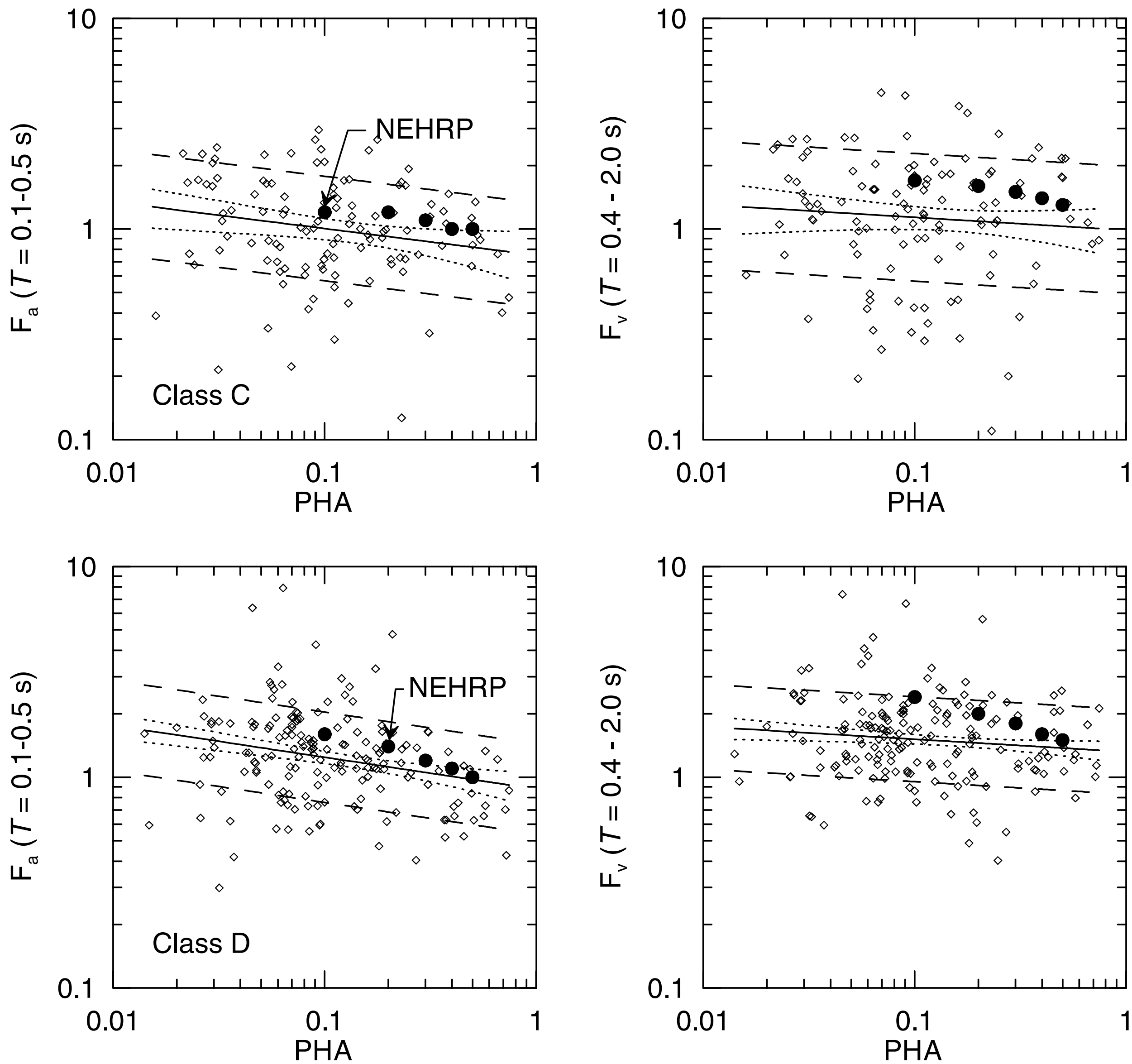

Fig. 5.14(b). Amplification factors at short- and long-period ranges from Stewart et al. (2001) compared to site factors in NEHRP provisions (BSSC, 1998).

Ground motion amplification factors have been evaluated by Stewart et al. (2001) using the geotechnical classification scheme proposed by Rodriguez-Marek et al. (2001). The results indicated distinct spectral de-amplification for Category B (intact rock), larger levels of amplification for Categories C and D (shallow and deep stiff soil, respectively) that were similar to each other at low- to intermediate periods, and large weak-motion amplification and nonlinearity for Category E (soft clay).

An important issue is the relative consistency of ground motions within site categories defined by the surface geology, 30-m V_s, and geotechnical classification schemes. Stewart et al. have judged the "quality" of classification schemes by compiling inter-category standard errors, σ_R, which represent for a given categorization scheme the average dispersion of data from all site categories in the scheme relative to amplification-adjusted reference motions. Standard error results for spectral acceleration in soil categories are plotted as a function of period in Figure 5.15. The largest error terms at all periods are obtained from the 30-m V_s and geotechnical classification schemes. The smallest error terms are from detailed geology schemes such as age + depositional environment or age + material texture. Maximum differences in the category dispersion values are as large as 0.1 in natural logarithmic units, which is a significant variation. Also shown for reference are the error terms from the Abrahamson and Silva (1997) attenuation relationship. Note that the Abrahamson and Silva error terms are strongly magnitude dependent, an effect not observed by Stewart et al. for amplification-adjusted residuals. Based on these results, Stewart et al. concluded that detailed surface geology (i.e., age + depositional environment or age + material texture) provides a reasonable basis for site categorization for evaluation of spectral acceleration amplification factors.

Further advances in the characterization of site effects on spectral acceleration may require the use of parameters that represent features of the site other than characteristics of near-surface sediments. Such parameters may include basin depth and/or distance from basin edge. Some promising preliminary results in this regard have been obtained recently by Field et al. (2000), Lee and Anderson (2000), and Steidl (2000) for sites in the Los Angeles basin. These studies found amplification to increase significantly with basin depth (defined as depth to V_s = 2.5 km/s isosurface), with representative results shown in Figure 5.16. The amplification factors in Figure 5.16 are defined relative to the prediction appropriate to each site class (i.e., not relative to a particular geologic formation or V_s = 760 m/s). Further study of these effects is needed for other basins, and using additional basin parameters.

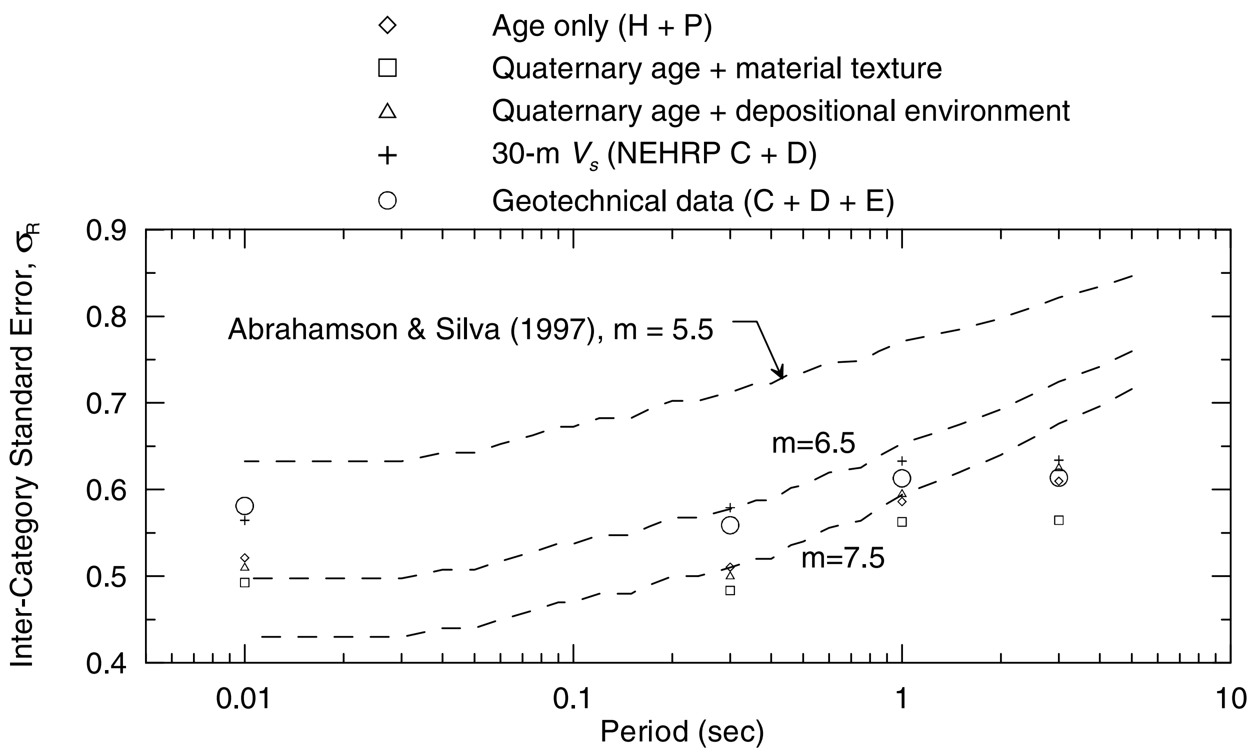

Fig. 5.15. Inter-category standard error terms for spectral acceleration by Stewart et al. (2001) and error terms derived by Abrahamson and Silva (1997), soil categories.

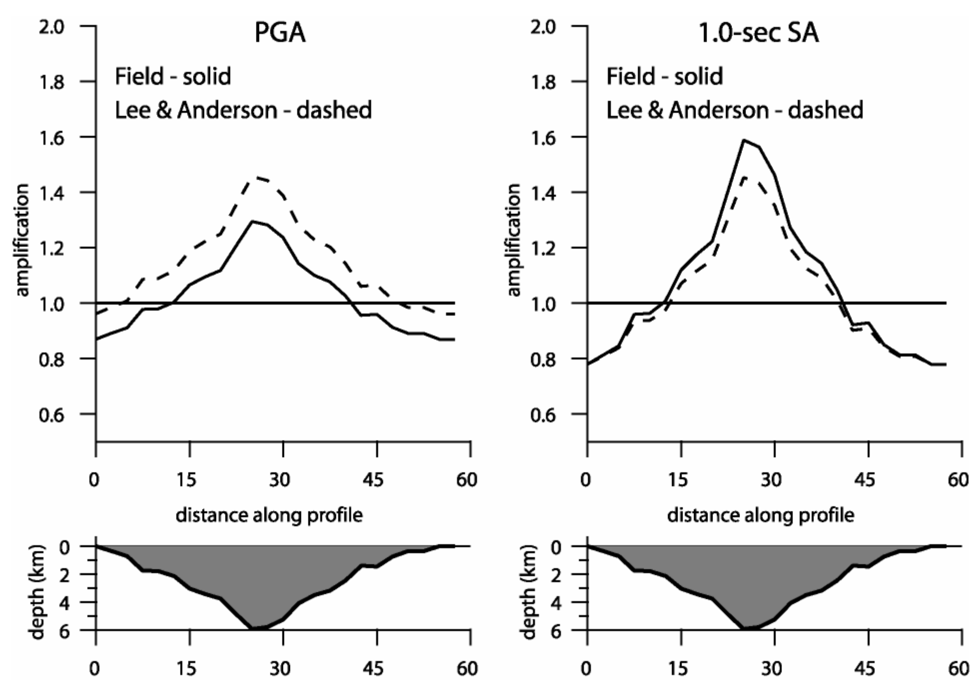

Fig. 5.16. Basin depth amplification factors implied by the attenuation relationships by Lee and Anderson (2000) and Field (2000) for sites along cross section through Los Angeles basin, after Field et al. (2000).

The above findings provide insight into the critical influence of reference site condition on amplification factors. The reference site condition for the Steidl and Stewart et al. studies (e.g., Figure 5.13) is based on "rock" recordings in active regions (most from California). The predominant site condition at these recording sites is "soft rock." Amplification factors derived in this way are generally lower than those identified from studies in which reference motions were taken from relatively competent rock sites (e.g., Figures 5.8-5.9, 5.11). For practical application, it is critical that reference site conditions for attenuation relations and amplification factors be compatible, to avoid the introduction of bias. For California, "rock" attenuation relations apply for a soft rock condition, and so this would appear to be the most appropriate reference site condition for amplification factors.

(d) ***Variability/uncertainty in site amplification factors***

Preceding figures (e.g., Figures 5.8-5.11, 5.14) illustrated a significant level of variability among amplification factors within a given site category. When amplification is defined using a non-reference site approach in which reference motions are derived from attenuation relations, this variability largely reflects the uncertainty associated with the reference motion model. However, even if reference motions are well defined (i.e., nearby rock station), amplification factors for a specific site derived from multiple events will be subject to variability as a result of variations in sediment nonlinearity, wave incidence angle, backazimuths, and wave types, as well as ground motion incoherence.

Across a collection of sites within a given category, variability of site response for a given event would be expected due to variations in physical site characteristics. To the extent that these variations are predictable as a result of their dependence on site condition, this variability can be said to contribute epistemic uncertainty to the amplification model. The sources of epistemic uncertainty to an amplification error term depend on the sophistication of the amplification function. For example, if a factor such as reference motion amplitude is incorporated, then epistemic uncertainty associated with nonlinear sediment response is reduced. Similarly, if site categories are well defined, epistemic uncertainty associated with site-to-site geologic/soil variability is minimized.

Given these sources of variability, an important question is how should amplification function error terms be used? The answer depends on the manner in which amplification functions are derived. When derived using attenuation estimates of reference motions, the intra-category amplification error term becomes the appropriate ground motion error term for that site condition (although an adjustment for inter-event variability should be made if reference motions are derived using an event term, see Stewart et al., 2001). When derived using reference site methods, the amplification error term must be combined with the reference motion error term to evaluate the appropriate ground motion error term. For example, if the amplification function (F) varies linearly with PHA (e.g., Eq. 5.1), then the ground motion error (σ) is calculated as (Bazzuro and Cornell, 1999a),

$$\sigma = \sqrt{(b+1)^2 \sigma_r^2 + \sigma_F^2} \tag{5.2}$$

where σ_r = reference motion error and σ_F = amplification function error. Note that if $b < 0$, which is generally the case if sediments soften with increasing shaking amplitude, then ground motion error (σ) can be less than reference motion error (σ_r).

(e) ***Summary and discussion***

In the previous sections we outlined critical features of observational studies of ground motion amplification. Most of these studies quantified ground motion variations relative to a "hard rock" reference site condition. The attractive feature of this approach is obvious — ground response at the reference site should be negligible. The drawback is that reference motions for such site conditions cannot be readily evaluated, because the data inventory for such conditions is insufficient to derive attenuation relationships. The ability to develop attenuation functions for the reference site condition is essential for practical application of amplification models. For California, the most logical choice may be weathered rock sites (mostly Tertiary), for which strong motion data is much more abundant than "hard" rock sites. Most of the above-referenced studies used a hard rock site condition, including the studies by Borcherdt and Glassmoyer (1994) that form the empirical basis for current U.S. seismic design code provisions. The evaluation of amplification functions for more representative conditions is an important research need recently addressed within PEER (e.g., Figure 5.14b).

Some important features of ground response illustrated by the aforementioned studies include

- There are significant differences between sediment response effects for marine clays (e.g., San Francisco Bay Mud) and alluvial sediments.

- Nonlinearity in sediment response has been well established at high frequencies, but is much less significant at low frequencies (f < ~1 Hz).
- Site amplification factors have generally been related to surface geology or a parameter directly correlated to surface geology such as 30-m V_s. Recent work has found that two detailed geologic classification schemes that incorporate information beyond age produce less scatter in amplification factors than a geologic age-only scheme, the NEHRP 30-m V_s scheme, and a scheme based on geotechnical data.
- Recent studies have found site amplification for a given surface geology to correlate well with depth to V_s = 2.5 km/s basement rock. Additional research is needed to gain further insights into "basin effects," and should consider other parameters known to affect basin response such as direction of wave propagation and distance to basin edge (see Section 5.4).

5.3 ONE-DIMENSIONAL GROUND RESPONSE

The term "one-dimensional ground response" refers to the modification of vertically (or nearly vertically) propagating body waves by sediment layers. Ground response is one of two processes contributing to the amplification at sediment sites relative to "rock" sites described in the section above (the other is basin response). The body of literature on ground response is extensive, and a complete review is beyond the scope of this report. Rather, the focus here is on how ground response analyses can be used to reduce bias and decrease uncertainty in hazard estimates at soil sites. The first two sections below briefly review critical dynamic soil properties for ground response and common analytical models. In the final section, we discuss uses of ground response analysis results in hazard calculations.

5.3.1 Critical Dynamic Soil Properties for Ground Response

The soil properties most commonly utilized in response analyses for horizontal ground motions include a profile of small strain shear wave velocity (V_S), and relationships for the variation of normalized shear modulus (G/G_{max}) and hysteretic soil damping (β) with shear strain (γ) within the soil. Shear wave velocity is related to maximum shear modulus as $G_{max} = V_s^2\rho$, where ρ = mass density of soil.

Profiles of V_S are best obtained from in situ measurements by downhole, crosshole, or suspension logging techniques. Geophysical techniques such as spectral analysis of surface waves can also be effective. If in situ measurements are unavailable, V_S can be estimated from correlations with other soil properties. The most accurate correlations are generally derived locally for specific soil formations (e.g., Dickenson, 1994 for San Francisco Bay Mud). More general correlations are available for clays (based on overconsolidation ratio and undrained shear strength, Weiler, 1988) and granular soils (based on penetration resistance and effective stress, Seed et al., 1986 for sand and Rollins et al., 1998 for gravel).

Modulus reduction and damping relations can be derived from material-specific testing, usually with simple shear (e.g., Dorourdian and Vucetic, 1995) or torsional shear devices. For most applications, however, "standard" curves for various soil types and material properties are used. These curves have generally been derived in one of two ways. First, laboratory-derived standard curves are available that are sensitive to soil plasticity for cohesive materials such as clays, and effective overburden stress for granular materials such as sands, low plasticity silts, and gravels. Second, curves can be derived from back-analysis of regional ground motion records (Silva et al., 1997). No formal consensus has been reached on standard curves that should be used for ground response studies. Recent studies by Stewart and Baturay (2001) and Silva et al. (1999, 2000) invoked the curve selection criteria listed in Table 5.5. Curves derived from laboratory tests (e.g., Table 5.5a) are well defined over a strain range of 10^{-3}% to 1% and for effective overburden stresses less than about 2-3 atmospheres. Ongoing work is expanding the database of available laboratory curves to strains as high as 10% (Hsu and Vucetic, 1999; Vucetic et al., 1998a) and overburden pressures as high as 4000 kPa. There is also a need for material characterization for silts, peats, loess, and weathered bedrock materials.

The modulus reduction and damping curves discussed above are derived from backbone curves established from the first cycle of cyclic tests conducted at frequencies typically on the order of one Hz. For granular materials, the curves do not incorporate the effects of pore-pressure generation under cyclic loading. When field conditions depart significantly from these test conditions, more sophisticated material characterization may be required. The specific case of soil liquefaction and cyclic mobility in granular soils is discussed in detail in a companion PEER report by Kramer and Elgamal (in preparation). For earthquakes of long duration (e.g., large-magnitude subduction zone events), cyclic modulus degradation may be important. Rate effects are generally neglected in practice, but may be important in some cases.

Table 5.5(a) Criteria used by Stewart and Baturay (2001) for selecting modulus reduction and damping curves

Soil Type	Condition[1]	Reference
Sand and silty sand	Z < 100 m	Seed et al. (1986), upper bound sand G/G_{max}, lower bound ?
	Z > 100 m	EPRI (1993): Z=251-500 ft.
Clays, silty clays, loams	PI=15 & Z<100m	Vucetic and Dobry (1991), PI=15[2]
	PI=15 & Z>100m	Stokoe (1999), CL curve, Z = 100-250 m
	PI >= 30	Vucetic and Dobry (1991)
	Bay Mud	Sun et al. (1988)
	Old Bay Clay	Vucetic and Dobry (1991), PI=30[3]
Bedrock	V_S < 900 m/s	Use soil curves for appropriate material type, depth, and PI
	V_S > 900 m/s	Schnabel (1973)

[1] Z=depth, PI = plasticity index

[2] Consistent with Stokoe (1999), CL curve, Z < 100 m

[3] Consistent with Guha et al. (1993) material testing

Table 5.5(b) Criteria used by Silva et al. (1999, 2000) for selecting modulus reduction and damping curves

Soil Type	Condition	Reference
Gravels, sands, low PI clays, and Quaternary/Tertiary rock	Located in San Francisco region	EPRI (1993), Silva et al. (1997)
Bay Mud, Old Bay Clay	All	Vucetic and Dobry (1991), PI=30
Peninsular range alluvium and Quaternary/Tertiary rock	Located in Los Angeles region	Silva et al. (1997)
Any	Depth > 150 m	Linear

5.3.2 Ground Response Models

Most ground response analysis models solve equations of motion for one-dimensional wave propagation. The principal characteristic distinguishing various analysis routines is the soil material model. Three general categories of material models are described below: equivalent-linear and nonlinear models for one horizontal direction of shaking, and nonlinear models for multiple directions of shaking.

(a) *Equivalent-linear model*

Nonlinear behavior of soil can be modeled by an equivalent-linear characterization of dynamic properties (Seed and Idriss, 1970). The most widely used computer program utilizing this model is SHAKE91 (Idriss and Sun, 1991), which is a modified version of the program SHAKE (Schnabel et al., 1972). The program uses an equivalent-linear, total stress analysis procedure to compute the response of a one-dimensional, horizontally layered viscoelastic system subjected to vertically propagating shear waves. The program uses the exact continuum solution to the wave equation adapted for use with transient motions through the Fast Fourier Transform algorithm.

The equivalent-linear method models the nonlinear variation of soil shear moduli and damping as a function of shear strain. The hysteretic stress-strain behavior of soils under symmetrical cyclic loading is represented by an equivalent modulus, G, corresponding to the secant modulus through the endpoints of the hysteresis loop and equivalent-linear damping ratio, β, which is proportional to the energy loss from a single cycle of shear deformation. An iterative procedure, based on linear dynamic analysis, is performed to find the shear moduli and damping ratios corresponding to the computed shear strains. Initial estimates of the shear strains and corresponding estimates of dynamic moduli and damping ratios are provided for the first iteration. For the second and subsequent iterations, moduli and damping ratio values corresponding to an "effective" strain are determined. This "effective" strain is calculated as a fraction of the maximum strain from the previous iteration.

An alternative solution to the ground response problem with equivalent-linear material characterization has been developed by W. J. Silva and co-workers (e.g., Silva and Lee, 1987; Schneider et al., 1993). In this approach, control motions are represented with power spectral density functions instead of time histories. The rock power spectrum is propagated through a one-dimensional soil profile using the plane wave propagators of Silva (1976). Random vibration theory (RVT) is used to compute probabilistic estimates of peak time-domain values of shear strain or acceleration from the power spectrum. This procedure is coded into the computer program RASCAL (Silva and Lee, 1987).

(b) *Nonlinear models: one horizontal direction of shaking*

Nonlinear models solve the one-dimensional wave equation by direct numerical integration in the time domain. A variety of material models are used, which range from relatively simple cyclic stress-strain relationships (e.g., Ramberg and Osgood, 1943; Finn et al., 1977; Pyke, 1979; Vucetic, 1990) to advanced constitutive models incorporating yield surfaces, hardening laws, and flow rules (e.g., Wang, 1990). A model by Pestana and Nadim (2000) allows the use of a relatively simple hysteretic nonlinear analysis (e.g., Salvati et al., 2001) or a more sophisticated analysis utilizing an advanced constitutive relationship (e.g., Biscontin et al., 2001). Nonlinear methods can be formulated in terms of effective stresses to allow modeling of the generation, redistribution, and eventual dissipation of excess pore pressure during and after earthquake shaking, whereas equivalent-linear methods can only perform total stress analysis.

Cyclic nonlinear models generally consist of a backbone curve and rules that describe unload-reload behavior, pore-pressure generation, and cyclic modulus degradation. Backbone curves can be constructed from modulus reduction curves coupled with the small strain modulus (G_{max}). Unload-reload rules can similarly be formulated to reproduce hysteretic damping values expected from standard curves of damping ratio vs. shear strain (e.g., Vucetic and Dobry, 1991; Seed et al., 1986). These formulations tend to predict damping ratios approaching zero at small strains, which is inconsistent with observed behavior (Vucetic et al., 1998b). This is resolved by the introduction of a viscous damping term that applies across all strain levels.

Several nonlinear modeling programs are summarized in Table 5.6. What differentiates these programs are (1) the numerical integration schemes used in the solution of the wave equation and (2) the constitutive models for cyclic stress-strain behavior, cyclic modulus degradation, and pore-pressure generation. The following discussion is focused on constitutive models.

Table 5.6 Computer codes for one-dimensional nonlinear ground response analyses

Program	Nonlinear Model	Reference	Comments
TESS	Pyke (1979)	Pyke (2000)	-
DESRA-2	Konder and Zelasko (1963); Masing (1926)	Lee and Finn (1978)	-
DESRAMOD	same as DESRA-2 + Dobry et al. (1985)	Vucetic (1986)	modified DESRA-2
D-MOD_2	Matasovic and Vucetic, (1993, 1995)	Matasovic and Vucetic (1993)	modified DESRA-2
MARDESRA	Martin (1975)	Mok (1990, *pers. com.*)	modified DESRA-2
DESRA-MUSC	same as DESRA-2 + Qiu (1997)	Qiu (1997)	modified DESRA-2

Note: Additional nonlinear codes for multi-directional shaking are discussed in the text.

Program DESRA-2 was developed by Lee and Finn (1978). The program evaluates the dynamic response of a multiple-degree-of-freedom lumped mass system. Model parameters were developed only for sandy soil deposits. The computer program DESRAMOD was modified from DESRA-2 by Vucetic (1986), who replaced the original pore water pressure model for sand with that of Dobry et al. (1985). Matasovic and Vucetic (1993) further modified the program by replacing the stress-strain (backbone curve) model of Kondner and Zelasko (1963) with the MKZ model, and the modified program was named D-MOD. In addition, the Matasovic and Vucetic (1995) cyclic degradation-pore water pressure generation model for clay was incorporated into the program. D-MOD takes into account the possible negative pore pressures that may develop in overconsolidated clays during earthquake shaking. D-MOD_2 is the most recent version of D-MOD, which has been adjusted to simulate seismically induced slip that may occur along weak interfaces (Matasovic, *personal communication*). MAR-DESRA and DESRA-MUSC are other modified versions of DESRA-2. MAR-DESRA varies from DESRA-2 in that it incorporates the Martin-Davidenkov model for nonlinear soil behavior (Martin, 1975; Martin and Seed, 1982). The DESRA-MUSC program has been further modified as described by Qiu, 1997.

(c) ***Nonlinear models: multi-directional shaking***

Each of the analysis routines discussed in Section (b) above analyzes only one horizontal component of ground response. The effects of simultaneous shaking in three directions can be considered with advanced constitutive models, which are implemented into programs such as DYNA1D (Prevost, 1989), SUMDES (Li et al., 1992), SPECTRA (Borja and Wu, 1994), and AMPLE (Pestana and Nadim, 2000). These models incorporate a yield surface that describes the limiting stress conditions for which elastic behavior is observed, hardening laws that describe changes in the size and shape of the yield surface as plastic deformation occurs, and flow rules that relate increments of plastic strain to increments of stress. Such models require a larger number of parameters than the simple models discussed above in Sections (a) and (b), and the associated parametric uncertainty in the analysis results is generally poorly defined. A detailed discussion of these models is beyond the scope of this report. Also beyond the scope of this report are site response models for two- or three-dimensional soil systems.

(d) *Verification studies*

Many studies have been performed using SHAKE and various nonlinear codes to verify the effectiveness of one-dimensional wave propagation analysis routines. These routines can be most effectively verified when the input motion is reasonably well known, which is the case when a rock recording is available near a soil recording, or from vertical array data. We focus here on these types of verification studies. However, it is noted that additional verification studies of the equivalent-linear technique have been performed using input motions calculated from a seismological simulation technique (EPRI, 1993; Silva et al., 1997).

A number of verification studies have utilized data from pairs of nearby rock/soil recordings. The rock motion is taken as input to ground response analyses, and the computed and recorded soil motions are compared. Several examples of studies of this type are summarized in Table 5.7(a). At the soft soil sites considered in these studies, ground response effects as modeled by SHAKE and MARDESRA were able to predict reasonably well variations between soil/rock spectra across a broad period range (e.g., Figure 5.17). Results were mixed for deep stiff soil sites, with relatively good predictions at northern California deep clay sites for $T \leq 1$ s (e.g., Figure 5.18a), and relatively poor predictions for many Los Angeles area alluvial sites (e.g., Santa Monica site in Figure 5.18b). The difference in model accuracy at Bay Area and Los Angeles area sites may be associated with basin effects (particularly at long periods), as the basin geometry at the Bay Area sites is relatively wide and flat as compared to the Los Angeles-area sedimentary basins.

One noteworthy outcome of these studies is that the prediction accuracy for soil spectra is strongly dependent on rock (control) motion characteristics. For example, as shown in Figure 5.19, Idriss (1993) found predicted spectra at the Treasure Island (soil) recording site to provide a good match to the recorded spectrum when the control motion is taken from the nearby Yerba Buena Island (rock) seismograph (top frame of Figure 5.19), but a highly variable match when control motions are taken from other rock stations in the San Francisco-Oakland-Berkeley area (bottom frame). Since rock motion characteristics cannot be known a priori, this suggests that significant uncertainty is introduced to ground response analysis results from uncertainty and variability in input motion characteristics.

Table 5.7 Verification studies of ground response analysis codes

Earthquake	Soil Condition - Recording Locations	Reference	Codes Investigated
(a) Nearby Rock-Soil Pairs			
1985 Michoacan-Guerrero	Soft clay - Mexico City (2)	Seed et al. (1987)	SHAKE
1989 Loma Prieta	Bay mud - San Francisco Bay Area (11 sites)	Idriss (1990); Dickenson (1994)	SHAKE; SHAKE, MARDESRA
1989 Loma Prieta	Deep stiff clay - Oakland, Emeryville; Gilroy (4 sites)	Chang (1996); Darragh and Idriss (1997)	SHAKE, DMOD; SHAKE
1994 Northridge	Deep alluvium - Sylmar, Hollywood, Santa Monica (3 sites)	Chang et al. (1996)	SHAKE, DMOD
(b) Vertical Arrays			
unnamed m=6.2, 7.0 events	Soft silt - Lotung	Chang et al. (1990) and Li et al. (1998); Beresnev et al. (1995); Borja et al. (1999); Elgamal et al. (1995)	SUMDES; DESRA2; SPECTRA; unnamed code
1995 Kobe	Liquefiable sand - Kobe Port Island	Wang et al.(2001); Elgamal et al. (1996)	SUMDES; unnamed code
1987 Superstition Hills	Liquefiable sand - Wildlife site, CA	Matsovic and Vucetic (1996)	DMOD

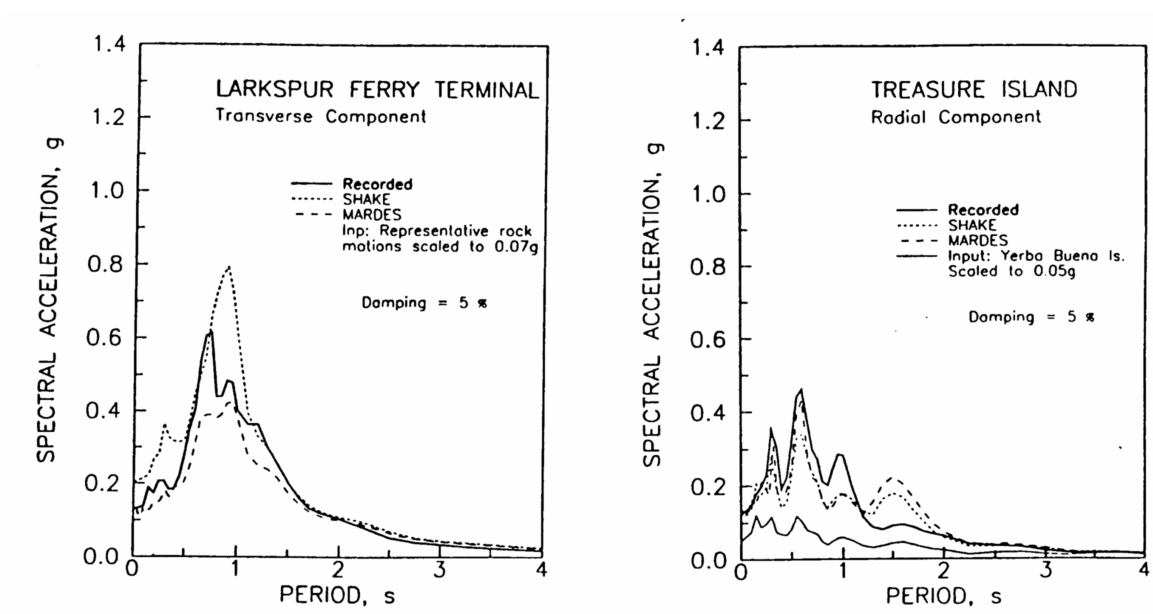

Fig. 5.17. Comparison between recorded and calculated response spectra at representative soft clay sites, from Dickenson (1994).

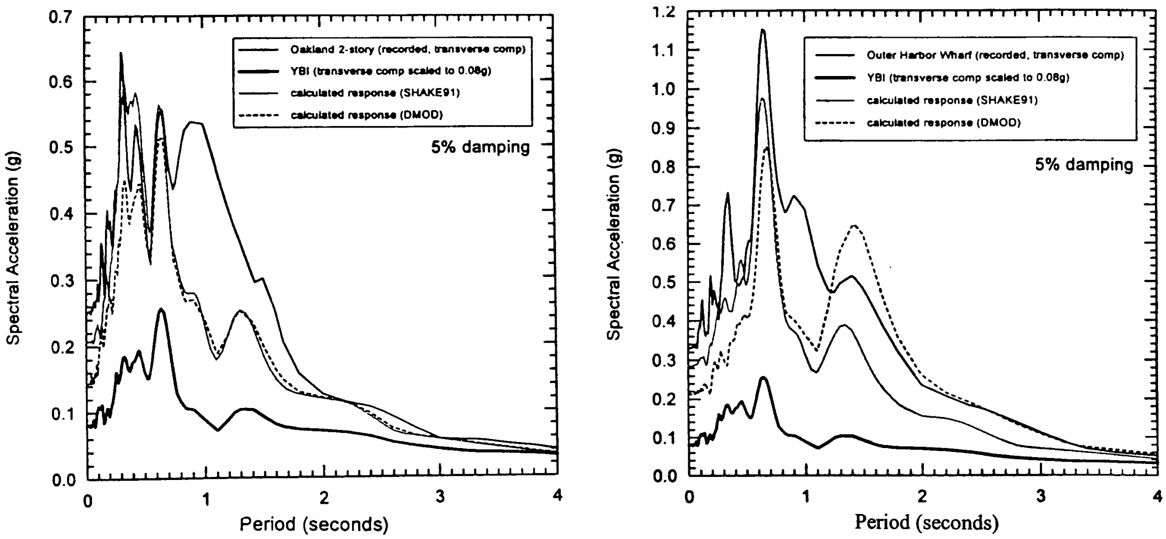

Fig. 5.18(a). Comparison between recorded and calculated response spectra at selected deep stiff clay sites in San Francisco Bay Area, from Chang (1996).

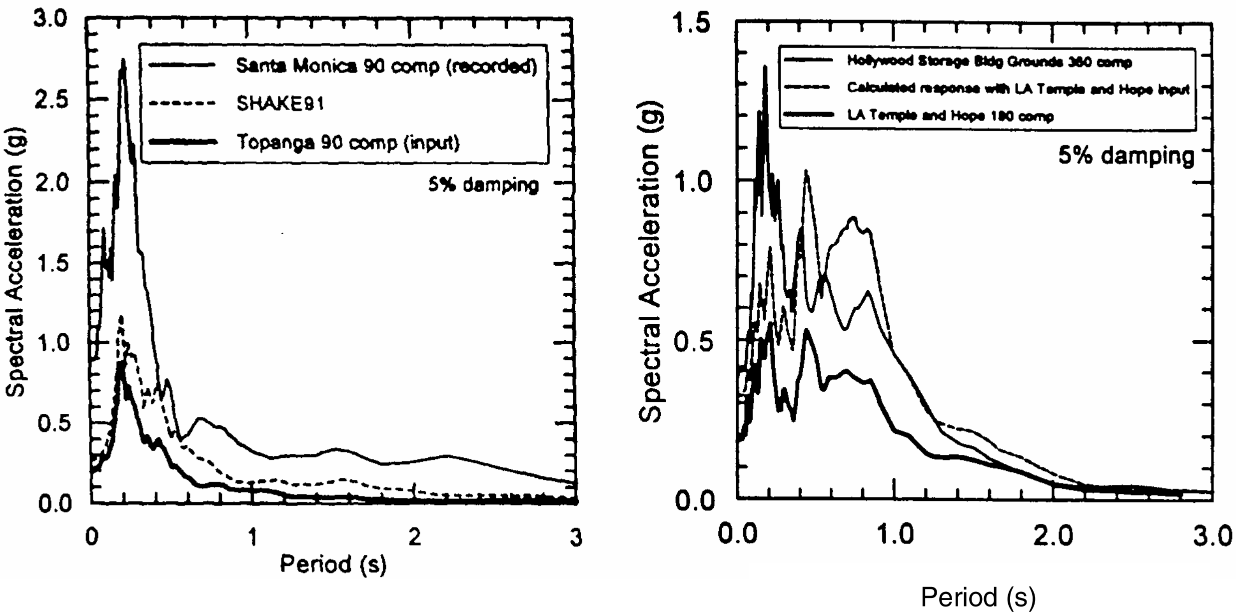

Fig. 5.18(b). Comparison between recorded and calculated response spectra at selected deep alluvial sites in Los Angeles area, from Chang (1996).

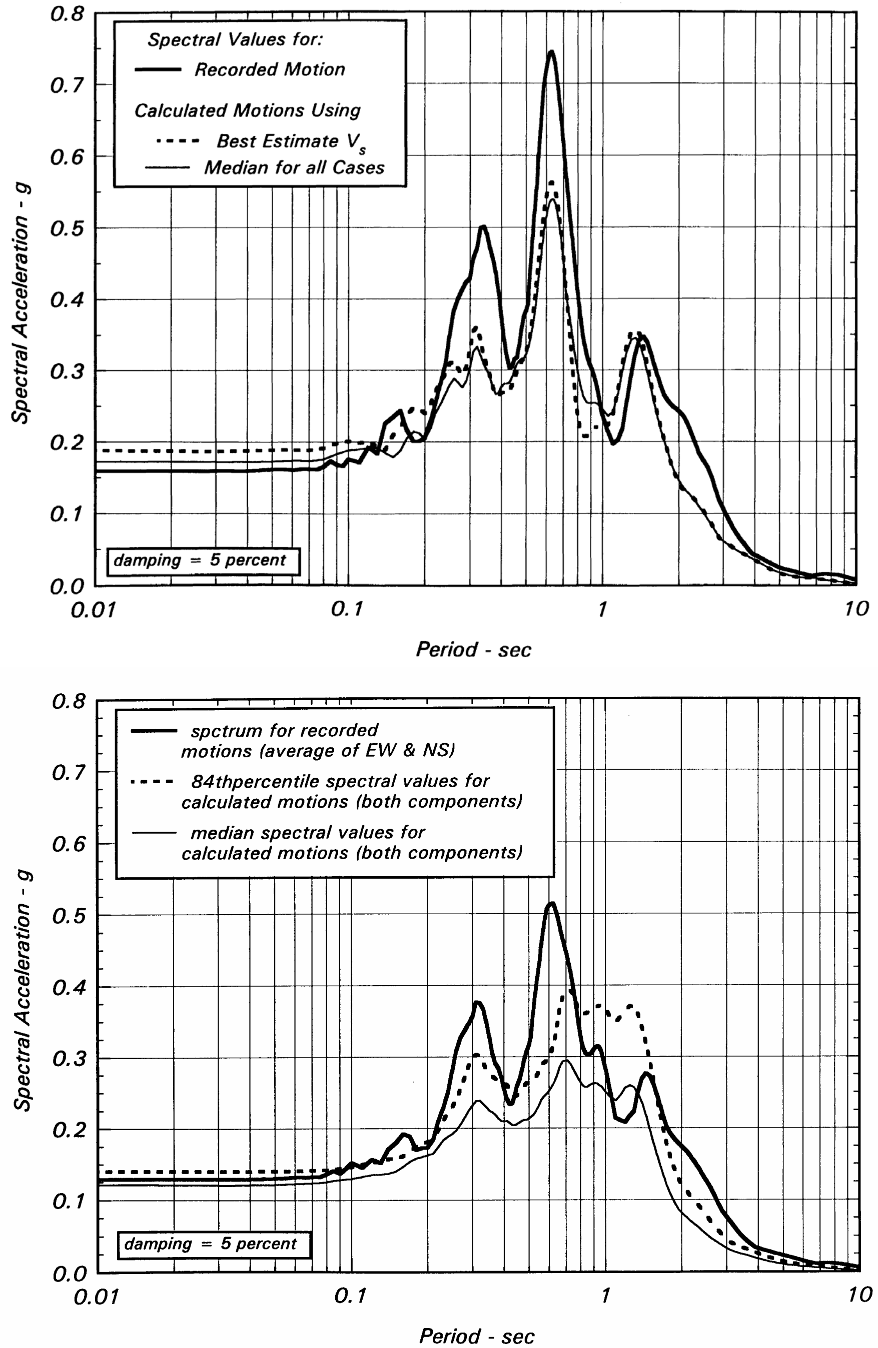

Fig. 5.19. Comparison of acceleration response spectrum of recorded motion at Treasure Island strong motion site (1989 Loma Prieta earthquake) with calculated spectra from ground response analyses. Calculations in upper frame utilized nearby rock recording (Yerba Buena Island) as control motion; lower frame presents statistical variation in calculated spectra for suite of control motions from rock sites in region surrounding Treasure Island. From Idriss, 1993.

A more direct verification of one-dimensional ground response analysis procedures is enabled by recordings from vertical arrays. Many such arrays have been installed worldwide, and a few that have recorded strong ground motion (i.e., PHA > 0.1g) are listed in Table 5.7(b). Data from one of these arrays, the Lotung large-scale seismic test site in Taiwan, have been used to validate several one-dimensional ground response analysis codes including SUMDES (Chang et al., 1990; Li et al., 1998; Wang et al., 2001), DESRA2 (Beresnev et al., 1995), SPECTRA (Borja et al., 1999), and an unnamed research code (Elgamal et al., 1995). Example results from these analyses are shown in Figure 5.20, which applies for the SPECTRA code. Both the fully nonlinear SPECTRA analysis and the equivalent-linear SHAKE analysis provide excellent matches in the time domain to the recorded motions. Other studies have shown improved matches in the time domain for nonlinear codes (e.g., Chang et al., 1990; Wang et al., 2001).

An important outcome of many of the verification studies cited above is that prediction residuals from nonlinear methods were not significantly smaller than those from equivalent-linear methods (a notable exception is the Kobe Port Island site, which liquefied). However, the amplitude of shaking at each of these sites was relatively small in comparison to typical design-basis ground motions in seismically active regions such as California. While not true "verifications" in the manner defined at the beginning of this section, several studies have compared the results of equivalent-linear and nonlinear analyses (EPRI, 1993, Silva et al., 2000). Silva et al. (2000) used simulated motions (from the Stochastic Ground Motion model, Section 6.3) with a wide range of amplitudes as input into equivalent-linear (RASCAL, Silva and Lee, 1987) and nonlinear (DESRA-MUSC, Qiu, 1997) ground response analyses for the calculation of amplification factors. In general, there was good agreement between the two approaches over most of the frequency range 0.1-100 Hz. However, for large input motions and soft soil profiles, the nonlinear damping exceeded that for the equivalent-linear damping, and the nonlinear amplification factors were below the equivalent-linear factors. Which of these sets of amplification factors is more nearly "correct" (based on comparisons to data) is unknown, and further comparative study of nonlinear and equivalent-linear analyses is therefore needed.

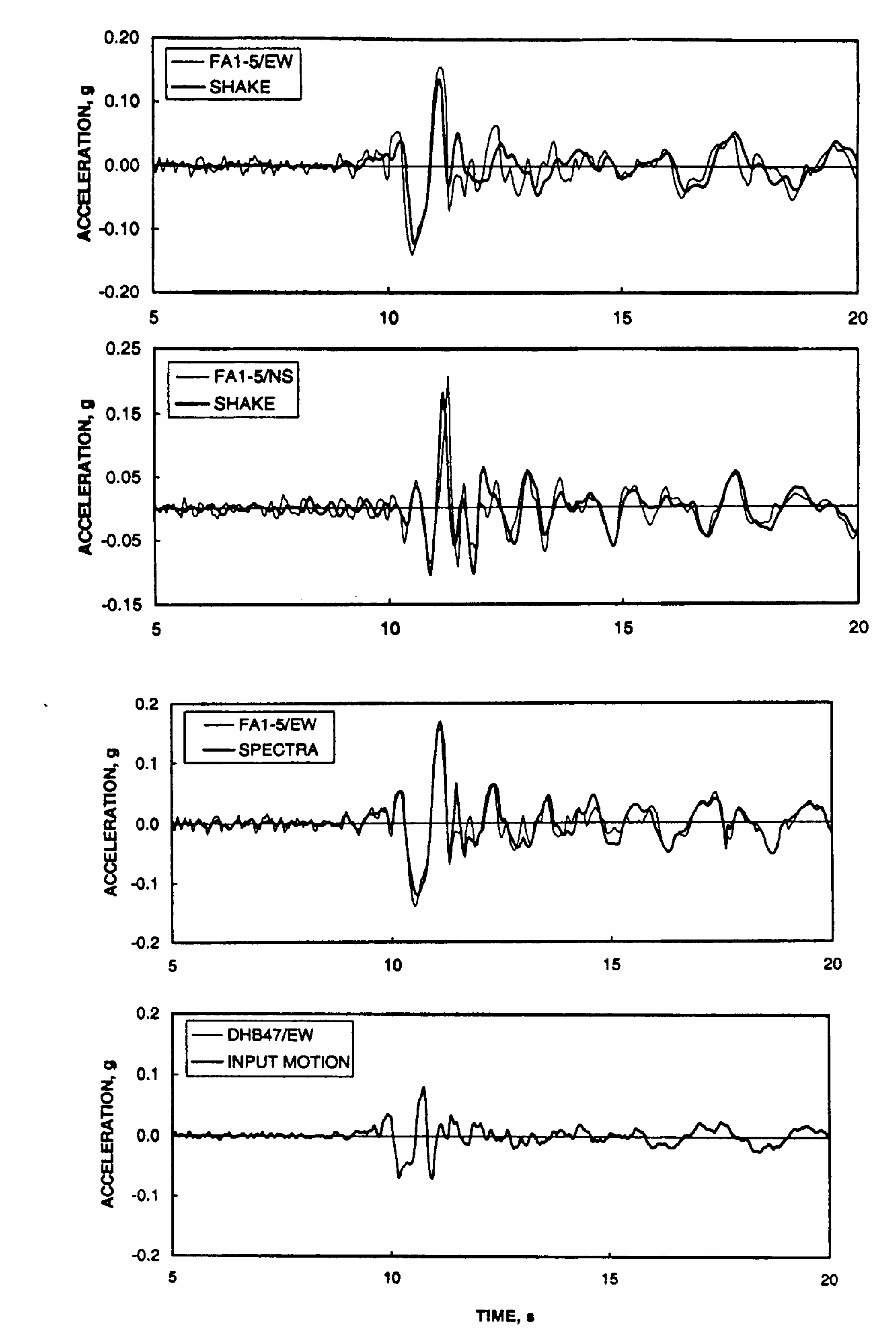

Fig. 5.20. Comparison of recorded ground surface accelerations and predictions by SHAKE (top two frames) and SPECTRA (third frame from top). Bottom frame shows recording at base of array (47-m depth). After Borja et al., 1999.

5.3.3 Use of Ground Response Analysis Results in Hazard Calculations

Ground response analyses have found two principal applications within the context of hazard analyses: (1) definition of amplification factors as a function of generic site conditions and (2) derivation of site-specific amplification factors. Work related to these applications is discussed below.

(a) ***Amplification factors for generic site categories defined from ground response analysis***

Silva et al. (1999) developed amplification factors for the San Francisco Bay (SFB) and Los Angeles (LA) areas as a function of surface geology, depth to basement (defined as V_s = 1 km/s, note distinction from definition in Section 5.2.2d), and control motion amplitude. Amplification is defined relative to Franciscan rock in SFB and granite in LA, both being Mesozoic in age. The amplification factors were derived by developing generic velocity profiles for various geologic units, defining control motions for the reference site condition using a stochastic point-source model, and performing ground response analyses with the equivalent-linear, frequency-domain analysis routine described in Section 5.3.2(a). To capture variations in ground conditions within geologic categories, V_s profiles and modulus reduction and damping relations for soil were randomized according to prescribed probability density functions. Basement depth was also randomized within prescribed ranges.

Distinct amplification levels for SFB were resolved for Tertiary bedrock, Quaternary/Tertiary bedrock, Quaternary alluvium, and Bay Mud. Amplification levels for LA geology were less distinctly resolved, but can be divided into Quaternary alluvium and a combined category of older alluvium and Tertiary bedrock. Averaged median amplification levels for these categories are summarized in Figure 5.21(a) for SFB and 5.21(b) for LA. These factors apply for the broadest depth category for the geologic units, which is generally 10 to 195-300 m (except Bay Area Tertiary rock, for which basement depths are shallow). These results indicate weak motion amplification at high frequencies (i.e., F_a) in all categories. High-frequency amplification decreases with control motion amplitude due to nonlinearity, with the "crossover" between amplification and de-amplification occurring at about 0.2-0.5g for Bay Mud and alluvium, and 0.7-0.8g for old alluvial/Tertiary materials. Low-frequency amplification (i.e., F_v) exhibits significantly less nonlinearity, except for Bay Mud. The largest weak motion

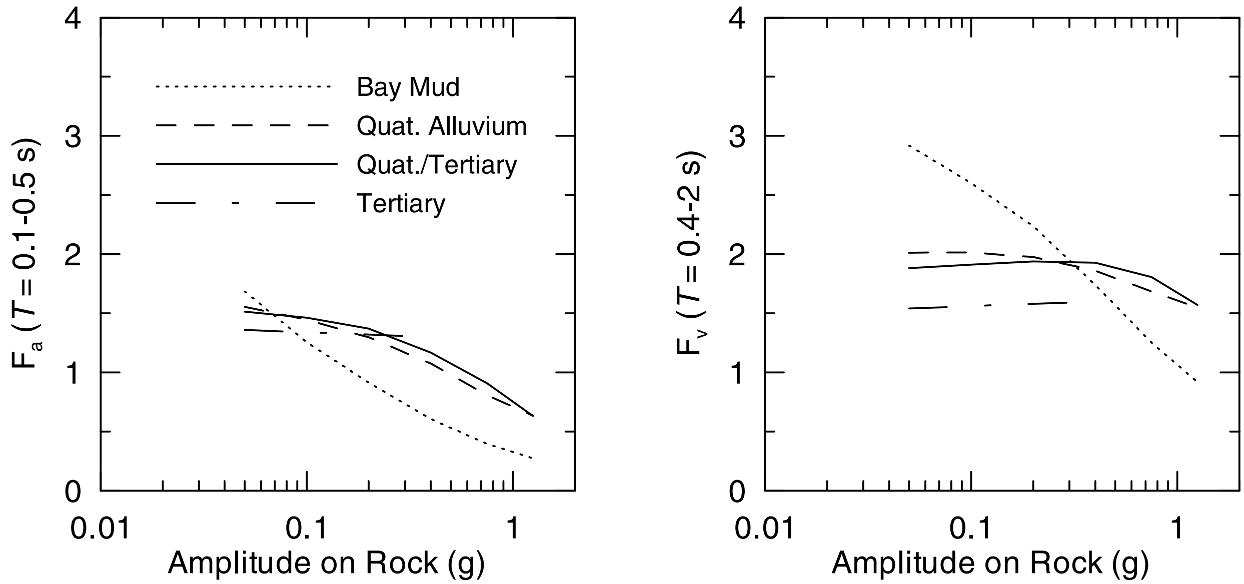

Fig. 5.21(a). Averaged median spectral amplification vs. reference motion amplitude for San Francisco Bay area geology, evaluated from ground response studies by Silva et al. (1999). Factors are for the broadest defined depth range for each category.

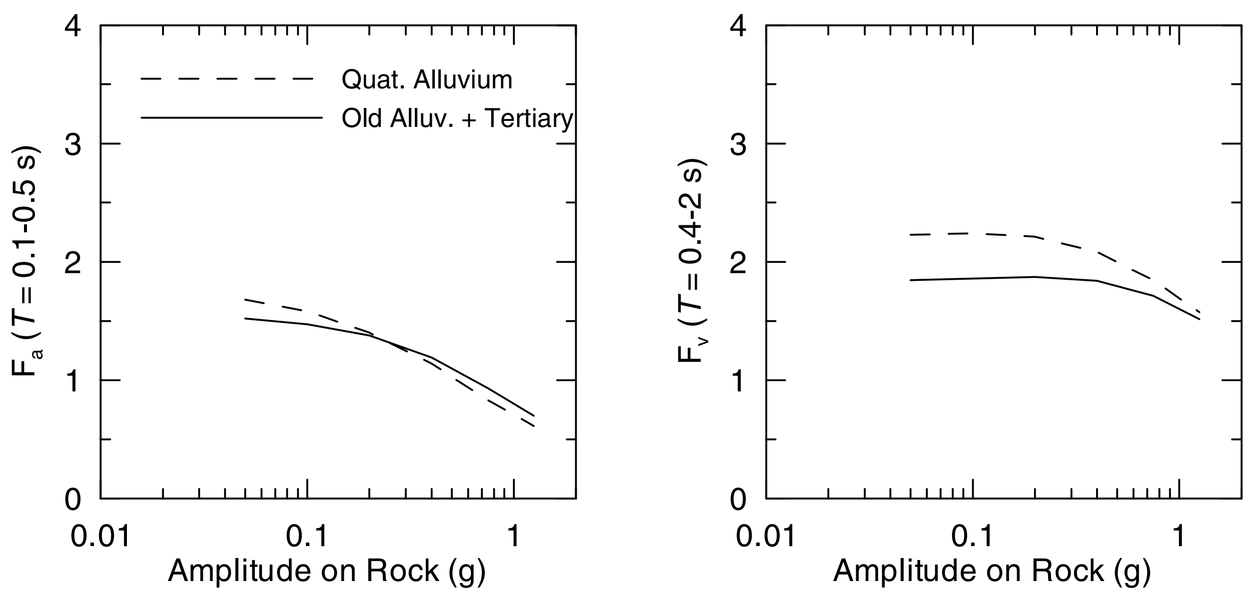

Fig. 5.21(b). Averaged median spectral amplification vs. reference motion amplitude for Los Angeles area geology, evaluated from ground response studies by Silva et al. (1999). Factors are for the broadest defined depth range for each category.

amplification and nonlinearity occur in the most poorly consolidated sediments (i.e., Bay Mud), which is consistent with observations discussed in Section 5.2. The effect of basement depth for SFB and LA is shown in Figures 5.21(c) and (d) for Quaternary alluvial sediments and control motion amplitude = 0.2g. The results indicate a shifting of the peak amplification to lower frequencies as depth to basement increases, and a reduction of high-frequency amplification due to material damping. Similar results were found for other control motion amplitudes.

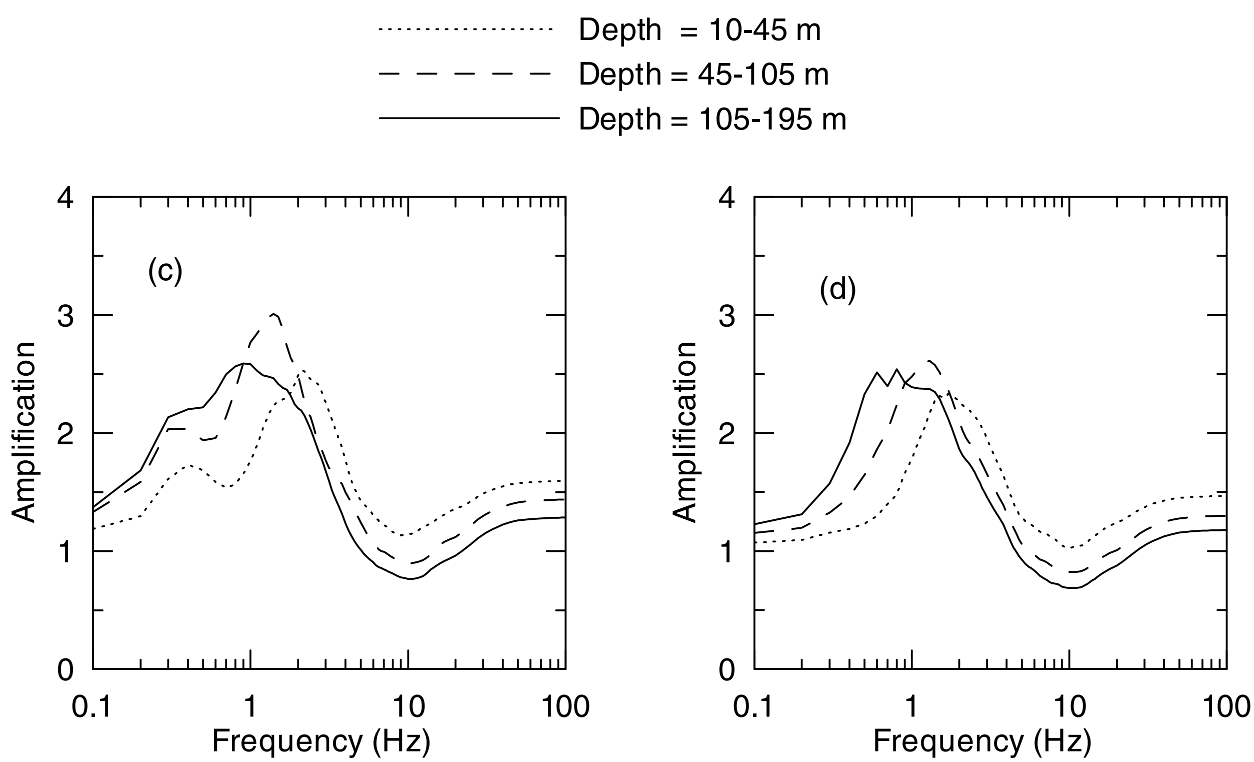

Fig. 5.21(c)-(d). Median amplification for different depth categories for Quaternary alluvium in (c) San Francisco area alluvium and (d) Los Angeles areas. Reference motion amplitude = 0.2g. After Silva et al. (1999).

Silva et al. (2000) performed a similar study to that described above, except that sites were classified based on NEHRP 30-m V_s categories (i.e., Table 5.3), and equivalent-linear results for soil categories were compared to nonlinear results obtained with the program DESRA-MUSC. Amplification factors obtained from this study are different from those derived for geologic categories because the V_s at the mid-point of the NEHRP categories does not correspond to median V_s values for natural geologic formations. However, the general trends in the results are similar to those discussed previously. The nonlinear equivalent-linear comparison was discussed previously in Section 5.3.2d.

The median amplification values provided in the Silva et al. (1999, 2000) studies have uncertainty as a result of parametric variability in the V_s profile, modulus reduction and damping curves, and basement depth. These values are typically on the order of 0.1-0.4 (natural log units), the larger values occurring at low frequencies and large shaking amplitudes. Overall error terms for soil motions are obtained by coupling these error terms with the reference motion error term as indicated in Eq. 5.2.

(b) *Amplification factors derived from site-specific analysis*

Ground response analyses are performed with the expectation that accounting for nonlinear sediment response reduces bias and uncertainty in estimated motions at soil sites. Two studies are discussed here that provide insight into the "benefits" of performing costly site-specific characterization and analysis work. We first discuss a pair of simulation exercises that evaluated the variability in soil motions arising from parametric variability in source, path, and site effects (Silva, 1992; Roblee et al., 1996). The results provide insight into the relative importance of having information on the various effects when ground motions are estimated with simulations. The second study compares the ability of soil attenuation relations and ground response analyses to predict the response spectra of recorded motions at soil sites (Stewart and Baturay, 2001). The ground response analyses utilized large suites of control motions that were scaled to match a modified rock attenuation median. Ground motions estimated from these response analyses incorporate the variability in source/path effects that is present in design situations for a fixed m and r. Hence, the results indicate the effect on bias and uncertainty of performing ground response analyses. The outcomes of these studies are discussed in the following paragraphs.

Roblee et al. (1996) used a stochastic model that incorporates a finite source, a range of source-to-site distances, and an equivalent-linear analysis of 1D ground response. The Silva (1992) study was similar in scope, but utilized a point-source model. Variability in site effects was assessed by randomizing within three site categories (rock, deep soil, marine clay) a range of modulus reduction and damping relations and a range of site geometries (e.g., depth of shear wave velocity characterization). It should be noted that these ranges were large; i.e., variability is interpreted across a knowledge space ranging from zero (no information) to complete (perfect characterization). It was shown that the variability in ground motions arising from variability in soil properties can overwhelm the parametric variability of source and path for T <~ 1 s. The relative significance of ground response variability as compared to source/path variability increased with decreasing site-source distance, and increasing site period. The effect of the depth of detailed subsurface exploration on the uncertainties associated with site effects was investigated, and it was found that details of the velocity profile down to depths of 100 m can significantly affect the characteristics of surface motions. These findings indicate that ground response effects need to be properly characterized to develop from simulations meaningful low-period ground motion estimates.

The Stewart and Baturay (2001) study considered 36 sites, each of which had well characterized near-surface geotechnical conditions and at least one strong motion recording (only one recording was used for each site). The sites were categorized as

I. Shallow stiff soil over rock (soil depth < 30 m)

II. Moderate depth stiff soil (soil depth = 45-90 m)

III. Deep stiff soil (soil depth > 120 m)

IV. Soft soil ($V_s \leq 150$ m/s; soft soil depth > 3 m)

Control motions were selected from "rock" recordings (either Tertiary or Mesozoic), and for each site were selected to have similar m, r, and near-fault geometric parameters to the soil recording. For most sites, the number of control motions was between 10-30. These motions were then scaled to a target spectrum in a manner that ensured the ensemble median matched the target, while maintaining the inherent variability of the suite. The target spectrum consisted of a prediction from a rock attenuation relationship adjusted for rupture-directivity effects and event terms. The top frame of Figure 5.22 shows for an example site the distribution of control motion spectra along with the target spectrum. Using these input motions, ground response effects were calculated using an equivalent-linear technique. The middle frame of Figure 5.22 shows for the example site the distribution of predicted spectra from ground response analyses along with the spectra of the recorded motion. The bottom frame compares the spectra of the recorded motion to the prediction from a soil attenuation relation. A comparison of the prediction misfits in the second and third frames provides a qualitative assessment of the "benefit" of ground response analysis for this site. For each site, residuals were compiled between the observed spectrum and the ordinates corresponding to the 50% and 84% percentile predictions. These residuals were then compiled across the four site categories listed previously. Results for Categories III and IV are presented in Figure 5.23.

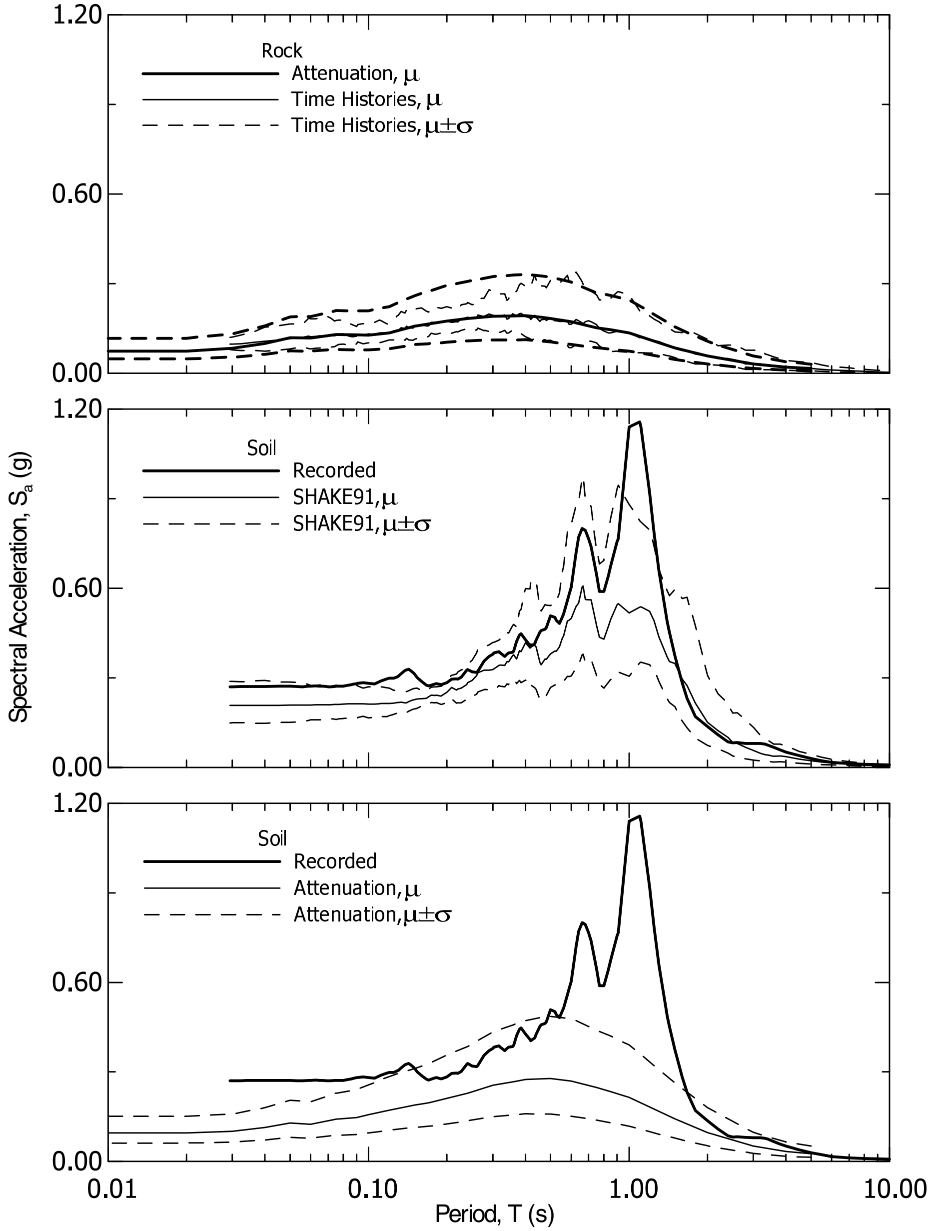

Fig. 5.22. Spectral accelerations at 5% damping. Input motions (top frame), ground response results (middle frame), and soil attenuation results (bottom frame). Site is Apeel #2 Redwood Shores, fault-normal direction, 1989 Loma Prieta earthquake. After Stewart and Baturay (2001).

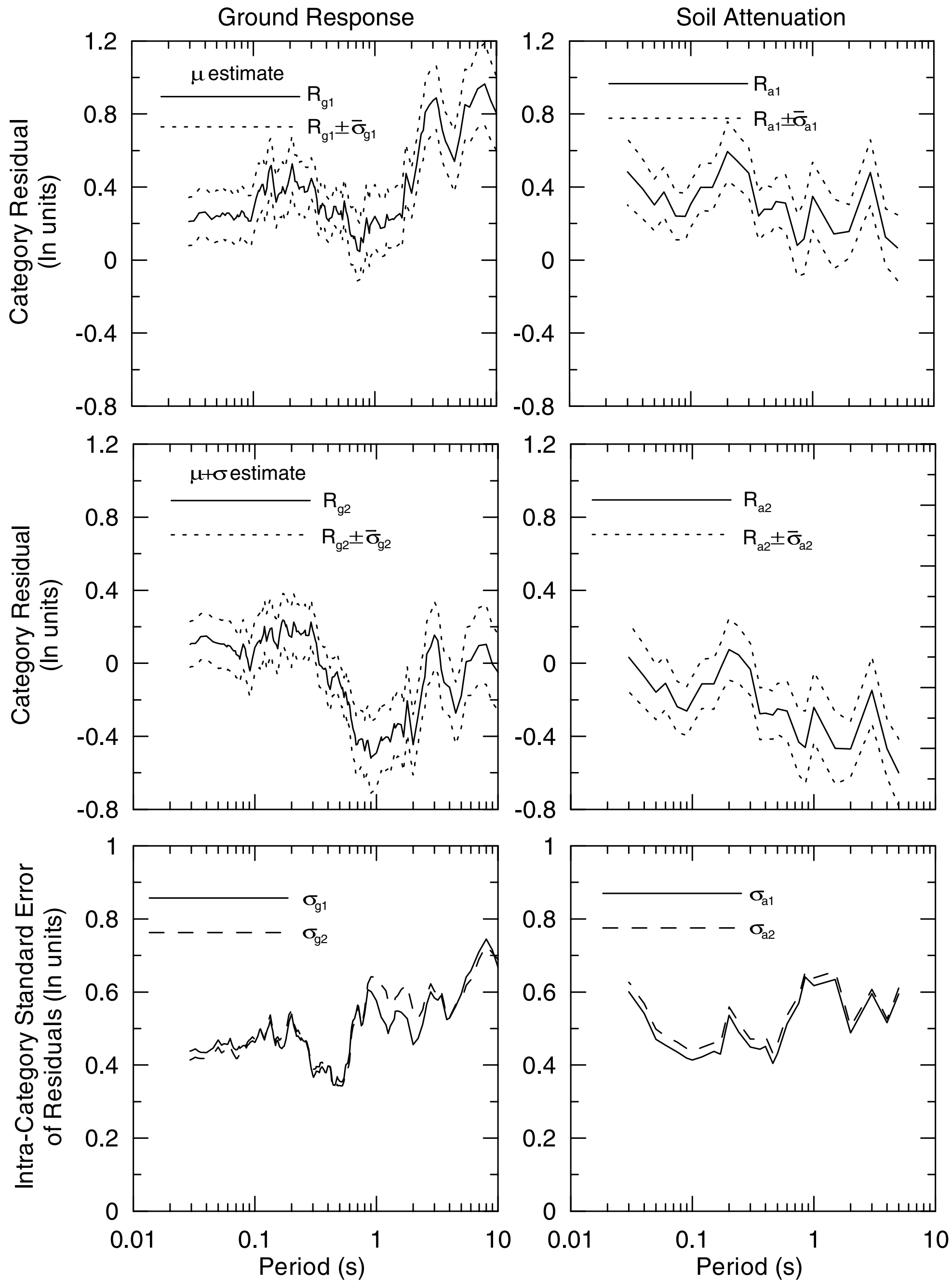

Fig. 5.23(a). Category median residuals and standard error terms, Type III sites (deep stiff soil, depth > 120 m). Stewart and Baturay (2001).

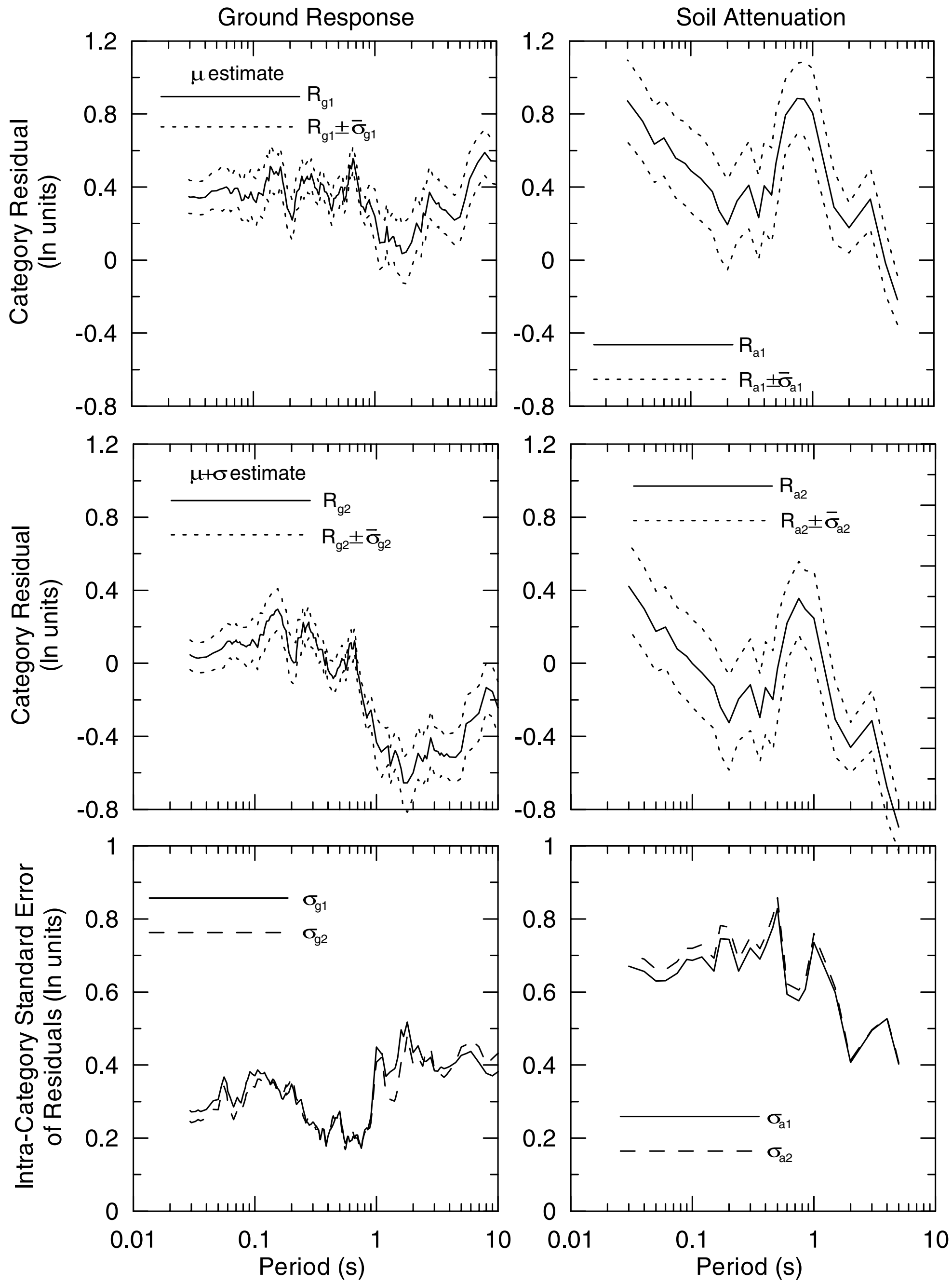

Fig. 5.23(b). Category median residuals and standard error terms, Type IV sites (soft clay). Stewart and Baturay (2001).

The benefit of performing ground response analysis was assessed by comparing category residuals and standard errors for the median ground response and soil attenuation ground motion estimates. A smaller residual from ground response indicates a more accurate overall prediction, and a smaller standard error implies relatively consistent residuals within the category. Category residuals were smaller for the ground response estimates for $T < 1$ s in all categories, but the difference was only statistically significant for Categories I and IV. Intra-category standard errors for ground response were significantly reduced only for Category IV. These results indicate a clear benefit to performing ground response analyses for soft clay sites, but suggest little benefit to such analyses for other site conditions. A second issue raised by these results is potential bias in ground motion estimates from response analyses. Positive residuals were found in Categories II-IV for median predictions from ground response analyses (e.g., Figure 5.23), which indicate an underprediction. The cause of this underprediction is unknown. However, it is noted that the soil attenuation results also show a positive bias, indicating that the recordings from the sites investigated are unusually large relative to the median attenuation prediction.

The above findings regarding benefits and bias in ground response predictions require verification through study of additional sites and strong motion records. Moreover, there is a need to examine whether more sophisticated nonlinear ground response analysis routines reduce the bias and/or dispersion in the median predictions. Such efforts are being undertaken within the PEER Lifelines Program.

5.4 BASIN RESPONSE

5.4.1 Introduction

Many urban regions are situated on deep sediment-filled basins. A basin consists of alluvial deposits and sedimentary rocks that are geologically younger and have lower seismic wave velocities than the underlying rocks upon which they have been deposited. Basins have thickness ranging from a 100 m to over 10 km. Waves that become trapped in deep sedimentary basins can produce up to 50% stronger amplitudes at intermediate and low frequencies ($f < \sim 1$ Hz) than those recorded on comparable surface materials outside basins, and their durations (measured using the Husid plot) can be twice as long (e.g., Graves et al., 1998).

Although past studies of basin response have typically been limited to ground motions with frequencies less than about 1 Hz, it is possible that basin response effects are also important at higher frequencies (e.g., Davis et al., 2000), or can affect structures having higher fundamental-mode frequencies. With respect to the former point (importance of basin effects at high frequencies), available information is not sufficient to assess the importance of basin effects relative to shallow ground response effects, and further investigation of this issue is an important research need. With respect to the later point (importance of longer-period ground motions, known to be affected by basin effects, on damage), recent studies of the 1994 Northridge and 1995 Kobe earthquakes suggest that the spatial distribution of structural damage correlates best with peak ground velocity having a dominant frequency of about 1 Hz (e.g., Kawase and Nagato, 2000, Boatwright et al., 2001). This correlation holds even for "short" structures, which may have fundamental frequencies of about 2 or 3 Hz. These results suggest that increasing our understanding of the processes that affect ground motions at intermediate frequencies (like basin response) is an important step toward developing improved amplification factors for use in performance-based engineering.

5.4.2 Mechanism for Basin Response

Conventional criteria for characterizing site response are typically based on the distribution of shear wave velocity with depth in the upper 30 m as determined from field measurements. The response of this soil layer is usually modeled assuming horizontal layering and 1D wave propagation, following the method illustrated on the left side of Figure 5.24. The wave that enters the layer may resonate in the layer but cannot become trapped within the layer. Recent weak motion studies by Hartzell et al. (2000) have shown that in some cases 1D modeling is capable of accounting for observed amplification at intermediate to low frequencies (f<2Hz), whereas in other cases 2D and 3D models are necessary to explain observed amplification levels, particularly when the measure of amplification is sensitive to duration. Use of the 2D and 3D models was necessary for locations near a steeply sloping basin edge.

At frequencies around 1 Hz and less, seismic waves have wavelengths that are much longer than 30 m, and their amplitudes are controlled by geological structure having depths of hundreds or thousands of meters which in many cases, such as in sedimentary basins, is not horizontally layered. If the wave is propagating in the direction in which the basin is thickening and enters the basin through its edge, it can become trapped within the basin if post-critical incidence angles develop. The resulting total internal reflection at the base of the layer is illustrated at the top right of Figure 5.24. In the lower part of Figure 5.24, simple calculations of the basin response are compared with those for the simple horizontal layered model. In each case, a plane wave is incident at an inclined angle from below. The left side of the figure shows the amplification due to impedance contrast effects that occurs on a flat soil layer overlying rock (bottom) relative to the rock response (top). A similar amplification effect is shown for the basin case on the right side of the figure. However, in addition to this amplification, the body wave entering the edge of the basin becomes trapped, generating a surface wave that propagates across the basin. Current empirical ground motion attenuation relations do not distinguish between sites located on shallow alluvium and those in deep sedimentary basins, and therefore might be expected to underestimate the ground motions recorded in basins.

The importance of basin response on strong ground motions was first recognized following the 1971 San Fernando earthquake. The availability of high-quality ground motion recordings throughout the San Fernando and Los Angeles basins during this event allowed for detailed analyses of wave propagation effects along various profiles which traversed the basins (Hanks, 1975; Liu and Heaton, 1984). These data clearly showed the development of basin-generated surface waves, which lead to amplified ground motions and extended durations of shaking within the sedimentary basins. Further confirmation of these ideas was provided by Vidale and Helmberger (1988), who successfully modeled these data using 2D finite difference calculations.

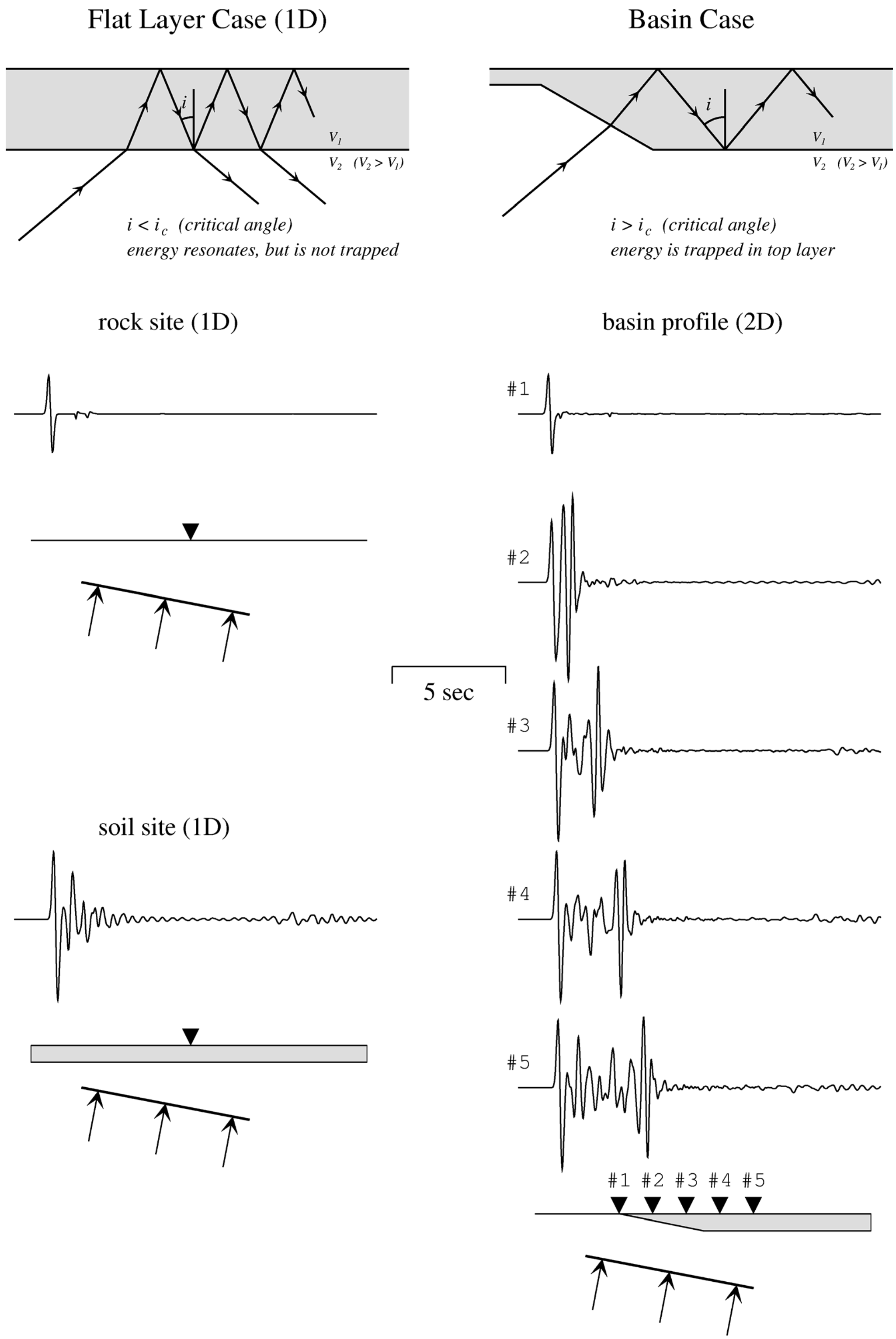

Fig. 5.24. Schematic diagram showing that seismic waves entering a sedimentary layer from below will resonate within the layer but escape if the layer is flat (left) but become trapped in the layer if it has varying thickness and the wave enters the layer through its edge (right). Source: Graves (1993).

For more recent earthquakes, the comparison of strong ground motion measurements with the results of computer simulations has continued to substantially increase our understanding of basin effects. For example, Figure 5.25 shows strong motion velocity time histories of the 1994 Northridge earthquake recorded on a profile of stations that begins in the San Fernando Valley, crosses the Santa Monica mountains and extends into the Los Angeles basin (Graves et al., 1998). The two dashed lines indicate the arrival of shear waves from the two predominant subevents of the earthquake. The time histories recorded on rock sites in the Santa Monica Mountains are brief, and are dominated by the direct waves. In contrast, the time histories recorded in the Los Angeles basin have long durations, and the peak velocities are associated not with the direct waves but from later arriving waves that are known to be waves generated at the northern edge of the Los Angeles basin (bottom right of Figure 5.25).

5.4.3 Basin Edge Effects

The 1994 Northridge and 1995 Kobe earthquakes have shown that large ground motions may be generated by the geological structure of fault-controlled basin edges. The largest ground motions in the Los Angeles basin during the Northridge earthquake were recorded just south of the Santa Monica fault. In this region, the basin-edge geology is controlled by the active strand of the westward-striking Santa Monica fault, shown in map view and cross section in the upper part of Figure 5.25. Despite having similar surface geology, sites to the north of the fault (that are closest to the earthquake source) show relatively modest amplitudes, whereas more distant sites to the south of the fault exhibit significantly larger amplitudes, with a clear and immediate increase in amplification occurring at the fault scarp. The same pattern is dramatically reflected in the damage distribution as indexed by red-tagged buildings, which are concentrated immediately south of the fault scarp in Santa Monica. The strong correlation of ground motion amplification pattern with the fault location suggests that the underlying basin-edge structure is strongly affecting the site response. Two mechanisms by which this geologic structure could affect amplification levels have been investigated. The first involved 1D ground response analyses, and was unsuccessful (see Figure 5.18b, Chang, 1996). The second involved 2D modeling of the basin edge, and found large amplification (that was consistent with observation) south of the fault from constructive interference of direct waves with the basin-edge generated surface waves (Figure 5.25).

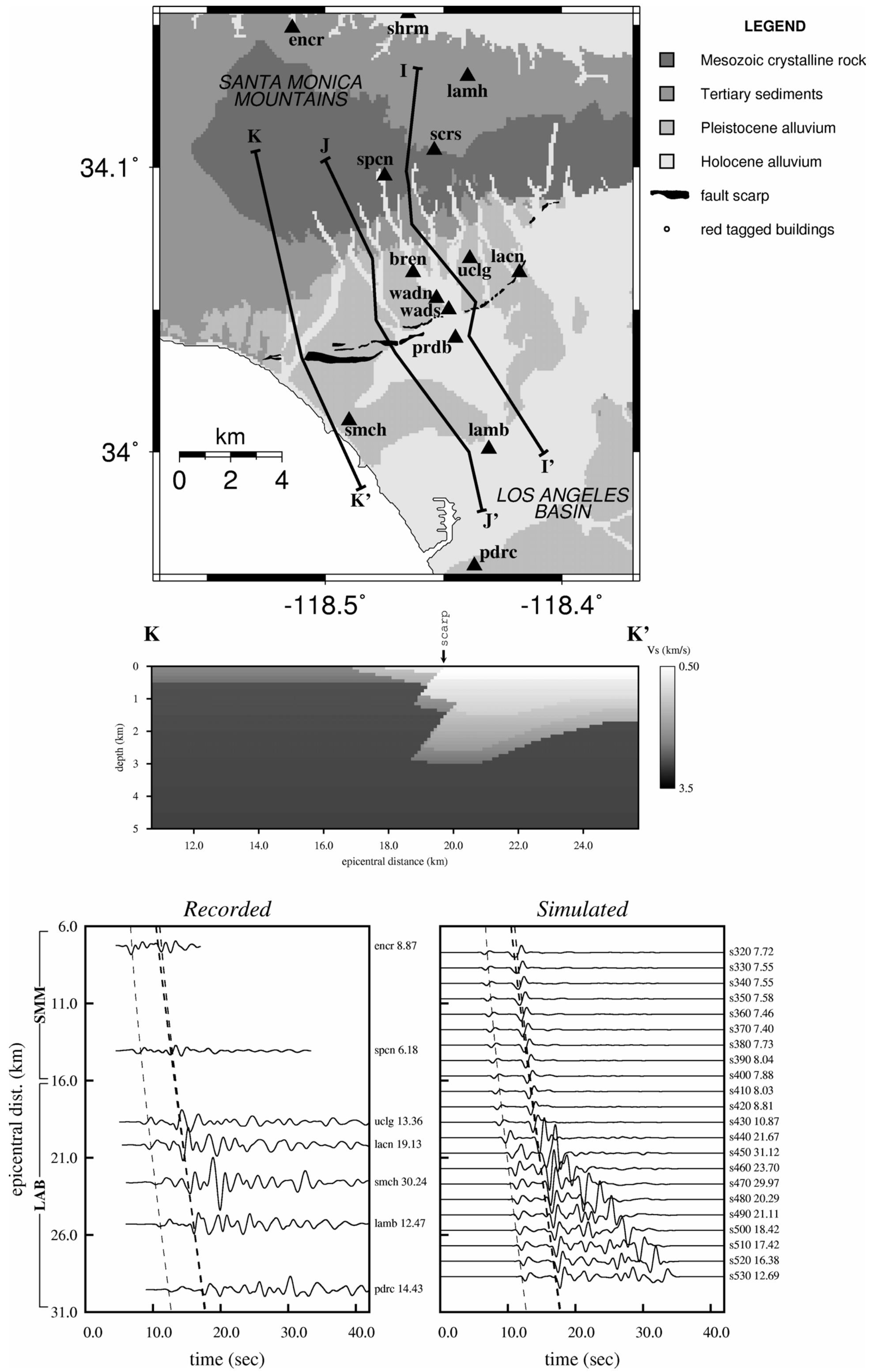

Fig. 5.25. Basin effects in Santa Monica from the 1994 Northridge earthquake. See text for explanation. Source: Graves et al. (1998).

The 1995 Kobe earthquake provided further evidence from recorded strong motion data, supported by wave propagation modeling using basin edge structures, that ground motions may be particularly large at the edges of fault-controlled basins. Severe damage to buildings due to the Kobe earthquake was observed in a zone about 30 km long and 1 km wide, and offset about 1 km southeast of the fault on which the earthquake occurred (Figure 5.26). The Kobe region is very heavily populated with dense urbanization extending up into the foothills north of the surface fault trace. The density and type of construction is similar throughout the urban region, suggesting that zones of concentrated damage reflect locally amplified ground motion levels rather than spatial variations in the built environment. Numerical simulations suggest that near-fault ground motions in the Kobe earthquake were amplified by the basin edge effect. This effect is caused by the constructive interference between direct seismic waves that propagated vertically upward through the basin sediments from below, and seismic waves that diffracted at the basin edge and proceeded laterally into the basin (Kawase, 1996; Pitarka et al., 1998).

The aforementioned concentrated damage zone (parallel to, but offset from, the fault) is represented by the zone of JMA Intensity VII shown in Panel (a) of Figure 5.26. This zone is reproduced in the map of simulated peak velocity (Panel c), generated using a 3D model of the basin edge (Panel b). The strong influence of the basin edge is demonstrated in the lower part of the figure (Panel d), which shows vertically aligned time histories from 3D simulations for the actual basin geometry (left side) and a flat layered model with no basin edge (right side). The basin structure produces a strongly asymmetrical zone of large amplitudes offset laterally about 1 km from the fault trace and running parallel to the edge of the basin, which is roughly coincident with the concentrated damage zone. Kawase (1996) demonstrated that this zone of amplification is present in both ground velocity and ground acceleration, suggesting that the basin edge effect may be a rather broadband phenomenon.

It should be noted that amplification by soft surficial materials was also likely to have contributed to ground motion amplification within the heavily damaged zone in Kobe, particularly at high frequencies (Suetomi and Yoshida, 1998). The quality of available shear wave velocity data for shallow sediments are limited, although Silva and Costantino (1999) note that most of the lateral variability in shear wave velocities (estimated from soil penetration resistance) between soft soil (where damage was severe) and hard soil (where damage was relatively modest) exists in the topmost 50 m, with a maximum deviation of about 20%. Limited previous studies of 1D ground response effects in the Kobe area have not been able to establish

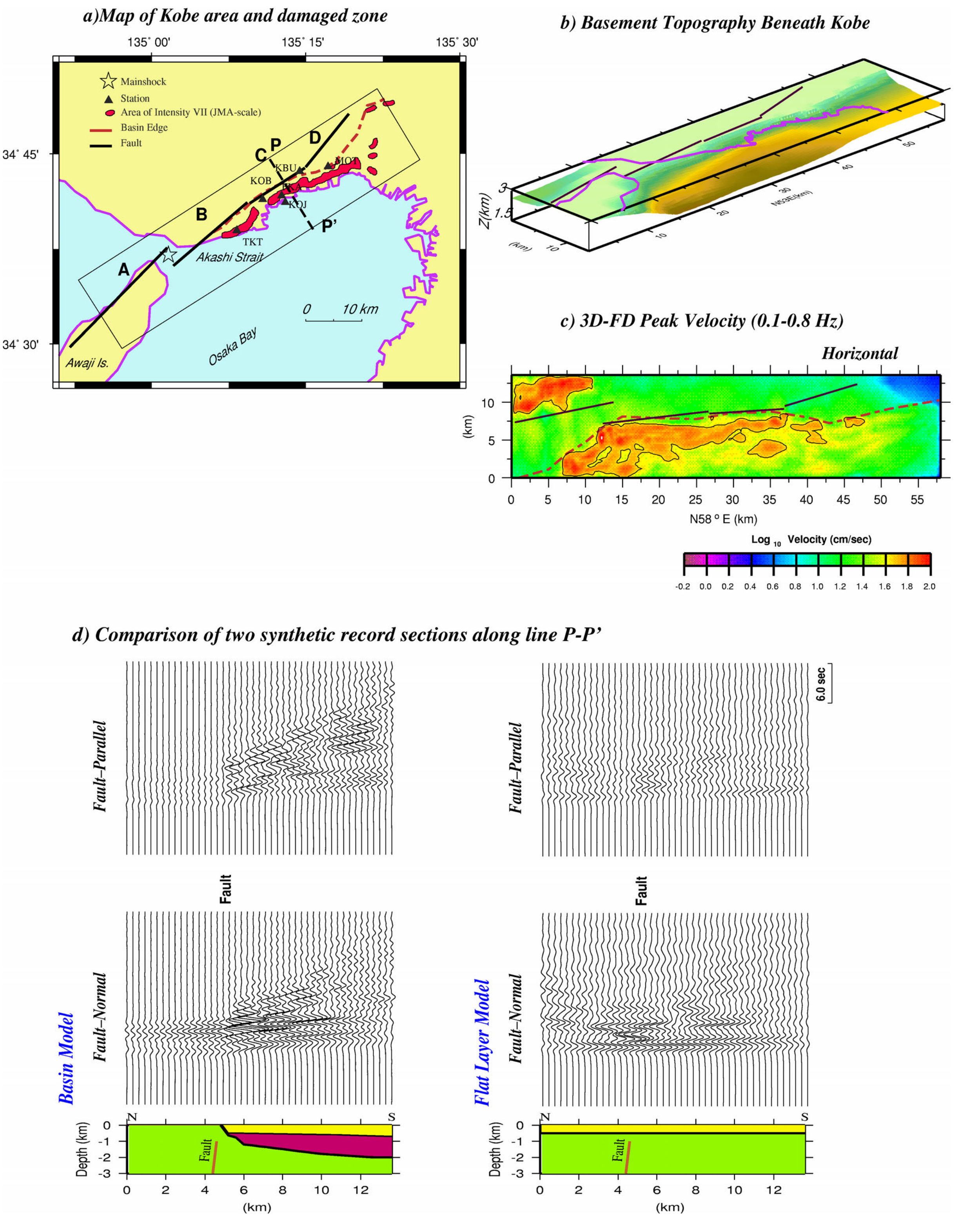

Fig. 5.26. Basin edge effects in the 1995 Kobe earthquake. See text for explanation. Source: Pitarka et al. (1998).

that this impedance difference alone can explain both the location of the concentrated damage zone (including its offset from the fault trace) and the observed level of amplification within this zone. However, further study of such effects is certainly warranted.

5.4.4 Focusing Effects

The damage pattern caused by the Northridge earthquake included pockets of localized damage such as those in Sherman Oaks and Santa Monica that were not clearly correlated with surficial soil conditions (Hartzell et al., 1997). These observations have produced important new insights into the causes of localized zones of damage. During the Northridge earthquake, deeper lying geological structure may have had as much influence on strong motion patterns as the upper 30 m that are conventionally used to characterize site response. This deeper structure may include sedimentary structures in the upper few kilometers of sedimentary basins, as well as topography on the underlying sediment/basement interface. These structures, in the form of folds and buried basins, may focus energy (like a lens) in spatially restricted areas on the surface, in some cases becoming the dominant factor in the modification of local ground motion amplitudes (Stephenson et al., 2000; Davis et al., 2000).

5.4.5 Seismic Zonation in Sedimentary Basins

The conventional approach to zonation of ground shaking hazards in urban regions is to assume that the geology can be characterized by a horizontally stratified medium, and that only the shallowest few tens of meters influence the ground motion characteristics. Seismic zonation then consists of linking together site-by-site estimates of site response generated using methods such as that shown on the left-hand side of Figure 5.24. However, as demonstrated on the right-hand side of Figure 5.24 and illustrated in Figures 5.25 and 5.26, this simple approach may significantly underestimate the amplitudes and durations of strong ground motions, especially at periods of about one second and longer, that can become trapped within sedimentary basins due to critical reflections that are set up at the edges of the basin. These effects are due to the geometry of the interface between the sedimentary materials and the underlying crystalline rocks, and cannot be explained by the shallow soil profile alone. Many elements of the urban infrastructure, such as bridges, multi-story buildings, dams and storage tanks, are susceptible to long-period ground motions, which may be influenced by basin effects.

New computational procedures have the potential for enhancing the reliability of seismic zonation of urban regions located in sedimentary basins. For these regions (e.g., Los Angeles, San Francisco, Seattle), it is expected that wave propagation computations using sophisticated 2D and 3D numerical techniques will be used to supplement the use of simple 1D models of shallow ground response (e.g., Page et al., 1998). The rapid increase in the speed and memory of computers, and the development of efficient computational methods for modeling seismic wave propagation in laterally varying geological structure, enable us to model the effects of sedimentary basins on ground motions generated by scenario earthquakes. By using finite difference (Graves, 1996) or finite element (Bao et al., 1998) techniques, the complete wave field can be computed up to a given frequency threshold throughout an entire urban region. This capability has the potential to greatly enhance the seismic zonation of urban regions located on sedimentary basins. Instead of obtaining ground motion estimates at a set of discrete locations using local flat-layered geological models, which may be inaccurate because they do not account for the effects of the basin structure, we are able to calculate the seismic wave field continuously throughout the model region. This allows the ground motion estimates at each location to incorporate the effects of the laterally varying geologic structure in the vicinity of the site.

In the approach outlined above, the degree and extent of basin response will likely be dependent on the location of the earthquake source. This dependence necessitates the use of simplifying assumptions for the adequate representation of basin effects in probabilistic ground motion estimation. A preliminary attempt to quantify the effect of basin response on probabilistic analyses has been performed by the SCEC Phase III Working Group (Field et al., 2000). Their results indicate a noticeable correlation between observed ground motion amplification and basin depth. However, other parameters (e.g., distance to basin margin in the direction of the source) may also exhibit the same degree of correlation. More work is needed to distinguish the level of influence of these various parameters, and the variability of the resulting ground motion estimates associated with parameter uncertainty.

5.4.6 Current Capabilities and Limitations in Estimating Basin Response

Finite difference and finite element methods used in the simulation of basin response have been successfully verified in the course of the PEER Lifelines Program. Individual finite difference methods have been validated against limited recorded data. Work is now proceeding on the more systematic validation of these methods against recorded data. Taking account of different procedures used in representing the earthquake source and velocity models is an important aspect of this validation process.

Realistic simulations in basin response can be made only for basins whose seismic shear wave velocity structure is fairly well known. Developing such 3D models is now a major focus of the U.S. Geological Survey internal and external research programs. To date, the most detailed models have been developed for the Los Angeles region (Magistrale et al., 2000). Preliminary models are also available for the San Francisco Bay region, the Puget Trough region (Seattle and surroundings), and the Portland and Tualatin basins. The Santa Clara Valley and the Puget Trough region are currently the focus of data gathering activities using dense arrays of ground motion instrumentation (e.g., Frankel et al., 2001). The goal of these dense arrays is twofold: (1) to develop empirical estimates of basin response with a dense spatial coverage and (2) to help construct validated 3D basin velocity models for use in numerical simulations of future hypothetical earthquakes.

Using workstation computers, it is currently feasible to compute 3D ground motions reliably up to frequencies of about 0.5 - 1 Hz in large urban regions. The modeling of 3D wave propagation effects is bandlimited to longer periods for several reasons. First, the fineness of the element spacing controls the highest frequencies that can be modeled. The lower the seismic velocity, the finer the element spacing required to model a given frequency. For stiff sediments (NEHRP C, 560 m/sec), a grid spacing of about 100 m is needed to model frequencies up to 1 Hz. For softer sediments (NEHRP D, 270 m/sec), a grid spacing of about 50 m is needed to model frequencies up to 1 Hz.

Using standard finite difference calculations, the memory requirements and computational effort scale as the inverse third and fourth powers, respectively, of the grid spacing. Thus halving the grid spacing results in an eightfold increase in the memory requirement and a sixteenfold increase in the computational effort. For a given model region, these factors place a practical limit on the frequencies that can be modeled. This limitation can be reduced substantially by using variable grid spacing methods (Pitarka, 1999; Aoi and Fujiwara, 1999) or by using non-structured mesh techniques such as finite element or spectral element methods.

Another factor affecting the frequency resolution is that, in many areas, the seismic velocity model has limited spatial resolution, which places a knowledge-based limit on the frequencies that can be modeled. For example, certain areas of the Los Angeles basin have undergone detailed subsurface exploration by the oil industry, and these data are being used to develop detailed images of the 3D velocity structure (e.g., Magistrale et al., 2000; Suess et al., 2000). In other areas, such as the northern portion San Fernando basin, the subsurface structure is much less well defined, thus inherently limiting the frequency resolution of the calculations. Typically, the spatial resolution of the subsurface structure (and associated velocities) is better in the near surface and decreases as a function of depth. Ground motion simulations will provide a key component in the further development and refinement of these models.

5.5 EFFECT OF SURFACE TOPOGRAPHY

In this section we discuss variations in ground motions between level sites and areas with irregular surface topography. Obviously, many geometries can give rise to topographic effects on ground motion. The discussion here is limited principally to two-dimensional geometries, which can be generally categorized as ridges, canyons, or slopes (Figure 5.27). In the following sections we briefly review amplification factors predicted by models for these various geometries. Limited available observational studies used for model calibration are also discussed.

5.5.1 Ridges

Numerous studies have investigated topographic effects for an isolated, two-dimensional, homogeneous ridge on the surface of a homogeneous halfspace, as illustrated in the top frame of Figure 5.27. Comprehensive literature reviews by Geli et al. (1988) and Bard (1995) found levels of crest-to-base time-domain amplification (e.g., ratios of peak motions) from 11 analytical studies to vary from about 1-2 (average ≈ 1.5) for shape ratios H/L ≈ 0.3-0.5. Frequency-domain amplification at several points along a ridge with H/L ≈ 0.4 subjected to vertically incident SH waves is illustrated in Figure 5.28. Broadband crest amplification occurs that is maximized at dimensionless frequency $\eta = 2L/\lambda = 2$, which corresponds to a wavelength (λ) equal to the ridge half-width. The maximum spectral amplification is about 1.6 for this case. Geli et al. found that amplification is generally lower for incident P waves than S waves, and the amplification is slightly greater for horizontal motion in the plane of the models than for out-of-plane motions. Amplification is also sensitive to the vertical angle of the incident wave field (Pedersen et al., 1994), although in a complex manner (i.e., simple and repeatable trends in the results could not be identified).

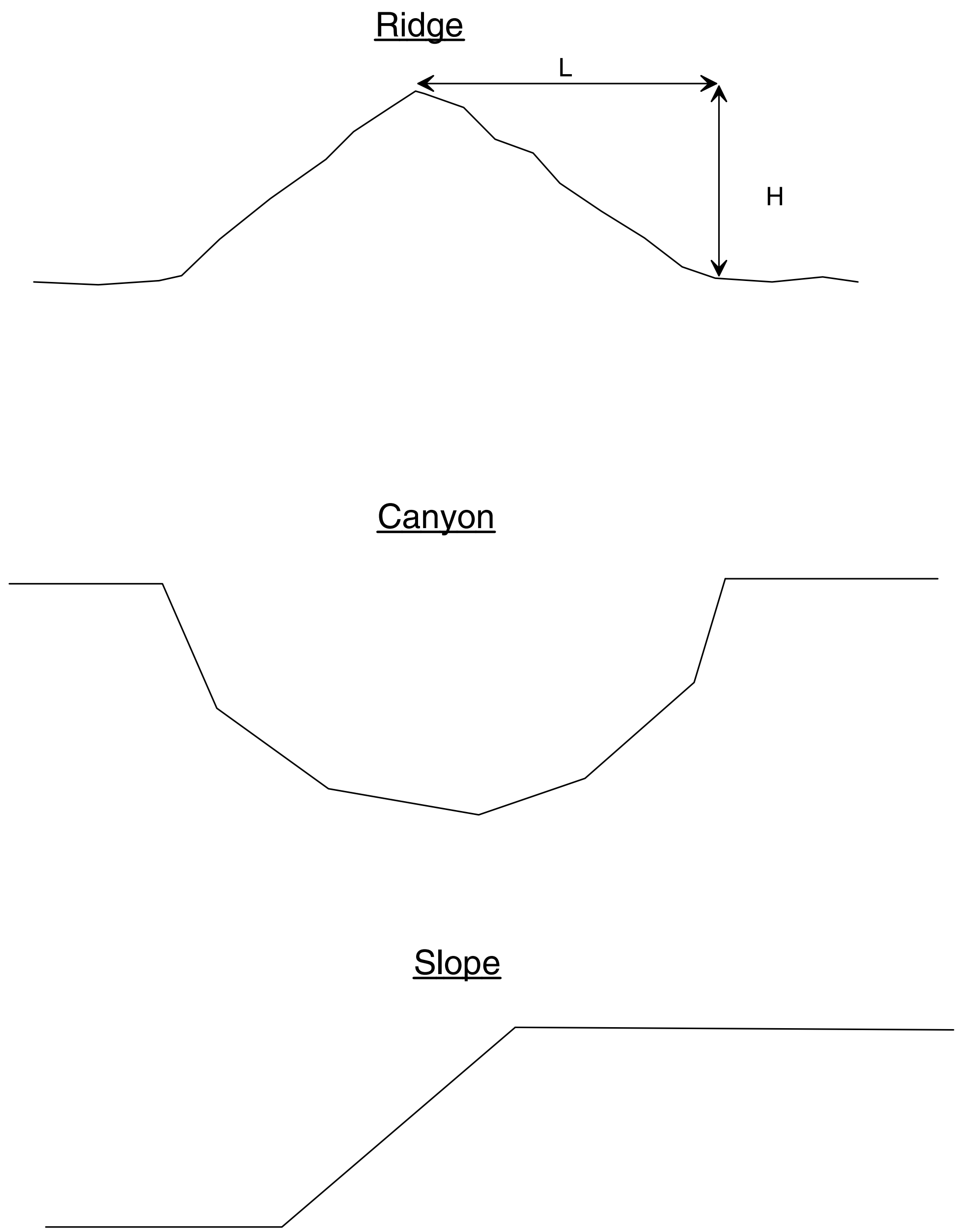

Fig. 5.27. Generalized 2D geometries of irregular surface topography.

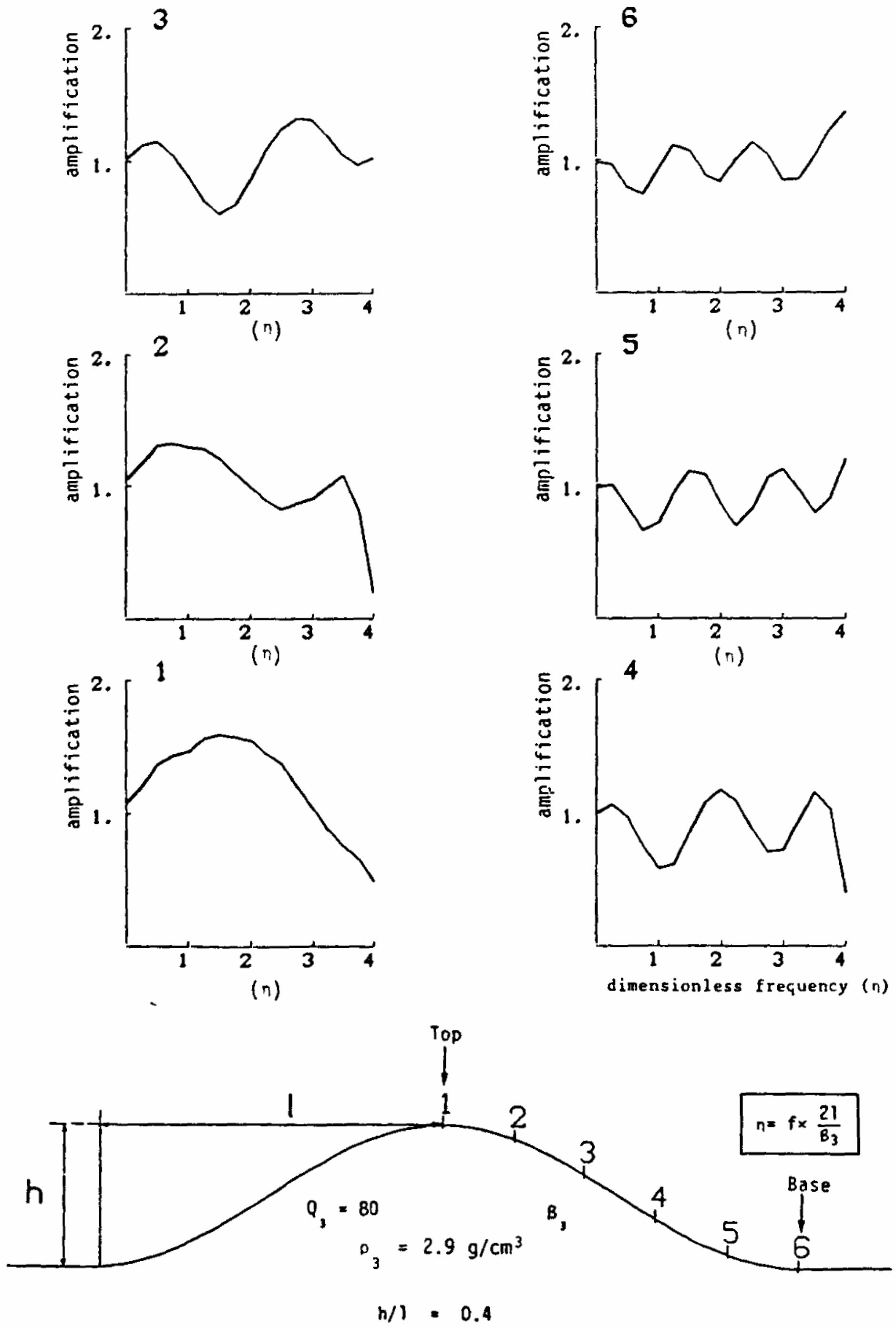

Fig. 5.28. Amplification as a function of normalized frequency across ridge subjected to vertically incident SH wave. After Geli et al. (1988).

Verification studies for topographic effects across ridges have been limited, despite the fact that most observational studies of topographic effects are performed on ridge geometries. These studies are generally based on interpretations of weak motion data from arrays across two- or three-dimensional surface geometries. Table 5.8 summarizes several such studies in which amplification effects are evaluated in the frequency domain from direct interpretation of surface recordings. Unfortunately, ground motion variations identified in these studies generally result from a combination of ground response variability (due to non-identical soil/rock conditions underlying the seismograph sites) and topographic effects. At none of the sites listed in Table 5.8 was subsurface characterization performed at each of the seismometers, and in most cases no attempt was made to remove potential bias in identified amplification factors associated with ground response variability. Accordingly, the results may not be useful for engineering application. Nonetheless, as discussed by Geli et al. (1988), the studies are consistent with theory in their findings of crest amplification that is typically maximized at wavelengths corresponding to the ridge half-width. However, due perhaps in part to the lack of ground response corrections, the amount of amplification observed in field experiments varies widely, and often significantly exceeds theoretical predictions.

5.5.2 Canyons

Significant interest in ground motion variations across canyon geometries was generated by recordings of unusually large amplitude on a canyon rim near Pacoima Dam during the 1971 San Fernando earthquake. This led to studies of the effects of canyon topography on ground motion by Trifunac (1973) and Wong and Trifunac (1974), among others. These investigators generally assumed a linear-elastic medium and a simple canyon geometry (e.g., semi-cylinder or semi-ellipse).

A general overview of ground motion variations across a simplified canyon geometry is provided in Figure 5.29, which indicates ground motion amplitude at various locations across a canyon as a function of normalized frequency $\eta = 2a/\lambda$ for vertically incident SH waves (where λ=wavelength). Amplification is strongly frequency dependent, being significant when wavelengths are similar to or smaller than the canyon dimension. A maximum amplification of about 1.4 occurs near the canyon edge, which remains approximately constant for $\eta > 0.5$. The maximum base de-amplification is about 0.5. If the same canyon geometry were subjected to an

Table 5.8 Observations of horizontal ground motion amplification transverse to predominant ridge line

Site	Earthquake	Slope Faces[1]	Approx. Slope Angle (deg.)	Slope Height (m)	Peak Crest Motion	Max Spectral Amp.	Approx. Freq. of Max. Amp.[2]	Crest/Base Geology	Reference
Kagel Mountain, CA	1971 San Fernando AS	3-D	28	430	na	10-30[a]	1.0	similar	Davis and West, 1973
Josephine Peak, CA	1971 San Fernando AS	3-D	17	910	na	3[a]	0.9	similar	Davis and West, 1973
Butler Mountain, NV	Explosions	ridge	36	150-180	na	5-7[a]	0.8	similar	Davis and West, 1973
Tien Shan Mtns., USSR	Microtremors	ridge	na	na	na	8[b]	na	loess/bsmt	Tucker et al., 1984
W. Nag. Prefec., Japan	1984 W. Nagana Prefec. AS	ridge	46	50-100	na	10	na	andesite/ash	Umeda et al. 1986
Canal Beagle, Chile	1985 Chilean AS	ridge	14	20	0.01 cm/s	5-10[b]	na	similar	Celebi, 1987
Coalinga Anticline, CA	1983 Coalinga AS	ridge	10-15	30	0.05 g	4-8[b]	na	similar	Celebi, 1991
Superstition Mtn., CA	1987 Sprstn. Hills AS	na	4	na	0.04 cm/s	20	na	similar	Celebi, 1991
Robinwood Ridge, CA	1989 Loma Prieta AS	ridge	25	100	0.02 cm/s	1.5-4[b]	0.8-2	similar[3]	Hartzell et al., 1994
Sourpi, Central Greece	Microtremors	ridge	30	300	na	3[b]	broad	similar	Pedersen et al., 1994
Mont St. Eynard, France	Microtremors	ridge	65	350	na	3.5[b]	na	similar	Pedersen et al., 1994
Nice, France	Microtremors	ridges	35-40	80-120	na	7-9[b]	na	similar	Nechtschein et al., 1995
Tarzana, CA	1994 Northridge AS	ridge	14	15	na	4.5b	1.1	similar[3]	Spudich et al., 1996
Epire, Greece	Microtremors	ridge	23-26	90	na	2[c]	broad	na	Chavez-Garcia et al. 1996

na = not available

[1]Slope face descriptions: 3-D = three-dimensional geometry; ridge = approximate 2-D geometry with two slope faces
[2]Normalized frequency equivalent to ridge half width (W) normalized by wavelength, not available if V_S not reported
[3]Potential for geologic amplification noted by authors

[a] pseudo relative velocity response spectra
[b] Fourier amplitude ratio
[c] Based on Horizontal to vertical spectral ratio (HVSR)

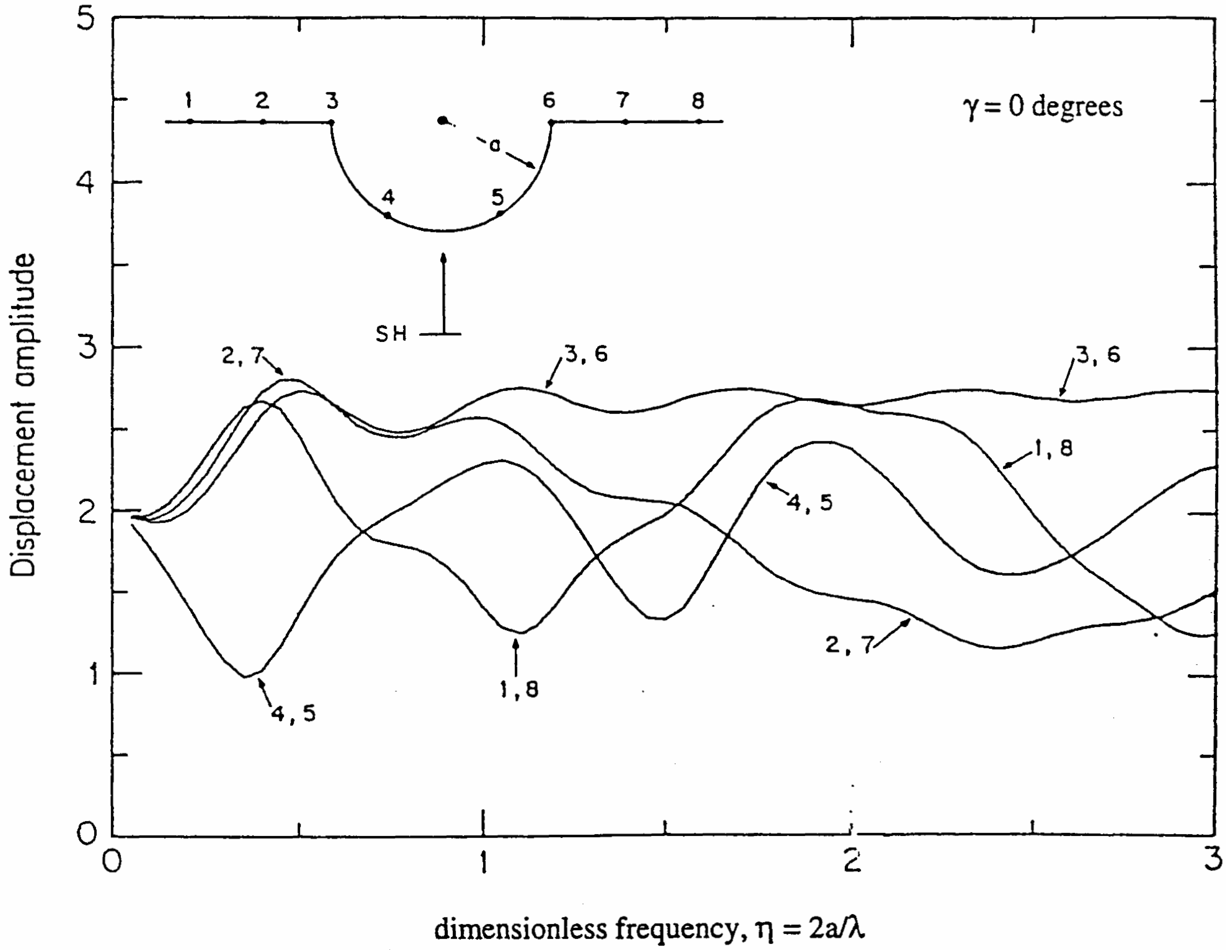

Fig. 5.29. Amplification as a function of normalized frequency across canyon subjected to vertically incident (γ=0) SH waves. After Trifunac (1973).

inclined SH wave arriving from the left, wave trapping on the left canyon wall would cause higher amplification levels than on the right side, with amplification levels as high as two being possible for horizontally propagating waves. Similar studies for P and SV waves have been performed by Wong (1982) and Lee and Cao (1990), and indicate amplification levels generally smaller than those for SH. Canyon geometry is also significant, with amplification being negligible for shallow canyons (ratio of depth to width < 0.05). For deep canyons, edge amplification is not significantly different than that discussed above, but more base de-amplification occurs (Wong and Trifunac, 1974).

Accelerograph arrays across several dam sites provide good candidate data sets for verifying analytical models. These sites include Pacoima Dam and Long Valley Dam in California, and Feitsui Dam in Taiwan. Each dam site has recordings from the canyon base and rim. Future research should utilize these data in verification exercises, with appropriate allowance for variable ground response effects.

5.5.3 Slopes

Single slope faces geometries have been investigated by Sitar and Clough (1983), Ashford et al. (1997), and Ashford and Sitar (1997). The later two studies analyzed a stepped halfspace subjected to plane SH waves and SV/P waves at various incidence angles. It was found that amplification generally increases with slope angle and proximity to crest, and is maximized for slope height (H) to wavelength (λ) ratios of H/λ = 0.2. Results by Ashford et al. (1997) for vertically incident SV waves are summarized in Figure 5.30a. In studies of stepped halfspaces with vertical slope faces, Ashford and Sitar (1997) found that the amplification indicated in Figure 5.30a can be increased significantly when incident waves are inclined such that they travel into the slope face. This is shown in Figure 5.30b, which shows a 50% increase in amplification for a vertical incidence angle of only -10 degrees.

Stewart and Sholtis (1999) evaluated topographic effects across a slope face from strong motion data, with appropriate corrections for ground response variability. The site is a water pumping plant for which recordings above and below a 21-m high cut slope are available from the m=6.4 1983 Coalinga mainshock and two aftershocks. Crest amplification of 5%-damped acceleration response spectra identified from the three recordings are presented in Figure 5.31. The maximum crest amplification is on the order of 1.2, which is reasonably consistent with published results by Ashford and Sitar (1997) and Ashford et al. (1997).

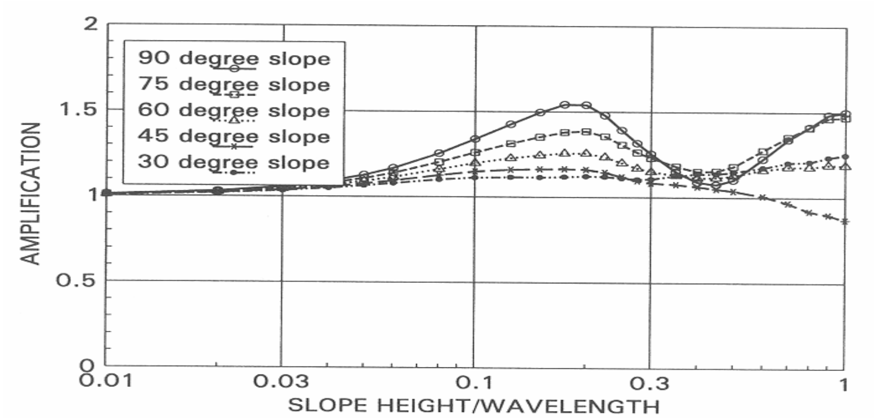

Fig. 5.30(a). Horizontal amplification at slope crest for a vertically incident SV wave (from Ashford et al., 1997).

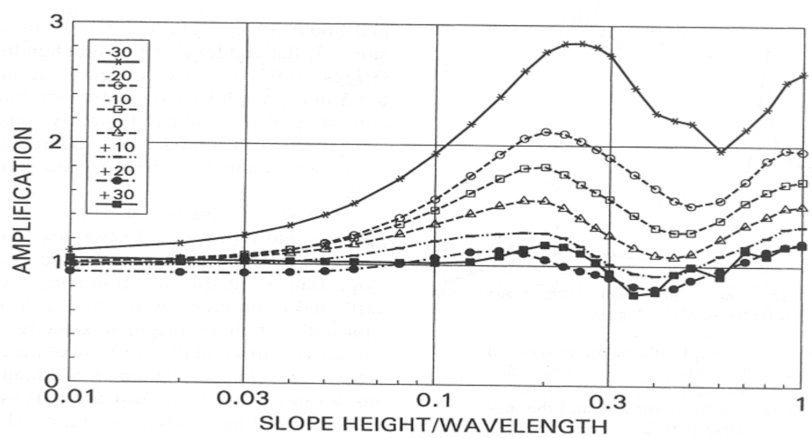

Fig. 5.30(b). Horizontal amplification at the crest of a vertical slope for inclined SV wave incident from -30° to +30° (from Ashford and Sitar, 1997). Negative incidence angles indicate wave propagation toward slope face.

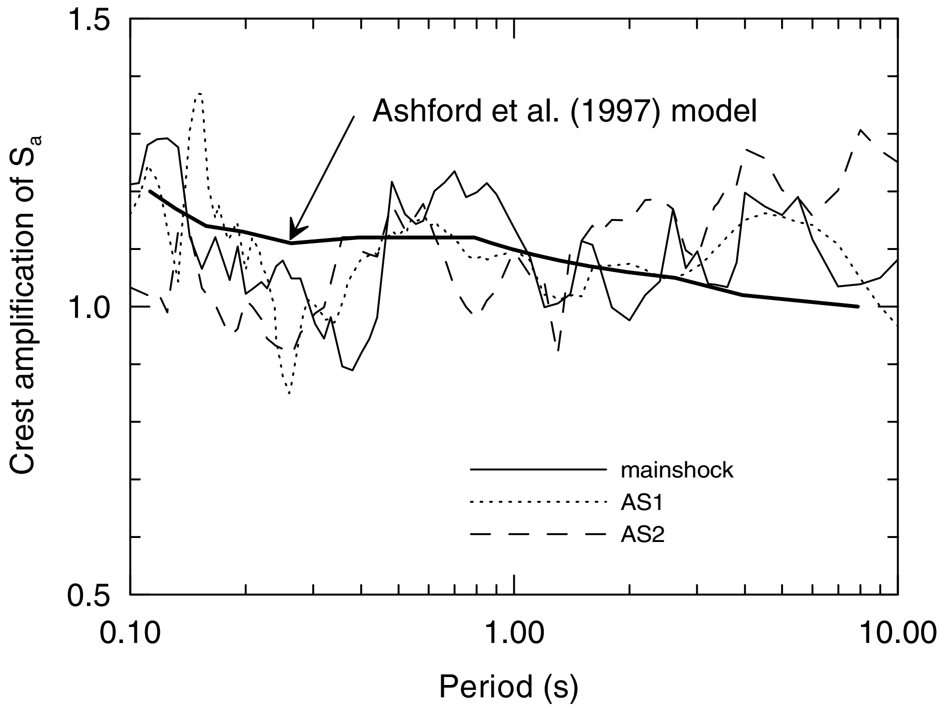

Fig. 5.31. Amplification at crest of 21-m tall, 3H:1V cut slope inferred from strong motion recordings and model prediction by Ashford et al. (1997) for vertically incident waves. After Stewart and Sholtis (1999).

5.5.4 Merging Topographic Effects into Hazard Calculations

As described in the sections above, a significant number of parameters affect model predictions of topographic effects. Most have not been suitably verified with observation. This state of knowledge does not allow rigorous treatment of topographic effects within hazard calculations. In order for this capability to be developed, there is a need for research to evaluate parametric variability on amplification factors using realistic ranges of model parameters. A parallel need that could help guide this process is verification studies using available strong motion recordings, and installation of new accelerograph arrays to enable more detailed future verification studies.

5.6 SYNTHESIS OF PEER RESEARCH

As noted in Section 1.3, at the time of PEER's inception, there was a lack of consensus on appropriate strategies for evaluating seismic site response effects associated with local soil conditions, basin response, and surface topography. Consensus on some of these issues remains elusive, but significant advances have been made through a coordinated plan of research involving the PEER Core and Lifelines programs, as well as the Phase III effort within the Southern California Earthquake Center (SCEC). Research in the Lifelines Program on these topics continues at present, in the first year of a three-year coordinated plan of work. In the following paragraphs we synthesize completed, ongoing, and planned research on ground response within the Lifelines Program. Only one project on ground response has been funded in the PEER Core Program, but this targeted project is complementary to the SCEC and PEER Lifelines work, and is also described.

The PEER Lifelines Program developed in 1997 a plan for research that sought to evaluate the impact of increasing levels of detail in site characterization on the accuracy of ground motion predictions. A series of complementary studies were funded in Phases I and II of the program that investigated the use of the following approaches for ground motion estimation: (1) qualitative surface geology and geotechnical site categories, (2) one-dimensional ground response analyses, and (3) basin response analyses.

The first of these three thrust areas of work was directed toward the evaluation of amplification factors based on either surface geology or geotechnical site conditions. Complementing this effort was the SCEC work and a PEER Core project in Thrust Area 2. Major strides have been made in the development of amplification factors through the following studies:

- "Characterization of Site Response, General Site Categories," PEER Lifelines Phase I (PI: Bray). This project developed the geotechnical classification scheme discussed in Section 5.2.2(c)
- "Surface Geology Based Strong Motion Amplification Factors for San Francisco and Los Angeles Areas," PEER Lifelines Phase II (PI: Silva). This project evaluated site amplification factors as a function of surface geology using equivalent-linear ground response analyses. Results presented in Section 5.3.3(a).

- "Empirical Characterization of Ground Response for Performance Based Design," PEER Core Project, Years 2-3 (PI: Stewart). Amplification factors were evaluated from empirical strong motion data for active regions as a function of surface geology, 30-m shear wave velocity, and a geotechnical-based classification scheme. Partial results presented in Section 5.2.3(c).

Complementing this work is a series of SCEC Phase III projects in which amplification factors were evaluated from empirical strong motion data for the southern California area. As described in Section 5.2.3(c), the results of the PEER work have provided insight into the merits of coarse vs. detailed geologic mapping (found to be beneficial) and detailed geologic mapping vs. 30-m shear wave velocity or geotechnical data. This work complemented and extended the SCEC study, and the results improve the accuracy with which ground motions can be estimated when detailed, site-specific analyses are not economically feasible. Moreover, the work allows the next-generation attenuation models to incorporate more rigorously defined site terms than had previously been possible.

The second thrust of work outlined above has sought to develop guidelines on the use of site-specific, one-dimensional ground response analyses. There are two components to this work. The first is evaluating the benefits of ground response analyses relative to soil attenuation relations. This work was initiated in PEER Lifelines Phase II in a project titled "Evaluation of Uncertainties in Ground Motion Estimates for Soil Sites," (PI: Stewart), and was described above in Section 5.3.3(b). The results have provided insight into the generalized site conditions for which equivalent-linear ground response analyses are justified in terms of their ability to reduce prediction dispersion relative to attenuation. Similar studies are being performed as part of an ongoing, multi-investigator project that is extending the number of sites considered and investigating the use of nonlinear analyses. The second component of the PEER ground response research is utilizing vertical geotechnical array data to more directly validate ground response analysis routines. A current project is assembling a comprehensive vertical array database (PI: Silva), and future work will utilize this data to gain insight into wave propagation characteristics and nonlinear soil behavior across these arrays, and to validate equivalent-linear and nonlinear ground response analysis routines. The analysis guidelines resulting from these two components of work will outline the site conditions for which ground response analyses of any type are justified, and the levels of shaking and types of intensity measures for which nonlinear analyses are needed in lieu of equivalent-linear.

The third thrust of work outlined above has sought to develop analytical models for basin response as a viable means by which to assess basin effects. Work organized through the PEER Lifelines Program (Phase I, PI: Day) has validated a series of leading basin response analysis routines against each other, and is now proceeding to calibrate these routines against a uniform set of ground motion recordings from basins. This work is discussed briefly in Section 5.4.6. The outcome of this work has been an improved understanding of the factors leading to damaging ground motions from basin response, which are discussed in detail in Section 5.4.2-5.4.4. Current and future work on basin response is seeking to further validate basin response codes against recordings, and then to use the validated codes to develop simplified empirical and parametric models for basin response.

In the above, we have described work performed within research thrust areas identified during the initial planning of PEER ground response research. Several additional topics have been identified and are planned for study in Stages 2 or 3 of the current, three-year PEER Lifelines Program. These include evaluation of ground motion variations across cut and fill areas, and studies to evaluate site amplification factors across shallow stiff soil sites and weathered rock sites. Both sets of studies will utilize microtremor measurements and engineering analyses to evaluate the respective amplification factors. Finally, it should be noted that the data collection projects described in Section 3.5 are of great value to site response research. These include updates to the ground motion database, characterization of ground conditions at strong motion stations, and development of models for nonlinear soil behavior.

6 GROUND MOTION SIMULATION

6.1 UTILIZATION OF SIMULATED EARTHQUAKE MOTIONS IN ENGINEERING PRACTICE

Simulated earthquake motions are used when strong motion recordings are not available for a particular earthquake engineering application. This can occur for particular geographical regions where recordings are sparse or for particular magnitude and distance ranges that may be of interest for a project. In either case, simulated earthquake motions represent synthetic data that can be used to supplement or supplant recorded motions. Two applications of simulations have been common in engineering design practice: (1) to provide design ground motions for structural or geotechnical response analyses for a particular project site and (2) to provide synthetic data for regions (geographic area, magnitudes, and distances) of sparse data to supplement or supplant recorded motions in developing attenuation relationships or design ground motions. One example of the first application is the SAC steel project (see Section 7.6.2) where near-fault acceleration time histories were simulated (Somerville et al., 1997b) and used as input time histories for structural analyses of steel moment-frame buildings. These simulated motions were needed to supplement the existing ground motion database for small source-to-site distances, as recordings with near-fault characteristics (such as fling step and directivity pulse) are poorly represented in the empirical database. An example of the second application is the use of simulated data to facilitate the development of spectral acceleration attenuation relationships for the central and eastern United States (Toro et al., 1997; Atkinson and Boore, 1995; Frankel et al., 1996), where again strong motion recordings are sparse. In this application, spectral acceleration data were simulated using region-specific source and crustal properties to develop the ground motion database used for the development of attenuation relationships.

6.2 BASIC FEATURES OF GROUND MOTION SIMULATION PROCEDURES

As shown in Figure 6.1, earthquake ground motion is the outcome of a complicated physical system that consists of three processes: seismic waves are generated as part of the strain energy released from the rupture of an active geologic fault (earthquake source process); seismic waves then propagate through the earth's crust (wave propagation) and approach the surface of the earth, where they undergo further modifications while propagating through shallow soils (shallow soil response). The outcomes of these processes are complex earthquake ground motions, with fundamentally different characteristics in the long-period and short-period ranges.

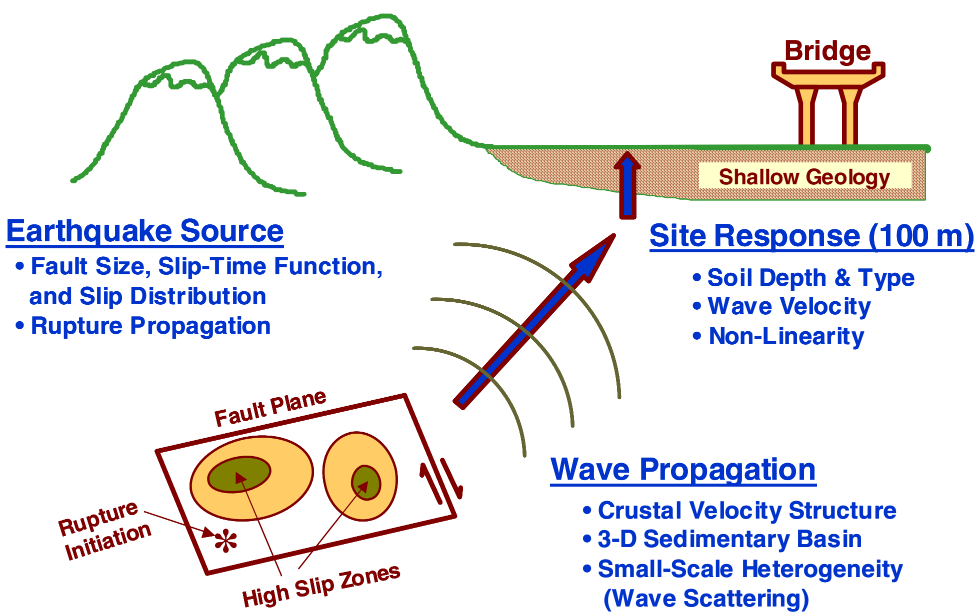

Figure 6.1. Schematic illustration of three physical processes that affect the generation and propagation of seismic waves.

It is generally accepted that long-period motions are deterministic, in the sense that one can reasonably predict their waveforms and spectral contents using seismological models that do not contain any stochastic element in either the input or the theoretical formulation. The first successful modeling of a near-fault record is the deterministic simulation of the displacement record at Station No. 2 of the 1966 Parkfield earthquake by Aki (1968) and Haskell (1969). It was demonstrated that the recorded displacement waveform at Station No. 2, which is only 0.8 km from the causative fault, can be successfully reproduced using a simple 5-parameter source model embedded in a homogeneous medium. Figure 6.2 provides another example of reasonable match to the long-period motion recorded at Arleta during the 1994 Northridge earthquake (Somerville et al., 1995).

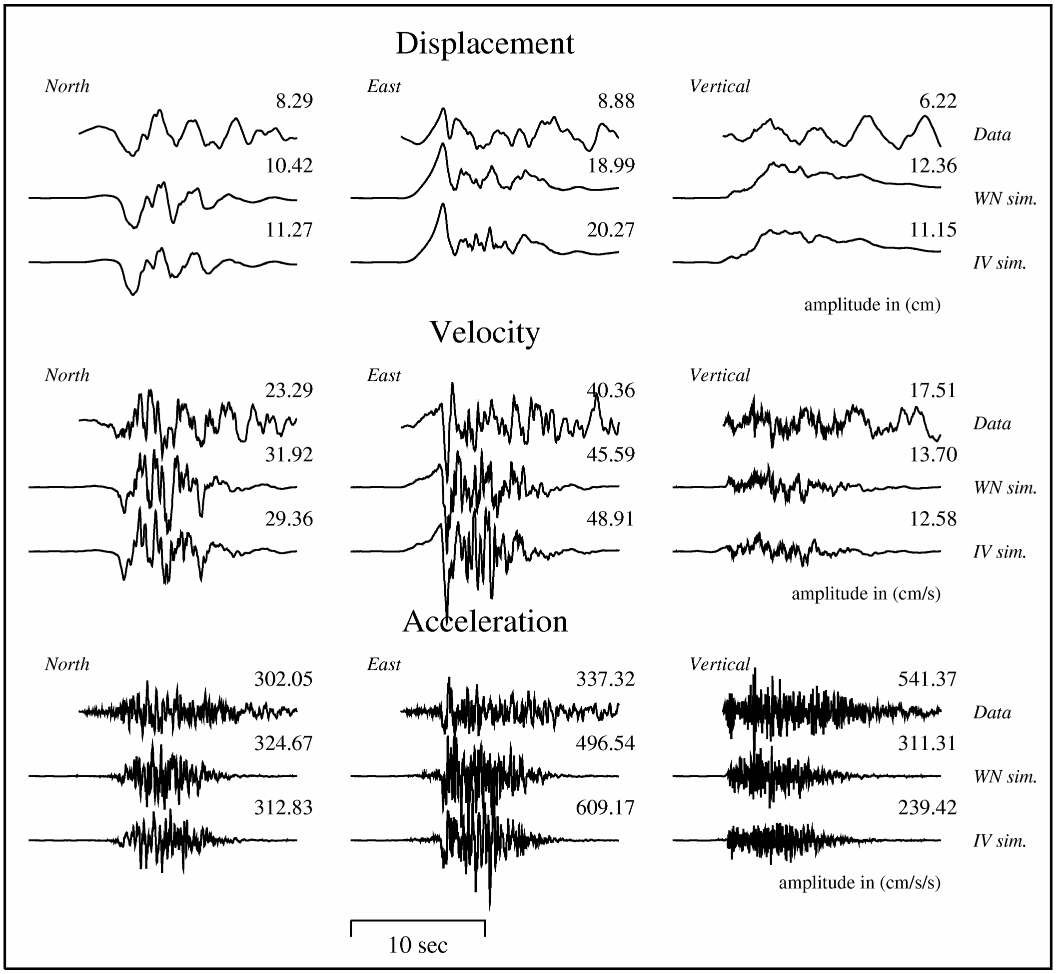

Figure 6.2. Comparison of recorded (top row) and simulated (middle and bottom rows) displacement, velocity, and acceleration time histories at Arleta from the 1994 Northridge earthquake, plotted on a common scale, with the peak value given in the top left corner. Source: Somerville et al., 1995.

Matches to the high-frequency waveforms of earthquake motions are relatively difficult to achieve using a deterministic approach. This is because source radiation and wave propagation become increasingly incoherent at short periods (e.g., Liu and Helmberger, 1985; Sato and Fehler, 1998) due to the existence of small-scale heterogeneities in the earthquake source process and crustal properties. Overall, the observed high-frequency motions behave stochastically. The period of transition from deterministic to stochastic behavior is uncertain, but is often taken as about $T \approx 1$s.

Seismologists have developed models to explain and approximate, with either deterministic or stochastic formulations, the effects of the above three physical processes on observed ground motions. Developers of different simulation procedures have adopted and implemented different models of the seismic source, wave propagation, and site response effects. An important question for engineers is the extent to which these procedures have been validated against recordings in both the long-period and short-period ranges. Extensive surveys of existing simulation procedures (and the seismological models they employ) are presented by EPRI (1995), Aki et al. (1995), Schneider et al. (1996), Hartzell et al. (1999), and Abrahamson and Becker (1999). In this section we describe basic features of seismological models that are essential to a simulation procedure. The following discussions focus on features related to the earthquake source and seismic wave propagation in the crust; a detailed description of site response effects has already been covered in Chapter 5 and will not be repeated here. It should be noted that, because the principle of linear superposition is used in their derivations, the simulation procedures described below are most suitable for estimating rock motions. The simulated rock motions can be used as input motions for ground response analyses (as described in Chapter 5) to account for the effects of nonlinear soil response on ground motions. Such nonlinear soil response analyses can be either conducted as part of a simulation procedure or performed by separate computer codes.

6.2.1 Earthquake Source Processes

(a) *Basic features of earthquake source processes*

The elastic rebound theory proposed by Reid (1911; see also Bolt, 1993) provides the fundamental framework for modern seismic source modeling of tectonic earthquakes. In Reid's theory, rupture occurs when stresses on a fault have accumulated to the point that the shear strength of the rock is exceeded, leading to rapid rupture across the fault. The rupture begins at a point called the hypocenter, and then spreads across the fault surface at a speed that is typically less than or close to the shear-wave velocity of the rock. As the rupture front passes a point on the fault, slip at that point begins to occur and it takes a finite amount of time (in seconds) for the slip to reach its final value and stop. The time between the initiation and termination of slip is defined as the rise time. In a simulation procedure, a kinematic source model[1] is typically used to describe such a fault slip process. Key parameters of a kinematic source model include fault

[1] Ideally, these source parameters should be determined from dynamics (balance of force and/or energy). However, they are often specified based on either observation or physical intuition.

rupture geometry (ruptured area, fault strike, and fault dip), rupture nucleation point, rupture velocity, slip direction (rake angle), and a slip-time function. The slip-time function describes the progression of slip at a point on the fault and includes information about rise time and final amount of slip. Example distributions of fault rupture area and final slip inferred from seismological data are given in Figure 6.3 for five crustal earthquakes with m=5.6-7.2.

(b) *Point source or finite source?*

The fault slip process is finite in both time and space. When a site is within a few fault lengths of the source of a large-magnitude earthquake, a finite source is essential to the simulation of the near-fault effects described in Chapter 4. Otherwise, at distances far from the fault, a finite source can be reasonably simplified to a point source in space for the purpose of simulating ground motions. Because a procedure using a point source model is computationally less involved than one using a finite source model, considerable cost savings can be achieved when the point source model is deemed appropriate.

(c) *Randomness in source process*

The fault slip process is complicated both spatially and temporally. Smooth (coherent) components of fault slip affect the generation of long-period waves, whereas small-scale (incoherent) components, as well as rupture arresting near the fault edge, control the excitation of high-frequency waves. Small-scale components are generally too complicated to be specified exactly; instead, they are treated as random phenomena and characterized stochastically. To implement stochastic source processes in a simulation procedure, small-scale random heterogeneity can be imposed on top of a specified source parameter. For example, random perturbations could be applied to a constant rupture velocity to produce a jerky rupture front and the resulting accelerations/de-accelerations of the rupture front efficiently generate high-frequency waves (Madariaga, 1977; Bernard and Madariaga, 1984; Spudich and Frazer, 1984; Hisada, 2001). Statistical models have been proposed to generate random slip distributions for future earthquakes (Silva, 1992; Herrero and Bernard, 1994; Joyner, 1995; Somerville et al., 1999; Hisada, 2000, 2001; Mai and Beroza, 2001). Parameters for such slip models are calibrated using slip distributions from past earthquakes and are constrained by the seismological observations of far-field motions. Similar randomization has been applied to other source parameters such as the rise time and rake angle.

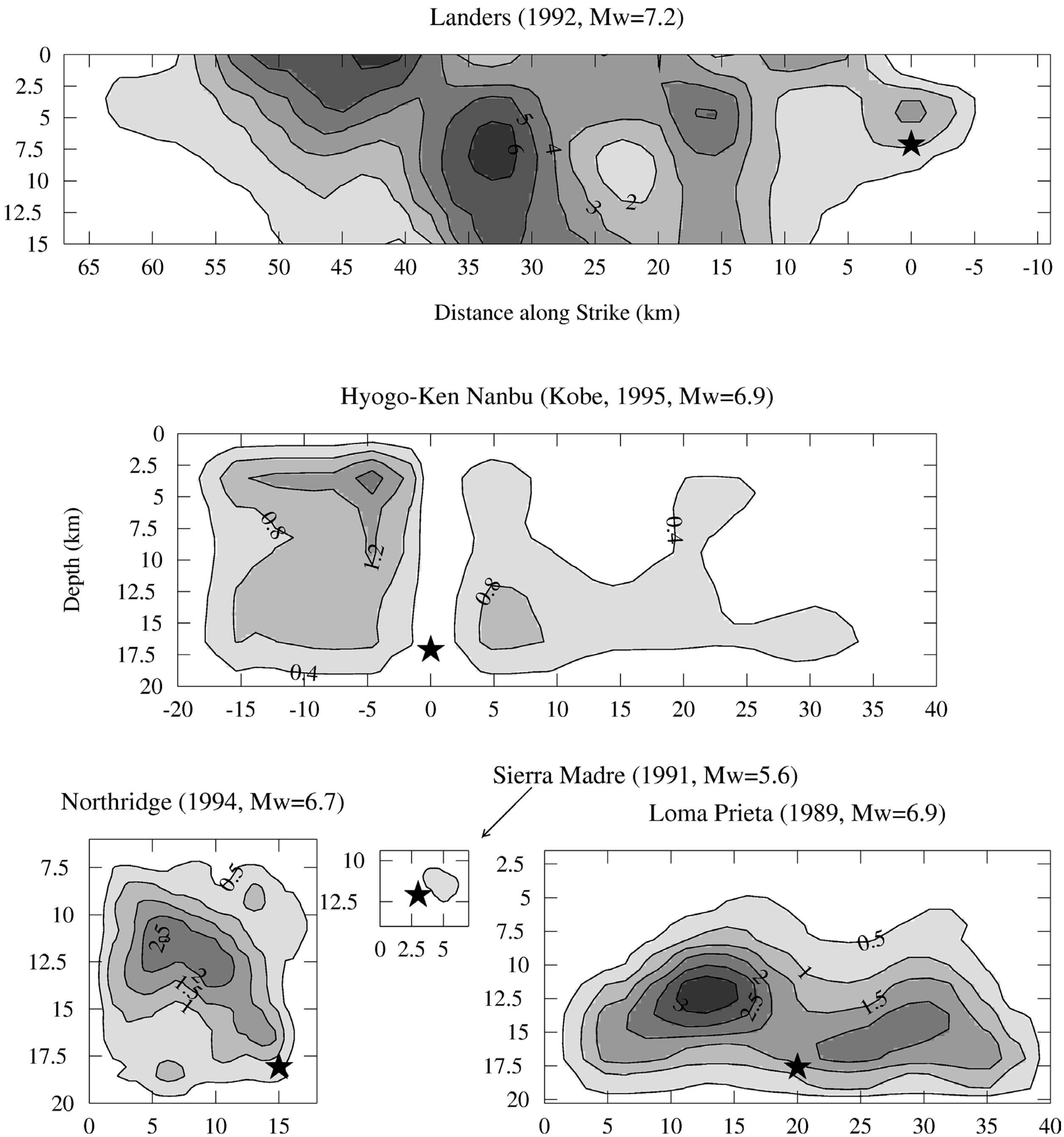

Figure 6.3. Fault slip in meters as a function of position on the fault plane of five recent earthquakes, derived from strong motion and teleseismic data. Source: Wald, 1996.

6.2.2 Wave Propagation

The effect of wave propagation in the earth's crust is also called the path effect. Typical path effects include attenuation of wave amplitude due to geometrical spreading and inelastic energy absorption, reflection and refraction at the interface of distinct rock types (large-scale heterogeneity), and wave scattering from small-scale heterogeneities in the crust. Green's functions[2] are used in simulation procedures to collectively represent the effects of wave propagation in a crustal structure model.

(a) *Analytical Green's function*

A Green's function may be calculated analytically for a given crustal model. In order to compute Green's functions, we need to understand properties of the crustal structure such as the compressional- and shear-wave velocities, density, and damping factor (or seismic Q factor, where $Q \approx 0.5/\beta$). Different assumptions of the crustal structure are used in different simulation procedures. Several stochastic procedures (e.g., Boore 1983; Silva and Lee 1987) use a $1/r_{hypo}$ (r_{hypo} = hypocentral distance) geometrical spreading term that is appropriate for the attenuation of shear waves in a homogeneous medium. Green's functions for more realistic models of layered crust (Helmberger et al., 1992; Olson et al., 1984; Luco and Apsel 1983) are also widely used. An example of the contributions of multiple seismic arrivals to the complexity of earthquake motions in a layered crustal model is given in Figures 6.4 and 6.5. The ray paths of the up-going and the down-going seismic waves leaving an earthquake source are shown in Figure 6.4 and their contributions to the ground motions are illustrated in Figure 6.5.

When a site is located in a sedimentary basin or on a hilltop, basin or topographic effects can be observed, respectively. Such effects can be modeled, but the key input to the modeling is the 2D or 3D earth structure, which is often poorly characterized. Finite difference or finite element methods are usually used to model wave propagation in a complex 2D or 3D earth structure. These methods remain computationally intensive and are often limited to long-period ($T > \sim 1$ s) calculations. Further research is required before these calculations can be used for routine engineering applications. Sections 5.4 and 5.5 of this report provide additional discussion on the effects of sedimentary basins and topography, respectively.

[2] Green's function is the response of the earth to a seismic point source. It is a function of the earth's velocity structure, site and source locations.

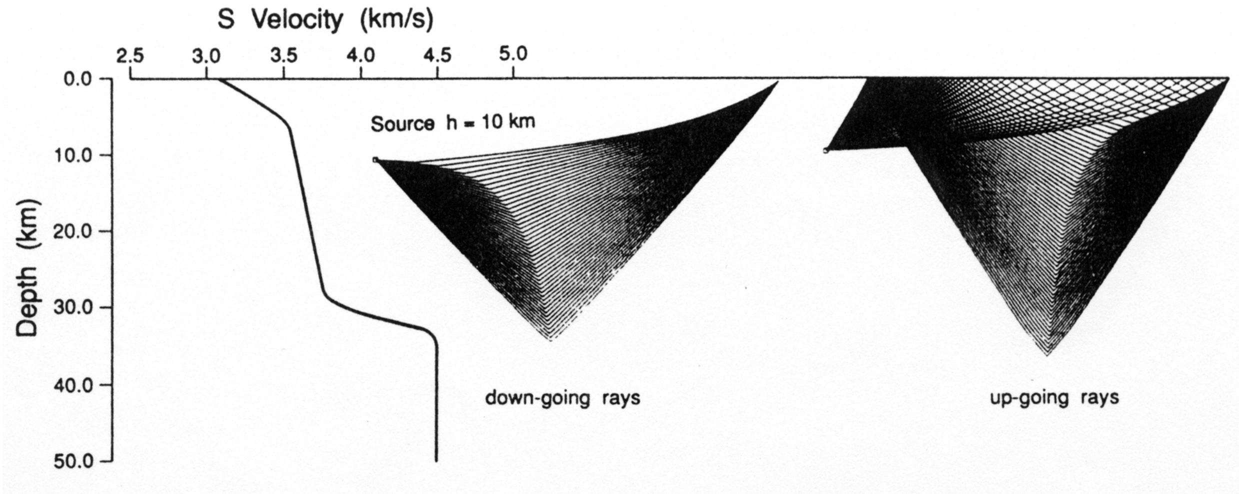

Figure 6.4. A smooth crustal velocity depth function and generalized ray paths contained in the Green's functions used to construct the synthetic seismograms shown in Figure 6.5. Source: Helmberger et al., 1992.

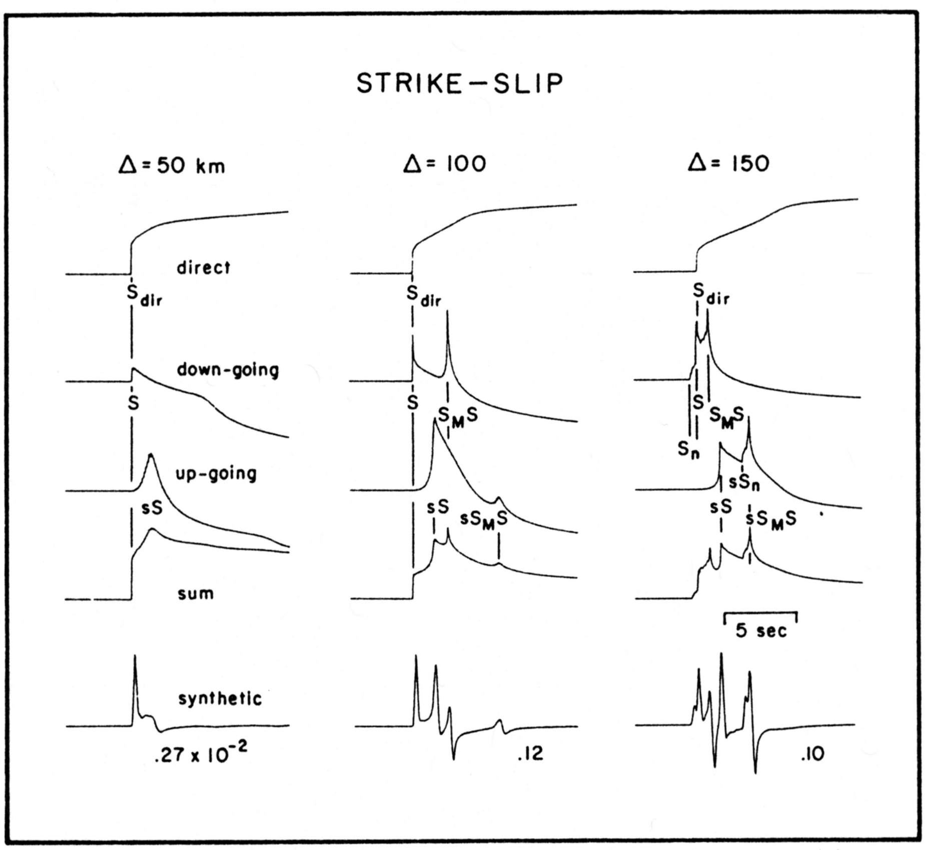

Figure 6.5. Decomposition of Green's functions showing the response of the direct arrival at the top followed by the contribution of downgoing paths (S) and upgoing paths (sS). The bottom row shows synthetic seismograms derived from these Green's function components. Source: Helmberger et al., 1992.

(b) *Randomness in wave propagation*

The analytical Green's functions described above do not include the effects of wave scattering at high frequencies. Scattered waves due to small-scale heterogeneities in the crust contribute significantly to the complex appearance of recorded acceleration time histories. They prolong the ground shaking duration, redistribute energy among the three orthogonal components of shaking, and contribute to the spatial incoherence of ground motions. As an example of the importance of scattered waves in recorded motions, it was found that neglecting scattered waves in simulations could lead to underprediction of strong motion duration of Northridge accelerations by factors ≥ 1.3 (Aki et al., 1995). The distribution of small-scale heterogeneities in the crust is for practical purposes random; therefore it is only possible to predict the average characteristics of the scattered waves (i.e. wave envelope, in the time domain, and mean power spectral density, in the frequency domain). See Sato and Fehler (1998) for an extensive review of seismological models for the synthesis of scattered waves. There are several simulation procedures that explicitly include scattered waves (e.g. Zeng, 1995; Zeng et al., 1995; Horton, 1994) as signal-generated noise in the simulated motions, the signal being the seismic wave arrivals contained in the analytical Green's function. Other procedures ignore or include empirically the scattered waves (for example, the empirical Green's function and empirical source function include scattered waves generated in the real earth).

(c) *Empirical Green's function*

An alternative approach, called the empirical Green's function approach (Hartzell, 1978, 1985; Irikura, 1983; Hutchings, 1994), has been used to obtain the Green's functions needed for the simulation of earthquake motions. This approach takes a recording (at the site of interest) from a small-magnitude earthquake, which is located close to the causative fault for the design earthquake, as an approximation to the Green's function. The empirical Green's function is considered more realistic than an analytical one because it contains wave propagation effects of the real earth, including scattered waves. The latter makes it attractive for the simulation of high-frequency motions, which are strongly influenced by scattered waves. One potential problem with empirical Green's function is that the signal-to-noise ratios of recordings are sometimes inadequate for low-frequency simulations. Another practical difficulty is acquiring a insufficient number of small earthquake recordings to cover the entire fault surface.

6.2.3 Ground Motion Representation Theorem

Given a fault slip model and Green's functions, the representation theorem is used to compute the total ground motion at a site due to a finite earthquake source. Comprehensive discussions of the representation theorem and its use in ground motion simulation are given in Aki and Richards (1980) and Spudich and Archuleta (1987). Numerical implementation of the theorem involves an integration that can be evaluated as a triple summation of weighted and time-lagged Green's functions over time and over a 2D grid of subfaults (see Figures 6.6 to 6.8). In the first summation, multiple Green's functions are summed together in order to build up a longer rise time. The second and third summations are performed over the 2D grid of subfaults, which represent a discretized finite fault. For a subfault with a larger assigned slip, a proportionally larger weight is given to the corresponding Green's functions. Time lags are applied to Green's functions to account for the rupture propagation and for the travel time needed for the seismic waves to propagate from a subfault to the site.

6.3 EXAMPLES OF GROUND MOTION SIMULATION PROCEDURES

In this section, descriptions of three simulation procedures widely used in engineering practice are given. These three procedures are based on different seismological models of earthquake source, wave propagation, and site response. Only brief summaries of the seismological models used in each procedure are provided here. For more comprehensive descriptions, see Silva and Darragh (1995), Silva et al. (1990, 1995, and 1999), Zeng et al. (1994, 1995), Zeng and Anderson (2000), Somerville (1993), and Somerville et al. (1996). In the following, we have attempted to avoid opining on the strengths and weaknesses of these procedures because the documentation of these procedures, and the available validation studies are not sufficiently thorough to enable such judgments to be made.

6.3.1 The Stochastic Ground Motion Model

There are two versions of this simulation procedure, one uses a point seismic source and the other uses a finite fault source. The point-source version uses a ω-squared source model (Brune, 1970, 1971) with a single corner frequency (f_c) and a constant stress drop ($\Delta\sigma$) (Boore, 1983; Atkinson, 1984) (Figure 6.6). The finite-source version combines aspects of the finite source described in Section 6.2.1 with the point-source ground motion model (Silva et al., 1990; Silva et al., 1995) (Figure 6.6). In the finite-source case, the approach of lagging-and-summing multiple Green's functions over a 2D grid of subfaults is used. The finite source model includes a heterogeneous slip distribution, and the rupture velocity is taken as 0.8 times the shear-wave velocity at the depth of dominant slip. To capture heterogeneity in fault rupture propagation, a random perturbation of 20% is applied to the rupture velocity. Validation results of point- and finite-source versions (Silva et al., 1999) indicate that the finite-source model, on average, gives more accurate predictions than the point-source model for spectral periods $T > 1$ s. For $T < 1$ s, both versions give comparable results in terms of the modeling bias and variability (Silva et al., 1999).

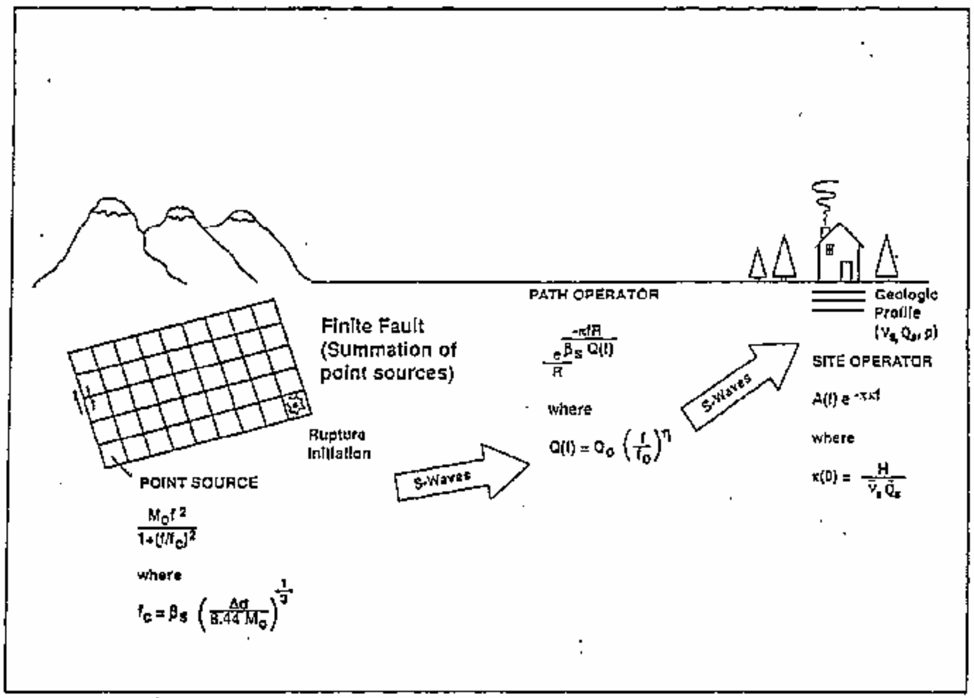

Figure 6.6. Schematic of Stochastic Finite-Fault Model. Source: Roblee et al., 1996.

The effects of wave propagation are simply modeled by $1/r_{hypo}$ (or $1/\sqrt{r_{hypo}}$ for surface wave) geometrical attenuation, crustal damping [modeled by a frequency-dependent quality factor, $Q(f)$], and crustal amplification due to the velocity gradient in the shallow crust. It is also possible to use either empirical or simplified numerical procedures (ray tracing) to account for the effects of reflection off crustal interfaces (such as Moho) (Ou and Herrmann, 1990; Boore, 1996).

An equivalent-linear model is used to account for nonlinear 1D ground response. A simple damping function, parameterized by κ (Figure 6.6), is used to model the damping effect in the very shallow crust directly below the site (Hough and Anderson, 1988; Silva and Darragh, 1995). This damping effect is an attempt to model the observed rapid fall off of Fourier amplitude spectra beyond a maximum frequency (Hanks, 1982; Silva and Darragh, 1995). This observed phenomenon truncates the high-frequency part of the spectrum, and along with corner frequency f_c, is responsible for the band-limited nature of predicted spectra from the stochastic ground motion model.

This procedure predicts the power spectral density of stochastic ground motions with attractive simplicity. The predicted power spectral density, and the assumptions of normality and stationarity about the stochastic character of time histories, permit stable estimates of peak values of ground motions to be made without computing detailed time histories (Hanks and McGuire, 1981; Boore, 1983). Under these two assumptions, random vibration theory is used to relate a time-domain peak value to the time-domain root-mean-square (RMS) value (Boore, 1983), which is calculated by integrating the power spectral density from zero frequency to the Nyquist frequency and applying Parsevall's relation.

Fourier phase spectra are needed to generate time-domain realizations of stochastic motions. One simple way is to generate random phases using a random number generator. A more attractive alternative is to carry the phase information (or time delays) in the finite-source procedure and, at the end, combine it with the phase spectrum of a real recording from an earthquake whose size is comparable to the subfault size (generally in the magnitude range of $m = 5 - 6.5$). The empirical phase spectrum permits the generation of a realistic time history, especially the high-frequency waveforms. Interestingly, this phase spectrum need not be from a recording in the region of interest (Silva et al., 1989). Combining the amplitude and phase spectra, and transforming the resulting complex-valued Fourier spectrum back into the time domain then results in one realization of the ground motion time history, which includes all of the aspects of a finite source, as well as path and site effects.

6.3.2 The Composite Source Method

In this procedure, a composite source model (Zeng et al., 1994) is used to represent the complex source process of an earthquake. The source is taken as a superposition of circular subevents with constant stress drop (Figure 6.7a). The number of subevents and their radius follows a power law distribution. The heterogeneous nature of the composite earthquake faulting is apparently characterized by the maximum subevent size and the subevents' stress drop, which are constrained by independent geophysical data. The random nature of the heterogeneities on a complex fault is simulated by distributing the subevents randomly on the fault plane. Rupture propagates from the initiation point at a constant rupture velocity. Each subevent initiates the radiation of a displacement pulse, calculated using a crack model (this displacement pulse is equivalent to the use of slip-time function in the other two procedures).

Wave propagation is modeled using analytical Green's functions calculated for a flat-layered medium (Figure 6.7b) in both short- and long-period ranges. The short-period components of the Green's functions are modified for the effects of random lateral heterogeneity by adding scattered waves into the Green's function (Zeng, 1995) (Figure 6.7c). The solution is then further modified by propagating the motions as vertically propagating plane waves through a near-surface 1D velocity profile. Thus, the complex high-frequency waveform of this simulation procedure is generated from the combination of a heterogeneous source, wave reverberation in a stratified shallow crustal structure, and scattering from lateral heterogeneity.

Linear site response may be directly incorporated in the Green's function computations. Similar to the Stochastic Ground Motion Model, inelastic effects in the shallow site response are modeled using a simple inelastic attenuation function (Hough and Anderson, 1988; Silva and Darragh, 1995) that represents the absorption of seismic energy in the shallow subsurface directly below the site. A ground response calculation may be used outside the computation to accommodate nonlinear site response.

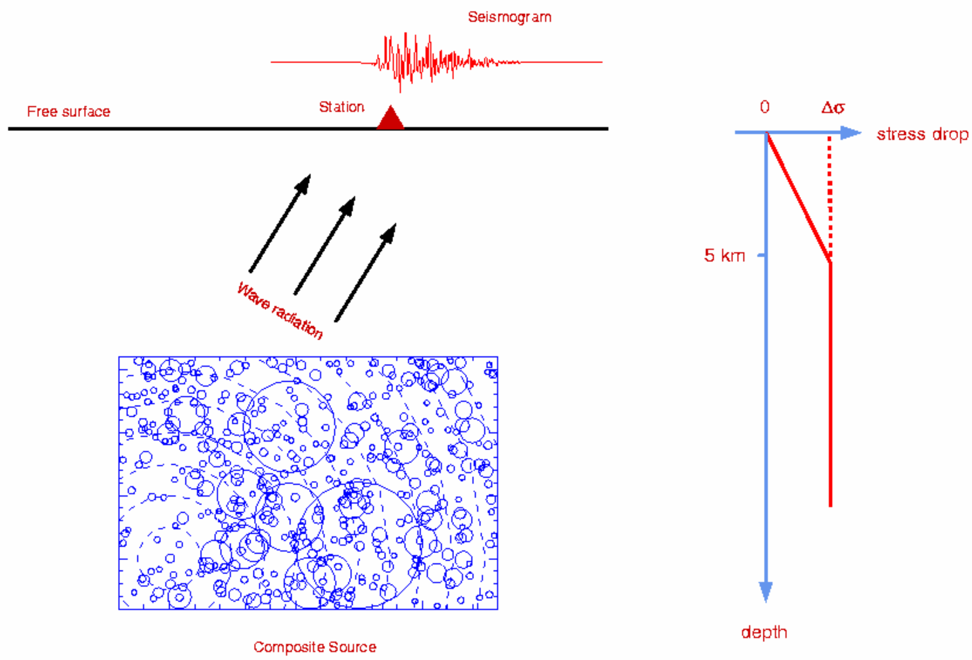

Figure 6.7(a). Schematic of source model in Composite Source Procedure. Source: Zeng and Anderson, 2000.

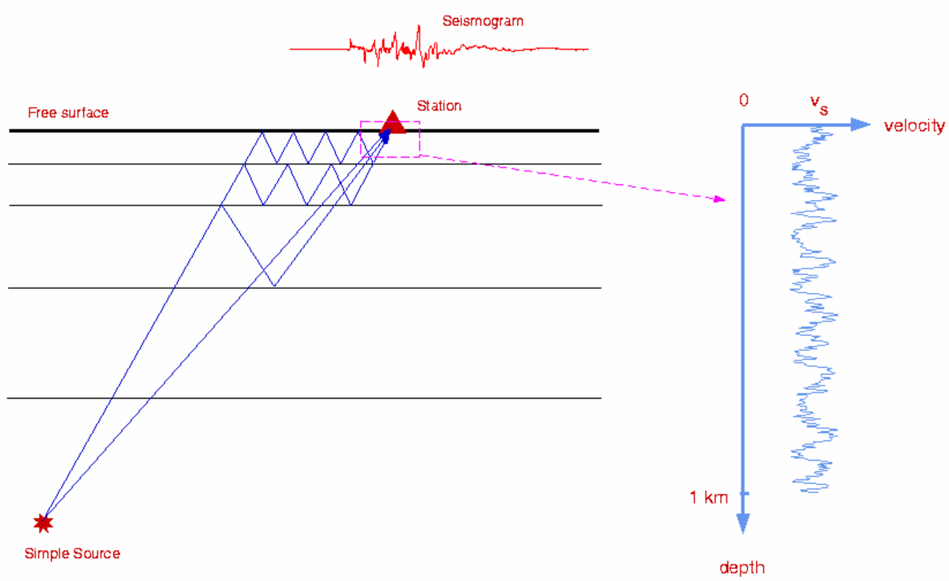

Figure 6.7(b). Schematic of flat-layered medium used for synthesis of Green's functions in Composite Source Procedure. Source: Zeng and Anderson, 2000.

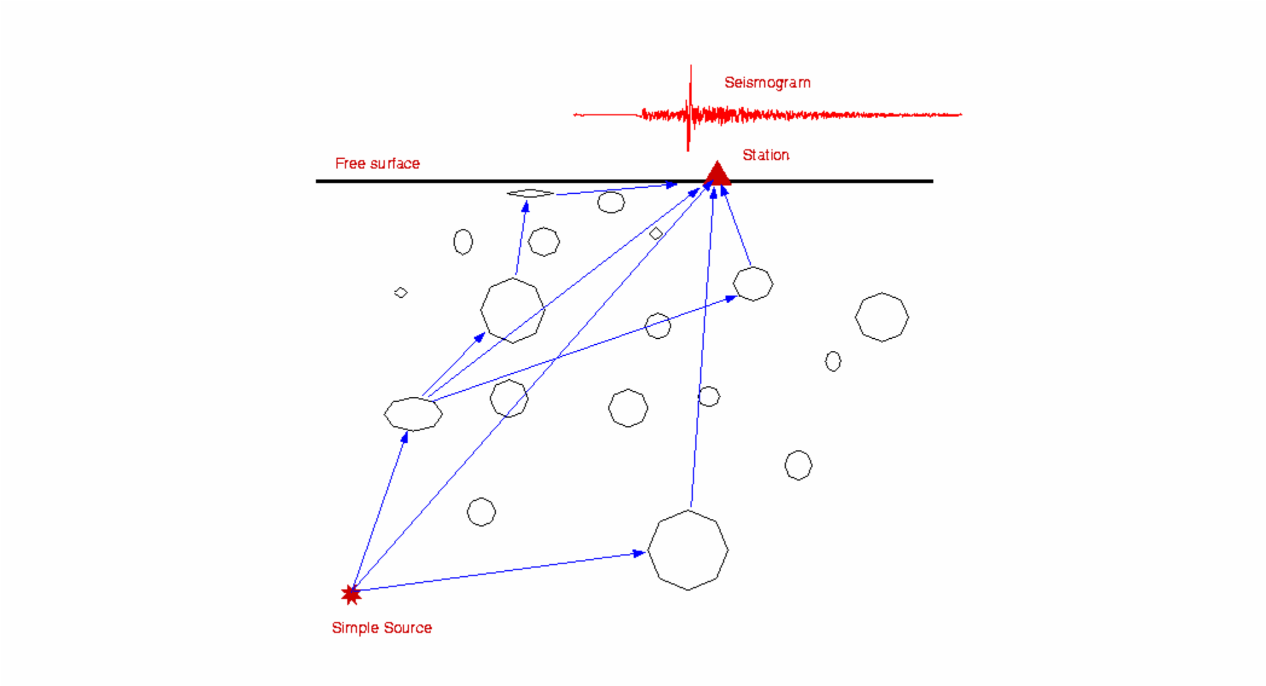

Figure 6.7(c). Schematic illustration of wave scattering and the effects of lateral crustal heterogeneity in Composite Source Procedure. Source: Zeng and Anderson, 2000.

6.3.3 The Hybrid Green's Function Method

This procedure uses a hybrid method to compute ground motions separately in the short- and long-period ranges, and then combines them into a single time history using matched filters at 1 Hz (Somerville, 1993; Somerville et al., 1996). The use of two separate approaches is motivated by the observation that ground motions have fundamentally different characteristics in the short- and long-period ranges: long-period motions behave in a more-or-less deterministic manner, while short-period motions behave stochastically. The transition from deterministic to stochastic behavior is thought to be associated with source radiation and wave propagation conditions being coherent at long periods and incoherent at short periods. At long periods, theoretical source models are used, which include the theoretical radiation pattern. At short periods, empirical source functions are used, which incorporate the radiation pattern and the wave scattering empirically.

The motivation for using an empirical source function is similar to that for using an empirical Green's function (Section 6.2.2c). However, of principal interest here is the complex source process included in the recording of a small earthquake, as well as the high-frequency scattered waves naturally included in this recording. A set of recordings representing the empirical source functions of one region could be transferred and used in another region after correcting for differences in path effects between the two regions (Somerville, 1993; Somerville et al., 1996).

In this procedure, the fault rupture plane is discretized into a grid of equal size subfault regions, and different values of slip can be assigned to each subfault element to incorporate non-homogeneous slip distribution across the fault (Figure 6.8). Empirical relationships are used to estimate the rise time of the design earthquake. An empirical source function is used as a subevent in the lag-and-sum procedure to build up a larger finite source. The subevent rise time, i.e., the rise time of the earthquake from which the empirical source functions are derived, is estimated independently. Heterogeneity of the source process is implemented by randomizing the selection of the empirical source function and by randomizing the location of the subevents within each subfault area. Additional details on this source characterization procedure are described in Somerville et al. (1999).

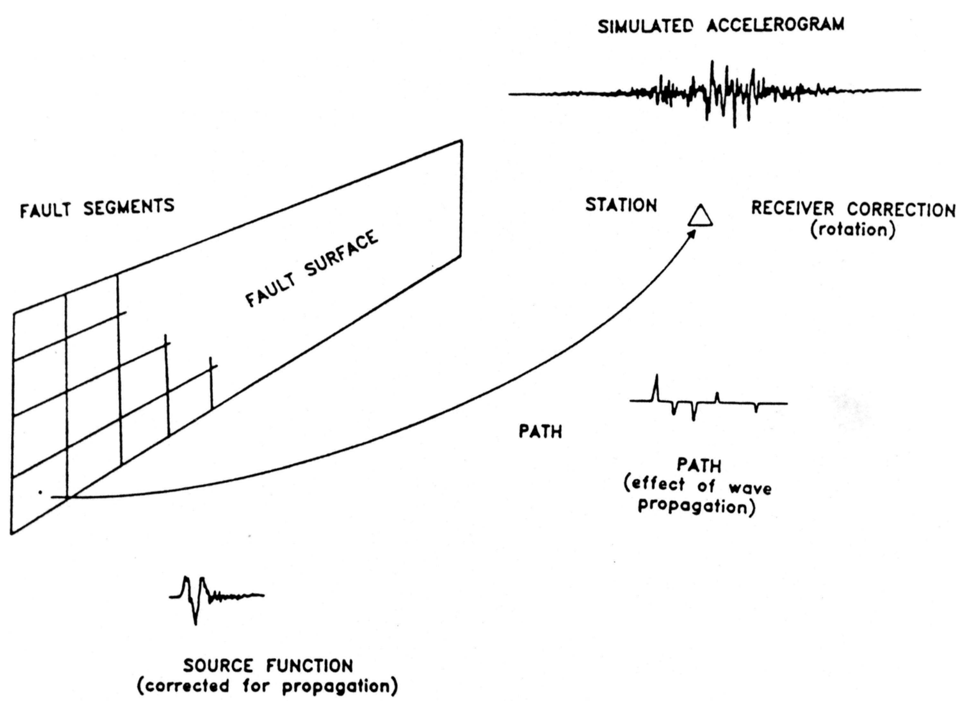

Figure 6.8. Schematic illustration of Hybrid Green's function method for simulating strong ground motion. Source: Somerville, 1993.

Wave propagation is represented by analytical Green's functions computed for the seismic velocity structure that contains the fault and the site. The Green's functions are usually calculated for a flat-layered crustal structure model using the frequency-wavenumber integration method in the long-period procedure and using generalized rays (direct and first multiple) in the short-period procedure. In the long-period procedure, the Green's function can also be calculated using a 3D model of crustal structure that contains a sedimentary basin.

Linear site response can be directly incorporated in the Green's function computations. Inelastic effects in the site response are modeled using a simple inelastic attenuation function (Hough and Anderson, 1988; Silva and Darragh, 1995) that represents the absorption of seismic energy in the shallow subsurface directly below the site. A ground response analysis may be used outside the computation to accommodate nonlinear site response.

6.4 VALIDATION OF SIMULATION PROCEDURES — MODELING VARIABILITY

Our first criterion to accept a simulation procedure for engineering application is whether the procedure is based on rational seismological models of earthquake source, wave propagation, and site response. Each of the procedures discussed in Section 6.3 meets this criterion. However, seismological models only approximate the effects of the real physical processes and it is critical to calibrate and validate these models against recordings from real earthquakes. Therefore, our second criterion to accept a simulation procedure is that it has undergone a thorough validation process against data from well-recorded past earthquakes (Abrahamson et al., 1990). By means of the validation, one can assess a procedure's effectiveness at predicting intensity measures such as peak ground acceleration, peak ground velocity, response spectral accelerations, duration, and waveform characteristics. It should be noted that validation exercises conducted to date are principally based on the intensity measures of peak acceleration and spectral acceleration. Some recent work has also used duration as a validation parameter (Aki et al. 1995; Abrahamson and Becker, 1999; Hartzell et al., 2000). Waveform characteristics have not been adequately addressed during validation exercises.

The effectiveness of a simulation procedure at predicting a particular intensity measure is measured in terms of the misfit[3]. The misfit is partly due to the fact that seismological models implemented in any simulation procedure are only approximations to the real physical processes. Another important factor contributing to misfit is the selection of values for model parameters. Values for most model parameters can be estimated from geophysical data, and are subject to

[3] Misfit, or residual, is computed as the difference between the logarithms of the observed and the predicted intensity measure.

defined levels of estimation uncertainty. However, some model parameters are not measurable, either because they are not observable or the required data is unavailable. In such cases, values for these parameters are educated guesses. For either type of parameter, there is obviously uncertainty associated with its selected value, and a particular set of parameter values used in a validation exercise may not be the optimal values that give the smallest misfit.

One might attempt optimizing parameter values to reduce misfit. This optimization could be performed for an individual earthquake (e.g., the slip distribution or rise time), in which case event-specific parameter values are used in the validation. Alternatively, parameters could be optimized across a suite of earthquakes (e.g., stress drop used in the stochastic ground motion model), in which case validation is performed with the parameter fixed at its optimal value for all earthquakes. A parameter optimization can also be "site-specific"; e.g., the κ value may be optimized for each soft rock site or for all of the soft rock sites. The distinction between "generic" parameters and "event-specific" (and site-specific) parameters used in validation is critical when attempting (1) to apply a procedure to simulate future earthquake motions and (2) to assess the total variability of the estimated motions (Abrahahmson et al., 1990; Roblee et al., 1996; Abrahamson and Becker, 1999). In general, as more "event-specific" parameters are included in the procedure, the modeling variability becomes lower, however, at the expense of introducing additional (parametric) variability associated with the unpredictability of these parameters for a future earthquake. This topic is discussed further in Section 6.5.

Misfits in a validation exercise are usually summarized by modeling bias and variance. Bias is the average misfit over the entire set of recordings used in the validation. The modeling variance is computed as the average squared misfit, and its square root (standard error) provides a measure of the expected difference between a recorded motion and a predicted motion. The predicted motion at a given site may have significant variability (e.g., a factor of 1.5), reflecting limitations in the ability of the simulation procedure to predict the detailed characteristics of individual recordings, even though the bias (which represents the average misfit over all recordings) may be quite small. The modeling variability, quantified by the variance (or the standard error) of the misfits, along with the parametric variability associated with the model parameters for a future earthquake, contribute to the total variability of predicted motions when the simulation procedure is used to predict ground motions for design (see Section 6.5).

Only a few simulation procedures have been thoroughly validated, most having been only partially validated against recordings from a few earthquakes. Abrahamson and Becker (1999) reported that at the time of a October 1997 workshop, only four out of the eight procedures represented at the MCEER Workshop on Ground Motion Methodologies for the Eastern United States were validated against recordings from a large number of earthquakes. The three procedures discussed in Section 6.3 are part of the four well-validated procedures. In 1997, five earthquakes had been used by Zeng and Anderson, 15 earthquakes by Silva, and six earthquakes by Somerville. Recently, additional validation of these three procedures was conducted in the PEER Lifelines Program (Phase II) against a standard set of near-fault recordings from five well-recorded shallow crustal earthquakes. The objective of the Phase II projects was to determine the appropriateness of these three procedures to model near-fault directivity effects on response spectral accelerations (reports of the Phase II Lifelines projects can be downloaded from **http://pier.saic.com/PGEDocs.asp**). Developers of these three procedures are currently being supported by the PEER Lifelines Program to conduct additional validations against recordings from the 1999 Kocaeli, Turkey, the 1999 Chi-Chi, Taiwan, and the 1999 Duzce, Turkey, earthquakes.

Figure 6.9a shows the bias and standard errors of spectral acceleration misfits from the stochastic finite-source model (Silva et al., 1999). The validation was conducted against 15 well-recorded earthquakes with m = 5.3 - 7.4, with recordings from 487 sites having site-source distances ranging from about 1 km to > 200 km. This represents the most comprehensive validation currently available. Another unique aspect of this validation is that rock and soil sites were modeled using generic rock and soil profiles and equivalent-linear site response. The modeling bias of the stochastic finite-fault procedure is close to zero over the entire frequency range analyzed. The standard error ranges from 0.5 to 0.7 for frequency higher than 1 Hz. These standard errors are low considering that more than half of the validation data set comes from earthquakes with m < 6.5 (recall from Section 3.2.2 that the variance of high-frequency ground motion increases with decreasing magnitude, particularly for m > 6.5, Youngs et al., 1995).

For the Composite Source procedure and Hybrid Green's Function procedure, compilations of bias and standard error of spectral acceleration across the full suite of recordings from multiple events are not available. However, results from both methods are available for the Northridge earthquake, and are shown in Figures 6.9b-c. For the Hybrid Green's Function procedure, the Northridge results are representative of the results for the larger set of earthquakes. The bias and standard error in these figures cannot be directly compared to those in Figure 6.9a, because of the large differences in the data sets used in the validation exercises.

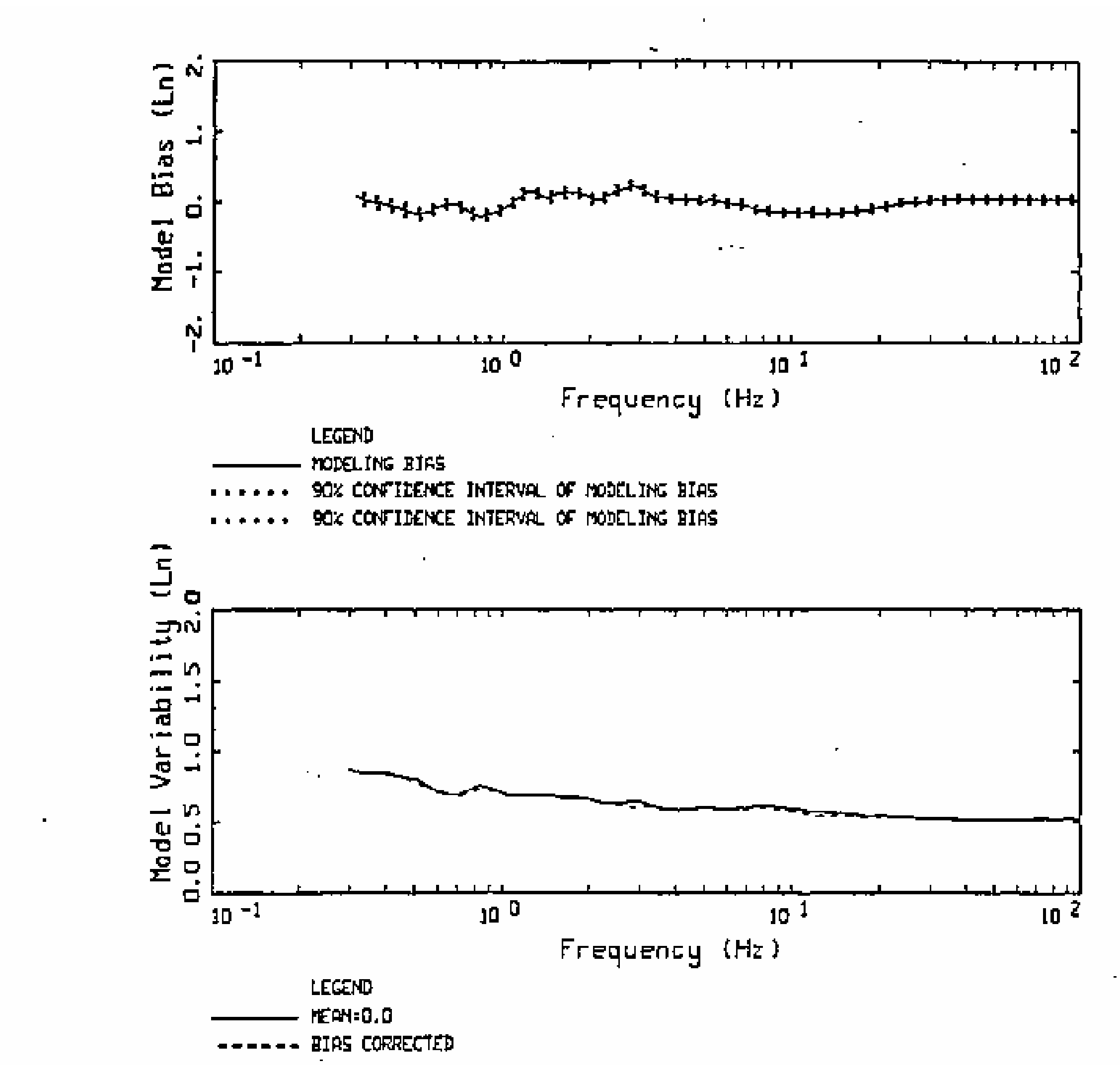

Figure 6.9(a). Model bias and variability of spectral acceleration from Stochastic Ground Motion model, based on 487 sites, 15 earthquakes, and finite-source model. Source: Silva et al., 1999.

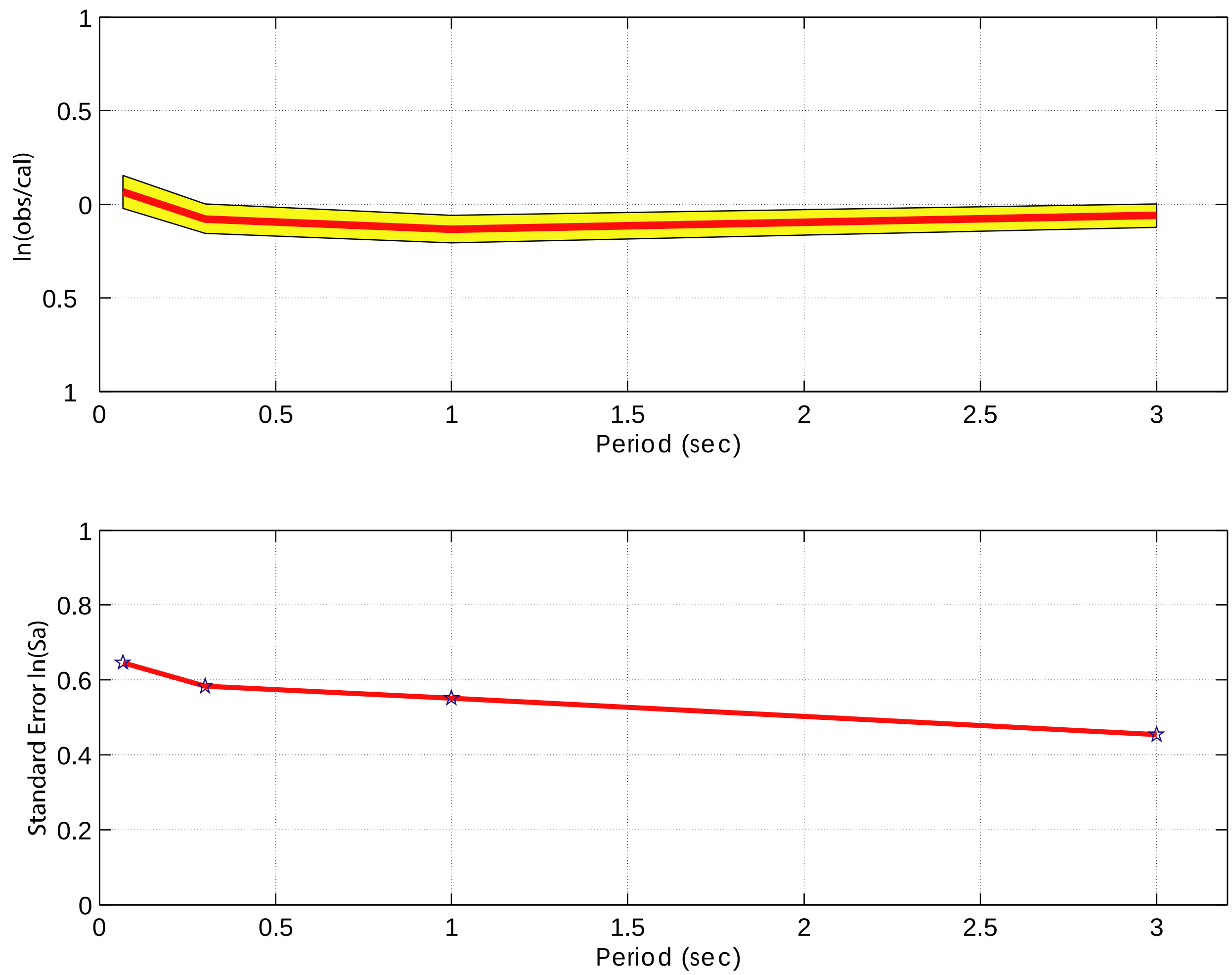

Figure 6.9(b). Model bias and variability of spectral acceleration at several periods from Composite Source Simulation method, based on 147 sites that recorded the Northridge earthquake. Source: Zeng, 2001, *personal communication*.

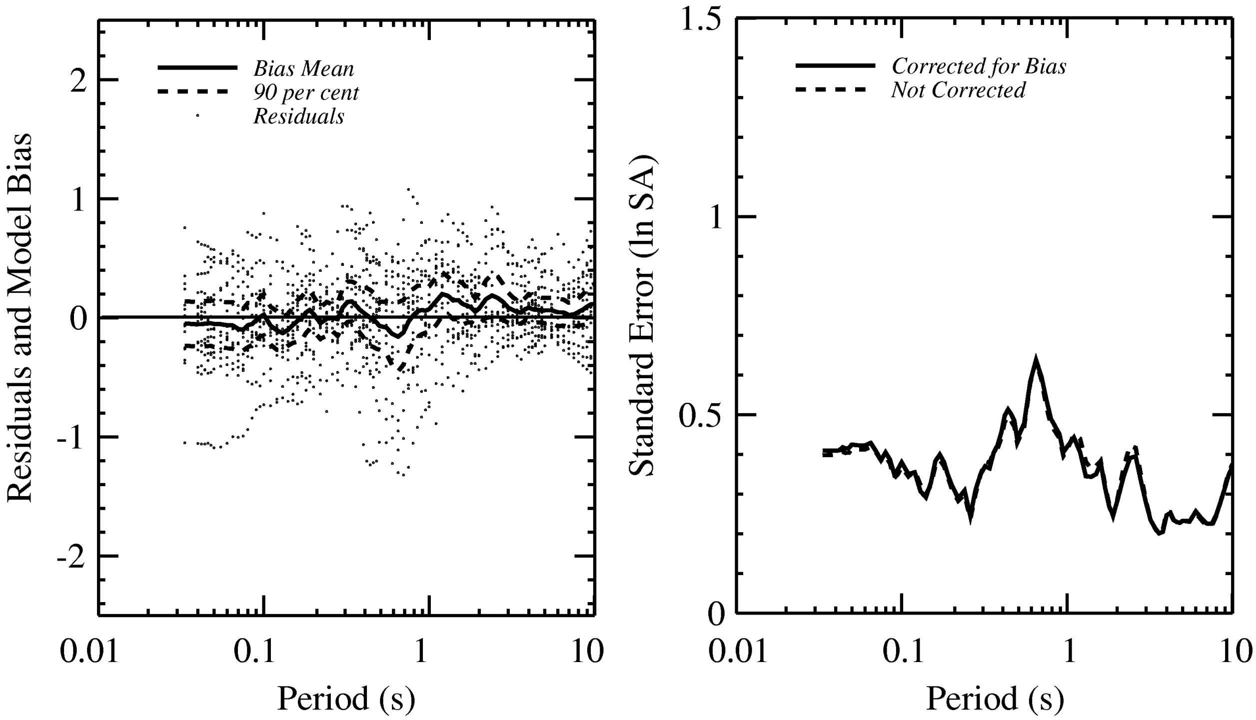

Figure 6.9(c). Model bias and variability of spectral acceleration from Hybrid Green's Function Simulation method, based on 15 sites in the San Fernando Valley that recorded the Northridge earthquake. Source: Somerville et al., 1995.

6.5 USE OF SIMULATIONS TO PREDICT GROUND MOTIONS FROM FUTURE EARTHQUAKES — PARAMETRIC AND MODELING VARIABILITY

To predict ground motion from a future earthquake, one or more simulation procedures should be used, each with multiple realizations of "event-specific" model parameters. The outcome of such analyses is usually a range of intensity measure estimates, which depend on the simulation procedure and the input parameter values. The predicted intensity measures are summarized by their median and standard deviation (prediction variability). For applications in performance-based engineering, the variability is as important as the median prediction. One needs to carefully track sources of variability and avoid any underestimation or double counting of the total variability.

Prediction variability is partitioned into "modeling variability" and "parametric variability." Modeling variability was discussed in Section 6.4, and is estimated with validation exercises. Parametric variability is due to our inability to reliably define "event-specific" parameter values for future earthquakes. Parametric variability is typically estimated through Monte Carlo simulation, in which random realizations of parameter values are used in a suite of simulations. It is important to emphasize that division between modeling and parametric variability is procedure-dependent; the same parameter could be treated as a fixed parameter in one procedure but as an "event-specific" parameter in another procedure. These two types of variability can be further viewed as having components of "uncertainty" and "randomness;" the division between these two components is also procedure-dependent. Table 6.1 outlines the four components of variability in the context of ground motion prediction. For a fixed parameter, which is part of the modeling variability, there might be "uncertainty" on the best fixed value due to the small number of earthquakes used in the validation, and this uncertainty is reducible when more earthquakes are used in the validation.

As an example of the total variability of prediction using the Hybrid Green's Function procedure, the variability for a *m*8 subduction zone earthquake is shown in Figure 6.10 (Ohtsuka et al., 1998). Four "event-specific" parameters are varied to estimate the parametric variability. They are the slip distribution, hypocenter location (rupture initiation point), rupture velocity, and rise time. The variability in the response spectrum due to each parameter was calculated with the other parameters fixed. The combined parametric variability is obtained by directly combining the variability arising from individual parameters, thus neglecting correlations between the effects of these four parameters. Global variability is derived from the whole set of simulations. The fact that global parametric variability is higher than the combined parametric variability suggests the presence of correlation between the effects of the four "event-specific" parameters. The modeling variability shown in Figure 6.10 is derived from the validation against recordings of the 1985 Michoacan earthquake alone. The total variability of ground motion prediction is obtained by combing the modeling variability and the global parametric variability.

Examples of prediction variability using the Stochastic Finite-Fault procedure is given in Silva (1992) and Roblee et al. (1996). In the later study, the parametric variability includes contributions from "event-specific" as well as "site-specific" parameters. Their results (Figure 6.11) show that for periods up to several tenths of a second, "site-specific" components of parametric variability comprise a significant fraction of total variability. For longer periods, modeling variability overshadows all sources of parametric variability.

Table 6.1 Contributions to total variability in ground motion prediction
(Source: Roblee et al., 1996)

	Modeling Variability	**Parametric Variability**
Uncertainty (also Epistemic Uncertainty)	<u>Modeling Uncertainty:</u> Variability in predicted response resulting from particular model assumptions, simplifications and/or fixed parameter values. *Can be reduced by adjusting or "calibrating" model to better fit observed earthquake response.*	<u>Parametric Uncertainty:</u> Variability in predicted response resulting from incomplete data needed to characterize parameters. *Can be reduced by collection of additional information which better constrains parameters.*
Randomness (also Aleatory Uncertainty)	<u>Modeling Randomness:</u> Variability in predicted response resulting from discrepancies between model and actual complex physical process. *Cannot be reduced for a given model form.*	<u>Parametric Randomness:</u> Variability in predicted response resulting from inherent randomness of parameter values. *Cannot be reduced a priori* by collection of additional information.*

Note: Some parameters (e.g., source characteristics) may be well defined after an earthquake.

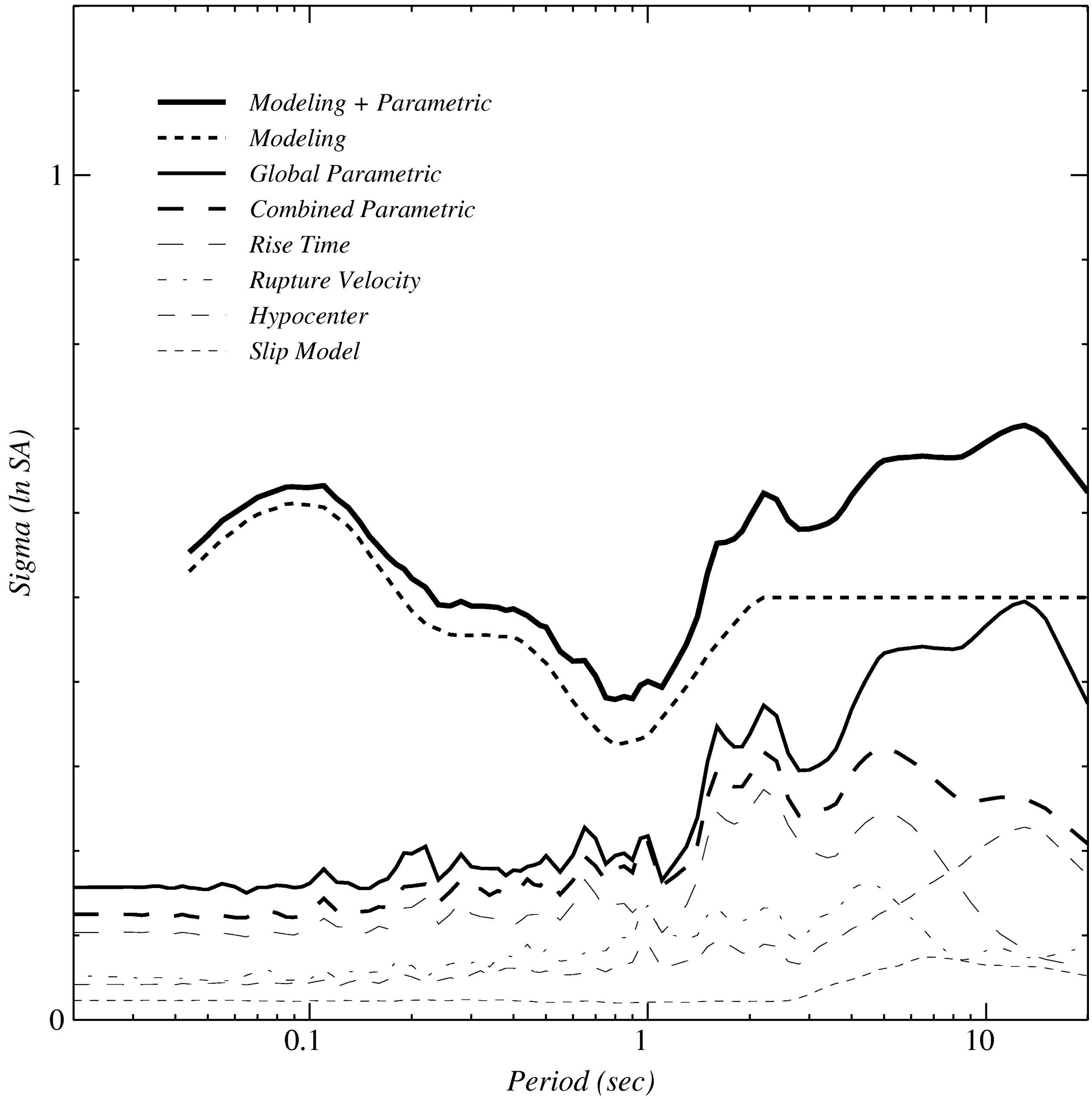

Figure 6.10. Overall standard error of Hybrid Green's Function simulation procedure (modeling + parametric), and its contributions from global parametric standard error and modeling standard error. Also shown are the partial standard error due to parametric variability of slip model, hypocenter location, rupture velocity and rise time, and the combination of these standard errors assuming no correlation between them. Source: Ohtsuka et al., 1998.

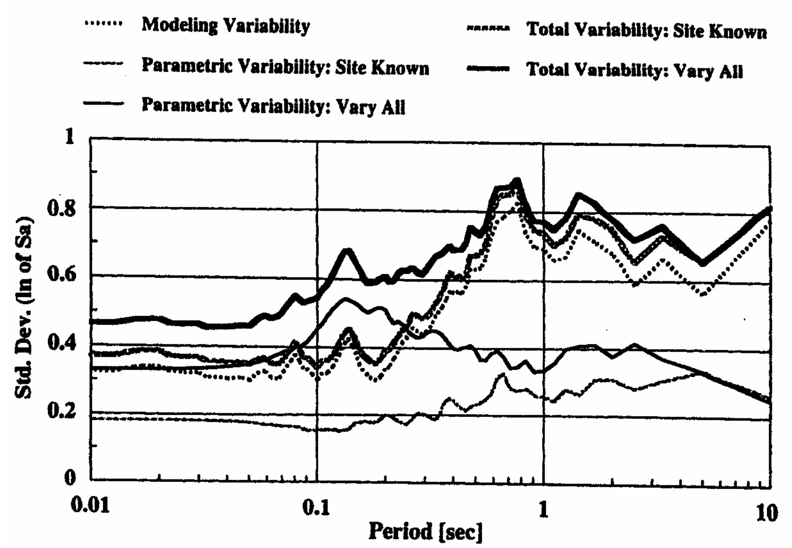

Figure 6.11. Comparison of components of variability for a scenario event and a stiff soil condition, Stochastic Ground Motion Model. Source: Roblee et al., 1996.

6.6 SUMMARY AND LIMITATIONS OF SIMULATION TECHNIQUES FOR GROUND MOTION PREDICTION

The various procedures for numerical simulation of strong ground motions have some common features. For example, the ground motion from a large-magnitude earthquake is computed by summing the ground motions from many smaller-magnitude earthquakes called subevents. The models differ in how they model the subevents and how they sum them together (size, location, and timing of subevents).

Theoretical seismology can be used to describe the subevents. At long period ($T > 1$ s), this approach works well using fairly simple models of the crustal structure, but at high frequencies, the observed ground motion amplitudes are not consistent with theoretical predictions. There is a systematic bias between the model predictions of response spectral values and the observed values.

To produce unbiased estimates of the high-frequency ground motions, the numerical simulation procedures must add some form of randomness into the high-frequency ground motions. The different procedures use different approaches for incorporating the randomness. In general, some randomness is added to the process or empirical recordings (which include the effects of randomness) are used for high-frequency ground motions.

For example, the "stochastic model" uses random vibration theory, which is based on random Fourier phase angles. The "composite source model" uses a fractal distribution of subevent sizes and subevents are randomly located on the fault plane. The "empirical Green's function" model uses empirical recordings for the subevents.

Since all of the procedures require random or empirical parts of the model, these aspects of the model can only be derived by calibrating the model using recorded ground motions. For this reason, numerical simulations at high frequencies typically do not do a better job of predicting high-frequency spectral accelerations than empirical attenuation models for magnitudes and distances for which there are empirical data. While simulations may do a better job of extrapolating to magnitudes and distances not well represented in the empirical data base since they have more physics behind them, they nonetheless suffer from the similar limitations as empirical models. Namely, since the high-frequency prediction is based on calibration to empirical data, how do we know that the randomness in the numerical simulation is appropriate for magnitude-distance pairs outside of the empirical data range?

6.7 SYNTHESIS OF PEER RESEARCH

PEER has taken a strong interest in ground motion simulation procedures because of their ability to generate synthetic time histories for situations that are critical from an engineering standpoint, but for which available recordings are sparse. One such situation is near-fault ground motions from large-magnitude earthquakes. This topic was addressed in Phases I and II of the PEER Lifelines Program, with the objective being to test the ability of three simulation procedures to reproduce key features of near-fault ground motions (PIs: Graves/Somerville, Silva, and Zeng/Anderson). In the Phase I work, a forward blind prediction of near-fault effects for a hypothetical earthquake produced very different results. The Phase II research explored the reasons for these differences, and validated the procedures against data from five earthquakes, as discussed in Section 6.4. This work is continuing with validation exercises utilizing data from the 1999 Kocaeli, Turkey, and Chi Chi, Taiwan, earthquakes.

Despite the recent progress toward developing well-validated simulation procedures, several critical tasks still need to be undertaken. These include

1. A PEER panel should objectively identify a standard set of validation recordings as adequate to assess the modeling bias and variability. The final validation results of each procedure must be based on this standard set of recordings.
2. Validations based on intensity measures other than the spectral accelerations need to be conducted, with particular emphasis on intensity measures that better represent the damaging features of ground motion time histories.
3. A comprehensive documentation of each procedure's formulation and input parameters is required. To properly assess and compare the total prediction variability of each procedure, all of the model parameters need to be identified as either fixed (generic) or free (event-specific or site-specific) parameters. Documentation should also include descriptions of how the fixed parameter values are determined and how the free parameters are to be varied for future earthquakes.
4. Reviews of simulated motions by a PEER panel are required before PEER formally adopts these simulated motions for use in research.
5. PEER user feedback regarding the strengths and limitations of the simulated motions needs to be solicited and used to guide future improvements.

7 TIME HISTORY SELECTION

Performance-based earthquake engineering (PBEE) is based on the probabilistic specification of strong ground motions. In PBEE, each performance objective is associated with a specified annual probability of exceedance, with increasingly undesirable performance characteristics caused by increasing levels of strong ground motion having decreasing annual probability of exceedance. A probabilistic seismic hazard analysis (PSHA) takes into account the ground motions from the full range of earthquake magnitudes that can occur on each fault or source zone that can affect the site. The PSHA produces response spectral ordinates (or other intensity measures) for each of the annual probabilities that are specified for performance-based design. In PBEE, the ground motions may need to be specified not only as intensity measures such as response spectra, but also by suites of strong motion time histories for input into time-domain nonlinear analyses of structures. The focus of this chapter is on procedures for developing these suites of time histories.

7.1 DE-AGGREGATION OF SEISMIC HAZARD

A constant hazard response spectrum derived from PSHA represents the aggregated contribution of a range of earthquake magnitudes occurring at various rates on each of several discrete faults or seismic source zones located at various distances from the site, and includes the effect of random variability in the ground motions for a given magnitude and distance. The spectrum applies for a given annual probability of exceedance, or hazard level. The same could be said for other intensity measures, but for convenience, the discussion that follows will focus on spectral acceleration. In order to provide ground motion time histories that represent the constant hazard spectrum, we must choose one or more discrete combinations of magnitude, distance, ε, and possibly other parameters, to represent the probabilistic ground motion. The parameter ε is defined as the number of standard deviations above or below the median ground motion level for that magnitude and distance that is required to match the probabilistic spectrum. The magnitude, distance, and ε values are estimated through de-aggregation of the probabilistic seismic hazard (Bazzurro and Cornell, 1999b; Chapman, 1995; Cramer and Peterson, 1996; Harmsen et al., 1999; McGuire, 1995).

The de-aggregation can be displayed by histograms in a variety of ways. One method is to use magnitude and distance on the horizontal axes, and show the contributions of different ε values on the vertical axis (Figure 7.1). Another method is to show the source location on a map with relative contribution indicated on the vertical axis (Figure 7.2). This method allows the contribution of individual faults to the hazard to be readily identified, and shading of the relative contribution bars indicates the magnitude.

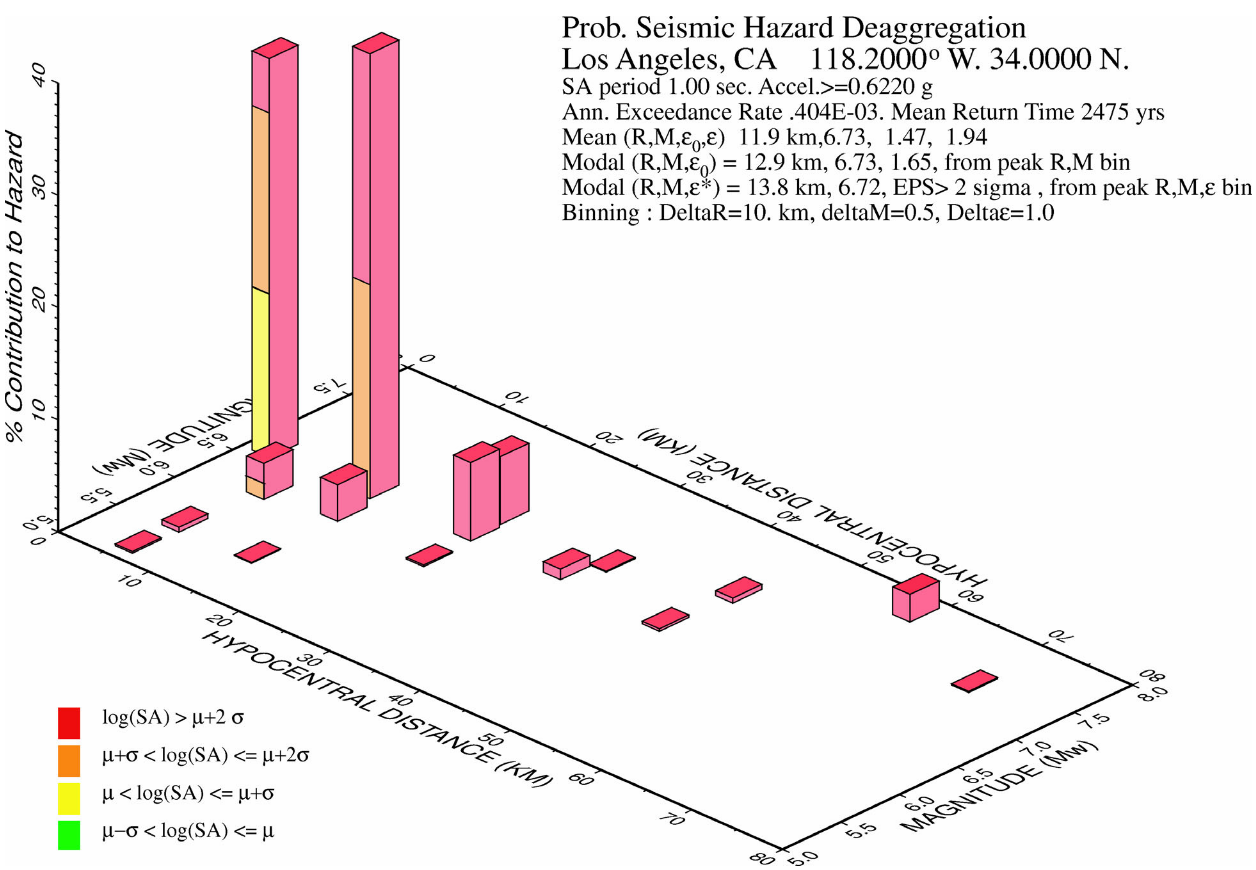

Figure 7.1. De-aggregation of the seismic hazard in Los Angeles using magnitude and distance on the horizontal axes and the probability level of ground motions relative to the median on the vertical axis. Source: U.S. Geological Survey.

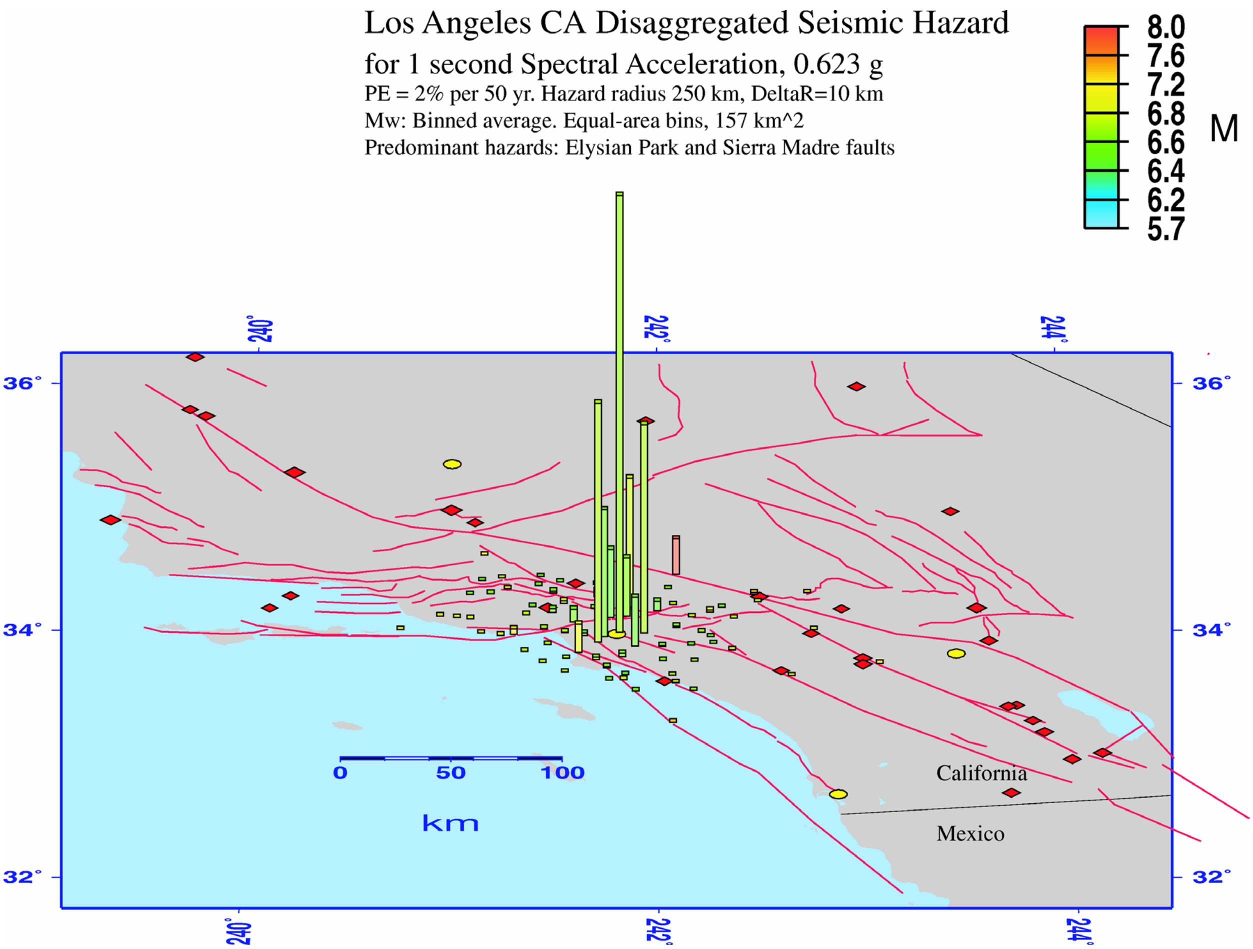

Figure 7.2. De-aggregation of the seismic hazard in Los Angeles in map view using magnitude on the vertical axis. U.S. Geological Survey.

It is now possible for seismic hazard calculations for near fault sites in California to include the effect of rupture-directivity on the spectral acceleration hazard (Abrahamson, 2000), using the model of Somerville et al. (1997a). In this model, the amplitude of the ground motion, controlled by the rupture-directivity parameter, depends not only on the closest distance to the fault, but also on where the rupture begins and terminates. In addition to randomizing the location of the fault rupture, the location of the initiation of rupture (the hypocenter) is randomized in the PSHA. The de-aggregation of the hazard can be displayed by the magnitude and the directivity parameter on the horizontal axes (Figure 7.3). These parameters, together with the de-aggregated distance (which is the closest distance to the fault for near fault sites), can be used to select time histories containing the appropriate degree of rupture directivity. It is found that even for relatively high annual probabilities of exceedance (1/475), the hazard near very active faults is dominated by strong forward rupture-directivity effects (Abrahamson, 2000). Guidelines for selecting time histories having forward-directivity effects are described in the following section.

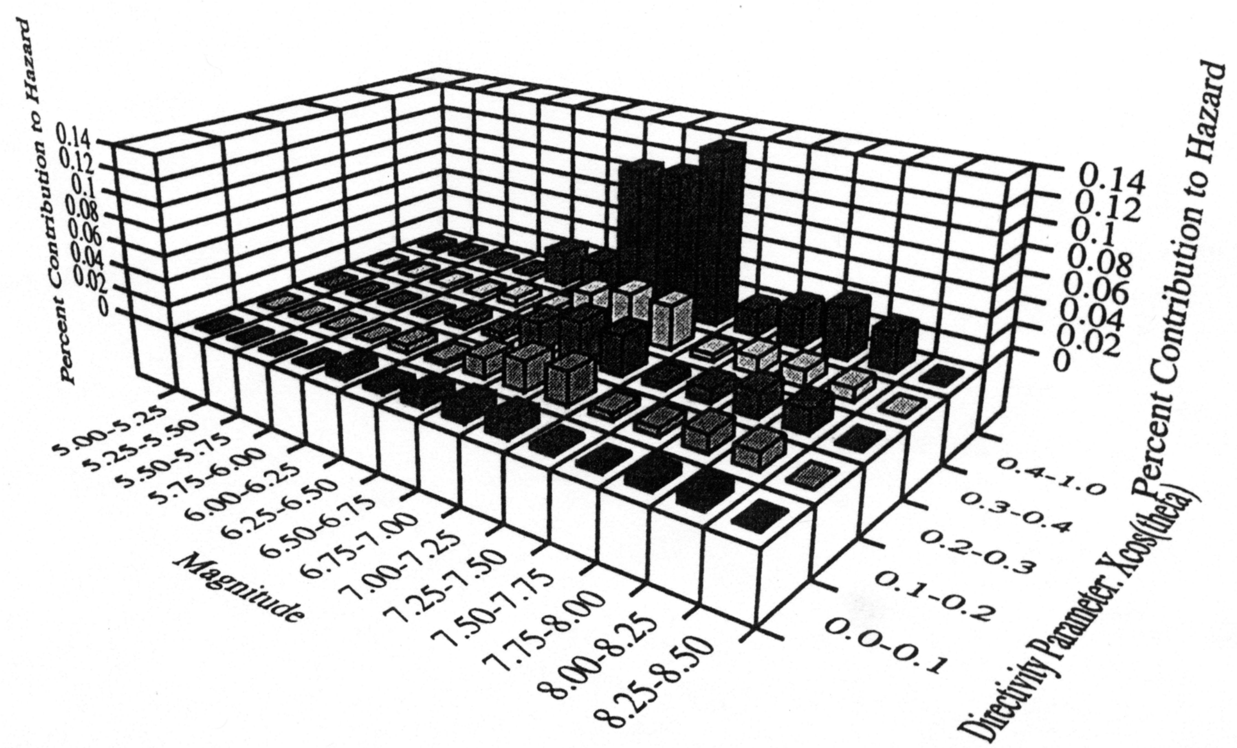

Figure 7.3. De-aggregation of the seismic hazard in San Francisco using magnitude and directivity parameter on the horizontal axes. Source: Abrahamson, 2000.

7.2 SELECTION OF GROUND MOTION TIME HISTORIES

The ground motion time histories that are used to represent an intensity measure corresponding to a particular hazard level (or return period) should reflect the magnitude, distance, site condition, and other parameters that control the ground motion characteristics. These parameters are obtained by de-aggregating the hazard for that intensity measure.

Selection of records having appropriate magnitudes is important because magnitude strongly influences frequency content and duration of ground motion. It is desirable to use earthquake magnitudes within 0.25 magnitude units of the target magnitude. This represents a difference of a factor of 2.4 in seismic moment, corresponding to differences of a factor of 1.33 in fault length, fault width and fault displacement.

Selection of records having appropriate distances is important especially for near-fault sites, because the characteristics of near-fault ground motions differ from those of other ground motions. In selecting time histories for near-fault sites, it is important to account for rupture-directivity and/or fling-step effects. As described in Section 4.1.1, fling-step displacements occur over a discrete time interval of several seconds and are distinct from the dynamic displacement referred to as the "rupture-directivity pulse" (see Figures 4.3 and 4.4). For seismic design, it is preferable to estimate the static and dynamic components of the ground displacement separately, and then combine them because the combination of static and dynamic displacements in a given recording may not be appropriate to the conditions at the site. Current empirical procedures for predicting ground motions only address the dynamic components and do not address the static displacement field. Separate models for calculating the static displacement component need to be developed. Ground motion time histories calculated by simulation methods (see Chapter 6) can include both the static and dynamic displacements.

It is commonly assumed that near-fault ground motion time histories close to large earthquakes should have a long duration. This is true only for backward directivity, which produces long, low-amplitude ground motions. Forward directivity causes nearly all of the seismic radiation from the fault to arrive in a single brief pulse of motion, unless the earthquake consists of multiple discrete rupture events. Combining several near-fault records containing brief pulses to make up for the short duration that is characteristic of forward rupture-directivity effects is not appropriate unless the earthquake scenario involves the rupture of multiple discrete faults.

Ground motions recorded in basins may have long trains of locally generated surface waves, with periods of one second and longer, following the direct shear wave arrivals. The velocity time histories of such records have long significant (Husid) durations, although the acceleration time histories may have normal significant durations. Spectral accelerations at intermediate to long periods may also be affected by basin response. Factors affecting basin response are described in Section 5.4. Time histories selected to represent the ground motions in basins should contain these characteristics. Current methods for developing design response spectra do not usually include consideration of the difference between sites situated inside and outside basins. Consequently, the basin site recordings that are selected may have systematically larger values of some intensity measures (e.g., duration and intermediate to long-period spectral shapes) than recordings from non-basin sites. In each case, it may be preferable to allow the response spectra of the time histories to deviate from the design spectrum at the longer periods if the design response spectrum does not consider the presence or absence of basin effects.

7.3 SCALING OF TIME HISTORIES

7.3.1 General Considerations

Unlike design response spectra, which are usually smooth, the response spectra of recorded ground motion time histories have peaks and troughs. The linear response of a structure can often be obtained using only a single time history to represent the seismic hazard. However, the time history should be spectrally modified (see following discussion) so that its response spectrum matches the design response spectrum.

The nonlinear response of structures is strongly dependent on the phasing of the input ground motion and on the detailed shape of its spectrum. Accordingly, it is not generally possible to obtain the nonlinear response of a structure using a single time history that has been matched to the target spectrum at a single period. Instead, it is necessary to use a suite of time histories having phasing and spectral shapes that are appropriate for the characteristics of the earthquake source, wave propagation path, and site conditions that control the design spectrum. The purpose of using a suite of time histories is to provide a statistical sample of the response of the structure to this variability in phasing and spectral shape. The median estimate of the response should be unbiased, and the dispersion, which is inversely proportional to the square root of the number of time histories used, should be acceptably low (Shome et al., 1998).

Building codes prescribe the use of three or seven time histories. For many applications, three time histories are too few to provide an adequate statistical sample. Consequently, if only three time histories are used, it may be appropriate to spectrally match the time histories to the smooth design spectrum, removing their peaks and troughs, so that the results of the structural analyses are not unduly controlled by the particular time histories that are chosen.

It is preferable to use a large number of time histories without modifying their response spectral shapes, in order to sample the response of the structure to ground motions having different phasing and response spectral shape. The time histories are scaled by a constant factor that makes their response spectrum match the design spectrum at a single period (e.g. the period of the fundamental mode of the structure) or over a period range of interest for the structure. This simple uniform scaling procedure preserves the peaks and troughs in the response spectra of the recorded time histories, allowing the structural response analyses to sample a range of different response spectral shapes. Shome et al. (1998) show that seven simply scaled time histories may provide an acceptably low dispersion in the estimated response of the structure.

The spectral matching of time histories to a design spectrum can be done either in the frequency domain or in the time domain. Frequency-domain methods have the disadvantage of adding harmonic components throughout the record, so it is important to use the phase spectrum to control the phasing of the ground motion (Silva and Lee, 1987). Time-domain methods have the advantage of allowing the addition of wave packets of various periods having discrete durations. These wave packets are added at times where there is significant amplitude in the ground motions of the same period. This approach has been implemented by Abrahamson (1993). An example of the spectral matching process is shown in Figure 7.4. The spectrum of the unmodified time history is shown by the dashed line; the target design spectrum is shown by the solid line, and the matched spectrum after filtering, baseline correction and scaling to match the target, which is shown by the dotted line, overlays the target spectrum. The initial and matched waveforms are shown in the bottom part of the figure.

7.3.2 Scaling of Near-Fault Time Histories

In selecting time histories to represent near-fault rupture-directivity effects, it is important to select time histories that contain the near-fault pulse. This is true even if the time history is to be spectrally matched to a design spectrum, because the spectral matching process cannot build a rupture-directivity pulse into a record where none is present to begin with.

Ordinarily, the two horizontal components are treated as being interchangeable because they have similar characteristics. However, the near-fault pulse is polarized in the strike-normal direction, causing its response spectrum to be stronger than the strike-parallel component at intermediate periods. Different design spectra for strike-normal and strike-parallel components are required to properly represent near-fault ground motions. If different design spectra are specified, then time histories oriented in the strike-normal and strike-parallel directions should be scaled separately to their respective response spectra. If only a single design response spectrum is prescribed, but it is desired to correctly represent the orientation of near-fault ground motions, then a scale factor should be found which scales the average of the two horizontal time history components to the design spectrum, and then be applied individually to the strike-normal and strike-parallel time histories, thus preserving the relationship between these two components.

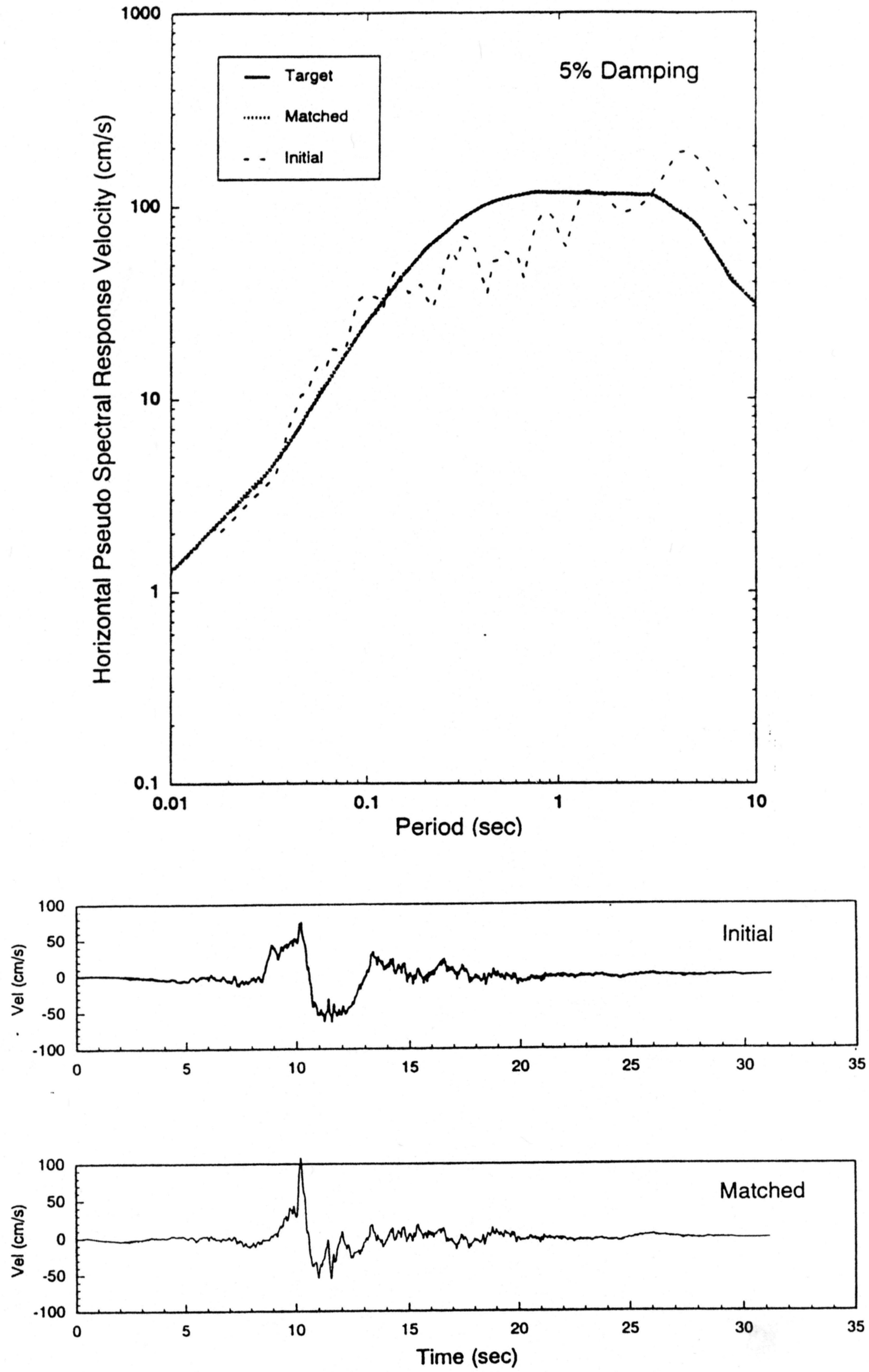

Figure 7.4. Spectral matching of a time history to a design response spectrum. The top panel shows that the response spectrum of the matched time history overlies the target, and the bottom panel compares the velocity time histories before and after spectral matching.

7.3.3 Spectral Modification of Time Histories for Site Conditions

Ideally, time histories should be selected from seismograph sites having ground conditions similar to those at the site under consideration. However, in some instances, it may be desirable to modify the spectral content of a recorded time history to match a site condition different from that at the accelerograph site. For a simple rock/soil parameterization of site condition, an approximate way of doing this is to take the ratio of soil to rock response spectra for the appropriate magnitude and distance using an empirical ground motion attenuation relation, multiply the response spectrum of the recording by this ratio to generate a response spectral shape that is appropriate for the new site condition, and then match the recorded time history to this modified response spectrum. This procedure is broadband, and retains the peaks and troughs in the original response spectrum.

Although the procedure described above produces a modified time history that is spectrum compatible, it may not necessarily include phase characteristics that vary across site categories. For example, it is not possible to generate a time history containing a long train of basin-generated surface waves from a strong motion recording on a hard rock site, even though its response spectrum has been made to be compatible with that of the basin record. Also, it may not be possible to convert near-fault records on rock to soil site conditions using current empirical ground motion models. The ratio of soil to rock ground motions in some of these models is less than unity at short periods and greater than unity at intermediate and long periods. Since the peak acceleration in these records is controlled by the intermediate periods contained in the directivity pulse, not by the short periods, it may not be feasible to increase the intermediate and long periods and reduce the short periods as required to modify a rock recording to soil site conditions. Alternative parameterizations of near-fault motions (as described in Section 4.1.2) may be required in such cases.

7.4 USE OF RECORDED AND SYNTHETIC TIME HISTORIES

A large number of ground motion time histories have been recorded during the past three decades. Many of these time histories are available on the PEER and COSMOS websites. However, it may still be difficult to satisfactorily fill certain magnitude-distance bins with sets of recorded time histories. This is especially true for large magnitudes at close distances.

Consequently, it may be desirable in some situations to use simulated ground motion time histories to supplement recordings for use in these magnitude-distance bins. Ground motion simulation procedures are discussed in Chapter 6.

Most engineers feel more comfortable using recorded time histories than simulated time histories because recorded time histories are actual realizations, and because they do not feel familiar enough with the methods used to generate simulated time histories to have confidence in their reliability. It is possible to objectively assess the adequacy of simulated time histories by comparing simulated with recorded ground motions (i.e., see Section 6.4). However, as noted in Section 6.6, such calibrations are not possible where empirical data are sparse. Therefore, the conditions for which simulations are most attractive (e.g., sparsely populated magnitude-distance ranges) are unfortunately the same conditions that are difficult to calibrate. This limitation is especially significant for low-period ground motions (i.e., $T < \sim 1$ s).

A potential advantage of simulated time histories for site-specific analyses is that they can be made much more site-specific than recorded ground motions, which are from a different earthquake and represent different wave propagation and site conditions than those that pertain to the site. Simulated time histories can potentially contain not only the exact magnitude but also other source parameters, not only the exact distance but also other source-site geometry and crustal structure characteristics, and not only the same site category but also the precise site conditions. However, some of these parameters cannot be known *a priori*, and therefore proper treatment of parametric and model variability is vital when using simulations to predict ground motions (as discussed in Section 6.5).

Simulation procedures provide a means of generating suites of ground motions whose magnitude, distance, site condition and other parameters can be exactly prescribed. Such suites of time histories are useful for assessing the sensitivity of structural response to these parameters. Although bins of recorded time histories that occupy ranges of these parameters can be assembled, such suites of time histories cannot represent exact values of these parameters. Moreover, the influences of source, path, and site conditions in these recorded time histories are difficult to separate, whereas the controlled nature of simulated time histories makes this separation straightforward.

7.5 SETS OF GROUND MOTION TIME HISTORIES

7.5.1 PEER Time Histories

The PEER website **(http://peer.berkeley.edu)** contains sets of near-fault ground motion recordings and long-duration ground motion recordings on both soil and rock sites. Each set contains five recordings. The recordings are all for large earthquakes. They have not been scaled or spectrally modified in any way and do not represent a specified seismic hazard level. This website also has a much larger database of time histories for active tectonic regions.

7.5.2 FEMA/SAC Time Histories

The FEMA/SAC Steel Program website contains sets of ground motions used in topical investigations, case studies, and trial applications. The ground motions are described in Somerville et al. (1997b). The ground motions were developed for three locations of the United States (Boston, Seattle, and Los Angeles) corresponding to seismic zones 2, 3 and 4 respectively. Suites of ten time histories are available for each of two probabilities of occurrence (2% in 50 years and 10% in 50 years) in each of these three locations for firm soil conditions. Time histories are also provided for 50% in 50 years for Los Angeles. In all cases, the time histories were scaled so that their response spectra matched the spectra in the 1994 NEHRP Provisions mainly in the period range of one to four seconds, modified for firm soil conditions. Time histories for soft soil profiles are also provided for 10% in 50 years in all three locations. Twenty near-fault time histories are also provided for seismic zone 4 conditions. In each of these data sets, simulated time histories were used to augment recorded time histories because not enough recorded time histories were available.

7.6 SYNTHESIS OF PEER RESEARCH

The PEER Center sponsored a workshop attended by seismologists and engineers in which representative time histories were selected for various applications, as discussed in Section 7.5.1. The Lifelines Program has sponsored several efforts to develop suites of synthetic time histories for applications related to ground failure studies (Phase II, PIs: Somerville and Silva). Beyond those efforts, the center has sponsored relatively little research on the development of time history selection procedures, such as those described in this chapter.

8 CONCLUSIONS

The preceding chapters have presented contemporary procedures for evaluating ground motion hazard for utilization within the performance-based design framework. The objective of ground motion research sponsored by the PEER Center has been to provide data, models, and methods needed to reduce the earthquake vulnerability of the civil infrastructure in the western U.S. and other seismically active regions. A number of important studies have been completed which, when combined with ongoing/future studies, are redefining the process by which ground motions are evaluated for performance-based design applications.

The research performed within the PEER Center can be broadly classified into three categories: data, models, and methods.

- Research projects classified as **data** produce the scientific or engineering data sets that are necessary for subsequent studies. The data can be either empirical observations or synthetic data generated as part of numerical or experimental studies. In general, data are not the useable result, but rather are the input for the development of models or methods as discussed below. An example of a data project is the documentation of site conditions at strong motion stations.
- Research projects classified as **models** produce simplified descriptions of data. Models can be either parametric descriptions of data (such as regression equations) or maps. An example of a model project is deriving an algorithm for the amount of amplification of the ground motion expected for a given site condition.
- Research projects classified as **methods** develop new procedures or evaluate existing ones for using models or data to compute a desired parameter. An example method project is the evaluation of the relative accuracy of different procedures for predicting site response.

As noted in Chapter 1, PEER research on ground motions has addressed the broad topics of travel path and site response effects. In the following, we briefly synthesize the major contributions of PEER research in these two important areas within the framework of data, models, and methods described above. We first discuss PEER accomplishments based on completed and ongoing research, and then discuss future research directions.

8.1 PEER ACCOMPLISHMENTS

8.1.1 Path Effects

Studies of path effects on earthquake ground motions are no better than the databases from which they are derived or against which they are calibrated. The PEER Lifelines Program has taken on the costly, yet vital task of developing critical databases for ground motion studies, and web-enabling these databases for the earthquake engineering community. There have been several principal thrusts to these data compilation efforts:

- Strong motion data: PEER researchers have web-enabled a comprehensive, uniformly processed strong motion data set for active regions (available from **http://peer.berkeley.edu),** and have recently supplemented this data set with uniformly processed motions from the 1999 Turkey and Taiwan earthquakes.
- Geologic/geotechnical data: PEER researchers have performed field studies to develop high-quality documentation of geotechnical conditions at critical strong motion recording sites in California and Turkey, and are developing classifications of ground conditions at strong motion sites based on uniform criteria.

Utilizing these data resources, PEER researchers have developed engineering models for important path effects such as forward rupture-directivity effects on critical intensity measures. Moreover, as described below, work is under way on the development of a new generation of attenuation relations incorporating the data from the 1999 earthquakes. The results of this PEER research will likely become the new industry standard for evaluations of ground motion attenuation in active regions.

Available data resources are inadequate to constrain models for a number of important problems such as ground motions from very large-magnitude earthquakes, near-fault ground motions, and basin effects. Accordingly, PEER has invested in fundamental research necessary to develop seismological simulation methods that can be used to supplement empirical data sets with synthetic data sets. Work within PEER has validated a number of leading simulation methods against each other, and has begun the process of calibrating these codes against uniform data sets from several earthquakes. Work of this type is required to enable engineers and seismologists to have confidence in these methods so that they can serve as a viable tool to assist in engineering model development.

8.1.2 Site Response Effects

The data compilation work discussed above for path effects is equally vital to studies of site response. This work was discussed in the previous section.

As discussed in Chapter 5, PEER research has developed several state-of-the-art models for characterizing site response effects. These models, derived both from field recordings (Section 5.2.3c) and ground response analysis results (Section 5.3.3a), provide a practical means by which ground conditions represented by a site category can be readily incorporated into ground motion hazard analyses. Additional models based on basin response parameters are in development. The intent of these efforts is to minimize the bias and uncertainty in ground motion estimates from hazard analyses that do not incorporate detailed site response analyses (which, in turn, require the acquisition of costly geotechnical subsurface data).

PEER researchers have also been involved in the development of next-generation methods for site response analyses. These studies fall into two general categories, one contrasting the ability of different models to predict observed ground motions at soil sites, the other developing new methods for site response analysis. The first of these method studies has identified the general site conditions where site response analyses are found to produce a demonstrable improvement in ground motion predictions relative to attenuation relationships. The second class of method studies involves the calibration of both one-dimensional ground response analysis procedures and basin response codes against appropriate field recordings. These studies are in progress.

The method studies and model development discussed above are providing engineers with several options for evaluating site response for hazard calculations. The least amount of effort involves the use of attenuation relations for broadly defined site categories (e.g., rock or soil). For a small additional effort in which the near-surface ground conditions are categorized, the attenuation estimate can be adjusted using amplification factors from simple models. Finally, for a (presumably) more precise characterization of site response, basin and/or ground response codes can be implemented, but of course at the expense of field characterization of site conditions. When site response evaluation for practical application is viewed within this framework, the influence of PEER research is apparent. With regard to the first and second options, PEER research is helping to define the attenuation relationships for critical ground motion parameters that incorporate the important data sets from Turkey and Taiwan, and has developed models for ground motion amplification as a function of surface geology, 30-m shear wave velocity, and geotechnical classifications. PEER research is also developing guidelines on when use of the relatively costly third option is worthwhile, and is developing and calibrating the methods by which such analyses should be performed.

8.2 FUTURE RESEARCH DIRECTIONS

The PEER Center has formulated a research plan for coming years that builds on the present momentum with the objective of developing rational, calibrated procedures for estimating ground motion intensity measures. It is not our intention in this section to provide a complete inventory of future PEER ground motion projects. Rather, we discuss general research directions for the PEER Core and Lifelines programs.

The PEER Core Program has three principal objectives in ground motion research. The first is to identify existing or define new intensity measures (*IM*s) that provide the best possible correlation to damage measures for structures. These critical *IM*s are being defined in fundamental research characterizing the nonlinear dynamic response of geotechnical and structural systems in Thrust Areas 2 and 3. Once these critical *IM*s are defined, the second objective is to develop procedures for estimating these parameters with due consideration of near-fault and site effects. The third objective is to develop vector hazard capabilities, as the nonlinear response of many structures is described by multiple *IM*s. These later two objectives will be pursued in Thrust Area 2.

The PEER Lifelines Program is currently engaged in the first stage of a three-year program of research on earthquake ground motions. The following reviews some of the general topic areas being addressed:

- Seismological basin models: Projects are validating a series of basin response analysis methods against each other, and then calibrating them against strong motion data sets. The calibrated analysis methods will then be used to help develop engineering models for basin response.
- Validation of ground motions from very large earthquakes: Objective of projects is to develop data that can be used to constrain attenuation and directivity models for large

earthquakes, for which empirical data are scarce. Initial work is incorporating Turkey and Taiwan strong motion data into existing relations. Additional potential "data" sources that are being investigated as possible means of constraining the attenuation relations include the dating of precarious rocks near active faults, and simulation exercises. Physical models will be investigated as a means to evaluate rupture-directivity effects.

- Dynamic and differential displacements: Projects will develop attenuation relations for velocity, displacement, and differential displacement.
- Fault studies: Projects will seek to develop improved recurrence models through trenching studies and earthquake cataloguing exercises. Additional projects will characterize fault rupture displacement hazards.
- Characterization of strong motion station sites: Field studies to characterize geotechnical properties at strong motion stations are being undertaken using drilling and suspension logging, as well as SASW techniques. Additional research will perform laboratory testing to evaluate nonlinear soil properties.
- Utilization of vertical array data: Data from vertical arrays will be used to calibrate geotechnical site response methods, and to gain insight into wave propagation characteristics and nonlinear soil properties across the arrays.
- Nonlinear ground response analysis methods: Studies will evaluate the effectiveness of different ground response analysis methods relative to predictions from simple models (e.g., attenuation relations or attenuation predictions adjusted by amplification factors). Objectives are to establish guidelines for when detailed response analyses are justified in terms of their ability to reduce prediction dispersion, and to develop guidelines on the use of equivalent linear vs. nonlinear response analyses.
- Other studies: Studies are planned to develop guidelines for the analysis of vertical ground motions; to evaluate ground motion variations across cut/fill sites; and to evaluate amplification factors for shallow, stiff soils sites relative to weathered rock sites.

In short, the PEER Lifelines Program is developing data, models, and methods that are needed to meet the ground motion characterization needs for contemporary performance-based earthquake-risk management for highway and electric power systems. This work is highly synergistic with planned work in the PEER Core Program, which will define the ground motion characterization needs for the next-generation of analysis and design methodologies for other classes of structures such as buildings. The solid foundation of data and experience gained through the Lifelines Program will streamline the model development process for new intensity measures defined in the Core Program. All will benefit from close collaboration and coordination between these two equally vital research programs.

REFERENCES

Abrahamson, N.A. (1993). "Spatial variation of multiple support inputs," *Proc. First U.S. Symp. Seism. Eval. Retrofit Steel Bridges*, U.C. Berkeley, October 18.

Abrahamson, N.A. (2000). "Effects of rupture directivity on probabilistic seismic hazard analysis," *Proc. 6th Int. Conf. on Seismic Zonation*, *Palm Springs*.

Abrahamson, N.A., and Becker, A. (1999). *Proceedings of the MCEER Workshop on Ground Motion Methodologies for the Eastern United States*. MCEER Technical Report MCEER-99-0016.

Abrahamson, N.A., and Shedlock, K.M. (1997). "Overview (of modern attenuation relationships)," *Seism. Res. Letters*, 68(1), 9-23.

Abrahamson, N.A., and Silva, W.J. (1996). *Empirical ground motion models*, Report to Brookhaven National Laboratory.

Abrahamson, N.A., and Silva, W.J. (1997). "Empirical response spectral attenuation relations for shallow crustal earthquakes," *Seism. Res. Letters*, 68(1), 94-127.

Abrahamson, N.A., and Somerville, P.G. (1996). "Effects of the hanging wall and footwall on ground motions recorded during the Northridge earthquake," *Bull. Seism. Soc. Am.*, 86, S93-S99.

Abrahamson, N.A., and Youngs, R.R. (1992). "A stable algorithm for regression analyses using the random effects model," *Bull. Seism. Soc. Am.*, 82, 505-510.

Abrahamson, N.A., Somerville, P.G., and Cornell, C.A. (1990). "Uncertainty in numerical strong motion predictions," *Proc. 4th U.S. National Conference on Earthquake Engineering,* 1, 407-416.

Aki, K. (1968). "Seismic displacement near a fault," *J. Geophy. Res*., 73, 5359-5376.

Aki, K., and Richards, P.G. (1980). *Quantitative seismology*, Vol. 1, W.H. Freeman, San Francisco, CA.

Aki, K., Martin, G. R., Chin, B. H., Abrahamson, N.A., Cornell, A.C., and Mahdyiar, M. (1995). *Final task report on the characteristics of earthquake ground motions for seismic design; Task H-7, probabilistic seismic hazard analysis and development of earthquake scenario time histories for southern California sites*, Southern California Earthquake Center, University of Southern California, Los Angeles, CA.

Alavi, B., and Krawinkler, H. (2000) "Consideration of near-fault ground motion effects in seismic design," *Proc. 12th World Conference on Earthquake Engineering*, New Zealand, 8 pp.

Anderson, J.G. (1997). "Nonparametric description of peak acceleration above a subduction thrust," *Seism. Res. Letters*, 68(1), 86-93.

Anderson, J.G. (2000). “Expected shape of regressions for ground motion parameters on rock,” *Bull. Seism. Soc. Am.*, 90, S43-S52.

Andrews, D.J. (1986). “Objective determination of source parameters and similarity of earthquakes of different size,” in *Earthquake Source Mechanics*, S. Das, J. Boatwright, and C.H. Scholz (eds.), American Geophysical Union, Washington D.C., 259-268.

Aoi, S., and Fujiwara, H. (1999). “3D finite difference method using discontinuous grids,” *Bull. Seism. Soc. Am.*, 89, 918-930.

Arias, A. (1970). “A measure of earthquake intensity,” in *Seismic Design for Nuclear Power Plants*, R.J. Hansen, ed., MIT Press, Cambridge, MA, 438-483.

Ashford, S.A., and Sitar, N. (1997). “Analysis of topographic amplification of inclined shear waves in a steep coastal bluff,” *Bull. Seism. Soc. Am.*, 87, 692-700.

Ashford, S.A., Sitar, N., Lysmer, J., and Deng, N. (1997). “Topographic Effects on the Seismic Response of Steep Slopes,” *Bull. Seism. Soc. Am.*, 87, 701-709.

Atkinson, G.M. (1984). “Attenuation of strong ground motion in Canada from a random vibration approach,” *Bull. Seism. Soc. Am.,* 74, 2629-2653.

Atkinson, G.M. (1995). “Empirical ground motion relations for earthquakes in the Cascadia region,” *Canadian J. Civil Engrg.*, 24, 64-77.

Atkinson, G.M., and Boore, D.M. (1995). “New ground motion relations for eastern North America,” *Bull. Seism. Soc. Am.*, 85, 17-30.

Atkinson, G.M., and Boore, D.M. (1997a). “Stochastic point source modeling of ground motions in the Cascadia region,” *Seism. Res. Letters*, 68(1), 74-85.

Atkinson, G.M., and Boore, D.M. (1997b). “Some comparisons between recent ground motion relations,” *Seism. Res. Letters*, 68(1), 24-40.

Atkinson, G.M., and Silva, W.J. (1997). “An empirical study of earthquake source spectra for California earthquakes,” *Bull. Seism. Soc. Am.* 87, 97-113.

Bao, H., Bielak, J., Ghattas, O., Kallivokas, L. F., O'Hallaron, D. R., Shewchuk, J. R., and Xu, J. (1998). “Large scale simulation of elastic wave propagation in heterogeneous media on parallel computers,” *Comput. Meth. Appl. Mech. Eng.*, 152, 85-102.

Bard, P-Y. (1995). “Effects of surface geology on ground motion: recent results and remaining issues,” *Proc. 10th European Conference on Earthquake Engineering*, Duma (ed.), Rotterdam, 305-323.

Bazzuro, P., and Cornell, A.C. (1999a*). Efficient PSHA for nonlinear soil sites with uncertain properties,* Report, Civil Engineering Dept., Stanford University (in progress).

Bazzuro, P., and Cornell, A.C. (1999b). “Disaggregation of seismic hazard,” *Bull. Seism. Soc. Am.,* 89, 501-520.

Beresnev, I.A., Wen, K.L. and Yeh Y.T. (1995) “Seismological evidence for nonlinear elastic ground behavior during large earthquakes,” *Soil Dynamics and Earthquake Engineering*, 14 (2), 103-114.

Bernard, P., and Madariaga, R. (1984). “A new asymptotic method for the modeling of near-field accelerograms,” *Bull. Seism. Soc. Am.*, 74, 539 – 557.

Biscontin, G., Pestana, J.M., Nadim, F., and Anderson, K. (2001). “Seismic response of normally consolidated cohesive soils in gently inclined submerged slopes,” *Proc. 4th Int. Conf. Recent Advances in Geotech. Eqk. Engrg. Soil Dyn.*, Paper 5.32.

Boatwright, J., Seekins, L.C., and Mueller, C.S. (1991). “Ground motion amplification in the Marina,” *Bull. Seism. Soc. Am.*, 81, 1980-1997.

Boatwright, J., Thywissen, K., and Seekins, L. (2001). “Correlation of ground motion and intensity for the January 17, 1994 Northridge, California earthquake,” *Bull. Seism. Soc. Am.*, 91, 739-752.

Bolt, B.A. (1969). “Duration of strong motion,” *Proc. 4th World Conf. Earthquake Engrg.*, Santiago, Chile, 1304-1315.

Bolt, B.A. (1993). *Earthquakes,* W.H. Freeman, NY.

Bommer, J.J., and Martinez-Pereira, A. (1999). “The effective duration of earthquake strong motion,” *J. Earthquake Engrg*., 3(2), 127-172.

Bonilla, L.F., Lavallee, D., and Archuletta, R.J. (1997). “Site amplification in the San Fernando Valley, California,” *Bull. Seism. Soc. Am*., 87, 710-730.

Bonilla, M. G. (1970) “Surface faulting and related effects,” in Earthquake Engineering, Weigel, R.L., ed., New Jersey, Prentice-Hall, 47-74.

Boore, D.M. (1983). “Stochastic simulation of high-frequency ground motions based on seismological models of the radiated spectra,” *Bull. Seism. Soc. Am.* 73, 1865-1894.

Boore, D.M. (1996). *SMSIM— Fortran Programs for Simulating Ground Motions from earthquakes: Version 1.0,* Open File Report 96-80-A, U.S. Geological Survey.

Boore, D.M., Joyner, W.B., and Fumal, T.E. (1997). “Equations for estimating horizontal response spectra and peak acceleration from western North American earthquakes: A summary of recent work,” *Seism. Res. Letters*, 68(1), 128-153.

Borcherdt, R.D. (1970). “Effects of local geology on ground motion near San Francisco Bay,” *Bull. Seism. Soc. Am*., 60, 29-61.

Borcherdt, R.D. (1994). “Estimates of site-dependent response spectra for design (methodology and justification),” *Earthquake Spectra*, 10(4), 617-653.

Borcherdt, R.D. (1996). “Preliminary amplification estimates inferred from strong ground motion recordings of the Northridge earthquake of January 17, 1994,” *Proc. Int. Workshop on Site Response Subjected to Strong Ground Motion*, Vol. 1, Port and Harbor Research Institute, Yokosuka, Japan.

Borcherdt, R.D. (2001-in review). “Empirical evidence for acceleration-dependent amplification factors,” submitted to *Bull. Seism. Soc. Am*.

Borcherdt, R.D., and Gibbs, J.F. (1976). “Effects of local geological conditions in the San Francisco Bay region on ground motions and the intensities of the 1906 earthquake,” *Bull. Seism. Soc. Am*., 66, 467-500.

Borcherdt, R.D., and Glassmoyer, G. (1994). “Influences of local geology on strong and weak ground motions recorded in the San Francisco Bay region and their implications for site-specific building-code provisions,” *The Loma Prieta, California Earthquake of October 17, 198—-Strong Ground Motion,* U. S. Geological Survey Professional Paper 1551-A, A77-A108

Borja, R.I., and Wu, W.H. (1994). “Vibration of foundations on incompressible soils with no elastic region,” *J. Geotech. Engrg.*, ASCE, 120(9), 1570-1592.

Borja, R.I., Chao, H.Y., Montans, F.J. and Lin, C.H. (1999). "Nonlinear ground response at Lotung LSST site," *J. Geotech. & Geoenv. Engrg.*, ASCE, 125 (3), 187-197.

Bozorgnia, Y., Campbell, K.W., Niazi, M. (1999). “Vertical ground motion: Characteristics, relationships with horizontal component, and building code implications,” *Proc. SMIP99 Seminar on Utilization of Strong Motion Data*, California Strong Motion Instrumentation Program, Sacramento, CA, 23-50.

Bray, J.D. (2001) “Developing mitigation measures for the hazards associated with earthquake surface fault rupture,” in *Seismic Fault-Induced Failures Workshop,* Japan Society for the Promotion of Science, University of Tokyo, Japan, pp. 55-79, January 11-12.

Bray, J.D., Rathje, E.M., Augello, A.J., and Merry, S.M. (1998). “Simplified seismic design procedure for geosynthetic-lined, solid-waste landfills,” *Geosynthetics International*, 5(1-2), 203-235.

Bray, J.D., Seed, R. B., Cluff, L.S. and Seed, H.B. (1994) “Earthquake fault rupture propagation through soil,” *J. Geotech. Engrg.*, ASCE, 120(3), 543-561.

Brillinger, D.R., and Priesler, H.K. (1984). “An exploratory analysis of the Joyner-Boore attenuation data,” *Bull. Seism. Soc. Am.*, 74, 1441-1450.

Brillinger, D.R., and Priesler, H.K. (1985). “Further analysis of the Joyner-Boore attenuation data,” *Bull. Seism. Soc. Am.*, 75, 611-614.

Brocher, T.M., et al. (1998). "San Francisco Bay area 3D velocity model, revision 1," USGS, Menlo Park, CA, unpublished manuscript.

Brune, J.N. (1970). "Tectonic stress and the spectra of seismic shear waves from earthquakes," *J. Geophys. Res.*, 75, 4997-5009.

Brune, J.N. (1971). "Correction," *J. Geophys. Res*., 76, 5002.

Building Seismic Safety Council, BSSC (1998). *NEHRP Recommended Provisions for Seismic Regulations for New Buildings and Other Structures, Part 1 — Provisions and Part 2 — Commentary*, Federal Emergency Management Agency, Washington D.C., February.

Bullen, K.E. (1965). *An introduction to the theory of seismology*, Cambridge Univ. Press, Cambridge, U.K.

Byerly, P., and DeNoyer, J. (1958) "Energy in earthquakes as computed from geodetic observations," in *Contributions in Geophysics: In Honor of Beno Gutenberg,* Pergamon Press, NY.

Campbell, K.W. (1981). "Near source attenuation of peak horizontal acceleration," *Bull. Seism. Soc. Am.*, 71, 2039-2070.

Campbell, K.W. (1982). "Near-source scaling characteristics of peak horizontal acceleration for moderate-to-large earthquakes," in *The Dynamic Characteristics of Faulting Inferred from Recordings of Strong Ground Motion*, Vol. I , Open-File Report 82-591,U.S. Geological Survey, Menlo Park, California, 120-184.

Campbell, K.W. (1997). "Empirical near-source attenuation relations for horizontal and vertical components of peak ground acceleration, peak ground velocity, and pseudo-absolute acceleration response spectra," *Seism. Res. Letters*, 68(1), 154-179.

Campbell, K.W. (2000). Erratum to Campbell, 1997, *Seism. Res. Letters*, 71(3), 352-354.

Campbell, K.W. (2001). Erratum to Campbell, 2000, *Seism. Res. Letters*, 72(4), p 474.

Carver, D., and Hartzell, S.H. (1996). "Earthquake site response in Santa Cruz, California," *Bull. Seism. Soc. Am.*, 86, 55-65.

Celebi, M. (1987). "Topographical and geological amplifications determined from strong-motion and aftershock records of the 3 March 1985 Chile earthquake," *Bull. Seism. Soc. Am.*, 77, 1147-1167.

Celebi, M. (1991). "Topographic and geological amplification: Case studies and engineering implications," *Structural Safety*, 10, 199-217.

Chang, C.-Y., Mok, C.M., Power, M.S., Tang, Y.K., Tang, H.T., and Stepp, J.C. (1990). "Equivalent linear versus nonlinear ground response analyses at Lotung seismic experiment site," *Proc. 4th U.S. National Conf. Eqk. Engrg.*, Vol. 1.

Chang, S.W. (1996). "Seismic response of deep stiff soil deposits," Ph.D. Dissertation, Univ. of California, Berkeley.

Chang, S.W., Bray, J.D., and Seed, R.B. (1996). "Engineering implications of ground motions from the Northridge earthquake," *Bull. Seism. Soc. Am.*, 86, S270-S288.

Chapman, M.C. (1995). "A probabilistic approach to ground motion selection for engineering design," *Bull. Seism. Soc. Am.,* 85, 937-942.

Chavez-Garcia, F.J., Sanchez, L.R., and Hatzfeld, D. (1996). "Topographic site effects and HVSR. A comparison between observations and theory, *Bull. Seism. Soc. Am.*, 86, 1559-1573.

Chopra, A.K. (2000). *Dynamics of structures*, 2nd Ed., Prentice Hall, Upper Saddle River, NJ.

Cornell, C.A. (1968). "Engineering seismic risk analysis," *Bull. Seism. Soc. Am.*, 58, 1583-1606.

Cramer, C.H., and Peterson, M.D. (1996). "Predominant seismic source distance and magnitude maps for Los Angeles, Orange, and Ventura Counties, California," *Bull. Seism. Soc. Am.,* 86, 1645-1649.

Crouse, C.B. (1991). "Ground-motion attenuation equations for earthquakes on the Cascadia subduction zone," *Earthquake Spectra*, 7(2), 201-236.

Darragh, R.B., and Idriss, I.M. (1997). "A tale of two sites: Gilroy #2 and Treasure Island – Site response using and equivalent linear technique," NEHRP Professional Fellowship Report, EERI, Oakland, CA.

Davis, L.L., and West, L.R. (1973). "Observed effects of topography on ground motion," *Bull. Seism. Soc. Am.*, 63, 283-298.

Davis, P.M., Rubenstein, J.L., Liu, K.H., Gao, S.S. and Knopoff, L. (2000). "Northridge earthquake damage caused by geologic focusing of seismic waves," *Science*, 289, 1746-1750.

Dickenson, S.E. (1994). "The dynamic response of soft and deep cohesive soils during the Loma Prieta earthquake of October 17, 1989," Ph.D. Dissertation, Univ. of California, Berkeley.

Dobry, R., Pierce, W.G., Dyvik, R., Thomas, G.E., and Ladd, R.S. (1985). *Pore pressure model for cyclic straining of sand,* Research Report, Civil Engineering Department, Rensselaer Polytechnic Institute, Troy, New York

Doroudian, M., and Vucetic, M. (1995). "A direct simple shear device for measuring small-strain behavior," *Geotech. Testing J.*, ASTM, 18(1), 69-85.

Earthquake Engineering Research Institute, EERI (1995). *Scenario for a magnitude 7.0 earthquake on the Hayward fault*, Chapter 6, September, 109 p.

Electrical Power Research Institute, EPRI (1993). "Guidelines for determining design basis ground motions. Volume 1: Method and guidelines for estimating earthquake ground motion in eastern North America," *Rpt. No. EPRI TR-102293*, Palo Alto, CA.

Electric Power Research Institute. (1995). "Proceedings of Workshop on Modeling Earthquake Ground Motion at Close Distances," *EPRI Report TR-104975*, Palo Alto, CA.

Elgamal, A.W., Zeghal, M., Tang, H.T., and Stepp, J.C. (1995). "Lotung downhole array. I: Evaluation of site dynamic properties," *J. Geotech. Engrg.*, ASCE, 121(4), 350-362.

Elgamal, A.-W., Zeghal, M., and Parra, E. (1996). "Liquefaction of reclaimed island in Kobe, Japan," *J. Geotech. Engrg.*, 122 (1), 39-49.

Ellsworth, W.L., Matthews, M.V., Nadeau, R.M., Nishenko, S.P., Reasenberg, P.A., Simpson, R.W. (1999). "A physically based earthquake recurrence model for estimation of long-term earthquake probabilities," *Proc. Workshop on Earthquake Recurrence*, Rome, Italy.

Field, E.H. (2000). "A modified ground motion attenuation relationship for southern California that accounts for detailed site classification and a basin depth effect," *Bull. Seism. Soc. Am.*, 90, S209-S221.

Field, E.H., and Jacob, K.H. (1995). "A comparison and test of various site-response estimation techniques, including three that are not reference-site dependent," *Bull. Seism. Soc. Am.*, 85, 1127-1143.

Field, E.H. et al. (2000). "Accounting for site effects in probabilistic seismic hazard analyses of southern California: Overview of the SCEC Phase III report," *Bull. Seism. Soc. Am.*, 90, S1-S31.

Finn, W.D.L., Lee, K.W., and Martin, G.R. (1977). "An effective stress model for liquefaction," *J. Geotech. Engrg. Div.*, ASCE, 103 (6), 517-553.

Frankel, A., and Stephenson, W. (2000). "Three dimensional simulation of ground motions in the Seattle region for earthquakes in the Seattle fault zone," *Bull. Seism. Soc. Am.*, 90, 1251-1265.

Frankel, A.D., Mueller, C., Barnhard, T., Perkins, D., Leyendecker, E.V., Dickman, N., Hanson, S., and Hopper, M. (1996). "National seismic hazards maps, June 1996 documentation," *Open File Report 96-532*, U.S. Geological Survey.

Frankel, A., Carver, D., Cranswick, E., Bice, T., Sell, R., and Hanson, S. (2001). "Observation of basin ground motions from a dense seismic array in San Jose, California," *Bull. Seism. Soc. Am.*, in press.

Fumal, T.E., and Tinsley, J.C. (1985). "Mapping shear-wave velocities of near-surface geologic materials," *U.S. Geological Survey Prof. Paper 1360*, 127-150.

Geli, L., Bard, P-Y., and Jullien, B. (1988). "The effect of topography on earthquake ground motion: a review and new results," *Bull. Seism. Soc. Am.*, 78, 42-63.

Graves, R.W. (1993). "Modeling three-dimensional site response effects in the Marina District, San Francisco, California," *Bull. Seism. Soc. Am.*, 83, 1042-1063.

Graves, R.W. (1996). "Simulating seismic wave propagation in 3D elastic media using staggered-grid finite-differences," *Bull. Seism. Soc. Am.*, 86, 1091-1106.

Graves, R.W., Pitarka, A., and Somerville, P.G. (1998). "Ground motion amplification in the Santa Monica area: effects of shallow basin edge structure," *Bull. Seism. Soc. Am.*, 88, 1224-1242.

Guha, S., Bray, J.D., and Drnevich, V.P. (1993). *Characteristics of the deep old bay clay deposits in the east San Francisco bay area,* Rpt. No. UCB/GT/93-09, Univ. of California, Berkeley.

Gutenberg, B., and Richter, C.F. (1944). "Frequency of earthquakes in California," *Bull. Seism. Soc. Am.*, 34, 1985-1988.

Hanks, T.C. (1975). "Strong ground motion of the San Fernando, California earthquake: Ground displacements," *Bull. Seism. Soc. Am.*, 65, 193-225.

Hanks, T.C. (1982). "f_{max}," in *The dynamic characteristics of faulting inferred from recordings of strong ground motion,* U.S. Geological Survey Open-File Report 82-591, 405-436, Vol. I.

Hanks, T.C., and Kanamori, H. (1979). "A moment magnitude scale," *J. Geophy. Res.*, 84, 2348-2350.

Hanks, T.C., and McGuire, R.K. (1981). "The character of high-frequency strong ground motion," *Bull. Seism. Soc. Am.,* 71, 2071-2095.

Harmsen, S.C. (1997). "Determination of site amplification in the Los Angeles urban area from inversion of strong motion records," *Bull. Seism. Soc. Am.*, 87, 866-887.

Harmsen, S., Perkins, D., and Frankel, A. (1999). "Deaggregation of probabilistic ground motions in the central and eastern United States," *Bull. Seism. Soc. Am.,* 89, 1-13.

Hartzell, S. (1978). "Earthquake aftershocks as Green's functions," *Geophysical Research Letter,* 5, 1-4.

Hartzell, S. (1985). "The use of small earthquake as Green's functions," in *Strong Motion Simulation and Earthquake Engineering Applications*, Publication 85-02, R.E. Scholl and J.L. King, ed., Earthquake Engineering Research Institute, El Centro, CA.

Hartzell, S.H., Carver, D.L., and King, K.W. (1994). "Initial investigation of site and topographic effects at Robinwood Ridge, California," *Bull. Seism. Soc. Am.*, 84, 1336-1349.

Hartzell, S.A., Leeds, A., Frankel, A., and Michael, J. (1996). "Site response for urban Los Angeles using aftershocks of the Northridge earthquake," *Bull. Seism. Soc. Am.*, 86, S168-S192.

Hartzell, S.A., Cranswick, E., Frankel, A., Carver, D., and Meremonte, M. (1997). "Variability of site response in the Los Angeles urban area," *Bull. Seism. Soc. Am.*, 87, 1377-1400.

Hartzell, S.A., Harmsen, S., Frankel, A., Carver, D., Cranswick, E., Meremonte, M., Michael, J. (1998). "First generation site response maps for the Los Angeles region based on earthquake ground motions," *Bull. Seism. Soc. Am.*, 88, 463-472.

Hartzell, S., Harmsen, S., Frankel, A., and Larsen, S., (1999). "Calculation of broadband time histories of ground motion; Comparison of methods and validation using strong-ground motion from the 1994 Northridge earthquake," *Bull. Seism. Soc. Am.,* 89, 1484-1504.

Hartzell, S.A., Carver, D., Cranswick, E., and Frankel, A. (2000). "Variability of site response in Seattle, Washington," *Bull. Seism. Soc. Am.*, 90, 1237-1250.

Haskell, N.A., (1969). "Elastic displacements in the near-field of a propagating fault," *Bull. Seism. Soc. Am*., 59, 865-908.

Helmberger, D., Stead, R., Ho-Liu, P., and Dreger, D. (1992). "Broadband modeling of regional seismograms; Imperial Valley to Pasadena," *Geophysical Journal International*, 110 (1), 42-54.

Herrero, A., and Bernard, P. (1994). "A kinematic self-similar rupture process for earthquake," *Bull. Seism. Soc. Am*., 83, 1216-1228.

Hisada, Y. (2000). "A theoretical omega-square model considering the spatial variation in slip and rupture velocity," *Bull. Seism. Soc. Am.*, 90 387-400.

Hisada, H. (2001). "A theoretical omega-square model considering spatial variation in slip and rupture velocity, Part 2: Case for a two-dimensional source model," *Bull. Seism. Soc. Am*., 91, 651-666.

Horton, S.P. (1994). "Simulation of strong ground motion in eastern North America," *Proceedings of the 5th U.S. National Conference on Earthquake Engineering*, Earthquake Engineering Research Inst., Vol. III, p 251-260.

Hough, S.E., and Anderson, J.G. (1988). "High-frequency spectra observed at Anza, California: Implications for Q structure," *Bull. Seism. Soc. Am*., 78, 692-707.

Hsu, C.C., and Vucetic, M. (1999). *Results of cyclic and dynamic simple shear tests on soils from Tarzana and Rinaldi sites conducted for ROSRINE project and other research purposes,* Report No. UCLA/ENG-99-205, Univ. of California, Los Angeles.

Hudson, D.E., and Housner, G.W. (1958). "An analysis of strong motion accelerometer data from the San Francisco earthquake of March 22, 1957," *Bull. Seism. Soc. Am.*, 48, 253-268.

Husid, L.R. (1969). "Caracteristicas de terremotos. Analisis general," *Revista del IDIEM*, 8, Santiago de Chile, 21-42.

Hutchings, L., (1994). "Kinematic earthquake models and synthesized ground motion using empirical Green's functions," *Bull. Seism. Soc. Am*., 84, 1028-1050.

Idriss, I.M. (1990). "Response of soft soil sites during earthquakes," *Proc. H. Bolton Seed Memorial Symposium*, J.M. Duncan (ed.), Vol. 2, 273-290.

Idriss, I.M. (1991). "Procedures for selecting earthquake ground motions at rock sites," Report to U.S. Department of Commerce, revised 1993.

Idriss, I.M. (1993). "Assessment of site response analysis procedures," Report to National Institute of Standards and Technology, Gaithersburg, Maryland, Dept. of Civil & Environmental Engrg., Univ. of California, Davis.

Idriss, I.M. (1994). Personal communication regarding revision to Idriss 1991 document to incorporate Northridge recordings.

Idriss, I.M., and Sun, J.I. (1992). "SHAKE91: A computer program for conducting equivalent linear seismic response analyses of horizontally layered soil deposits," Center for Geotech. Modeling, Univ. of California, Davis.

Irikura, K. (1983). "Semi-empirical estimation of strong ground motions during large earthquakes," *Bulletin, Disaster Prevention Research Institute,* Kyoto University, Kyoto, Japan, Vol 33, pp 63-104.

Inoue, T., and Cornell, C.A. (1990). *Seismic hazard analysis of multi-degree-of-freedom structures,* Report No. RMS-8, Stanford University.

Joyner, W. (1995). "Stochastic simulation of near-source earthquake ground motion," *Proceedings of Workshop on Modeling Earthquake Ground Motion at Close Distance*s, Report TR-104975, Electric Power Research Institute, Palo Alto, CA.

Joyner, W.B., and Boore, D.M. (1981). "Peak horizontal acceleration and velocity from strong motion records including records from the 1979 Imperial Valley, California, earthquake," *Bull. Seism. Soc. Am.*, 71, 2011-2038.

Joyner, W.B., and Boore, D.M. (1993). "Method for regression analysis of strong motion data," *Bull. Seism. Soc. Am.*, 83, 469-487.

Joyner, W.B., and Boore, D.M. (1994). "Errata: Method for regression analysis of strong motion data," *Bull. Seism. Soc. Am.*, 84, 955-956.

Joyner, W.B., Warrick, R.E., and Fumal, T.E. (1981). "The effect of Quaternary alluvium on strong ground motion in the Coyote Lake, California earthquake of 1979," *Bull. Seism. Soc. Am.*, 71, 1333-1349.

Kawase, H. (1996). "The cause of the damage belt in Kobe:'The basin edge effect,' constructive interference of the direct S-wave with the basin induced diffracted/Rayleigh waves," *Seism. Res. Lett.*, 67(5), 25-34.

Kawase, H., and Nagato, K. (2000). "Structural damage impact of strong motions evaluated by the nonlinear analyses of a set of building models," *Proc. Sixth Int. Conf. Seism. Zonation*, Palm Springs, CA.

Kayen, R.E., and Mitchell, J.K. (1997). "Assessment of liquefaction potential during earthquakes by Arias Intensity," *J. Geotech.& Geoenv. Engrg.*, ASCE, 123(12), 1162-1174.

Kondner, R.L., and Zelasko, J.S. (1963). "A hyperbolic stress-strain formulation of sands." Proceedings of 2nd Pan American Conference on Soil Mechanics and Foundation Engineering, Sao Paulo, Brasil, 289-324

Kramer, S.L. (1996). *Geotechnical Earthquake Engineering*, Prentice Hall, Upper Saddle River, NJ.

Krawinkler, H., and Alavi, B. (1998) "Development of improved design procedures for near-fault ground motions," *SMIP98, Seminar on Utilization of Strong Motion Data*, Oakland, Calif.

Lazarte, C.A, Bray, J.D., Johnson, A.M., and Lemmer, R.E. (1994) "Surface breakage of the 1992 Landers earthquake and its effects on structures," *Bull. Seism. Soc. Am.*, 84, 547-561.

Lee, M.K.W., and Finn, W.D.L. (1978). "Dynamic effective stress response analysis of soil deposits with energy transmitting boundary including assessment of liquefaction potential," The University of British Columbia, Faculty of Applied Science.

Lee, V.W., and Cao, H. (1989). "Diffraction of SV waves by circular canyons of various depths," *J. Engrg. Mech.*, ASCE, 115 (9), 2035-2056.

Lee, Y., and Anderson, J.G. (2000). "A custom southern California ground motion relationship based on analysis of residuals," *Bull. Seism. Soc. Am.*, 90, S170-S187.

Lermo, J., and Chavez-Garcia, F.J. (1993). "Site effect evaluation using spectral ratios with only one station," *Bull. Seism. Soc. Am.*, 83, 1574-1594.

Li, X.S., Wang, Z.L., and Shen, C.K. (1992). "SUMDES: A nonlinear procedure for response analysis of horizontally layered sites subjected to multi-directional earthquake loading," Dept. of Civil Engineering, Univ. of California, Davis.

Li, X.S., Shen, C.K., and Wang, Z.L. (1998). "Fully coupled inelastic site response analysis for 1986 Lotung earthquake," *J. Geotech. & Geoenv. Engrg.*, ASCE, 124 (7), 560-573.

Liu, A.H., Stewart, J.P., Abrahamson, N.A., and Moriwaki, Y. (2001). "Equivalent number of uniform stress cycles for soil liquefaction analysis," *J. Geotech. & Geoenv. Engrg.*, ASCE, 127(12).

Liu, H., and Helmberger, D.V. (1985). "The 23:19 aftershock of the October 1979 Imperial Valley earthquake: More evidence for an asperity," *Bull. Seism. Soc. Am.,* 75, 689-708.

Liu, H.L., and Heaton, T.H. (1984). "Array analysis of the ground velocities and accelerations from the 1971 San Fernando California earthquake," *Bull. Seism. Soc. Am.*, 74, 1951-1968.

Luco, J.E., and Apsel, R.J. (1983). "On the Green's functions for a layered half-space, I," *Bull. Seism. Soc. Am.,* 73, 909-929.

Madariaga, R. (1977). "High-frequency radiation from crack (stress-drop) models of earthquake faulting," *J.R. Astr. Soc*., 51, 625 – 651.

Magistrale, H., Day, S., Clayton, R., and Graves, R. (2000). "The SCEC southern California reference three-dimensional seismic velocity model version 2," *Bull. Seism. Soc. Am.*, 90, S65-S76.

Mai, M.P., and Beroza, G.C. (2001). "A spatial random-field model to characterize complexity in earthquake slip," *J. Geophy. Res*. (in review).

Margheriti, L., Wennerberg, L., and Boatwright, J. (1994). "A comparison of coda and s-wave spectral ratios as estimates of site response in the southern San Francisco Bay area," *Bull. Seism. Soc. Am.*, 84, 1815-1830.

Martin, G.M., editor (1994). *Proceedings of the NCEER/SEAOC/BSSC Workshop on Site Response During Earthquakes and Seismic Code Revisions*, Univ. of Southern Calif.

Martin, P.P. (1975). "Non-linear methods for dynamic analysis of ground response"" Ph. D. Dissertation, Univ. of California, Berkeley.

Martin, P.P., and Seed, H.B. (1982), "One-dimensional dynamic ground response analyses," *J. Geotech. Engrg. Div.*, ASCE, 108 (7), 935-952.

Masing, G. (1926). "Eigenspannungen und Verfertigung Beim Messing," *Proc. 2nd Int. Congress on Applied Mechanics*, Zurich.

Matasovic, N., and Vucetic, M. (1993). *Seismic response of horizontally layered soil deposits,* Report No. ENG 93-182, School of Engineering and Applied Science, University of California, Los Angeles.

Matasovic, N., and Vucetic, M. (1995). "Generalized cyclic degradation-pore pressure generation model for clays." *J. Geotech. Engrg.*, ASCE, 121 (1), 33-42.

Matasovic, J., and Vucetic, M. (1996). "Analysis of seismic records from the Wildlife Liquefaction site," *Proc. 11th World Conf. Earthquake Engrg.*, Disc 1, Paper 209.

Mathews, M.V. (1998). "A stochastic model for recurrent earthquakes," *J. Geophy. Res.* (in review).

McGuire, R.K. (1995). "Probabilistic seismic hazard analysis and design earthquakes: closing the loop," *Bull. Seism. Soc. Am.,* 86, 1275-1284.

Morton, D.M., Hauser, R.M., and Ruppert, K.R. (1999). *Preliminary Digital Geologic Map of the Santa Ana 30' x 60' Quadrangle, Southern California,* Open-File Report 99-172, U.S. Geological Survey, Menlo Park, CA.

Nechtschein, S., Bard, P.Y., Gariel, J.C., Meneroud, J.P., Dervin, P, Cushing, M., Gaubert, C., Vidal, S., and Duval, A.M. (1995). "A topographic effect study in the Nice region," *Proc. 5th Int. Conf. on Seismic Zonation*, Vol. II, Nice, France, 1067-1074.

Ohtsuka, H., Somerville, P.G., and Sato, T. (1998). "Estimation of broadband strong ground motions considering uncertainty of fault parameters," *J. Struct. Mech. Earthq. Eng.*, JSCE, No.584/I-42, 185-200.

Olson, A.H., Orcutt, J.A., and Frazier, G.A. (1984). "The discrete wavenumber/finite element method for synthetic seismograms," *J.R. Astr. Soc*., 77, 421 – 460.

Ou, G.B., and Herrmann, R.B. (1990). "A statistical model for ground motion produced by earthquakes at local and regional distances," *Bull. Seism. Soc. Am.,* 80, 1397-1417.

Page, R.A., Mori, J., Roeloffs, E.A., and Schweig, E.S., (1998). *Earthquake hazards program five year plan 1998-2002,* USGS Open-File Report 98-143, 35 pp.

Park, S., and Elrick, S. (1998). "Prediction of shear wave velocities in southern California using surface geology," *Bull. Seism. Soc. Am.*, 88, 677-685.

Pedersen, H.A., Le Brun, B., Hatzfeld, D., Campillo, M., and Bard, P.-Y. (1994). "Ground motion amplification across ridges," *Bull. Seism. Soc. Am.*, 84, 1786-1800.

Pestana, J.M., and Nadim, F. (2000). "Nonlinear site response analysis of submerged slopes," *Report No. UCB/GT/2000-04*, Dept. of Civil & Environmental Engrg., U.C. Berkeley.

Petersen, M.D., Bryant, W.A., Cramer, C.H., Cao, M.S., Reichle, M.S., Frankel, A.D., Lienkaemper, J.J., McCroroy, P.A., and Schwartz, D.P. (1996). *Probabilistic seismic hazard assessment for the State of California,* Open File Report 96-08, California Division of Mines and Geology, *Open File Report 96-706*, U.S. Geological Survey.

Petersen, M.D., Cramer, C.H., Reichle, M.S., Frankel, A.D., and Hanks, T.C. (2000). "Discrepancy between earthquake rates implied by historic earthquakes and a consensus geologic source model for California," *Bull. Seism. Soc. Am.*, 90, 1117-1132.

Pitarka, A. (1999). "3D elastic finite-difference modeling of seismic motion using staggered grids with nonuniform spacing," *Bull. Seism. Soc. Am.*, 89, 54-68.

Pitarka, A., Irikura, K., T. Iwata and H. Sekiguchi (1998). Three-dimensional simulation of the near-fault ground motion for the 1995 Hyogo-ken Nanbu (Kobe), Japan, earthquake. *Bull. Seism. Soc. Am*. 88, 428-440.

Prevost, J.H. (1989). DYNA1D — *A computer program for nonlinear seismic site response analysis: Technical documentation,* Rpt. No. NCEER-89-0025, National Center for Earthquake Engineering Research, Buffalo, NY.

Pyke, R.M. (1979). "Nonlinear soil models for irregular cyclic loadings" *J. Geotech. Engrg. Div.*, ASCE, 105 (6), 715-726.

Pyke, R.M. (2000). "TESS Users' Manual," TAGA Engineering Software Services, Lafayette, CA.

Qiu, P. (1997). "Earthquake induced nonlinear ground deformation analyses," Ph.D. Dissertation, Univ. of Southern California.

Ramberg, W., and Osgood, W.R. (1943) *Description of stress-strain curves by three parameters,* Technical Note 902, National Advisory Committee for Aeronautics, Washington, D.C.

Rathje, E.M., Abrahamson, N.A., and Bray, J.D. (1998). "Simplified frequency content estimates of earthquake ground motions," *J. Geotech.& Geoenv. Engrg.*, ASCE, 124(2), 150-159.

Rathje, E., Idriss, I.M., and Somerville, P. (2000). "Chapter 4: Strong ground motions and site effects," *Earthquake Spectra*, 16, Supplement A, 65-96.

Reid, H.F. (1911). "The elastic-rebound theory of earthquake," *University of California Publications in the Geological Sciences,* 6, 13-44.

Roblee, C.J., Silva, W.J., Toro, G.R., and Abrahamson, N.A. (1996). "Variability in site-specific seismic ground motion design predictions," *ASCE Geotech. Special Publication No. 58*, Uncertainty in the Geologic Environment: From Theory to Practice, C.D. Shakelford, P.P. Nelson (eds.), Vol. 2, 1113-1133.

Rodriguez-Marek, A. (2000) "Near-fault seismic site response," Ph.D. Dissertation, Department of Civil Engineering, University of California, Berkeley, August, 451 pp.

Rodriguez-Marek, A., Bray, J.D., and Abrahamson, N.A. (2001). "An empirical geotechnical seismic site response procedure," *Earthquake Spectra*, 17(1), 65-87.

Rogers, A.M., Borcherdt, R.D., Covington, P.A., and Perkins, D.M. (1984). "A comparative ground response study near Los Angeles using recordings of Nevada nuclear tests and the 1971 San Fernando earthquake," *Bull. Seism. Soc. Am.*, 74, 1925-1949.

Rollins, K.M., Evans, M.D., Diehl, N.B., and Daily, W.D. (1998). "Shear modulus and damping relationships for gravels," *J. Geotech. Geoenv. Engrg.*, ASCE, 124 (5).

Sadigh, K. (1993). "A review of attenuation relationships for rock site conditions from shallow crustal earthquakes in an interplate environment," *Proc. Int. Workshop on Strong Motion Data*, 2, 179-236, Menlo Park, CA.

Sadigh, K., Chang, C.-Y., Abrahamson, N.A., Chiou, S.J., and Power, M.S. (1993). "Specification of long-period ground motions: updated attenuation relationships for rock site conditions and adjustment factors for near-fault effects," *Proc. Seminar on Seismic Isolation, Passive Energy Dissipation, and Active Control*, Applied Technology Council Publication No. 17-1, Vol. 1, 59-70.

Sadigh, K., Chang, C.-Y., Egan, J.A., Makdisi, F., and Youngs, R.R. (1997). "Attenuation relations for shallow crustal earthquakes based on California strong motion data," *Seism. Res. Letters*, 68(1), 180-189.

Salvati, L.A., Lok, M.-H., and Pestana, J.M. (2001). "Seismic response of deep stiff granular soil deposits," *Proc. 4th Int. Conf. Recent Advances in Geotech. Eqk. Engrg. Soil Dyn.*, Paper 3.30.

Sasani, M., and Bertero, V.V. (2000) "Importance of severe pulse-type ground motion in performance-based engineering: historical and critical review," *Proc. 12th World Conference on Earthquake Engineering*, New Zealand, 8 pp.

Sato, H., and Fehler, M.C. (1998). *Seismic Wave Propagation and Scattering in the Heterogeneous Earth*, Springer-Verlag, Inc., NY.

Sato, T., Graves, R.W., and Somerville, P.G. (1999). "3D finite difference simulations of long period strong motions in the Tokyo metropolitan are during the 1990 Odawara earthquake (Mj 5.1) and the Great 1923 Kanto earthquake (Ms 8.2) in Japan," *Bull. Seism. Soc. Am.*, 89, 579-598.

Schnabel, P.B. (1973). "Effects of local geology and distance from source on earthquake ground motions," Ph.D. Dissertation, Univ. of California, Berkeley.

Schnabel, P.B., Lysmer, J., and Seed, H.B. (1972). *SHAKE: A computer program for earthquake response analysis of horizontally layered sites,* Rpt. No. EERC 72/12, Earthquake Engineering Research Center, Univ. of California, Berkeley.

Schneider, J.F., Silva, W.J., and Stark, C.L. (1993). "Ground motion model for the 1989 *m*6.9 Loma Prieta earthquake including effects of source, path, and site," *Earthquake Spectra*, 9(2), 251-287.

Schneider, J.F., Abrahamson, N.A., and Hanks, T.C. (1996). *Ground motion modeling of scenario earthquakes at Yucca Mountain: Provisional draft final report for Activity 9.3.1.17.3.3,* U.S. Geological Survey.

Schwartz, D.P., and Coppersmith, K.J. (1984). "Fault behavior and characteristic earthquakes: examples from the Wasatch and San Andreas faults," *J. Geophy. Res.*, 89, 5681-5698.

Seed, H.B., and Idriss, I.M. (1970). *Soil moduli and damping factors for dynamic response analyses,* Report EERC 70-10, Earthquake Engineering Research Center, University of California, Berkeley.

Seed, H.B., and Idriss, I.M. (1971). "Influence of soil conditions on building damage potential during earthquakes," *J. Struct. Engrg.*, ASCE, 97(2), 639-663.

Seed, H.B., and Idriss, I.M. (1982) *Ground motions and soil liquefaction during earthquakes*, Monograph Series, Vol. 5, Earthquake Engineering Research Institute.

Seed, H.B., Ugas, C., and Lysmer, J. (1976). "Site-dependant spectra for earthquake resistant design," *Bull. Seism. Soc. Am.*, 66, 221-243.

Seed, H.B., Wong, R.T., Idriss, I.M., and Tokimatsu, K. (1986). "Moduli and damping factors for dynamic analyses of cohesionless soils," *J. Geotech. Engrg.*, ASCE, 112 (11), 1016-1032.

Seed, H.B., Romo, M.P., Sun, J.I., Jaime, A., and Lysmer, J. (1987). *Relationships between soil conditions and earthquake ground motions in Mexico City in the earthquake of September 19, 1985,* Rpt. No. UCB/EERC-87/15, Earthquake Engineering Research Center, Univ. of California, Berkeley.

Silva, W.J. (1976). "Body waves in a layered anelastic solid," *Bull. Seism. Soc. Am.*, 66, 1539-1554.

Silva, W.J. (1992). "Factors controlling strong ground motion and their associated uncertainties," in *High-Level Nuclear Waste Repositories*, ASCE Struct. Div., 132-161.

Silva, W.J., and Costantino, C. (1999). "Assessment of liquefaction potential for the 1995 Kobe, Japan earthquake including finite source effects," report to U.S. Army Corps of Engineers, 163 pp.

Silva, W.J., and Darragh, R.B. (1995). "Engineering characterization of earthquake strong ground motion recorded at rock sites," *Report TR-102261*, Electric Power Research Institute, Palo Alto, CA.

Silva, W.J., and Lee, K. (1987). "WES RASCAL code for synthesizing earthquake ground motions," in State of the Art for Assessing Earthquake Hazards in the United States, Report 24, U.S. Army Engineers Waterway Experiment Station, *Misc. Paper S-73-1*.

Silva, W.J., Darragh, R.B., Stark, C., Wong, I., Stepp, J. C., Schneider, J. F., and Chiou, S.-J. (1990). "A methodology to estimate design response spectra in the near-source region of large earthquake using the band-limited-white noise ground motion model," *Proceedings of the 4th U.S. National Conference on Earthquake Engineerin*g, Palm Springs, CA, May 20-24, Earthquake Engineering Research Institute, El Cerrito, CA, 1, 487-494.

Silva, W.J., Darragh, R.B., Green R.K., and Turcotte, F.T. (1989). "Estimated ground motions for a New Madrid event," U.S. Army Engineer Waterways Experiment Station, Wash., DC, *Misc. Paper GL-89-17*.

Silva, W.J., Chiou, S.-J., and Somerville, M. (1995). "Finite and point source RVT modeling," *Proceedings of Workshop on Modeling Earthquake Ground Motion at Close Distance*s, Report TR-104975, Electric Power Research Institute, Palo Alto, CA.

Silva, W.J., Abrahamson, N., Toro, G., and Costantino, C. (1997). *Description and validation of the stochastic ground motion model,* Report to Brookhaven National Laboratory, Associated Universities, Inc., Upton, NY.

Silva, W.J., Li, S., Darragh, R., and Gregor, N. (1999). *Surface geology based strong motion amplification factors for the San Francisco Bay and Los Angeles areas,* Report to Pacific Earthquake Engineering Research Center.

Silva, W.J., Darragh, R., Gregor, N., Martin, G., Abrahamson, N., and Kircher, C. (2000). *Reassessment of site coefficients and near-fault factors for building code provisions*, Report to U.S. Geological Survey, National Earthquake Hazards Reduction Program.

Silva, W.J., Gregor, N., and Darragh, R.B. (2000). *Near fault ground motions*, Report to the PEER Program of Applied Earthquake Engineering Research on Lifeline Systems.

Sitar, N., and Clough, G.W. (1983). "Seismic response of steep slopes in cemented soils," *J. Geotech. Engrg.* 109(2).

Shome, N., Cornell, C.A., Bazzuro, P., and Carballo, E.J. (1998). "Earthquakes, records, and nonlinear responses," *Earthquake Spectra,* 14, 469-500.

Sokolov, V.Y. (1997). "Empirical models for estimating Fourier-amplitude spectra of ground acceleration in the northern Caucasus (Racha seismogenic zone)," *Bull. Seism. Soc. Am.*, 87, 1401-1412.

Sokolov, V.Y., Loh, C.-H., and Wen, K.-L. (2000). "Empirical study of sediment-filled basin response: The case of Taipei City," *Earthquake Spectra*, 16(3), 681-707.

Somerville, P. G. (1993). "Engineering applications of strong ground motion simulation," *Tectonophysics*, 218 (1-3), 195-219.

Somerville, P.G. (1998). "Development of an improved representation of near fault ground motions," *Proc. SMIP98 Seminar on Utilization of Strong Motion Data*, California Strong Motion Instrumentation Program, Sacramento, CA, 1-20.

Somerville, P.G. (2000). "Magnitude scaling of near fault ground motion," *Proc. Int. Workshop on Annual Commemoration of Chi-Chi earthquake*, Vol. 1, 59-70.

Somerville, P.G., Smith, N.F., and Dreger, D.S. (1992). *The influence of critical Moho reflections on strong ground motion attenuation in California*, A report to the California Division of Mines and Geology Strong Motion Instrumentation Program, 82 p.

Somerville, P.G., Smith, N.F., and Graves, R.W. (1994). "Effect of critical reflections from the Moho on the attenuation of strong ground motion," in *The Loma Prieta, California, earthquake of October 17, 1989 — Strong Ground Motion*, R.D. Borcherdt (ed.), U.S. Geological Survey Professional Paper 1551-A, A67-A76.

Somerville, P.G., Graves, R.W., and Saikia, C.K. (1995). "Characterization of Ground Motions during the Northridge Earthquake of January 17, 1994," *Program to Reduce the Earthquake Hazards of Steel Moment Frame Buildings,* SAC Report 95-03.

Somerville, P.G., Saikia, C., Wald, D., Graves, R. (1996). "Implications of the Northridge earthquake for strong ground motions from thrust faults," *Bull. Seism. Soc. Am.*, 86, S115-S125.

Somerville, P.G., Smith, N.F., Graves, R.W. and Abrahamson, N.A. (1997). "Modification of empirical strong ground motion attenuation relations to include the amplitude and duration effects of rupture directivity," *Seismological Research Letters* 68, 199-222.

Somerville, P., Smith, N.F., Punyamurthula, S., and Sun, J. (1997). *Development of ground motion time histories for Phase 2 of the FEMA/SAC Steel Project,* Report No. SAC/BD-97-04.

Somerville, P.G., Irikura, K., Graves, R., Sawada, S., Wald, D., Abrahamson, N.A., Iwasaki, Y., Kagawa, T., Smith, N., and Kowada, A. (1999). "Characterizing crustal earthquakes slip models for prediction of strong ground motion," *Seism. Research Letters*, 70(1), 59-80.

Spudich, P., and Archuleta, R.J. (1987). "Techniques for earthquake ground-motion calculation with applications to source parameterization of finite faults," in *Seismic Strong Motion Synthetics*, B.A. Bolt, ed., Academic Press.

Spudich, P., and Frazer, L.N. (1984). "Use of ray theory to calculate high-frequency radiation from earthquake source having spatially variable rupture velocity and stress drop," *Bull. Seism. Soc. Am.,* 74, 2061-2082.

Spudich, P. Hellweg, M., and Lee, W.H.K. (1996). "Directional topographic site response at Tarzana observed in aftershocks of the 1994 Northridge, California, Earthquake: Implications for mainshock motions," *Bull. Seism. Soc. Am.*, 86, S139-S208.

Spudich, P., Joyner, W.B., Lindh, A.G., Boore, D.M., Margaris, B.M., and Fletcher, J.B. (1999). "SEA99: A revised ground motion prediction relation for use in extensional tectonic regimes," *Bull. Seism. Soc. Am.*, 89, 1156-1170.

Steidl, J.H. (2000). "Site response in southern California for probabilistic seismic hazard analysis," *Bull. Seism. Soc. Am.*, 90, S149-S169.

Stein, R.S., and Hanks, T.C. (1998). "$m \geq 6$ earthquakes in Southern California during the twentieth century: no evidence for a seismicity or moment deficit," *Bull. Seism. Soc. Am.*, 88, 635-652

Stephenson, W.J., Williams, R.A., Odum, J.K., and Worley, D.M. (2000). "High-resolution seismic reflection surveys and modeling across an area of high damage from the 1994 Northridge earthquake, Sherman Oaks, California," *Bull. Seism. Soc. Am.*, 90, 643-654.

Stewart, J.P., and Baturay, M.B. (2001). "Uncertainties and residuals in ground motion estimates at soil sites," *Proc. 4th Int. Conf. Recent Advances in Geotech. Eqk. Engrg. Soil Dyn.*, San Diego, CA. Paper 3.14.

Stewart, J.P., and Sholtis, S.E. (1999). *Topographic effects on seismic ground motions above and below a cut slope in sand,* Report to U.S. Geological Survey, University of California, Los Angeles.

Stewart, J.P., Liu, A.H., Choi, Y. and Baturay, M.B. (2001). *Amplification factors for spectral acceleration in active regions,* Rpt. No. PEER-2001/10, Pacific Earthquake Engineering Research Center, Univ. of California.

Stokoe, K.H., Darendeli, M.B., Andrus, R.D., and Brown, L.T. (1999). "Dynamic soil properties: Laboratory, field and correlation studies," *Earthquake Geotechnical Engineering*, S. Pinto (ed.), Balkema, Rotterdam, Vol. 3, 811-845.

Suess, M.P., Stidham, C., Shaw, J.H., Tromp, J. (2000). "A 3D seismic velocity model of the Los Angeles basin developed from borehole sonic logs and stacking velocity data (abstract), "*EOS*, 78, Fall Meet. Suppl., F435-F436.

Suetomi, I., and Yoshida, N. (1998). "Nonlinear behavior of surface deposit during the 1995 Hyogoken-Nanbu earthquake," *Abstr. Special Issue of Soils and Foundations*, Japanese Geotechnical Society.

Sun, J.I., Golesorkhi, R., and Seed, H.B. (1988). *Dynamic moduli and damping ratios for cohesive soils,* Rpt. No. UCB/EERC-88/15, Earthquake Engineering Research Center, Univ. of California, Berkeley.

Tinsley, J.C., and Fumal, T.E. (1985). *Mapping Quaternary sedimentary deposits for areal variations in shaking response,* U.S. Geological Survey Prof. Paper 1360, 101-126.

Toro, G.R., Abrahamson, N.A., and Schneider, J.F. (1997). "Model of strong ground motions from earthquakes in central and eastern North America: Best estimates and uncertainty," *Seism. Res. Letters*, 68(1), 41-57.

Trifunac, M.D. (1973). "Scattering of SH waves by a semi cylindrical canyon," *Earthquake Engrg. Struct. Dyn.*, 1(3), 267-281.

Trifunac, M.D., and Todorovska, M.I. (1996). "Nonlinear soil response — 1994 Northridge, California earthquake," *J. Geotech. & Geoenv. Engrg.*, ASCE, 122 (9), 725-735.

Trifunac, M.D., and Todorovska, M.I. (1997). "Northridge, California, earthquake of 1994: density of red-tagged buildings versus peak horizontal velocity and intensity of shaking," *Soil Dyn. Earthquake Engrg.*, 16, 3, 209-222.

Tucker, B.E., King, J.I., Hatzfeld, D., and Nersesov, I.L. (1984). "Observations of hard-rock site effects," *Bull. Seism. Soc. Am.*, 74, 121-136.

Umeda, Y., Kuroiso, A., Ito, K, Ito, Y., and Saeki, T. (1986). "High accelerations in the epicentral area of the Western Nagana Prefecture, Japan, Earthquake of 1984," *J. Seism. Soc. Japan*, 39, 217-228.

Vidale, J.E., and Helmberger, D.V. (1988). “Elastic finite difference modeling of the 1971 San Fernando, California earthquake,” *Bull. Seism. Soc. Am.*, 78, 122-141.

Vucetic, M. (1986). “Pore pressure buildup and liquefaction of level sandy sites during earthquakes,” Ph.D. Dissertation, Rensselaer Polytechnic Institute, Troy, NY.

Vucetic, M. (1990). "Normalized behavior of clay under irregular cyclic loading," *Can. Geotech. J.*, 27 (1), 29-46.

Vucetic, M., and Dobry, R. (1991). “Effect of soil plasticity on cyclic response,” *J. Geotech. Engrg.*, ASCE, 117(1), 89-107.

Vucetic, M., Hsu, C.C., and Doroudian, M. (1998a). *Results of cyclic and dynamic simple shear tests on soils from La Cienega site conducted for ROSRINE project and other research purposes*, Report No. UCLA/ENG-98-200, Univ. of California, Los Angeles.

Vucetic, M., Lanzo, G., and Doroudian, M. (1998b). “Damping at small strains in cyclic simple shear test,” *J. Geotech. & Geoenv. Engrg.*, ASCE, 124(7), 585-594.

Wald, D.J. (1996). “Slip history of the 1995 Kobe, Japan, earthquake determined from strong motion, teleseismic and geodetic data,” *J. Phys. Earth*, 44, 489-503.

Wang, Z.L. (1990). “Bounding surface hypoplasticity model for granular soils and its applications,” Ph.D. Thesis, University of California, Davis, CA.

Wang, Z.L., Chang, C.-Y., and Mok, C.M. (2001). “Evaluation of site response using downhole array data from a liquefied site,” *Proc. 4th Int. Conf. Recent Advances in Geotech. Eqk. Engrg. Soil Dyn.*, Paper 4.30.

Weiler, W.A. (1988). “Small strain shear modulus of clay,” *Proc. ASCE Conf. Earthquake Engineering & Soil Dynamics II: Recent Advances in Ground Motion Evaluation*, Geotechnical Special Publication 20, ASCE, New York, 331-335.

Wells, D.L., and Coppersmith, K.J. (1994). “New empirical relationships among magnitude, rupture length, rupture width, rupture area, and surface displacement,” *Bull. Seism. Soc. Am.*, 84, 974-1002.

Wen, K-L., and Peng, H-Y. (1998). “Strong motion observations in the Taipei basin,” The Effects of Surface Geology on Seismic Motion, Recent Progress and New Horizon on ESG Study, *Proceedings of the Second International Symposium,* A.A. Balkema, Rotterdam, Vol. 1, p. 263-270.

Wesnousky, S.G. (1986). “Earthquakes, Quaternary faults, and seismic hazard in California,” *J. Geophy. Res.*, 91 (B12), 12587-12631.

Wesnousky, S.G. (1994). “The Gutenberg-Richter or characteristic earthquake distribution, which is it?,” *Bull. Seism. Soc. Am.*, 84, 1940-1959.

Wills, C.J., and Silva, W. (1998). "Shear wave velocity characteristics of geologic units in California," *Earthquake Spectra*, 14(3), 533-556.

Wills, C.J., Petersen, M., Bryant, W.A., Reichle, M., Saucedo, G.J., Tan, S., Taylor, G., and Treiman, J. (2000). "A site conditions map for California based on geology and shear wave velocity," *Bull. Seism. Soc. Am.*, 90, S187-S208.

Wilson, R.C. (1993). "Relation of Arias intensity to magnitude and distance in California," *Open File Rpt. No. 93-0556*, U.S. Geological Survey, Menlo Park, CA, 42 p.

Wong, H.L. (1982). "Effect of surface topography on the diffraction of P, SV, and Rayleigh waves," *Bull. Seism. Soc. Am.*, 72, 1167-1183.

Wong, H.L, and Trifunac, M.D. (1974). "Scattering of plane SH waves by a semi-elliptical canyon," *Earthquake Engineering Struct. Dyn.*, 3(2), 157-169.

Working Group on California Earthquake Probabilities (1995). "Seismic hazards in southern California: Probable earthquakes, 1994-2024," *Bull. Seism. Soc. Am.*, 85, 379-439.

Working Group on California Earthquake Probabilities (1999). *Earthquake probabilities in the San Francisco Bay Region: 2000 to 2030 — A summary of findings*, Open File Report 99-517, U.S. Geological Survey.

Youngs, R.R., and Coppersmith, K.J. (1985). "Implications of fault slip rates and earthquake recurrence models to probabilistic seismic hazard estimates," *Bull. Seism. Soc. Am.*, 75, 939-964.

Youngs, R.R., Abrahamson, N.A., Makdisi, F.I., and Sadigh, K. (1995). "Magnitude-dependent variance of peak ground acceleration," *Bull. Seism. Soc. Am.*, 85, 1161-1176.

Youngs, R.R., Chiou, S.-J., Silva, W.J., and Humphrey, J.R. (1997). "Strong ground motion attenuation relationships for subduction zone earthquakes," *Seism. Res. Letters*, 68(1), 58-73.

Zeng, Y. (1995). "A realistic synthetic Green's function calculation using a combined deterministic and stochastic modeling approach," *EOS, Trans. A.G.U.*, **7**6, F357.

Zeng, Y., and Anderson, J.G. (2000). *Evaluation of numerical procedures for simulating near-fault long-period ground motions using Zeng method,* Report to the PEER Program of Applied Earthquake Engineering Research on Lifeline Systems.

Zeng, Y., Anderson, J.G., and Yu, G. (1994). "A composite source model for computing realistic synthetics strong ground motions," *Geophysical Research Letters,* 21, 725-728.

Zeng, Y., Anderson, J.G., and Su, F. (1995). "Sub-event rake and random scattering effects in realistic strong ground motion simulation," *Geophysical Research Letters,* 22, 17-20.

PEER REPORTS

PEER reports are available from the National Information Service for Earthquake Engineering (NISEE). To order PEER reports, please contact the Pacific Earthquake Engineering Research Center, 1301 South 46th Street, Richmond, California 94804-4698. Tel.: (510) 231-9468; Fax: (510) 231-9461.

PEER 2001/09	*Ground Motion Evaluation Procedures for Performance-Based Design.* Jonathan P. Stewart, Shyh-Jeng Chiou, Jonathan D. Bray, Robert W. Graves, Paul G. Somerville, and Norman A. Abrahamson. $26.00
PEER 2001/06	*Development of an Electrical Substation Equipment Performance Database for Evaluation of Equipment Fragilities.* Thalia Agnanos. $15.00
PEER 2001/05	*Stiffness Analysis of Fiber-Reinforced Elastomeric Isolators.* Hsiang-Chuan Tsai and James M. Kelly. May 2001. $20.00
PEER 2001/04	*Organizational and Societal Considerations for Performance-Based Earthquake Engineering.* Peter J. May. April 2001. $15.00
PEER 2001/03	*A Modal Pushover Analysis Procedure to Estimate Seismic Demands for Buildings: Theory and Preliminary Evaluation.* Anil K. Chopra and Rakesh K. Goel. January 2001. $15.00
PEER 2001/02	*Seismic Response Analysis of Highway Overcrossings Including Soil-Structure Interaction.* Jian Zhang and Nicos Makris. March 2001. $20.00
PEER 2001/01	*Experimental Study of Large Seismic Steel Beam-to-Column Connections.* Egor P. Popov and Shakhzod M. Takhirov. November 2000. $15.00
PEER 2000/09	*Structural Engineering Reconnaissance of the August 17, 1999 Earthquake: Kocaeli (Izmit), Turkey.* Halil Sezen, Kenneth J. Elwood, Andrew S. Whittaker, Khalid Mosalam, John J. Wallace, and John F. Stanton. December 2000. $20.00
PEER 2000/08	*Behavior of Reinforced Concrete Bridge Columns Having Varying Aspect Ratios and Varying Lengths of Confinement.* Anthony J. Calderone, Dawn E. Lehman, and Jack P. Moehle. January 2001. $20.00
PEER 2000/07	*Cover-Plate and Flange-Plate Reinforced Steel Moment-Resisting Connections.* Taejin Kim, Andrew S. Whittaker, Amir S. Gilani, Vitelmo V. Bertero, and Shakhzod M. Takhirov. September 2000. $33.00
PEER 2000/06	*Seismic Evaluation and Analysis of 230-kV Disconnect Switches.* Amir S. J. Gilani, Andrew S. Whittaker, Gregory L. Fenves, Chun-Hao Chen, Henry Ho, and Eric Fujisaki. July 2000. $26.00
PEER 2000/05	*Performance-Based Evaluation of Exterior Reinforced Concrete Building Joints for Seismic Excitation.* Chandra Clyde, Chris P. Pantelides, and Lawrence D. Reaveley. July 2000. $15.00
PEER 2000/04	*An Evaluation of Seismic Energy Demand: An Attenuation Approach.* Chung-Che Chou and Chia-Ming Uang. July 1999. $20.00

PEER 2000/03 *Framing Earthquake Retrofitting Decisions: The Case of Hillside Homes in Los Angeles.* Detlof von Winterfeldt, Nels Roselund, and Alicia Kitsuse. March 2000. $13.00

PEER 2000/02 *U.S.-Japan Workshop on the Effects of Near-Field Earthquake Shaking.* Andrew Whittaker, ed. July 2000. $20.00

PEER 2000/01 *Further Studies on Seismic Interaction in Interconnected Electrical Substation Equipment.* Armen Der Kiureghian, Kee-Jeung Hong, and Jerome L. Sackman. November 1999. $20.00

PEER 1999/14 *Seismic Evaluation and Retrofit of 230-kV Porcelain Transformer Bushings*. Amir S. Gilani, Andrew S. Whittaker, Gregory L. Fenves, and Eric Fujisaki. December 1999. $26.00

PEER 1999/12 *Rehabilitation of Nonductile RC Frame Building Using Encasement Plates and Energy-Dissipating Devices.* Mehrdad Sasani, Vitelmo V. Bertero, James C. Anderson. December 1999. $26.00

PEER 1999/11 *Performance Evaluation Database for Concrete Bridge Components and Systems under Simulated Seismic Loads.* Yael D. Hose and Frieder Seible. November 1999. $20.00

PEER 1999/10 *U.S.-Japan Workshop on Performance-Based Earthquake Engineering Methodology for Reinforced Concrete Building Structures.* December 1999. $33.00

PEER 1999/09 *Performance Improvement of Long Period Building Structures Subjected to Severe Pulse-Type Ground Motions*. James C. Anderson, Vitelmo V. Bertero, and Raul Bertero. October 1999. $26.00

PEER 1999/08 *Envelopes for Seismic Response Vectors.* Charles Menun and Armen Der Kiureghian. July 1999. $26.00

PEER 1999/07 *Documentation of Strengths and Weaknesses of Current Computer Analysis Methods for Seismic Performance of Reinforced Concrete Members.* William F. Cofer. November 1999. $15.00

PEER 1999/06 *Rocking Response and Overturning of Anchored Equipment under Seismic Excitations.* Nicos Makris and Jian Zhang. November 1999. $15.00

PEER 1999/05 *Seismic Evaluation of 550 kV Porcelain Transformer Bushings.* Amir S. Gilani, Andrew S. Whittaker, Gregory L. Fenves, and Eric Fujisaki. October 1999. $15.00

PEER 1999/04 *Adoption and Enforcement of Earthquake Risk-Reduction Measures.* Peter J. May, Raymond J. Burby, T. Jens Feeley, and Robert Wood. $15.00

PEER 1999/03 *Task 3 Characterization of Site Response General Site Categories*. Adrian Rodriguez-Marek, Jonathan D. Bray, and Norman Abrahamson. February 1999. $20.00

PEER 1999/02 *Capacity-Demand-Diagram Methods for Estimating Seismic Deformation of Inelastic Structures: SDF Systems*. Anil K. Chopra and Rakesh Goel. April 1999. $15.00

PEER 1999/01 *Interaction in Interconnected Electrical Substation Equipment Subjected to Earthquake Ground Motions.* Armen Der Kiureghian, Jerome L. Sackman, and Kee-Jeung Hong. February 1999. $20.00

PEER 1998/08 *Behavior and Failure Analysis of a Multiple-Frame Highway Bridge in the 1994 Northridge Earthquake.* Gregory L. Fenves and Michael Ellery. December 1998. $20.00

PEER 1998/07 *Empirical Evaluation of Inertial Soil-Structure Interaction Effects.* Jonathan P. Stewart, Raymond B. Seed, and Gregory L. Fenves. November 1998. $26.00

PEER 1998/06 *Effect of Damping Mechanisms on the Response of Seismic Isolated Structures.* Nicos Makris and Shih-Po Chang. November 1998. $15.00

PEER 1998/05 *Rocking Response and Overturning of Equipment under Horizontal Pulse-Type Motions.* Nicos Makris and Yiannis Roussos. October 1998. $15.00

PEER 1998/04 *Pacific Earthquake Engineering Research Invitational Workshop Proceedings, May 14–15, 1998: Defining the Links between Planning, Policy Analysis, Economics and Earthquake Engineering.* Mary Comerio and Peter Gordon. September 1998. $15.00

PEER 1998/03 *Repair/Upgrade Procedures for Welded Beam to Column Connections.* James C. Anderson and Xiaojing Duan. May 1998. $33.00

PEER 1998/02 *Seismic Evaluation of 196 kV Porcelain Transformer Bushings.* Amir S. Gilani, Juan W. Chavez, Gregory L. Fenves, and Andrew S. Whittaker. May 1998. $20.00

PEER 1998/01 *Seismic Performance of Well-Confined Concrete Bridge Columns.* Dawn E. Lehman and Jack P. Moehle. December 2000. $33.00